

Copyright
By
Gregory Paul Turco
2007

**Durability Evaluation of Post-Tensioned Concrete Beam Specimens
After Long-Term Aggressive Exposure Testing**

by

Gregory Paul Turco, B.S.

Thesis

Presented to the Faculty of the Graduate School of
The University of Texas at Austin
in Partial Fulfillment
of the Requirements
for the Degree of

Master of Science in Engineering

The University of Texas at Austin

August 2007

**Durability Evaluation of Post-Tensioned Concrete Beam Specimens
After Long-Term Aggressive Exposure Testing**

**APPROVED BY
SUPERVISING COMMITTEE:**

John E. Breen

Sharon L. Wood

Dedication

To my family.

Acknowledgements

First of all, I would like to sincerely thank Dr. John Breen for his kindness, guidance and wisdom both in my research and in my coursework. He has given me countless career and life lessons which I will always remember.

I would also like to extend my gratitude to Jeff West and Andrea Schokker for creating this test program and building my beams for me even before I had graduated from high school. In addition, my most sincere thanks goes out to all those various, undergraduate, graduate, and doctorate student who over the past 8 years braved the hot Texas summers and cold winters to tend to the specimens.

I would also like to give a most heartfelt thanks and appreciation to my undergraduate assistants over the past 2 years-Lance Operhall, Sean Mac Lean, Kristen Donnelly, Katherine Abdou, Karl Kluever, Curtis Anderson, and Zach Webb. Without their help none of this would have been possible.

I would also like to thank both the administrative and technical staff here at the Ferguson Laboratory for all their help-Blake Stasney, Dennis Phillip, Greg Harris, Barbara Howard, Ella Schwartz and Cari Billingsley. In addition, I would like to thank Mike Rung and Dave Whitney from the Concrete Materials Research Group for their assistance as well.

And finally, I want to thank my parents and my sister for being so supportive and understanding.

May 25, 2007

Durability Evaluation of Post-Tensioned Concrete Beam Specimens After Long-Term Aggressive Exposure Testing

Gregory Paul Turco, M.S.E.

The University of Texas at Austin, 2007

SUPERVISOR: John E. Breen

This thesis focuses on the forensic analysis and evaluation of large-scale post-tensioned beam specimens after nearly 8 years of aggressive exposure testing. The research was funded jointly by both FHWA and TxDOT. The durability of post-tensioned bridge structures in aggressive environments has been of concern in recent years. Major concerns include the effectiveness of grouting materials, the splicing of ducts, and the soundness of anchorage zones. The relationship between durability performance and the following variables was evaluated in this study:

- Level of applied load & initial cracking
- Level of prestress
- Duct type
- Strand type
- Grout type
- Grouting method
- Use of encapsulated system for anchorage protection
- Galvanized duct splice type

In addition, the accuracy of non-destructive testing methods for evaluating corrosion was examined. These methods included half-cell potentials and chloride penetration tests.

Major findings include that mixed reinforcement (also known as partial prestressing), performed poorly from a durability standpoint. Only fully prestressed beams offered better durability performance than those which were not prestressed at all. Corrugated steel galvanized ducts were found to perform very poorly. Large holes were found in the ducts, and in some cases the ducts completely corroded away across several inches. Corrugated plastic ducts will offer better performance as long as they are “robust.”

Non-flowfilled epoxy coated strand and galvanized strand offered no significant improvement in long-term durability over conventional strand.

In addition, installing plastic caps over anchorheads rather than just filling the anchorage pocket with non-shrink grout increases the long-term durability of the anchorage.

Table of Contents

Chapter 1: Introduction	1
1.1 Background	1
1.2 Corrosion of Steel in Concrete	2
1.3 Durability in Post-Tensioning	3
1.4 Effect of Mixed Reinforcement	4
1.5 Durability of Post-Tensioning Anchorages	4
1.6 Thesis	5
1.6.1 Research Background	5
1.6.2 Thesis Objectives	6
1.6.3 Scope	7
Chapter 2: Test Specimens	8
2.1 Specimen Test Concept	8
2.2 Specimen Description	8
2.3 Specimen Variables	10
2.3.1 Control Specimens	10
2.3.2 Phase I Variables	11
2.3.3 Phase II Variables	15
2.4 Specimen Materials	18
2.5 Specimen Construction Details	19
2.5.1 Beam Fabrication	19
2.5.2 Post-Tensioning	20
2.5.3 Grouting Procedure	20
2.5.4 Anchorage Protection	21
2.6 Specimen Loading	22
2.7 Specimen Notation	23
Chapter 3: Experimental Procedure	27
3.1 Long-Term Exposure Set-up	27
3.1.1 Beam Exposure Cycles	27
3.1.2 Beam Anchorage Exposure	28
3.2 Measurements Taken During Exposure Testing	29
3.2.1 Visual Inspection	29
3.2.2 Crack Patterns and Crack Widths	29
3.2.3 Half-Cell Potential Measurements	30
3.2.4 Chloride Penetration	32
Chapter 4: Long-Term Exposure Test Results and Analysis	35
4.1 Half-Cell Potential Data	35
4.1.1 Phase I Half-Cell Readings	35
4.1.2 Phase II Half-Cell Readings	39
4.1.3 Analysis of Half-Cell Potential Data	40
4.2 Chloride Penetration Data	43
4.2.1 Phase I Chloride Penetration Data	43

4.2.2 Phase II Chloride Penetration Data.....	46
4.2.3 Analysis of Chloride Penetration Data	49
Chapter 5: Forensic Analysis.....	51
5.1 Autopsy Procedure.....	51
5.1.1 Beam Unloading	51
5.1.2 Cutting of Beams	53
5.1.3 Removal of Reinforcing Elements.....	56
5.1.4 Removal of Post-Tensioning Anchorages	58
5.1.5 Disassembly of Prestressing Tendons.....	58
5.1.6 Element Rating System.....	59
5.2 Results of Forensic Analysis.....	66
5.2.1 Phase I Beams	66
5.2.2 Phase II Beams.....	122
Chapter 6: Analysis of Results.....	182
6.1 Overall Observations From Forensic Analysis.....	182
6.1.1 Cracking.....	182
6.1.2 Reinforcing Bar Corrosion.....	182
6.1.3 Duct Corrosion and Grouting Voids.....	182
6.1.4 Strand Corrosion	182
6.1.5 Anchorages	183
6.2 Analysis of Phase I Variables	183
6.2.1 Level of Prestress, Applied Loading, and Crack Width	183
6.2.2 Duct Splice Type and Condition.....	188
6.3 Phase II Variables	189
6.3.1 Duct Type.....	190
6.3.2 Strand Type.....	193
6.3.3 Grouting Procedure.....	194
6.3.4 Grout Type	194
6.3.5 Anchorage Protection.....	194
6.4 Comparison of Data taken at the End of Exposure Testing With Results of Forensic Analysis.....	195
6.4.1 Half-Cell Potential Data.....	195
6.4.2 Chloride Penetration	200
6.5 Extent of Corrosion Damage and Length of Testing.....	203
6.6 Phase I Beams vs. Phase II Beams.....	206
Chapter 7: Design Recommendations & Implementation	211
7.1 Design Recommendations	211
7.1.1 Mixed Reinforcement	211
7.1.2 Duct Type.....	211
7.1.3 Duct Splice Type.....	211
7.1.4 Grout Type and Grouting Procedure.....	212
7.1.5 Strand Type.....	212
7.1.6 Anchorage Protection.....	212

7.1.7 Reinforcing Bars & Bar Chairs.....	213
7.1.8 Chloride Content.....	213
7.1.9 Half-Cell Potentials.....	213
Chapter 8: Summary, Conclusions, and Recommendations for Future Testing....	214
8.1 Summary	214
8.2 Conclusions.....	214
8.2.1 Level of Loading, Level of Prestress, and Initial Crack Width	214
8.2.2 Duct Type.....	215
8.2.3 Strand Type.....	215
8.2.4 Grout Type	216
8.2.5 Grouting Method.....	217
8.2.6 Anchorage Protection.....	217
8.2.7 Galvanized Metal Duct Splice Type & Condition.....	217
8.2.8 Accuracy of Non-Destructive Measurements Taken During Exposure Testing	218
8.3 Recommendations For Future Testing.....	218
Appendix A: Corrosion Ratings	220
Appendix B: Half-Cell Potential Data	221
References.....	223
Vita.....	225

List of Tables

Table 2.1: Specimen Designations.....	26
Table 3.1: Interpretation of Half-Cell Potentials for Mild Reinforcing Steel.....	31
Table 4.1: Half-Cell Potential Contour Map Color Indications.....	36
Table 5.1: Numerical Rating System For Mild Steel Bars and Stirrups.....	60
Table 5.2: Numerical Rating System for Galvanized Duct/Galvanized Splice.....	63
Table 5.3: Numerical Rating System for Prestressing Strand.....	64
Table 5.4: Beam 1.1-Corrosion Rating Summary.....	66
Table 5.5: Beam 1.2 Corrosion Rating Summary.....	70
Table 5.6: Beam 1.4 Corrosion Rating Summary.....	74
Table 5.7: Beam 2.1 Corrosion Rating Summary.....	77
Table 5.8: Beam 2.2 Corrosion Rating Summary.....	83
Table 5.9: Beam 2.4 Corrosion Rating Summary.....	89
Table 5.10: Beam 3.1 Corrosion Rating Summary.....	95
Table 5.11: Beam 3.4 Corrosion Rating Summary.....	101
Table 5.12: Beam 3.5 Corrosion Rating Summary.....	109
Table 5.13: Beam 4.1 Corrosion Rating Summary.....	116
Table 5.14: Beam 2.7 Corrosion Rating Summary.....	122
Table 5.15: Beam 2.7-Corrosion Rating Summary for Anchorages.....	139
Table 5.16: Beam 2.8 Corrosion Rating Summary.....	140
Table 5.17: Beam 2.9 Corrosion Rating Summary.....	146
Table 5.18: Beam 2.9-Corrosion Rating Summary for Anchorages.....	159
Table 5.19: Beam 2.10 Corrosion Rating Summary.....	160
Table 5.20: Beam 2.12 Corrosion Rating Summary.....	166
Table 5.21: Beam 2.12-Corrosion Rating Summary for Anchorages.....	181
Table A.1: Corrosion Ratings for Phase I and Phase II Beams (Center of Beams).....	220
Table A.2: Corrosion Ratings for Anchorages of Anchorage Exposure Beams.....	220

List of Figures

Figure 1.1: Typical Post-Tensioning Hardware.....	2
Figure 1.2: Corroded Anchorage (Bearing Plate with Strand Tails)	5
Figure 2.1: Test Specimen Elevation.....	9
Figure 2.2: Test Specimen Outside the Ferguson Structural Engineering Laboratory	9
Figure 2.3: Specimen Reinforcement Configurations	12
Figure 2.4: Duct Splice Types	14
Figure 2.5: Splice Configurations.....	15
Figure 2.6: VSL VSLAB+™ System (End Anchorage).....	18
Figure 2.7: Specimen Construction.....	19
Figure 2.8: Post-Tensioning Equipment Setup	20
Figure 2.9: Grouting Procedure	21
Figure 2.10: Anchorage Pocket Before Capping	22
Figure 2.11: Specimen Loading.....	23
Figure 3.1: Phase II Beams Under Exposure Testing.....	27
Figure 3.2: Anchorage Exposure System.....	28
Figure 3.3: Crack Width Measurement System.....	30
Figure 3.4: Half-Cell Potential Sampling Stations	31
Figure 3.5: Chloride Sample Locations for Typical Test Specimen.....	32
Figure 3.6: Chloride Sample Locations for Specimens 1.1 and 3.1	33
Figure 3.7: Chloride Sample Location for Anchorage Exposure Specimens	33
Figure 3.8: Block Specimens	34
Figure 4.1: Half-Cell Potential Contours at 3107 Days for Phase I Beams.....	37
Figure 4.2: Estimated Time of Initiation of Corrosion: Phase I Beams.....	38
Figure 4.3: Half-Cell Potential Readings at 2894 Days for Phase II Beams	39
Figure 4.4: Estimated Time of Initiation of Corrosion: Phase II Beams	40
Figure 4.5: Maximum Final Half-Cell Potential Readings for Phase I Beams.....	41
Figure 4.6: Maximum Final Half-Cell Potential Readings for Phase II Beams	42
Figure 4.7: Beam and Block Chloride Penetration for Phase I Beams	44
Figure 4.8: Beam Chloride Penetration for 27” and 32” Offsets (Beams 1.1 and 3.1).....	45
Figure 4.9: Beam and Block Chloride Penetration for Phase II Beams.....	47
Figure 4.10: Chloride Penetration for Anchorages of Phase II Beams Subjected to End Anchorage Exposure	48
Figure 4.11: Chloride Penetration at Reinforcing Bar Depth-Phase I Beams	49
Figure 4.12: Chloride Penetration at Bar Depth-Phase II Beams	50
Figure 5.1: Beam Unloading.....	51
Figure 5.2: Phase II Beams After Unloading.....	52
Figure 5.3: Reaction Beams Placed In Storage at FSEL	53
Figure 5.4: Beam Cutting Pattern	53
Figure 5.5: Cutting Pattern for Beams 1.1 and 3.1	54
Figure 5.6: Cutting of Beams (Phase I Beams Pictured)	55

Figure 5.7: Typical Center Block Removed from Beams (Phase II Beam 2.7 Shown) ...	55
Figure 5.8: Typical End Anchorage Block Removed from Phase II beams 2.7, 2.9, and 2.12.....	56
Figure 5.9: Breaking up of Block	56
Figure 5.10: Post-Tensioning Ducts Before Removal From Center Block	57
Figure 5.11: Mild Steel Reinforcing Cage After Removal From Beam	57
Figure 5.12: Removal of Post-Tensioning Anchorages.....	58
Figure 5.13: Mild Reinforcing Steel Rating Intervals	59
Figure 5.14: Galvanized Duct Rating System.....	62
Figure 5.15: Beam 1.1-Side View (Left) and Top View (Right).....	66
Figure 5.16: Beam 1.1 Crack Widths.....	67
Figure 5.17: Beam 1.1 Autopsy Elements	68
Figure 5.18: Beam 1.1-Crack Patterns and Corrosion Rating Graphs.....	69
Figure 5.19: Beam 1.2-Side View (Left) and Top View (Right).....	70
Figure 5.20: West End of Autopsy Block-Beam 1.2	71
Figure 5.21: Beam 1.2 Crack Widths.....	71
Figure 5.22: Beam 1.2 Autopsy Elements	72
Figure 5.23: Beam 1.2-Crack Patterns and Corrosion Rating Graphs.....	73
Figure 5.24: Beam 1.4-Top View (Left) and Side View (Right).....	74
Figure 5.25: Beam 1.4 Crack Widths.....	75
Figure 5.26: Beam 1.4 Autopsy Elements-Longitudinal Bar (Left) and Stirrup (Right)..	75
Figure 5.27: Beam 1.4-Crack Patterns and Corrosion Rating Graphs.....	76
Figure 5.28: Beam 2.1-Side View (Left) and Top View (Right).....	77
Figure 5.29: Beam 2.1 Crack Widths.....	78
Figure 5.30: Beam 2.1 Duct Splices	79
Figure 5.31: Beam 2.1 Autopsy Elements	81
Figure 5.32: Beam 2.1-Crack Patterns and Corrosion Rating Graphs.....	82
Figure 5.33: Beam 2.2-Side View (Left) and Top View (Right).....	83
Figure 5.34: Beam 2.2 Crack Widths.....	84
Figure 5.35: Beam 2.2 South Duct Splice	85
Figure 5.36: Beam 2.2 Autopsy Elements	87
Figure 5.37: Beam 2.2-Crack Patterns and Corrosion Rating Graphs.....	88
Figure 5.38: Beam 2.4-Side View (Left) and Top View (Right).....	89
Figure 5.39: Beam 2.4 Crack Widths.....	90
Figure 5.40: Beam 2.4 Duct Splices	91
Figure 5.41: Beam 2.4 Autopsy Elements	93
Figure 5.42: Beam 2.4- Crack Patterns and Corrosion Rating Graphs.....	94
Figure 5.43: Beam 3.1-Side View (Left) and Top View (Right).....	95
Figure 5.44: Beam 3.1 Duct Splices	96
Figure 5.45: Beam 3.1 Autopsy Elements	99
Figure 5.46: Beam 3.1-Crack Maps and Corrosion Rating Graphs.....	100
Figure 5.47: Beam 3.4-Side View (Left) and Top View (Right).....	101
Figure 5.48: Beam 3.4 Crack Widths.....	102
Figure 5.49: Beam 3.4 Duct Splices	104
Figure 5.50: Beam 3.4-Crack Patterns and Corrosion Rating Graphs.....	107
Figure 5.51: Beam 3.4 Autopsy Elements	108

Figure 5.52: Beam 3.5-Side View (Left) and Top View (Right).....	109
Figure 5.53: Beam 3.5 Crack Widths.....	110
Figure 5.54: Beam 3.5 Duct Splices	111
Figure 5.55: Beam 3.5 Autopsy Elements	114
Figure 5.56: Beam 3.5-Crack Patterns and Corrosion Rating Graphs.....	115
Figure 5.57: Beam 4.1-Side View (Left) and Top View (Right).....	116
Figure 5.58: Beam 4.1 Crack Widths.....	117
Figure 5.59: Beam 4.1 South Duct Industry Standard Splice.....	118
Figure 5.60: Beam 4.1 Autopsy Elements	120
Figure 5.61: Beam 4.1-Crack Patterns and Corrosion Rating Graphs.....	121
Figure 5.62: Beam 2.7-Side View (Left) and Top View (Right).....	122
Figure 5.63: Beam 2.7 Crack Widths.....	123
Figure 5.64: Beam 2.7 Industry Standard Duct Splices.....	124
Figure 5.65: Beam 2.7-Evidence of Abrasion of Epoxy Coating from Strand on Bottom of South Duct	125
Figure 5.66: Beam 2.7-South Duct Strand With Coating (Left) and After Removal of Coating (Right)	126
Figure 5.67: Beam 2.7-Example of Strand Coating Damage to North Duct Strand.....	127
Figure 5.68: Beam 2.7- North Duct Strand Damage Ratings	128
Figure 5.69: Beam 2.7 Autopsy Elements (From Center Portion of Beam).....	129
Figure 5.70: Beam 2.7-Crack Maps and Corrosion Rating Graphs	130
Figure 5.71: Beam 2.7 Anchorage Zones	131
Figure 5.72: Beam 2.7 West End Anchorages After Removal (Controls).....	132
Figure 5.73: Beam 2.7-West End Anchorage Zone (Control) Autopsy Elements.....	134
Figure 5.74: Beam 2.7 East End Anchorages (Dripped End).....	135
Figure 5.75: Beam 2.7-East End Anchorage Zone (Dripped End) Autopsy Elements...	137
Figure 5.76: Beam 2.7-Corrosion Rating Graphs for Anchorages	138
Figure 5.77: Beam 2.8-Side View (Left) and Top View (Right).....	140
Figure 5.78: Beam 2.8 Crack Widths.....	141
Figure 5.79: Beam 2.8 Duct Splices).....	142
Figure 5.80: Autopsied Galvanized Strand (Bottom) vs. New Galvanized Strand (Top)	143
Figure 5.81: Beam 2.8 Autopsy Elements	144
Figure 5.82: Beam 2.8-Crack Patterns and Corrosion Rating Graphs.....	145
Figure 5.83: Beam 2.9-Side View (Left) and Top View (Right).....	146
Figure 5.84: Beam 2.9 Crack Width Data.....	147
Figure 5.85: Beam 2.9 Industry Standard Splices.....	148
Figure 5.86: Beam 2.9 Autopsy Elements (From Center of Beam).....	150
Figure 5.87: Beam 2.9-Crack Patterns and Corrosion Rating Graphs.....	151
Figure 5.88: Beam 2.9 Anchorage Zones	152
Figure 5.89: Beam 2.9: Bottom Corner of East End Anchorage Zone.....	152
Figure 5.90: Beam 2.9 West End Anchorages (Controls)	153
Figure 5.91: Beam 2.9-West End Anchorage Zone (Control) Autopsy Elements.....	155
Figure 5.92: Beam 2.9 East End Anchorages (Dripped End).....	156
Figure 5.93: Beam 2.9-East End Anchorage Zone (Dripped End) Autopsy Elements...	158
Figure 5.94: Beam 2.9-Corrosion Rating Graphs for Anchorage Zones	159

Figure 5.95: Beam 2.10-Side View (Left) and Top View (Right).....	160
Figure 5.96: Beam 2.10 Crack Widths.....	161
Figure 5.97: Beam 2.10 Industry Standard Duct Splices.....	162
Figure 5.98: Beam 2.10 Autopsy Elements	164
Figure 5.99: Beam 2.10-Crack Patterns and Corrosion Rating Graphs.....	165
Figure 5.100: Beam 2.12-Side View (Left) and Top View (Right).....	166
Figure 5.101: Beam 2.12 Crack Widths.....	167
Figure 5.102: Beam 2.12 During Autopsy.....	168
Figure 5.103: Beam 2.12-Abrasion Damage to Interior of North Duct (Left) and Strand From Same Location (Right)	169
Figure 5.104: Beam 2.12 Autopsy Elements (Center Portion of Beam)	171
Figure 5.105: Beam 2.12-Crack Patterns and Corrosion Rating Graphs (Center Portion of Beam).....	172
Figure 5.106: Beam 2.12 Anchorage Zones: East End Anchorage With Dripper (Left) and West End Anchorage Without Dripper (Right)	173
Figure 5.107: Beam 2.12-Cracking in East End Anchorage Zone	173
Figure 5.108: Beam 2.12 West End Anchorages (Control End).....	174
Figure 5.109: Beam 2.12 West End Anchorage (Control End) Autopsy Elements.....	176
Figure 5.110: Beam 2.12-Corroded Stirrup in East End Anchorage Zone (Dripped End)	177
Figure 5.111: Beam 2.12 East End Anchorages (Dripped End).....	178
Figure 5.112: Beam 2.12 East End Anchorage Zone (Dripped End) Autopsy Elements	180
Figure 5.113: Beam 2.12-Strand Corrosion Ratings for Anchorages.....	181
Figure 6.1: Phase I Beams- Crack Ratings	184
Figure 6.2: Phase I Beams- Stirrup and Longitudinal Bar Generalized Ratings vs. Crack Ratings	185
Figure 6.3: Phase I Beams-Generalized Duct Ratings (Organized by Splice Type)	186
Figure 6.4: Phase I Beams-Strand Generalized Ratings	187
Figure 6.5: Phase I Beams-Maximum Grout Chloride Content in Each Duct.....	188
Figure 6.6: Phase II Beams-Crack Ratings.....	189
Figure 6.7: Phase II Beams-Bar and Stirrup Ratings.....	190
Figure 6.8: Phase II Beams-Duct Generalized Ratings	191
Figure 6.9: Phase II Beams-Strand Generalized Ratings.....	191
Figure 6.10: Phase II Beams-Maximum Grout Chloride Content in Each Duct	192
Figure 6.11: Phase I Beams-Stirrup and Bar Generalized Ratings vs. Final Half-Cell Potential Readings	195
Figure 6.12: Phase I Beams- Galvanized Duct Ratings vs. Final Half-Cell Potential Readings.....	196
Figure 6.13: Phase II Beam Stirrup and Bar Generalized Ratings vs. Final Half-Cell Potential Readings	197
Figure 6.14: Phase II Beams-Duct Ratings vs. Final Half-Cell Potential Readings.....	197
Figure 6.15: Phase I Beams-Stirrup and Bar Generalized Ratings vs. Time to Initiation of Corrosion.....	198
Figure 6.16: Phase I Beams-Duct Generalized Ratings vs. Time to Initiation of Corrosion	199

Figure 6.17: Phase II Beams-Stirrup and Bar Generalized Ratings vs. Time to Initiation of Corrosion	200
Figure 6.18: Phase I Beams-Maximum Chloride Content at Bar/Duct Level vs. Bar and Stirrup Generalized Ratings	201
Figure 6.19: Phase I Beams-Maximum Chloride Content at Bar/Duct Level vs. Generalized Duct Ratings	201
Figure 6.20: Phase II Beams-Maximum Chloride Content at Bar/Duct Level vs. Bar and Stirrup Ratings	202
Figure 6.21: Phase II Beams-Maximum Chloride Content at Bar/Duct Level vs. Duct Generalized Ratings	203
Figure 6.22: Phase I Beams-8 Year Crack Ratings vs. 4 Year Crack Ratings ³	204
Figure 6.23: Phase I Beams-4 Year Duct Ratings vs. 8 Year Duct Ratings ³	205
Figure 6.24: Phase I Beams-4 Year Strand Ratings vs. 8 Year Strand Ratings ³	205
Figure 6.25: Phase I and Phase II Beams-Generalized Bar and Stirrup Ratings	207
Figure 6.26: Phase I and Phase II Beams-Generalized Duct Ratings	208
Figure 6.27: Phase I and Phase II Beams-Generalized Strand Ratings	209
Figure B.1: Phase I Beams-Maximum Half-Cell Potentials for Each Day of Sampling	221
Figure B.2: Phase II Beams-Maximum Half-Cell Potentials for Each Day of Sampling	222

Chapter 1: Introduction

1.1 BACKGROUND

Post-tensioned concrete has been used for bridge construction since the second half of the 20th century. Post-tensioned concrete, a form of prestressed concrete, allows for concrete members to be precompressed so that any applied service loads must overcome this pre-compression before cracking of the concrete. Post-tensioning allows for the attainment of longer span lengths with the use of smaller members, and for better crack control than typical reinforced concrete. In addition, it allows for reduced congestion of reinforcement as well as better continuity of reinforcement. Bonded post-tensioning systems involve the use of tubes (known as ducts) cast within the concrete: Typically, these ducts have curvature along the length of the structure. Following the attainment of the specified concrete strength, the post-tensioning force is applied through seven-wire strands placed inside the duct. The strands are then anchored by tapered wedges within an anchorhead (a typical post-tensioning hardware configuration is shown in Figure 1.1). Following this, grout is pumped into the duct forming a multilayer system of protection for the strand and, with internal tendons, bonding the strands to the structure. However, in recent years durability issues have arisen with the use of such systems. These include but are not limited to the use of mixed reinforcement and the soundness of anchorage zones.

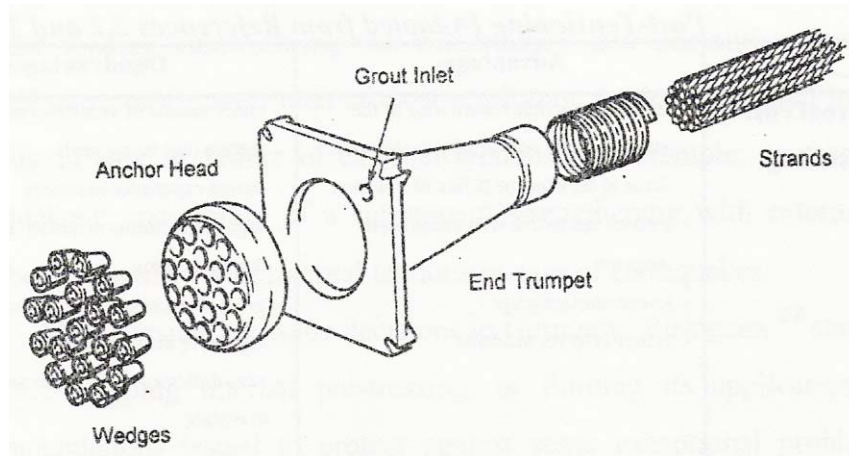


Figure 1.1: Typical Post-Tensioning Hardware³

1.2 CORROSION OF STEEL IN CONCRETE

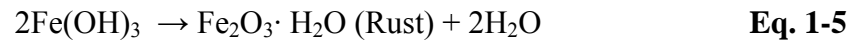
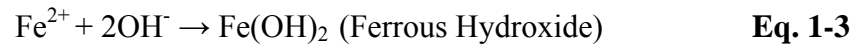
It has been estimated that corrosion of reinforced concrete structures is one of the most expensive corrosion problems in the United States, with an annual cost of \$8.3 billion.¹⁰ Due to its chemical nature, concrete is highly basic, or alkaline. In cured concrete, uncoated steel forms a protective layer known as a “passive” layer which basically consists of iron hydroxide.¹⁰ Thus, any corrosion in the steel is prevented. However, if the concrete is in a marine environment or in the presence of de-icing salts chlorides can find their way into the concrete either through high permeability (after a long period) or at a crack in the concrete. Once a threshold chloride concentration is reached (a typical value is 0.033% by weight of concrete³) the passive layer begins to break down and corrosion initiates.¹⁰ The location at which the passive layer breaks down is called the anode, and the reaction which takes place there is the anodic reaction, given by Equation 1-1.



Another location on the steel surface becomes the cathode, since the two electrons in the previous equations must be consumed in order to maintain the charge balance. This cathodic reaction is given by Equation 1-2.



These are the first steps in the corrosion process. The remainder of the process is given by the following three equations:



These iron oxides occupy up to ten times as much volume as the steel. Thus, extremely large expansive stresses are placed on the concrete. Since concrete is weak in tension, cracking and spalling result.¹⁰ In addition, when the iron in the steel begins to dissolve into solution, pits can form in the steel. Thus, the cross-sectional area of the bar or the strand is reduced. This is especially alarming in bonded post-tensioned concrete since the strand is under very high tensile stress. Thus, if the cross-sectional area of the strand wires is reduced, the stress in the strand can more easily reach the level of failure.

1.3 DURABILITY IN POST-TENSIONING

Typically in bridge construction, galvanized steel has been almost universally used for the ducts to provide protection for the strand. However, the duct is vulnerable for two reasons. The first is that galvanization is a type of sacrificial protection. In other words, the zinc coating will corrode instead of the steel. However, after all the zinc coating has reacted, the corrosion will begin to attack the steel in the duct directly, compromising its ability to protect the grout inside. The second reason for steel ducts behaving poorly is poor splice details that do not prevent chloride and moisture penetration into the duct. Typically, the splice method used in practice with galvanized steel ducts is an overlaid section of steel duct sealed at the ends with duct tape.

If the duct or the splice fails to provide the proper protection, the chlorides can reach the grout within the duct. While the grout should provide some additional protection for the strand, it can be unable to do so for several reasons, including voids and cracks in the grout. One of the ways in which voids form in grout is from bleed water accumulation in certain areas which causes voids to form once the water has evaporated. In addition, if proper venting is not used during grouting, air pockets can form at high points in the ducts also resulting in the formation of voids. Grout, unlike the surrounding

concrete, is not prestressed and will thus readily crack under service loads. Thus, if the duct is penetrated then the chlorides can attack the strands either through the grout voids or cracks and reduce their capacity due to cross-sectional area loss which has a detrimental effect on the structure as a whole.

Possible ways to reduce the possibility of corrosion in the strand are to use galvanized strand or epoxy coated strand, and several new coatings have also appeared on the market in recent years. However, like the galvanization in the ducts, the galvanization in the strand is a form of sacrificial protection which will no longer function once all the zinc has corroded. Severe damage to post-tensioning systems due to corrosion has been documented in Florida, where strands have actually failed due to corrosion.⁸ Reasons for these failures included poor grouting procedures and leakage in anchorage systems. Grouting deficiencies have also been found in the Boston Central Artery Bridges.⁸

In 2001 the American Segmental Bridge Institute established guidelines for grouting, and the Post-Tensioning Institute established new grouting specifications in February 2001.⁹ In recent years, the Texas Department of Transportation has actually banned the use of corrugated galvanized metal ducts and requires robust corrugated plastic ducts.¹¹

1.4 EFFECT OF MIXED REINFORCEMENT

One system allowed by AASHTO¹⁴ and used in practice is the use of mixed reinforcement in members. This means the use of both prestressed and non-prestressed reinforcement to share the tensile force when resisting loads. This is also referred to as “partial prestressing”. Advantages of mixed reinforcement include increased ductility compared to fully prestressed sections, and better creep and camber control.¹ However, there is a loss of crack control compared to fully prestressed members.

1.5 DURABILITY OF POST-TENSIONING ANCHORAGES

One major area of concern in post-tensioning systems is the anchorage. During stressing of the strands, the post-tensioning force is held by hydraulic rams. Upon completion of stressing, tapered wedges are driven into the holes into the anchorhead

typically using a power-seating system on the jack. Upon release of the force in the jack, the strand attempts to “jump” back into the duct but the metal teeth in the wedges “bite” into the strand and bear against the tapered holes in the anchorhead, maintaining the post-tensioning force. A detrimental effect from the wedges is a reduction in the cross sectional area of the strand wires, resulting in higher stresses than would be found along the length of the strand. Typically, post-tensioning anchorage areas are sealed with grout after stressing. However, if the chlorides penetrate the grout, either through cracks or because of high grout permeability, they can enter the rest of the post-tensioning system through the interstitial areas of the strand at the anchors. In addition, once the strands in the anchorage begin to corrode, the strand stress levels increase because of their smaller effective cross sectional area. Thus the strand can fail at the anchorage. Failures of this type have been observed in Florida.⁹ A corroded anchorage is shown in Figure 1.2.



Figure 1.2: Corroded Anchorage (Bearing Plate with Strand Tails)⁷

1.6 THESIS

1.6.1 Research Background

Research into post-tensioned durability issues has been an on-going effort at the University of Texas, jointly funded by both FHWA and TxDOT. The research has been performed at the Ferguson Structural Engineering Laboratory under contract with the

Center for Transportation Research. The research effort began in 1997 under project 1405, and has continued under project 4562, under the general supervision of Dr. John Breen. West¹ and Schokker² constructed beam specimens for long-term exposure testing under highly aggressive conditions, and final autopsy and analysis of approximately half of these specimens was completed by Kotys³ and Salas⁴ in 2003. Salas and Kotys conducted these autopsies after approximately four years of aggressive exposure testing, examining issues such as splice type, the effects of mixed reinforcement, grout type, as well as the effects of different loadings on durability. Sustained loading and aggressive exposure testing continued on the remaining 15 beam specimens for another 4 years until the autopsies reported in this thesis.

1.6.2 Thesis Objectives

The objectives of this thesis are:

- To evaluate the extent of corrosion found in all types of reinforcement in non-prestressed, fully prestressed and partially prestressed (mixed reinforcement) beam specimens after approximately 8 years of aggressive exposure testing, including drip exposure in the anchorage zone.
- To evaluate the effect of mixed reinforcement on corrosion protection with a comparison of fully prestressed, mixed reinforcement, and non-prestressed specimens.
- To evaluate the relationship between corrosion protection performance and the following variables in post-tensioned girder specimens:
 - Level of loading, including unloaded specimens
 - Level of prestress and initial crack width
 - Duct type
 - Strand type
 - Grout type
 - Grouting method
 - Use of encapsulated systems for anchorage protection
 - Galvanized duct splice type

- To evaluate the accuracy of non-destructive measurements taken during exposure testing.
- To use results obtained from long-term beam exposure testing and autopsy to develop durability design guidelines for bridge substructures.

1.6.3 Scope

The scope of this thesis includes:

- Examination of data taken during accelerated exposure testing of the remaining 15 large-scale beam specimens.
- Autopsy and analysis of the remaining 15 large-scale beam specimens under accelerated exposure testing.
- Recommendations for post-tensioned concrete durability design based on the autopsy observations.

Chapter 2: Test Specimens

2.1 SPECIMEN TEST CONCEPT

The specimen test concept and program was developed and implemented by West¹ and Schokker² in 1997 with the purpose of determining which combinations of materials, construction and design practices result in the best corrosion resistance in a bonded post-tensioned system. The specimen design developed was a beam element which would undergo rigorous exposure testing outside the Ferguson Structural Engineering Laboratory. The exposure testing included alternating wet/dry cycles with a 3.5 % NaCl solution. The test program was implemented in two phases: Phase I was implemented by West¹ and consisted of 16 beam specimens. Six of these specimens were autopsied in 2003 by Kotys⁴ and Salas³. In addition, two specimens were partially autopsied and then continued testing. Ten Phase I beams, including the two partial autopsies, remained to be autopsied in this study. Phase II was implemented by Schokker² and consisted of 11 beam specimens. Six Phase II specimens were autopsied by Kotys and Salas in 2003. Five remained to be autopsied in this study. Except for the experimental variables, the specimens of Phases I and II are basically identical in construction.

2.2 SPECIMEN DESCRIPTION

The full details of the specimen design process are outlined in References 1 and 2. An elevation of a typical test specimen is shown in Figure 2.1, and one of the actual test specimens is shown in Figure 2.2.

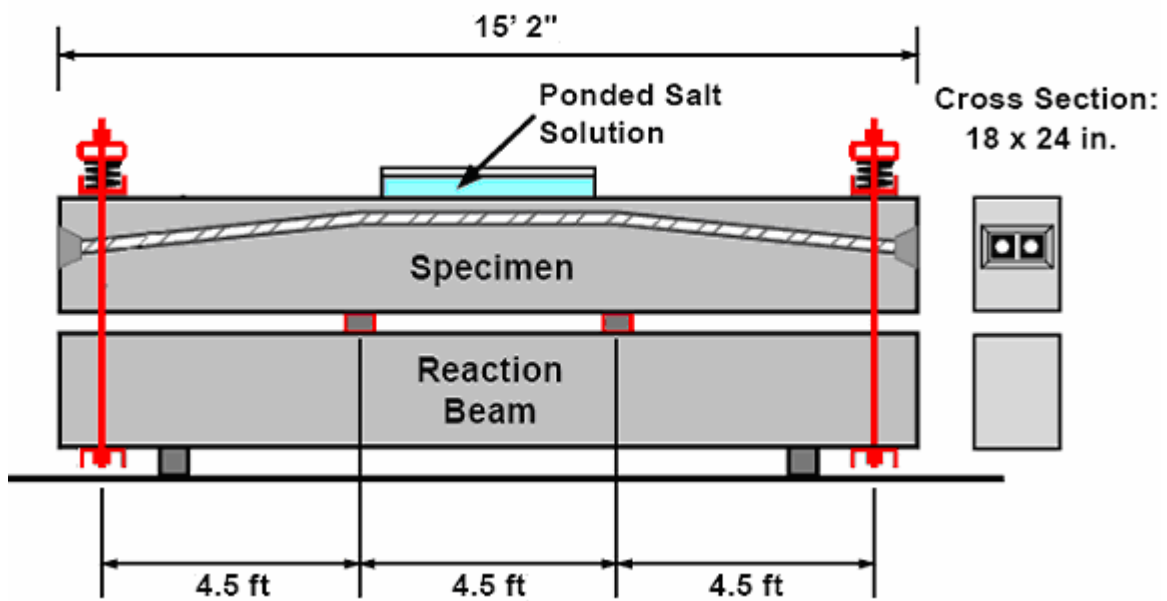


Figure 2.1: Test Specimen Elevation¹



Figure 2.2: Test Specimen Outside the Ferguson Structural Engineering Laboratory⁵

The specimens are 15'-2" long with a cross section of 18"x 24". These dimensions were chosen in order for the specimen to accommodate the materials to be tested and still be constructible in the laboratory setting. In order to study the effect of different levels of prestressing, four different specimen reinforcement arrangements were considered, each with varying levels of prestress and non-prestressed reinforcement (See Section 2.3.2.1). All the beam specimens are kept under sustained load at third points during exposure testing. Thus an essentially constant moment region exists in the center span of the beam. Details of beam loading are given in Section 2.6. Proper shear reinforcement was supplied, as well as confining spiral reinforcement in the anchorage zone. A non-prestressed reinforced concrete beam is placed beneath the specimen in order to provide the necessary reactions. The reaction beam is the same length as the test specimen and has the same cross-sectional dimensions. The details of the design of these reaction beams is found in Reference 1.

2.3 SPECIMEN VARIABLES

The test program includes several variables, as well as control specimens representing industry standards in the mid 1990's. The variables of Phase I include the level of prestress, level of loading, crack width, and duct splice type and condition.¹ The variables of Phase II consist of strand type and condition, the use of high performance, anti-bleed grout, grouting procedure, and the use of an encapsulated system for end anchorage protection².

2.3.1 Control Specimens

Controls are used which represented Texas Department of Transportation standard practices in 1997-the time of the implementation of the original test program. The control variables are as follows:¹

- **Concrete:** TxDOT Class C for bridge substructures was used, which requires a maximum water-cement ratio of 0.533 with Type I cement. The slump was specified at 4" with a maximum coarse aggregate size of ¾". Additives include

Rheocrete 300-R retarder and air entraining admixtures. Concrete clear cover was specified at 2”.

- **Cement Grout:** A water cement ratio of 0.44 was used with Type I cement. Inraplast-N expanding admixture was specified.
- **Duct:** Rigid galvanized steel duct was used.
- **Anchorage Protection:** Type V epoxy bonding agent coated all hardware in the anchorage, and the anchorage pocket was filled with non-shrink grout patch (Euclid non-shrink grout).

2.3.2 Phase I Variables

The variables for Phase I include level of prestressing, level of applied loading, crack width, as well as splice type and condition.

2.3.2.1 Level of Prestress

The effect of the level of prestress was one of the most critical variables of study in the test program. Overall, with higher levels of prestressing, the number and widths of cracks is typically reduced. In order to study the effect on durability four different reinforcement arrangements were tested. The four reinforcement configurations are as follows:

- Non-Prestressed (Non-PS)
- 2/3 or Partially Prestressed (2/3 PS)
- Fully Prestressed Designed by Ultimate Strength Method (100% U)
- Fully Prestressed Designed by Allowable Stress Design (100% S)

At the inception of the test program, strong consideration was being given to the use of mixed reinforcement (so called partial prestressing). There were apparent benefits in camber control and economy. However, the effect of partial prestressing on durability was uncertain at the time. The design calculations for each reinforcement configuration are found in Reference 1. The various reinforcement arrangements are shown in Figure 2.3.

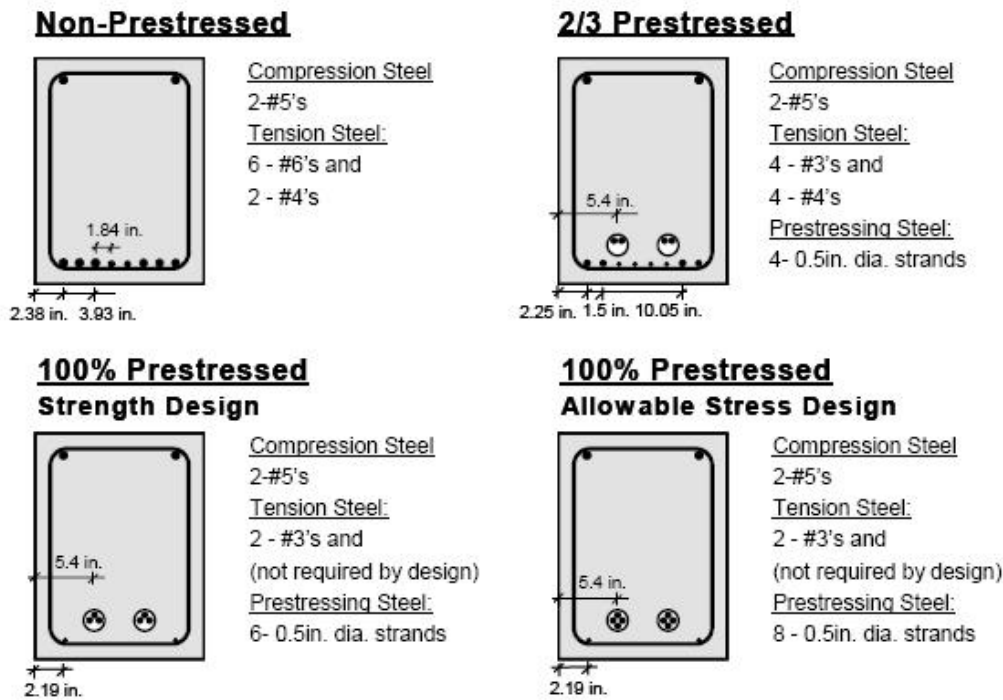


Figure 2.3: Specimen Reinforcement Configurations¹

The longitudinal bars in the 100% prestressed sections were installed in order to allow for reinforcing cage handling during construction. These bars were included when considering the section capacity. All sections were designed with the same maximum permissible service load moment of 2750 kip-in..

2.3.2.2 Level of Applied Loading and Crack Width

The effect of applied loading and crack width are directly related. Clearly if the level of prestress is held constant, crack width should increase with increased loading. Various levels of loading are applied for each reinforcement configuration:

Non-PS Loading Cases

- For the non-prestressed specimens, 3 different levels of loading were tested:
- Unloaded (No applied load)
 - Service Load
 - 25% Overload

The application of the overloading force was done at the beginning of exposure testing and then the specific specimen was lowered back down to service load.

2/3-PS Loading Cases

For the partially prestressed specimens, three different loading scenarios are considered.

- Small crack width
- Service Load
- 25% Overload

The overload and service load cases are similar to those for the Non-PS section. For the small crack width case the specimen was loaded until the defined “small” crack width was reached and then the load was held at this level for the duration of exposure testing. West¹ determined that the appropriate “small” crack width for the 2/3-PS section was 0.002 in..

100% U Loading Cases

In the case of the fully prestressed configuration (Ultimate Strength Design), it was originally intended to test the same loading cases as the Non-PS beams. However, for the specimen originally designated for service load (Beam Specimen 3.4), it was necessary to temporarily overload the specimen to produce cracking.¹ Thus the three loading cases are as follows:

- Unloaded (No applied load)
- 25% Overload
- 33% Overload (Specimen originally designated for service load)

100% S Loading Case

For the fully prestressed section (Allowable Stress Design), only the service load case was tested.

2.3.2.3 Duct Splice Type & Condition

The duct splice types tested are the industry standard (IS) splice and the heat shrink (HS) splice. The splices are shown in Figure 2.4.

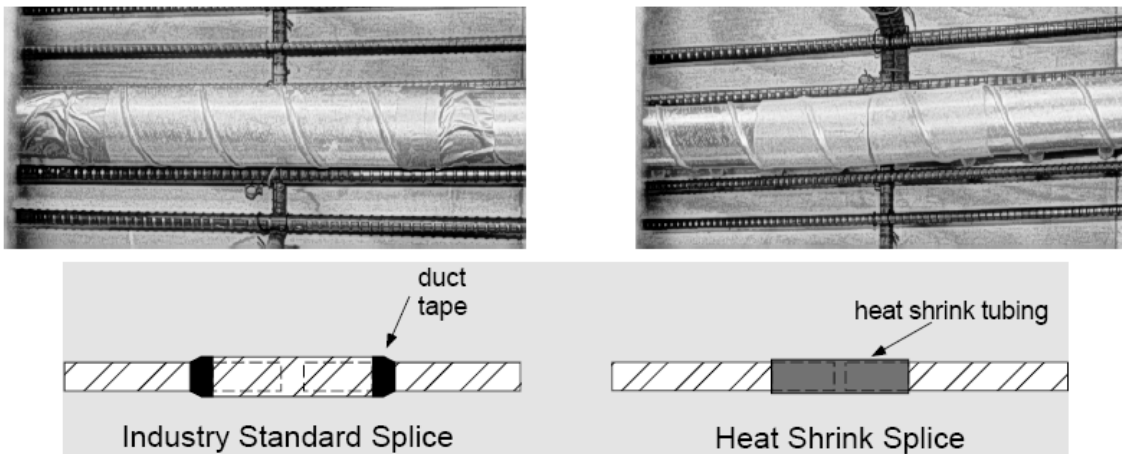


Figure 2.4: Duct Splice Types¹

The IS splice consists of a 12-in. long portion of oversized duct which wraps around the two duct sections being joined and is duct taped on the ends. The HS splice is an 8-in. piece of heat shrink tubing placed over the ends of the ducts being joined and then heated to seal the joint area. Five different splice configurations are used:

- Industry standard splice (IS)
- Heat shrink splice (HS)
- Damaged industry standard splice (ISD)
- Damaged heat shrink splice (HSD)
- No splice (NS)

The damaged cases are meant to study the effect of accidental damage on each splice type. Damage to the IS splice consists of poor or incomplete duct taping at the splice ends, while for the HS splice a 1-in. long cut was made at the point where the two ducts meet.¹ For comparison, ducts with no splices are also included to compare to the IS splice. The arrangements for the five duct splice configurations are shown in Figure 2.5.

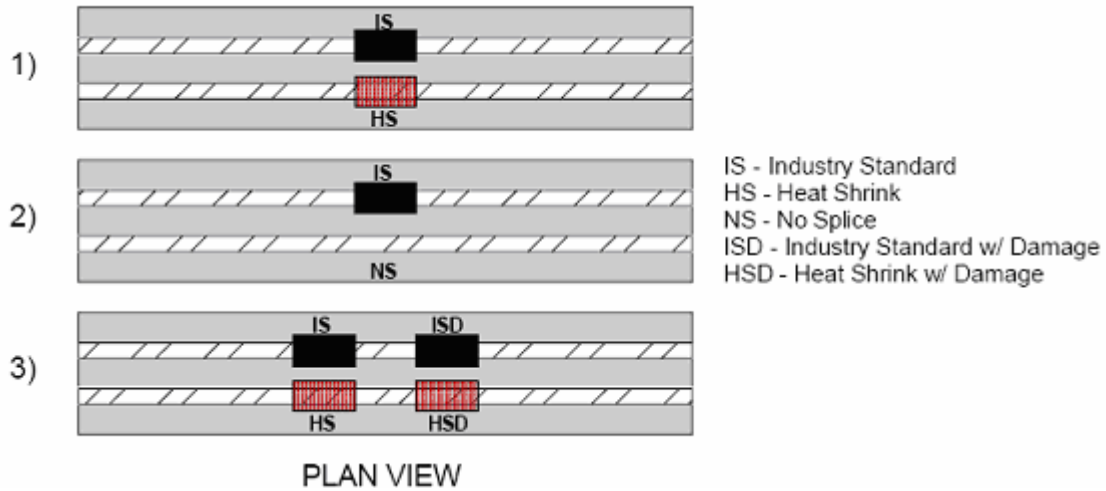


Figure 2.5: Splice Configurations¹

The use of two splices per duct in the damaged condition is so that a baseline of an undamaged splice can be compared to the damaged splice in each duct.

2.3.3 Phase II Variables

The variables for Phase II include duct type, strand type and condition, grout type, grouting procedure, and system protection. All of the beams from Phase II that were considered in this investigation were 2/3-PS beams kept at service load.

2.3.3.1 Duct Type

Two different duct types were tested. The first duct type is the galvanized metal duct, while the second is a plastic duct. The plastic ducts are unspliced and are those associated with the VSL VSLAB+™ System. Information on this system is given in Section 2.3.3.5.

2.3.3.2 Strand Type & Condition

Three different strand types were tested: galvanized and epoxy-coated, and conventional strand for comparison. All are ½” diameter and Grade 270 prestressing steel.

Hot-Dipped Galvanized Strand

The hot-dipped galvanized strand was donated by Florida Wire and Cable.² As with the galvanized duct, the galvanization is a type of sacrificial protection, so in a severely corrosive environment, the galvanized coating may not provide protection for the entire service life of the structure. However, since the coating is applied before the wires are assembled into the strand the coating covers the entire surface area of the wires, including the interstices.

Non-Flowfilled Epoxy Coated Strand

The epoxy coated strand was also donated by Florida Wire and Cable.² The epoxy-coated strand used in this test program only has coating covering the exposed portion of the wire. Thus the interstices of the strand are not protected, unlike galvanized strand. In order to investigate the effect of damage to the epoxy coating, intentional damage was done to one of the two tendons in the specimen with epoxy coated strand, while the other tendon was left undamaged. The damage consists of small squares of epoxy removed from the two strands in the tendon at five select locations, three of the locations coincided with the centerline crack and the cracks at 12" off the centerline. These crack locations were estimated based on the loadings of the Phase I 2/3-PS beams. The two other damaged locations coincided with the bends in the parabolic duct.² Often epoxy patch repair kits are supplied to repair any epoxy coating damaged during handling and construction. Therefore, the repair kit provided by Florida Wire and Cable was used to repair the damage on one of the two strands in the "damaged" tendon-the other strand was left damaged to determine the effectiveness of the patching system².

2.3.3.3 Grouting Procedure

The effect of improper grouting procedure was investigated in the test program. Poor grouting procedures such as not venting air properly can result in the formation of voids in the grout, which can in turn reduce the corrosion protection abilities of the grout. The proper grouting procedure used in all of the other prestressed specimens was done according to PTI specifications at the time of construction (1997), and is given in Section 2.5.3. The practices used for the poor grouting procedure included delays of up to 10

minutes during grouting, allowing air to enter the pump during grouting, and capping the grout vents at the first sign of grout at the exit vent².

2.3.3.4 Grout Type

High performance, anti-bleed grout was selected for use in the test program to compare to the typical grout specified by TxDOT specifications at the time of construction. The choice of this grout mix was based on fresh property and accelerated corrosion tests done by Schokker.² This anti-bleed grout contains an anti-bleed chemical admixture with superplasticizer, with a low water-cement ratio of 0.33.² During trials this mix exhibited very high resistance to bleed and good corrosion resistance compared to the other grout types tested.² The grout was mixed in buckets with hand-held mixers.

2.3.3.5 Anchorage Protection

To compare to the standard TxDOT anchorage details described in Section 2.3.1, an encapsulated system was used. VSL Inc. manufactures plastic duct systems for use in highly aggressive exposure environments. Unfortunately, the smallest multi-strand unit available at the time of specimen construction was for 12 strands.² However, VSL manufactures a two-strand encapsulated system for slab construction known as VSLAB+™, which has the same general properties of the larger-scale systems²-thus this system was used in the test program and is shown in Figure 2.6.

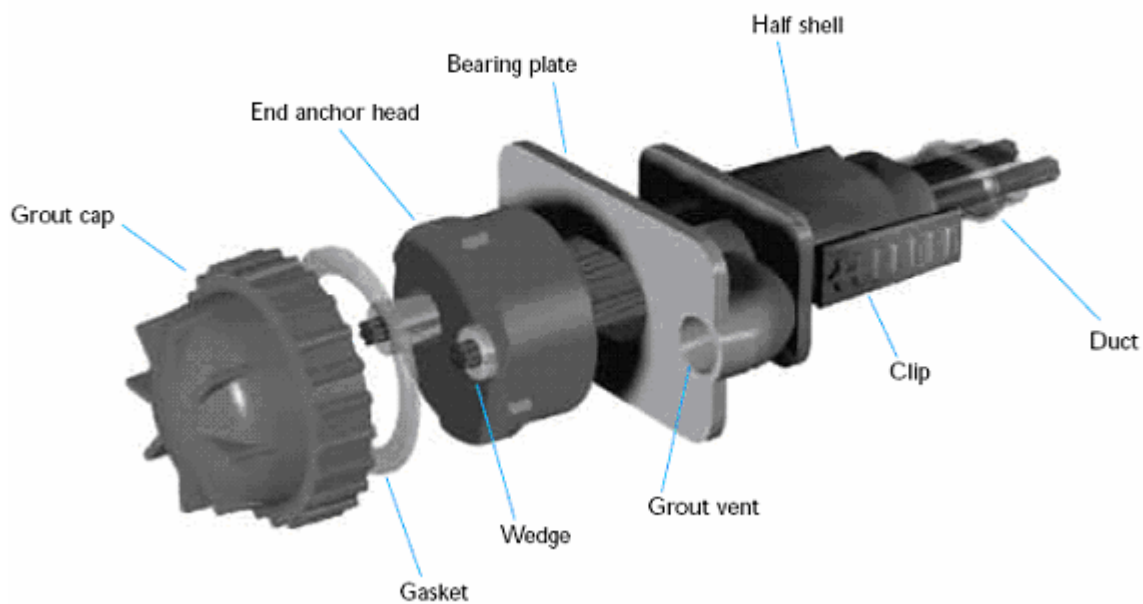


Figure 2.6: VSL VSLAB+™ System¹⁶ (End Anchorage)

A plastic cap is placed over the ends of the strands for protection, and a seal is made with a gasket. The connection between the plastic duct and the bearing plate is made with a half shell/clip connection, instead of the duct tape used in the TxDOT specifications at the time of specimen construction. The system is basically air and watertight.² However, because there is metal to metal contact between the anchorhead and the bearing plate, the system cannot be considered electrically isolated, so the system is not protected from stray currents¹. The use of this system allows for the study of both plastic ducts and anchorage protection¹.

2.4 SPECIMEN MATERIALS

All specimens were cast with TxDOT class C concrete. All reinforcing steel was uncoated Grade 60 reinforcement. For the Phase I beams, steel bolster strips with plastic feet were used to elevate the reinforcing bar cage while in the formwork. For the Phase II beams, plastic chairs were used.² Grout for post-tensioning ducts was batched in a

medium-sized mortar mixer.¹ The non-shrink grout for filling the post-tensioning anchorages was mixed in 5-gallon buckets with hand-held electric paddle mixers.¹

2.5 SPECIMEN CONSTRUCTION DETAILS

The specimens were constructed in the Ferguson Structural Engineering Laboratory. All construction activities were performed by the previous researchers.

2.5.1 Beam Fabrication

Before construction, all flexural reinforcement was cleaned with a wire brush wheel on an angle grinder in order to remove any pre-existing corrosion.¹ The post-tensioning hardware and the confining reinforcement in the anchorage were sandblasted for the same reason.¹ The specimens were cast upside down in wooden formwork at the Ferguson Structural Engineering Laboratory. Concrete was delivered by ready-mix trucks and then placed into the formwork using a bucket lifted by an overhead crane. The concrete was then vibrated by hand-held vibrators. Specimen construction photographs are shown in Figure 2.7.

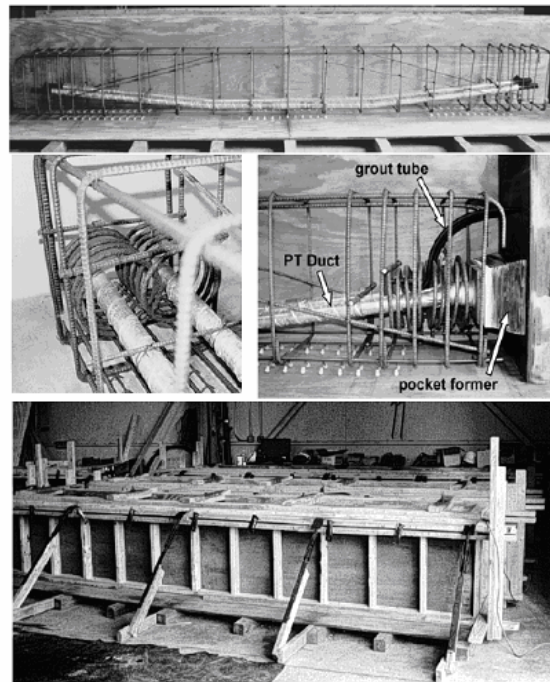


Figure 2.7: Specimen Construction^{3, 4}

2.5.2 Post-Tensioning

The beams were post-tensioned with equipment available at FSEL. The stressing was completed in accordance with TxDOT, PTI, and AASHTO LRFD specifications.¹ Staged stressing was used to compensate for elastic shortening losses.¹ Power seating was used to seat the wedges in order to minimize seating loss.¹ Hydraulic equipment from FSEL was adapted for the stressing because no commercial equipment with power seating was small enough for the number of strands in the tendons.¹ Further details of the post-tensioning process are given in Reference 1. The stressing set-up is shown in Figure 2.8.

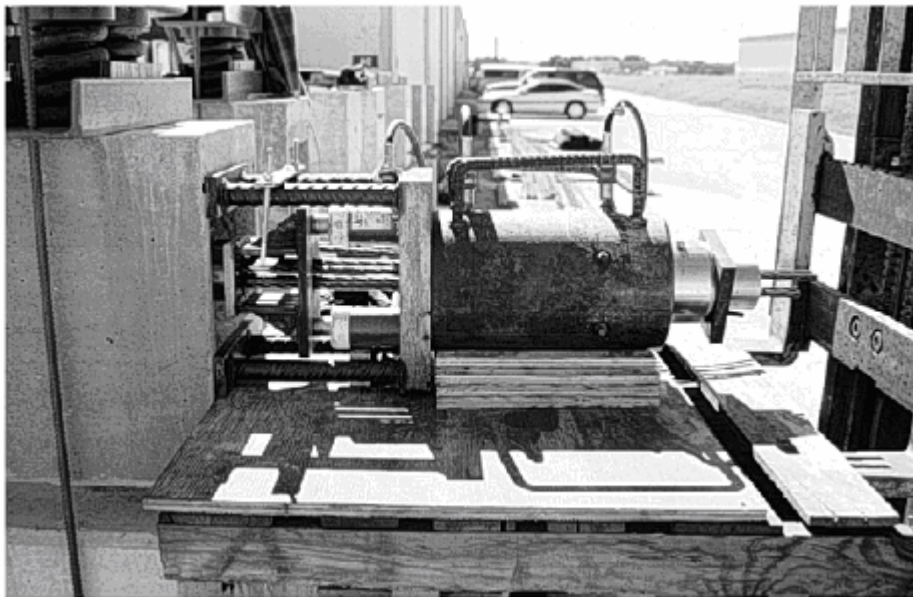


Figure 2.8: Post-Tensioning Equipment Setup¹

2.5.3 Grouting Procedure

Grouting was completed within three days after post-tensioning.¹ The end pockets were sealed with plywood and sealed with silicon after post-tensioning for moisture protection.¹ Grouting was completed in accordance with PTI specifications of the time. The grout was mixed as described in section 2.4 and then immediately pumped into the

ducts using an electric grout pump. The inlet/outlet setup for grouting is shown in Figure 2.9.

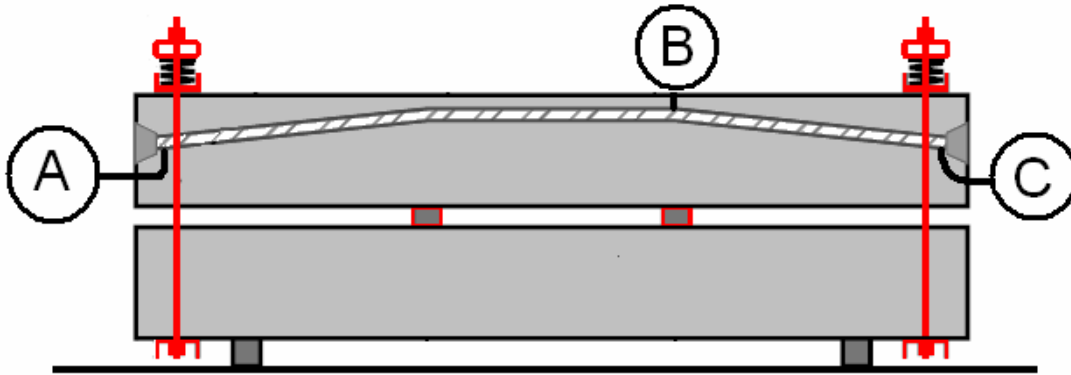


Figure 2.9: Grouting Procedure¹

The inlet at A and the vent at C consisted of $\frac{3}{4}$ -in. grout tubes with cutoff valves. Point B was drilled into the top of the specimen using a rotary hammer drill-this drilling was done before the strand was installed, and then the duct was blown clean.¹ It is interesting to note that PTI specifications of the time did not require Vent B, and under current specifications it would still not be required.¹³ The researchers added vent B based on tube tests performed by Schokker², which showed air accumulation could occur at the peak of the duct. The freshly mixed grout was transferred from the mixer using buckets and was continuously stirred in the reservoir to prevent segregation¹, and was then pumped through the inlet at A. Once continuous flow was observed at vent B, a dowel was inserted at vent B to stop the flow out of the vent. Pumping continued until venting occurred at C, at which time vent C was closed and the pump was stopped. Then the pump was restarted for a period of 2 to 3 seconds before closing the inlet valve at A.¹ Grout bleed water was normally observed exiting from around the wedges immediately after the grouting operation was complete.¹

2.5.4 Anchorage Protection

The anchorage protection provided was that required by TxDOT standards in 1997. The anchorage hardware was cleaned with a wire brush in order to eliminate any pre-

existing corrosion, and the hardware was coated with epoxy. Then the non-shrink grout, prepared as described in Section 2.4, was gravity fed through a funnel into a tube which went through a hole in the piece of the plywood at the end pocket¹. The grout contained silica sand and a non-shrink admixture.¹ Once the grout had cured, the plywood was removed and the entire end of the beam was rubbed with a mixture of cement, sand, and latex bonding agent to provide a uniform finish and fill any voids in the end pocket.¹ A typical anchorage before capping is shown in Figure 2.10.

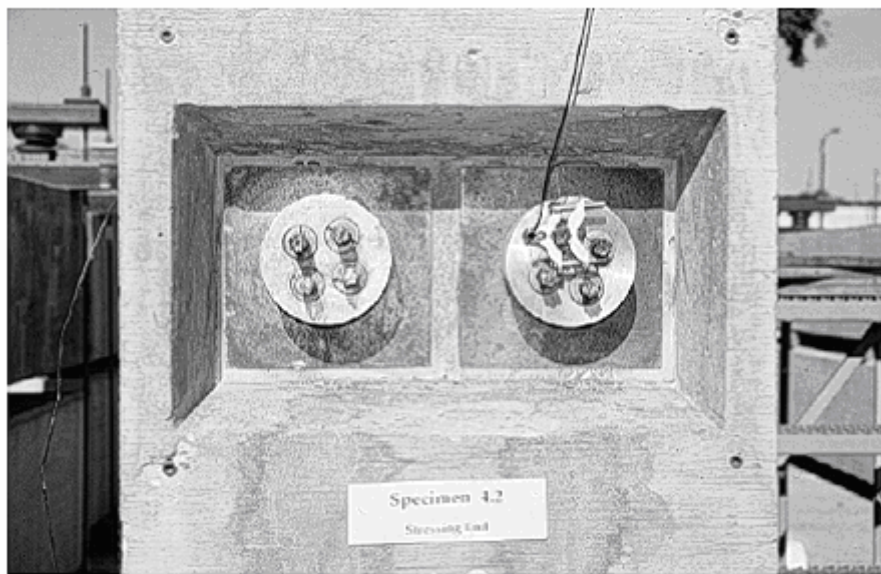


Figure 2.10: Anchorage Pocket Before Capping¹

2.6 SPECIMEN LOADING

The specimens were loaded with a 60-ton (120 kip) ram at each end of the beam. This is shown in Figure 2.11.

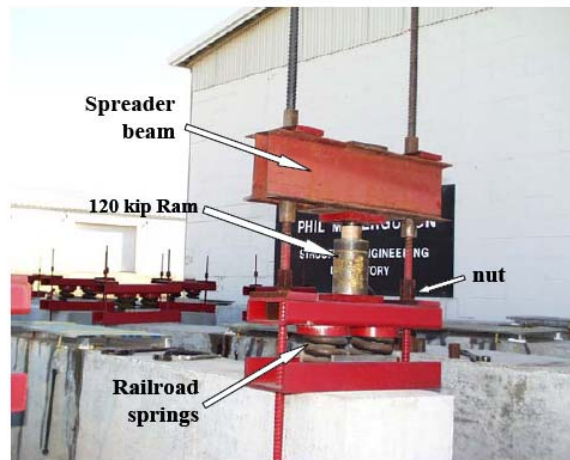


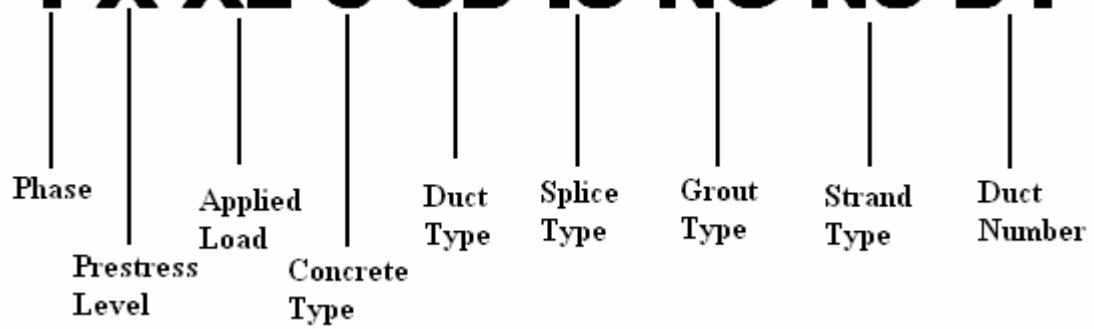
Figure 2.11: Specimen Loading³

The final service load level desired at each end of the beam was 50 kips.¹ In the case of specimens loaded based on small crack widths, the load was held once the sufficient crack width was reached. Rams at each end reacted against the spreader beam and compressed the springs. Once the desired force level was reached, the nuts on the top of the hollow steel section were tightened to maintain the load.¹ The railroad springs are designed to maintain the load on the specimen during exposure testing.

2.7 SPECIMEN NOTATION

At the beginning of the autopsies described in this thesis, a total of 15 beam specimens remained from Phase I and Phase II. The following notation scheme, adopted from Kotys⁴, describes the experimental variables for each specimen. The notation scheme uses a series of abbreviations to describe each specimen. Note that the variable of concrete type is not longer included in the test program, but will be used in the notation for continuity with the previous autopsies. For simplicity each specimen will typically be referred to by its two digit number shown in Table 2.1 throughout this thesis. Also note that some specific variables from Phase II are not included in this notation scheme-thus they are placed in the category “Other Variable.” The notation used for the specimen designations is as follows⁴:

1-X-XL-C-SD-IS-NG-NS-D1



Phase:

1 = Phase 1

2 = Phase 2

Prestress Level:

X = Non prestressed

P = 2/3 prestressed

U = 100% ultimate prestressed

S = 100% service prestressed

Applied Load:

XL = No load

SL = Service load

CL = Small crack load

OL = Overload (124%)

Concrete Type:

C = TxDOT Class C

F = 25 % fly ash*

H = High performance*

Duct Type:

SD = Galvanized steel duct

PD = Plastic duct

Splice Type:

IS = Industry standard

ISD = IS damaged

HS = Heat shrink

HSD = HS damaged

XS = No splice

Grout Type:

NG = Normal grout

AB = Anti-bleed grout

FA = 30% fly ash grout*

Strand Type:

NS = Normal strand

GS = Galvanized strand

ES = Epoxy coated strand

Duct Number:

D1 = Duct 1

D2 = Duct 2

* No longer part of this study, but included for clarity

Table 2.1: Specimen Designations

Phase I			
Specimen Number	Specimen Notation		
1.1	1 - X - XL - C		
1.2	1 - X - SL - C		
1.4	1 - X - OL - C		
2.1	1 - P - CL - C	SD - HS - NG - NS - D1	
	1 - P - CL - C	SD - IS - NG - NS - D2	
2.2	1 - P - SL - C - SD	XS - NG - NS - D1	
	1 - P - SL - C - SD	IS - NG - NS - D2	
2.4	1 - P - OL - C - SD	HS - NG - NS - D1	
	1 - P - OL - C - SD	IS - NG - NS - D2	
3.1	1 - U - XL - C - SD	HS - NG - NS - D1	
	1 - U - XL - C - SD	IS - NG - NS - D2	
3.4	1 - U - SL - C - SD	HS/HSD - NG - NS - D1	
	1 - U - SL - C - SD	IS/ISD - NG - NS - D2	
3.5	1 - U - OL - C - SD	HS - NG - NS - D1	
	1 - U - OL - C - SD	IS - NG - NS - D2	
4.1	1 - S - SL - C - SD	XS - NG - NS - D1	
	1 - S - SL - C - SD	IS - NG - NS - D2	
Phase II		Other Variable	
Specimen Number	Specimen Notation		
2.7	2 - P - SL - C - SD	IS - NG - ES - D1	Anchorage Exposure & Strand Coating Damage
	2 - P - SL - C - SD	IS - NG - ES - D2	
2.8	2 - P - SL - C - SD	HS - NG - GS - D1	
	2 - P - SL - C - SD	IS - NG - GS - D2	
2.9	2 - P - SL - C - SD	IS - NG - NS - D1	Poor Grouting Procedures & Anchorage Exposure
	2 - P - SL - C - SD	IS - NG - NS - D2	Anchorage Exposure
2.10	2 - P - SL - C - SD	IS - AB - NS - D1	
	2 - P - SL - C - SD	IS - AB - NS - D2	
2.12	2 - P - SL - C - PD	XS - NG - NS - D1	Anchorage Exposure
	2 - P - SL - C - PD	XS - NG - NS - D2	Anchorage Exposure

Chapter 3: Experimental Procedure

3.1 LONG-TERM EXPOSURE TESTING SET-UP

All Phase I and Phase II beams autopsied in the present study underwent approximately eight years of rigorous exposure testing outside the Ferguson Structural Engineering Laboratory. Specimens were exposed to saltwater both at mid-span and in some cases the anchorages. Non-destructive monitoring of the specimens took place during the testing period. The Phase II beams under exposure testing are shown in Figure 3.1.



Figure 3.1: Phase II Beams Under Exposure Testing

3.1.1 Beam Exposure Cycles

The specimens were exposed to a 3.5% NaCl solution (saltwater). This solution was used per ASTM G109 at the time, resulting in the most aggressive exposure possible. This standard has since been changed to 3%⁵, but 3.5% has been maintained throughout the eight years of testing for continuity in the exposure cycles. The saltwater was ponded above the cracked center portion of each beam. The ponding enclosure consisted of plexiglass walls epoxied to the surface of the specimen. For some specimens with large deformations due to overloading, the enclosure was divided in halves (with an additional

plexiglass panel in between) so that the enclosure could match the contour of the specimen more ideally. The enclosure was covered with plywood in order to prevent rainwater contamination of the solution, as well as protect the solution from wind. The plywood cover was secured to the beam by ropes and elastic tie-downs. To prevent saltwater leakage through the side face flexural cracks, the side face flexural cracks were sealed with epoxy. Each exposure cycle lasted approximately a month beginning with a two week wet cycle. At the end of the wet cycle, any remaining saltwater was soaked up with a sponge. Then the specimens were kept dry for the remainder of the month.

3.1.2 Beam Anchorage Exposure

In order to test anchorage protection, specimens 2.7 (Epoxy coated strands), 2.9 (Poor Grouting Procedures), and 2.12 (Encapsulated System) underwent exposure testing to their east-end anchorages using a dripper system. This is shown in Figure 3.2.



Figure 3.2: Anchorage Exposure System

The same NaCl solution used for the ponding portion of the beams was used. The saltwater was pumped from a container to a point above the specimens and then flowed down over the face of the anchorage. The saltwater was then collected in a plastic

container which was weighed down at its end by a concrete cylinder. The saltwater was then cycled back through the system. Due to leaks in the system, saltwater had to be periodically added during each cycle. The frequency of testing during the first several years of the test program was eight hours every two weeks², but for logistical reasons this was reduced to six hours once a month in the final years of testing.⁵ This is acceptable since all three anchorage exposure specimens still had the same exposure regimen.

3.2 MEASUREMENTS TAKEN DURING EXPOSURE TESTING

At various stages during exposure testing, the specimens were monitored by both non-destructive and destructive means.

3.2.1 Visual Inspection

The specimens were continuously observed for the appearance of any new cracking, spalling, or staining during exposure testing.

3.2.2 Crack Patterns and Crack Widths

Crack patterns and crack widths were taken at two stages during exposure testing. The first set of crack measurements was taken at the beginning of testing.¹ The second set of crack measurements was taken at the end of exposure testing. This was done since crack widths can increase due to creep and from stresses caused by the corrosion process. Also, the formation of longitudinal cracks aligned with the reinforcing bars is often a sign of severe corrosion, since these cracks form from the expansive effect of the corrosion of the bar or other steel components. Crack widths on the top surface of the beam were measured with a crack comparator or crack microscope if necessary. The method for crack width measurement is adopted from West¹ and is shown in Figure 3-3.

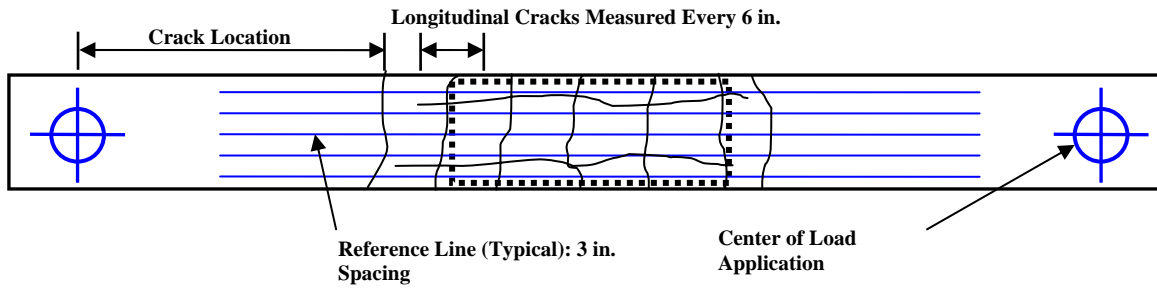


Figure 3.3: Crack Width Measurement System¹

Flexural cracks (or any crack running perpendicular to the longitudinal axis of the beam) were measured each time they crossed the reference lines. Longitudinal cracks were measured every 6 in. from the point at which they appeared. For specimens with anchorage exposure, any cracks in the anchorage zones were noted, and the width was measured at its apparent widest point. This was done at both anchorages in order to have the control of a non-exposed anchorage for comparison. This is valid comparison since the live and dead ends of the specimen are identical in construction.

3.2.3 Half-Cell Potential Measurements

Half-cell potentials are a non-destructive method for determining the probability of corrosion as well as when corrosion has initiated.¹ Half-cell potential readings require a wire connection to the reinforcing system, a reference electrode, and a voltmeter. Two wires were installed in the specimens—one clamped to the reinforcing cage before casting the concrete as well as a wire attached to the tail of the strands before backfilling of the anchorage occurred.¹ It was found by West¹ that the tendon system and reinforcing bar cage were electrically continuous, thus using either wire should produce the same results. Saturated calomel electrodes were used as the reference electrode in the testing program. The readings were done according to ASTM C876¹⁵ immediately after the end of the two week wet cycle. Initially, readings were taken with the saltwater still inside the ponding area, and readings done outside the ponding area required a wetting solution.¹ It was later found that more accurate readings could be taken if the saltwater was removed and the wetting solution was used in both the ponded and non-ponded areas of the specimen.³

The wetting solution used was soapy water. Initially, the locations of half-cell potential readings varied slightly with each beam type. However, later in the test program half-cell potentials were taken at the same locations regardless of the specimen (except for specimens 1.1 and 3.1). The locations of the test stations are shown in Figure 3.4.

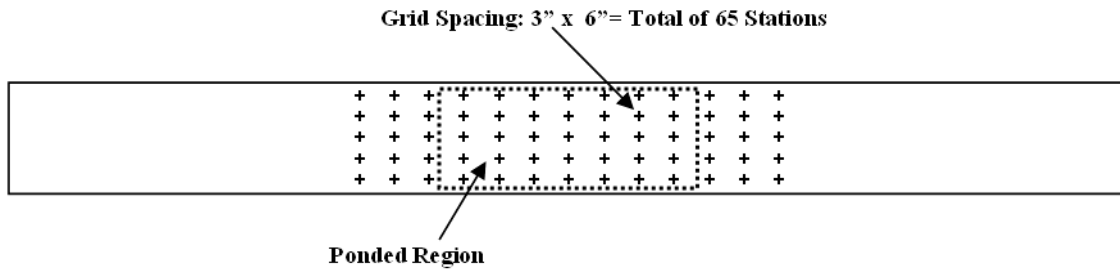


Figure 3.4: Half-Cell Potential Sampling Stations

For specimens 1.1 and 3.1 samples were only taken to one side of the centerline because of the partial autopsies performed on these specimens. The significance of the half-cell potential readings is shown in Table 3.1.

Table 3.1: Interpretation of Half-Cell Potentials for Mild Reinforcing Steel¹

Measured Potential (vs. SCE)	Probability of Corrosion
More Positive than -130 mV	Less than 10% Probability of Corrosion
Between -130 mV and -280 mV	Corrosion Activity Uncertain
More negative than -280 mV	Greater than 90% probability of corrosion

Note that the half-cell readings can only indicate the probability of corrosion, and that this system is for mild steel reinforcement only. Additionally, due to the presence of zinc in the galvanized post-tensioning ducts these values may not be appropriate for post-tensioned systems. The reading may actually be indicating the potential of zinc, which is more negative than mild steel.¹ This may lead to erroneous interpretations of the results.

For this reason regular half-cell potentials are not necessarily appropriate for post-tensioned systems.¹ However, the original researchers decided to use the regular half-cell potentials in this program since a sudden variation in voltage can indicate the onset of corrosion.¹

3.2.4 Chloride Penetration

Chloride penetration measurements were taken from both the beam specimens and from companion unloaded block specimens at different times during exposure testing. All drilling was done with a hammer drill, and the powder was collected for analysis. Multiple depths are sampled in order to determine the extent of chloride penetration. All samples were analyzed for acid-soluble chloride content using a specific ion probe (CL 500 Test System by James Instruments), and all sampling and analysis was done per AASHTO T260-94¹ during the entire 8-year testing period.

3.2.4.1 Specimens

The specimens were sampled for chloride content at the end of exposure testing. Samples were taken at depths of 0.5, 1, and 2 in.. Two in. corresponds to the depth of the reinforcement. Any damage inflicted on the specimen due to the drilling was noted for consideration in the later forensic analysis. The locations sampled for each specimen, adopted from Salas³, is shown in Figure 3.5.

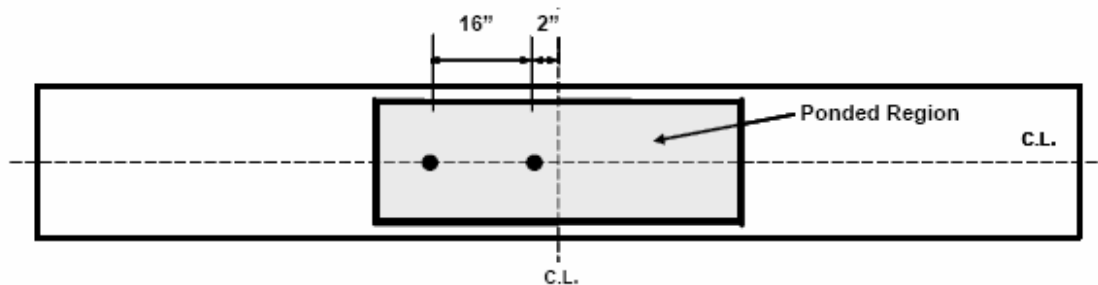


Figure 3.5: Chloride Sample Locations for Typical Test Specimen³

These two locations were used in the previous autopsies. Additional sample locations were done in the previous autopsies but it was decided that for the current

autopsies these additional points were no longer necessary. However, Specimens 1.1 and 3.1, which underwent partial autopsies by Salas³ and Kotys⁴, had the additional samples taken in order have comparable results with the previous autopsies. The sample locations are shown in Figure 3.6.

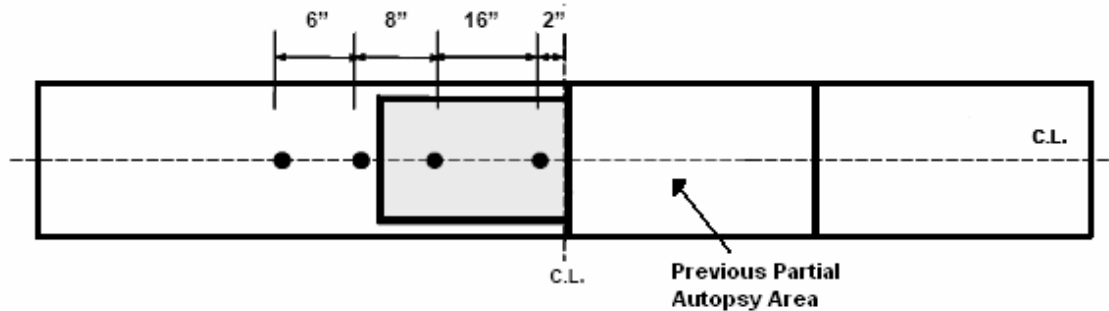


Figure 3.6: Chloride Sample Locations for Specimens 1.1 and 3.1³

For the three specimens with anchorage end drips chloride samples were taken at both beam ends at the center of the anchorage pockets. This is shown in Figure 3.7.



Figure 3.7: Chloride Sample Location for Anchorage Exposure Specimens

Samples were taken at depth of 0.5, 1, and 2 in.. The depth of two in. roughly corresponded to the depth of the tails of the strand. Samples were taken at the non-exposed end of the specimens in order to determine if any chloride ingress into the anchorages had occurred as a result of the ponding at the center portion of the beam.

3.2.4.2 Block Specimens

During casting of the beam specimens, two 12 x12 x 6 blocks were cast with each batch of concrete. One was designated as a ponding block and the other as a control block. The block specimens are shown in Figure 3.8.

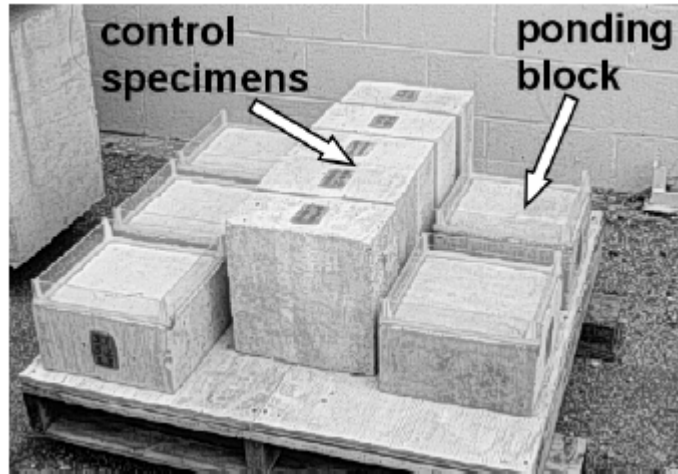


Figure 3.8: Block Specimens³

The ponding blocks had the same plexiglass enclosures installed as the beams. The blocks were subjected to the same exposure cycles at the specimens. The purpose of the ponding blocks was to measure chloride content due to the permeability of the concrete, and the sampling depths corresponded to those later used in the beam specimens. This was so drilling did not have to be done to the beam specimens during exposure testing. In addition, at the end of exposure testing the ponding blocks allowed for chloride ingress solely due to concrete permeability to be measured, since the ponding blocks were not cracked. The control blocks did not have enclosures and were used to measure the inherent chloride content in the concrete.¹

Chapter 4: Long-Term Exposure Test Results and Analysis

Exposure testing of the Phase I beams reported in this writing began in December 1997 and ended in June 2006 after 3107 days (8.5 years) of testing. Exposure testing of the Phase II beams described in this writing began in December 1998 and ended in November 2006 after 2894 days (approximately 8 years) of testing. During the testing period, half-cell potential data were collected each month and the specimens were continuously observed. The highest (most negative) monthly half-cell potential reading for each beam specimen over the entire 8-year testing period is given in Appendix B. Crack patterns and widths were taken at both the beginning and end of exposure testing. Crack data are given in Chapter 5 for each appropriate beam specimen.

4.1 HALF-CELL POTENTIAL DATA

The probability of corrosion for half-cell potentials is based on studies with plain reinforcing steel in the absence of any prestressing. Factors such as galvanization in either the strand or the duct may produce misleading results. As stated previously, readings were taken at several stations on each beam. In order to compare the specimens, the highest value for each day is used for comparison. Note that for some specimens there are periods of several months where readings were not taken due to beam maintenance issues⁴. Since the exposure times for Phases I and II are approximately the same, in some cases data were compared among specimens from both Phases I and II.

4.1.1 Phase I Half-Cell Readings

In Figure 4.1 contour plots of the final half-cell readings for the Phase I beams are shown. The contour scheme is based on that of Salas³ and Kotys⁴ from the previous autopsies for consistency. The contour color scheme is explained in Table 4.1. Note that all readings are based on the saturated calomel electrode. The probability of corrosion is based on ASTM C876.¹

Table 4.1: Half-Cell Potential Contour Map Color Indications

Potential	Color	Probability
< -580 mV_{SCE}	Purple	Extremely High
-430 to -580 mV_{SCE}	Red	Very High
-280 to -430 mV_{SCE}	Orange	High (At Least 90%)
-130 to -280 mV_{SCE}	Yellow	Uncertain
+20 to -130 mV_{SCE}	Light Blue	Low

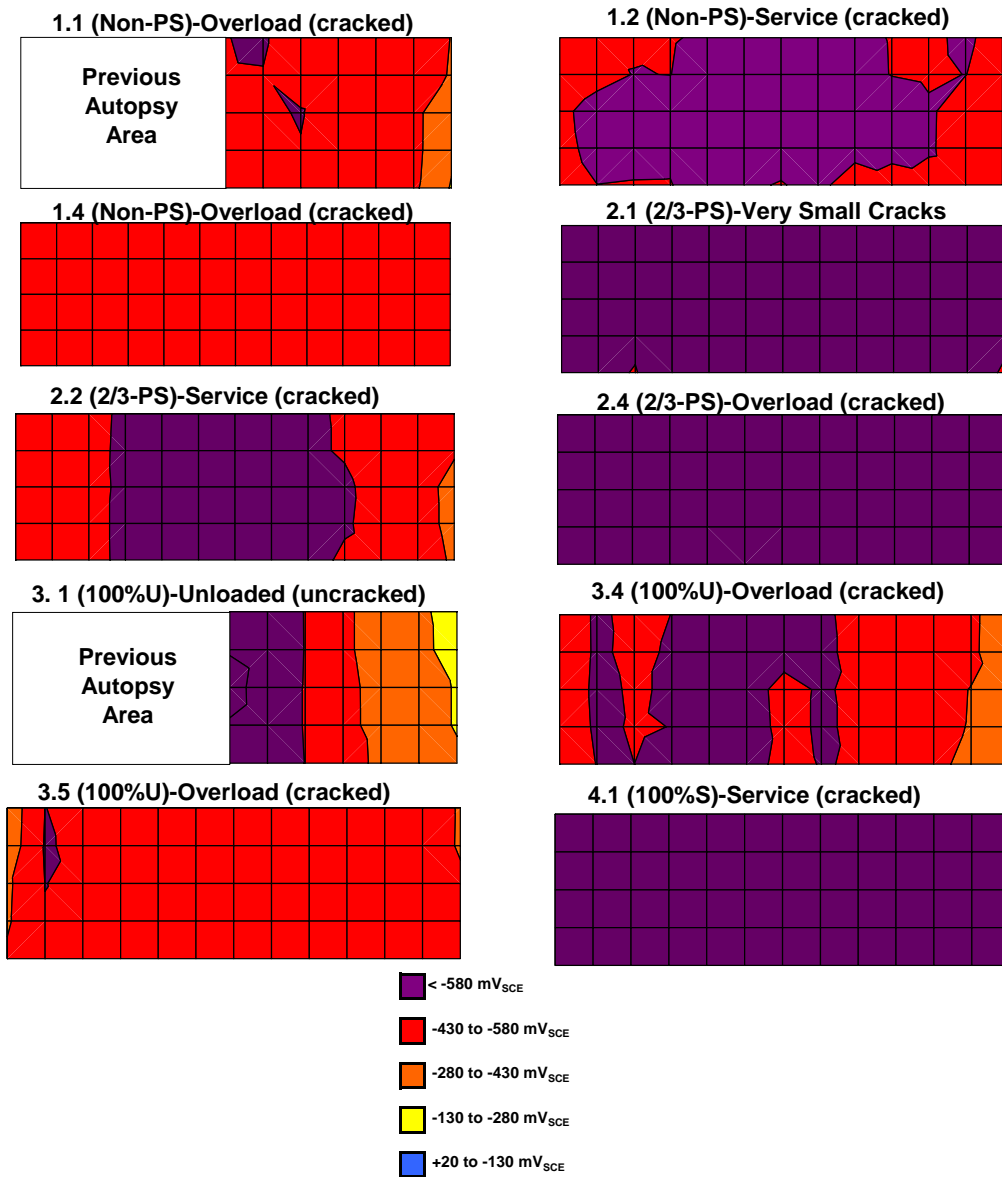


Figure 4.1: Half-Cell Potential Contours at 3107 Days for Phase I Beams

All Phase I specimens show high probabilities of corrosion. Only a small area of beam 3.1 falls in the uncertain range, while the rest of the beam shows a high probability of corrosion. Based on the -280 mV threshold for 90% probability of corrosion, the half cell data can also serve as a means to estimate the time of initiation of corrosion. This is done by examining the most negative monthly reading for each specimen. The estimated time to initiation of corrosion for the Phase I specimens is shown in Figure 4.2.

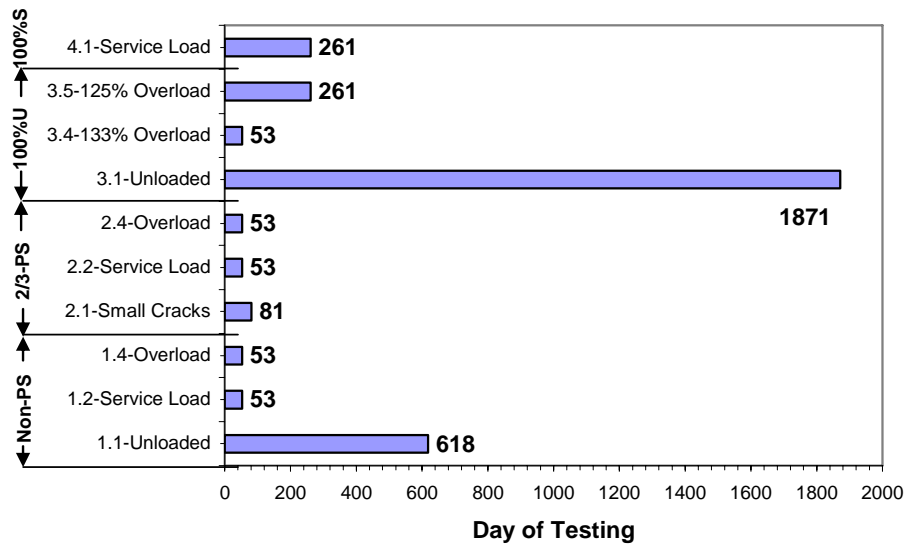


Figure 4.2: Estimated Time of Initiation of Corrosion: Phase I Beams

From Figure 4.2, the following is observed:

- All of the loaded specimens indicated corrosion within the first year of exposure testing, while the two unloaded specimens, 1.1 (Non-Prestressed) and 3.1 (100% Prestressed), showed a time to initiation of corrosion of 1.7 years and 5.1 years respectively. The delay in corrosion was likely due to the absence of cracking in these specimens.
- Among specimens with identical loading, the time to corrosion only increased when the specimen was fully prestressed, since the partially prestressed (2/3-PS) specimens and the non-prestressed specimens at service load began corroding at the same time as one another. The fully prestressed specimen (4.1) at service load had a much longer time for initiation of corrosion, most likely from better crack control since the specimen was fully prestressed.
- Among the partially prestressed and non-prestressed specimens, the overloaded and service load specimens began corroding at the same time. The partially prestressed specimen with small cracks (2.1) and the unloaded non-prestressed specimen (1.1) had a longer duration to initiation of corrosion. Thus, once cracks of sufficient size form, the time to initiation of corrosion is

not effected by any additional loading beyond the point at which the necessary crack width for corrosion is reached.

4.1.2 Phase II Half-Cell Readings

In Figure 4.3 the final half-cell contours for the Phase II beams are shown. All Phase II beams were partially prestressed and were cracked under service load.

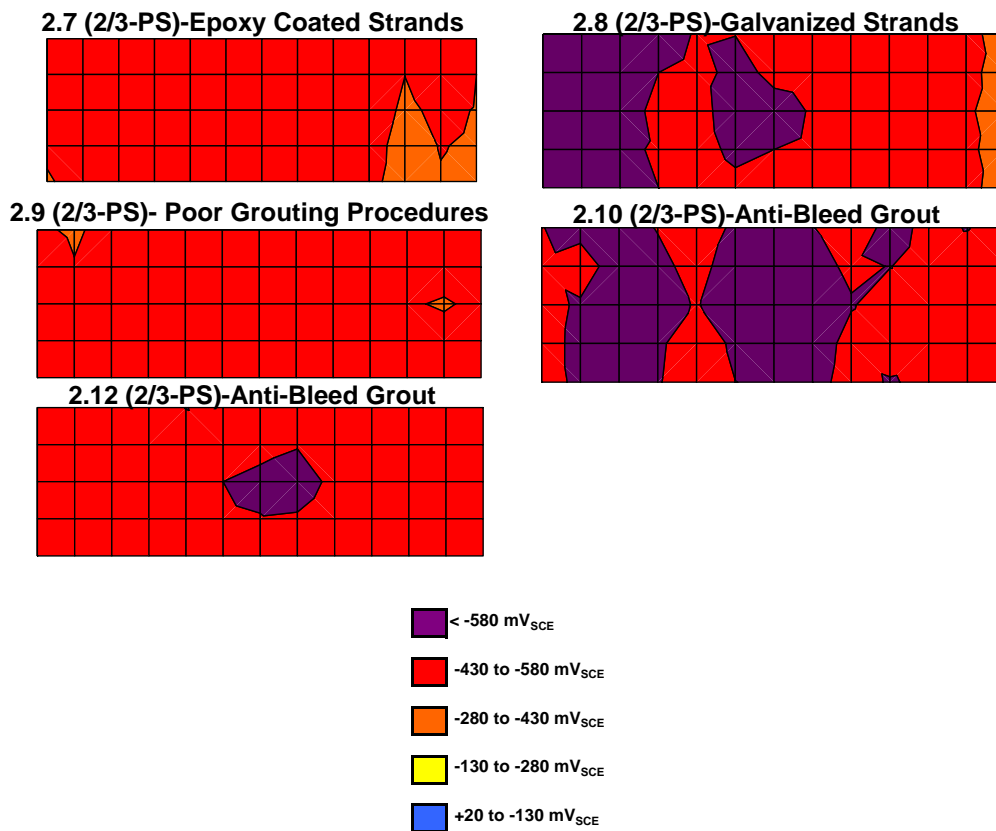


Figure 4.3: Half-Cell Potential Readings at 2894 Days for Phase II Beams

All Phase II beams had high probabilities of corrosion at the end exposure testing. The time to initiation of corrosion for the Phase II beams is shown in Figure 4.4

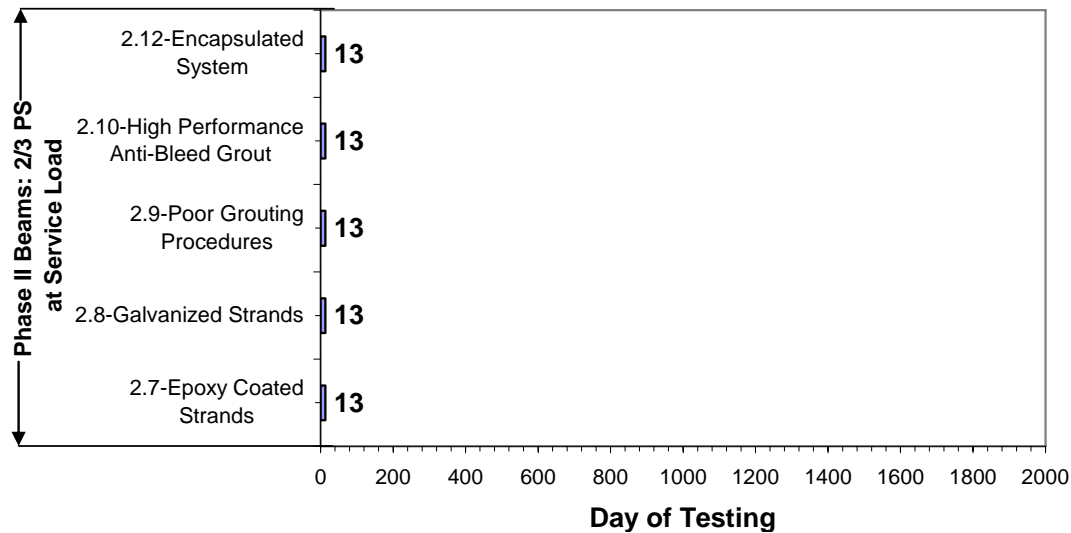


Figure 4.4: Estimated Time of Initiation of Corrosion: Phase II Beams

All Phase II Beams began corroding after only 13 days of testing. Even though all Phase II specimens had different post-tensioning details (either strand type, duct type, or grout type), the presence of cracking likely initiated the corrosion of the reinforcing bars at the same time in all five specimens. Thus, the corrosion in the reinforcing bars likely caused the crossing of the threshold.

4.1.3 Analysis of Half-Cell Potential Data

In Figure 4.5 the maximum final half-cell potential readings for all Phase I beams are shown. The symbols after the specimen number indicate the level of loading-NL indicates no load, CL indicates small crack load, SL is service load, and OL is overload.

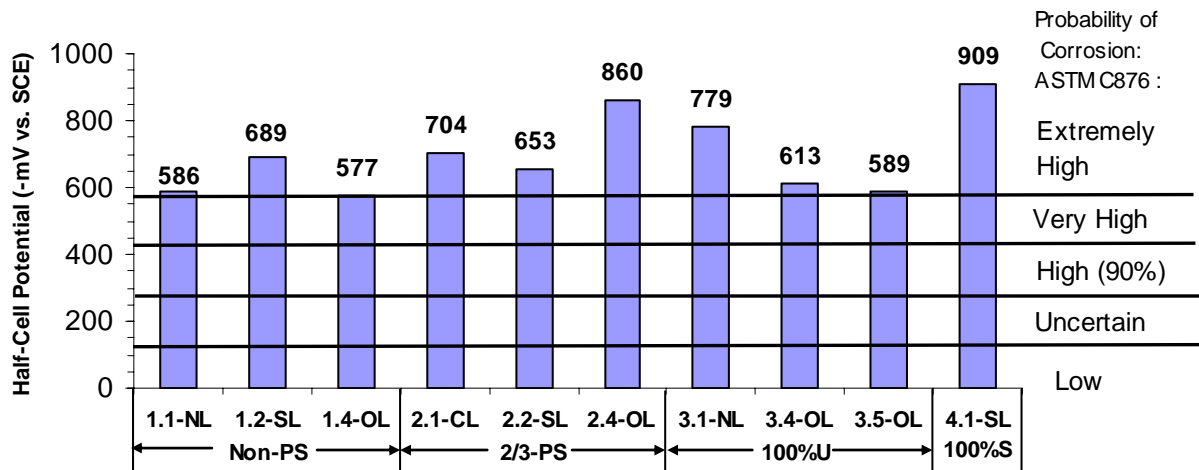


Figure 4.5: Maximum Final Half-Cell Potential Readings for Phase I Beams

When comparing specimens with the same levels of prestress, the following is observed about the level of loading:

- In the case of the non-prestressed and 2/3 prestressed specimens, there is no trend between increased loading and the half-cell readings. For the Non-PS specimens, the half-cell values did not increase (in terms of absolute value) with increased loading, and all three specimens were just at or above the extremely high probability of corrosion threshold. The same trend was observed in the 2/3-PS specimens, and all of those values were far above the threshold for extremely high probability of corrosion.
- For the 100% U specimens (fully prestressed), all specimens were above the threshold for extremely high probability of corrosion. The half-cell values did not increase with loading. Instead, they actually decreased.

Therefore, there is no overall trend between level of loading and the probability of corrosion after 8 years of testing.

When comparing specimens with the same levels of loading, the following is observed about the level of prestress:

- For the unloaded specimens (1.1 and 3.1), and the service load specimens (1.2, 2.2, and 4.1), there was no absolute decrease in the half-cell readings with increased prestress.

- In the case of the overloaded specimens (1.4, 2.4, 3.4, 3.5), a similar trend to that of the unloaded and service load specimens is observed

Therefore, according to the half-cell data, there is no correlation between the level of prestress and the probability of corrosion after 8 years of testing.

The maximum readings for the Phase II beams are given in Figure 4.6, along with the 2/3 PS service load beam from Phase I (Beam 2.2) for comparison.

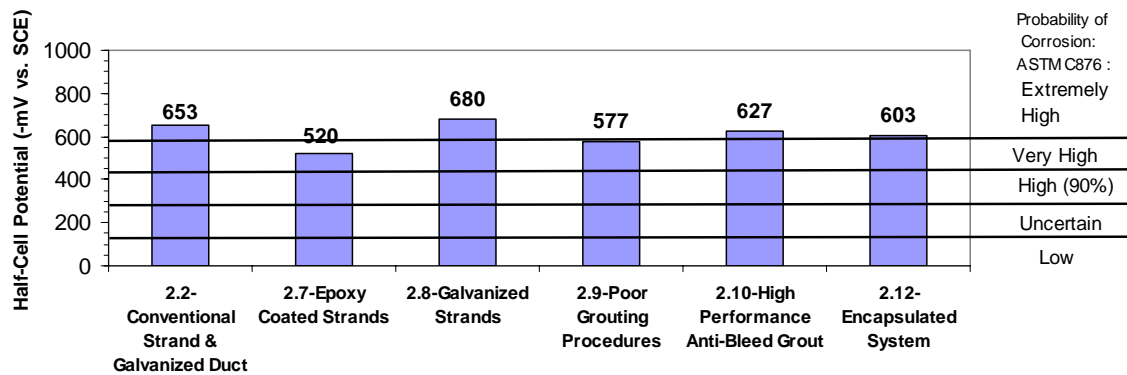


Figure 4.6: Maximum Final Half-Cell Potential Readings for Phase II Beams, Including Phase I Beam 2.2

Only the specimen with epoxy coated strands (2.7) had a probability of corrosion in the very high range. The remainder of the Phase II specimens were in the extremely high range. Beam 2.9 was essentially at the extremely high threshold (580 mV). It is interesting to note that according to the half-cell data, the use of the plastic duct did not decrease the probability of corrosion in relation to the other specimens. However, it needs to be stressed that the half cell readings include the conventional bars and metal ducts, since all the steel elements in the beam form a circuit. Therefore, the relative performance of only the post-tensioning hardware (namely the strand) cannot be readily estimated from the half-cell potential data.

In Chapter 6 the trends among the specimens indicated by the half-cell data are compared to the results of the forensic analyses of the specimens. Thus, it will be determined if the values of the half-cell readings can give an indication of the relative performance of the specimens. It will also be determined if the probabilities of corrosion suggested by the readings were correct.

4.2 CHLORIDE PENETRATION DATA

Chloride samples were taken from the unponded control blocks, ponding blocks, and the beam specimens as stated in Chapter 3. All unponded control blocks showed negligible acid soluble chloride content at all depths.

4.2.1 Phase I Chloride Penetration Data

The chloride content data for the Phase I beams is shown in Figure 4.7. The Cl^- threshold for corrosion is the same used by Salas³ which is 0.033% by weight of concrete. In Figure 4.8 the additional offsets outside the ponded region for unloaded beams 1.1 (Non-Prestressed) and 3.1 (100%U Prestressed) are shown.

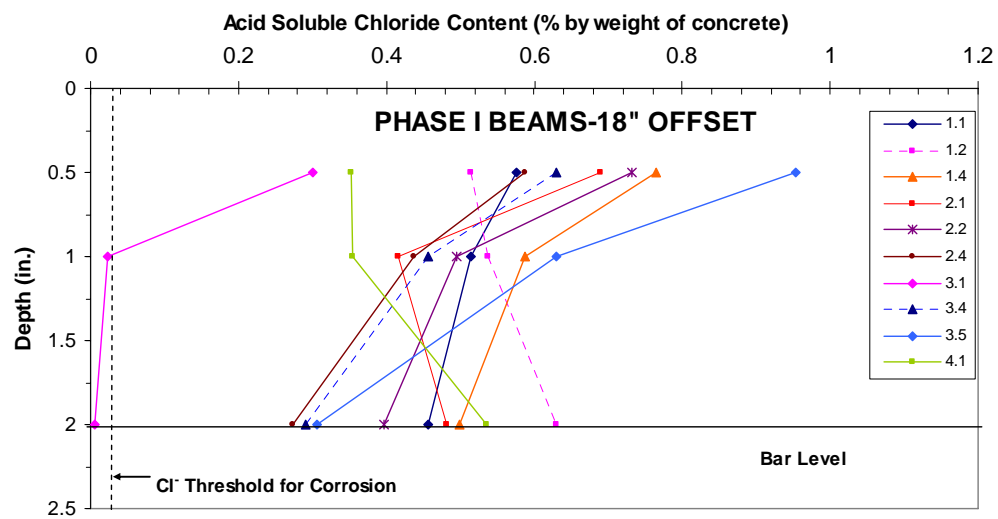
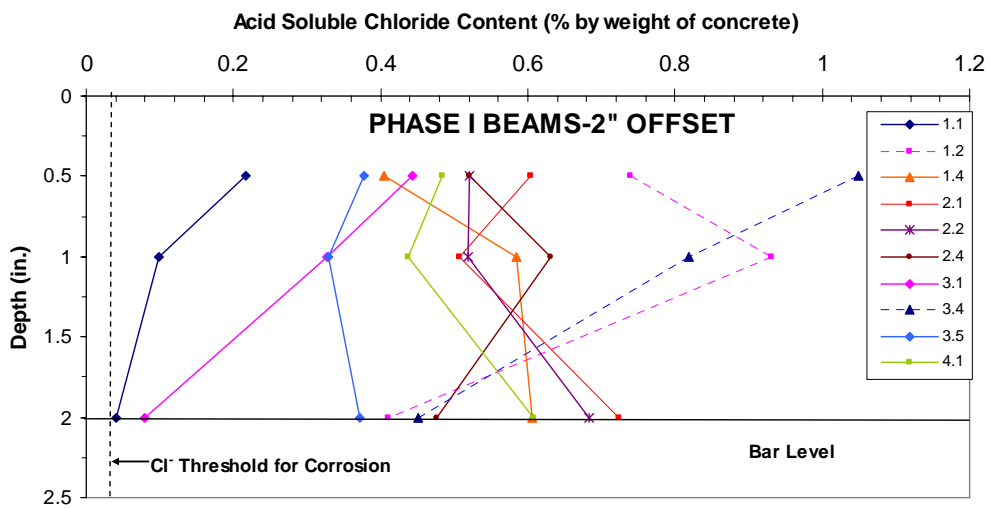
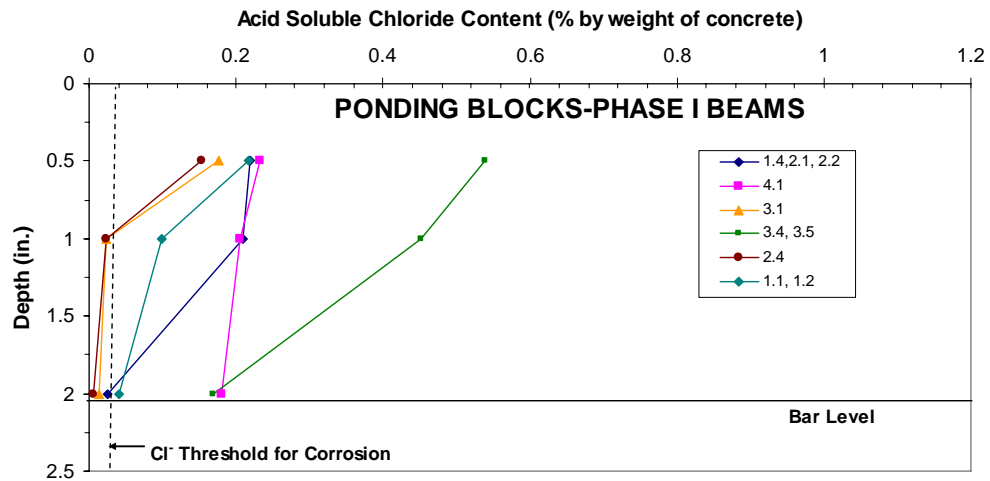


Figure 4.7: Beam and Block Chloride Penetration for Phase I Beams

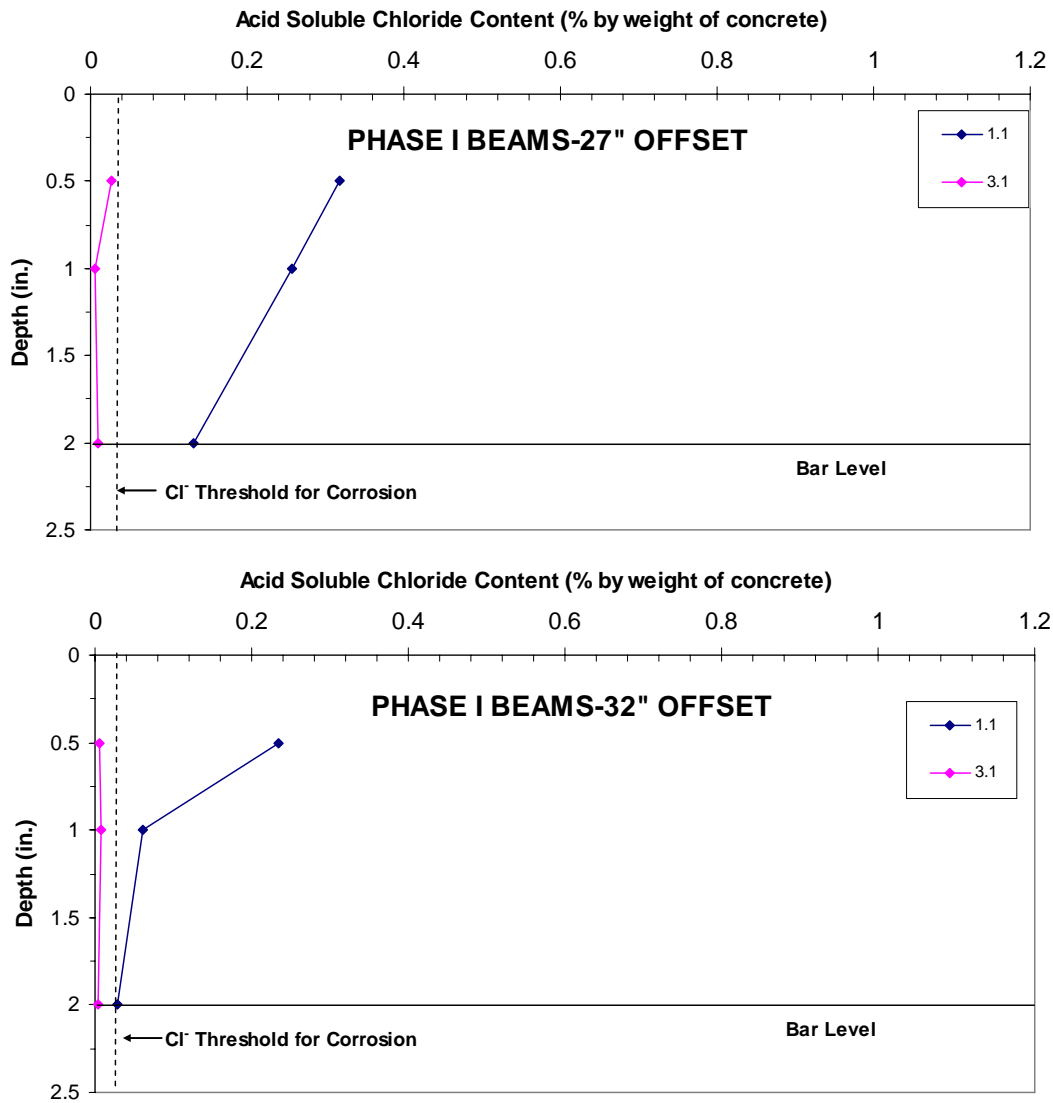


Figure 4.8: Beam Chloride Penetration for 27" and 32" Offsets (Beams 1.1 and 3.1)

For all Phase I ponding blocks the chloride content decreased appreciably with depth. In the ponding blocks with the concrete used in beams 3.4, 3.5, and 4.1 the chloride contents are far above the corrosion threshold at the level of the bars. This is significant because it suggests that even without cracking corrosion could occur in these specimens. In other words, the corrosion threshold could be reached just from the permeability of the concrete. Unlike the ponding block specimens, the chloride content did not always decrease with depth in the case of the beam specimens. The chloride

content at 2-in. depth was larger than that near the surface surely due to the large amount of cracking that was seen in the specimens (See Chapter 5). Also, the threshold for corrosion was reached at bar level for both offsets for all specimens, except the 18” offset for beam 3.1. The reason for this, as later stated in Chapter 5, is that beam 3.1 did not have any cracking in the vicinity of the 18” offset. In addition, outside the ponded region all samples for beam 3.1 were below the threshold for corrosion. In the case of beam 1.1, the samples outside the ponded region still showed values above the threshold for corrosion. A possible explanation for this is that the salt solution was leaking out of the salt bath onto the rest of the beam. This is supported by the fact that large amounts of staining were observed outside the ponded region in the case of beam 1.1.

4.2.2 Phase II Chloride Penetration Data

The chloride penetrations from the Phase II beams are shown in Figure 4.9.

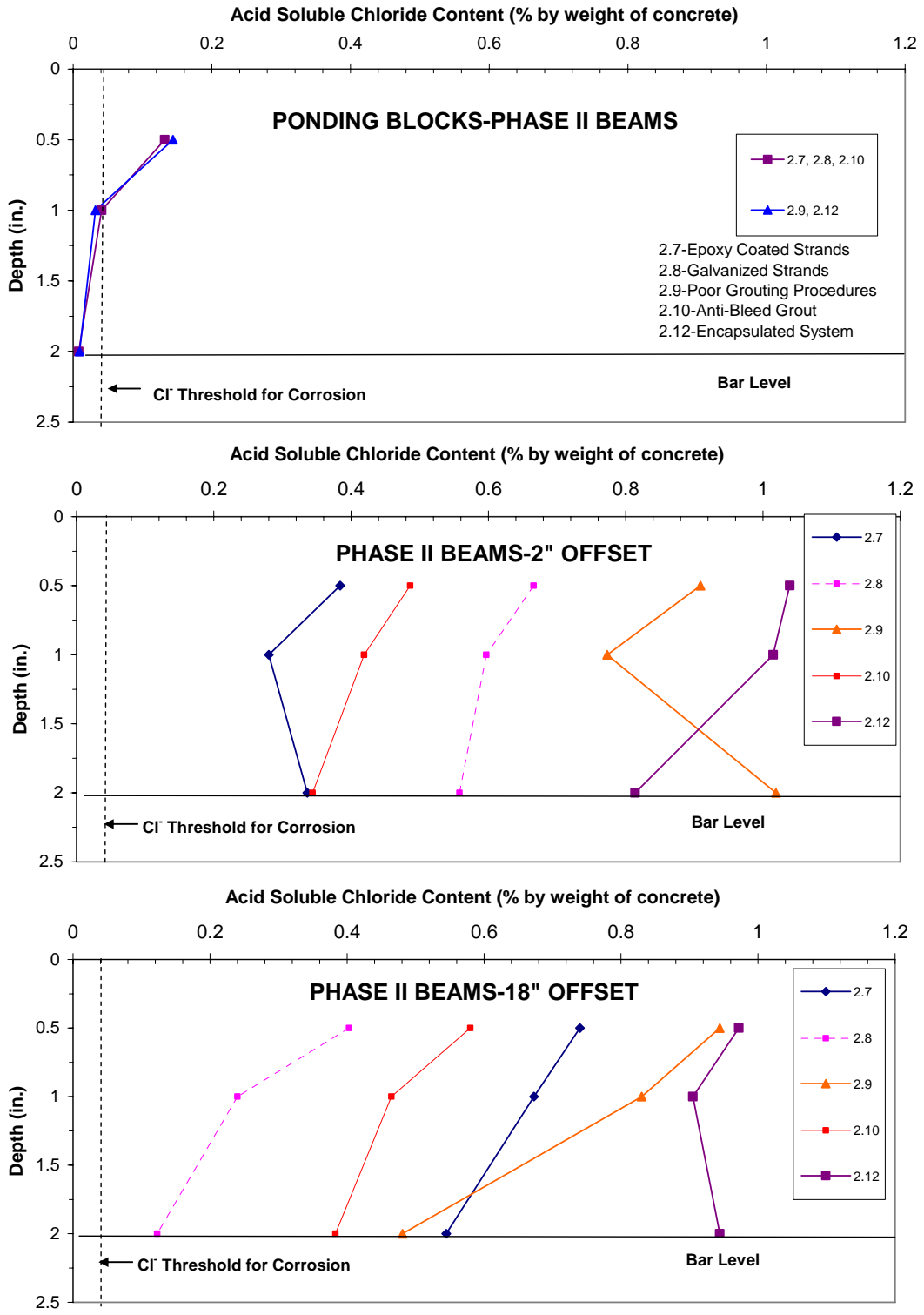


Figure 4.9: Beam and Block Chloride Penetration for Phase II Beams

In the case of the Phase II ponding blocks similar behavior was seen among all five specimens. At the depth of the reinforcing bars the ponding block chloride contents were far below the threshold for corrosion. In addition, the chloride content decreased appreciably with depth. In the case of the Phase II beam offsets, the values were substantially larger than the ponding blocks and did not always decrease with depth. At the depths of the bars all samples were far above the threshold for corrosion. As later shown in Chapter 5, the large amount of cracking in the Phase II specimens likely caused the chloride content to be higher at the bar level than at the surface. In addition, the profiles were not the same at both offsets. However, at both offsets all beams are well above the threshold for corrosion at the level of the bars.

In the case of the anchorages for beams 2.7 (Epoxy Coated Strand), 2.9 (Poor Grouting Procedure), and 2.12 (Encapsulated System), the end anchorages not subjected to the end drip exposure cycles showed negligible chloride content at all depths. The chloride content for the anchorages of beams which were subjected to the end exposure cycles are shown in Figure 4.10.

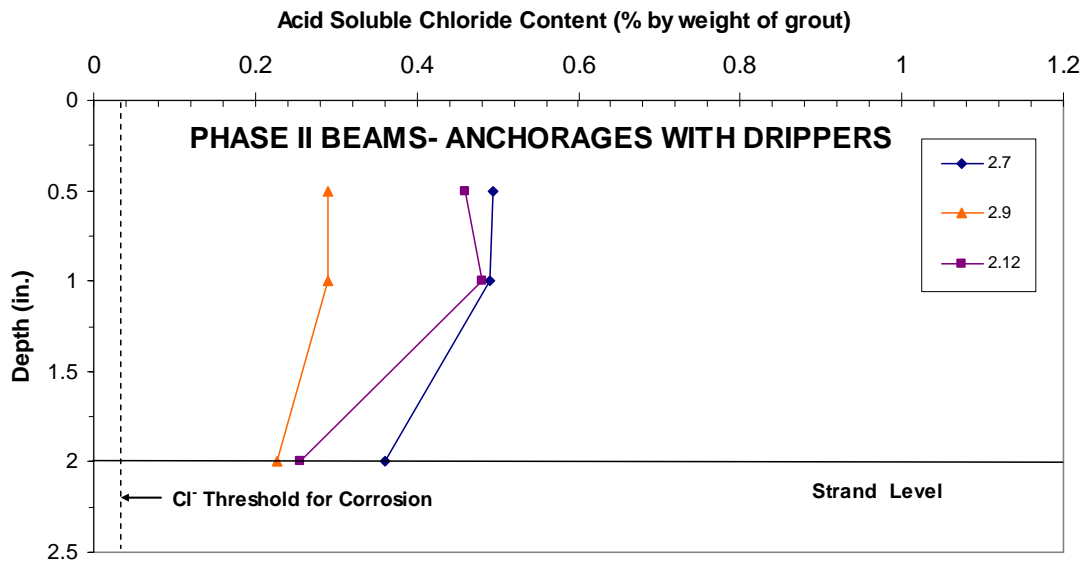


Figure 4.10: Chloride Penetration for Anchorages of Phase II Beams Subjected to End Anchorage Exposure

According to these data the anchorage exposure cycles were rigorous enough to produce corrosion in the anchorages. For all three specimens the chloride content at the level of the strand tails is far above the threshold for corrosion. The presence of any corrosion in the anchorages will be determined in the forensic analysis in Chapter 5.

4.2.3 Analysis of Chloride Penetration Data

The chloride penetration data at the level of the reinforcing bars for the Phase I beams is shown in Figure 4.11.

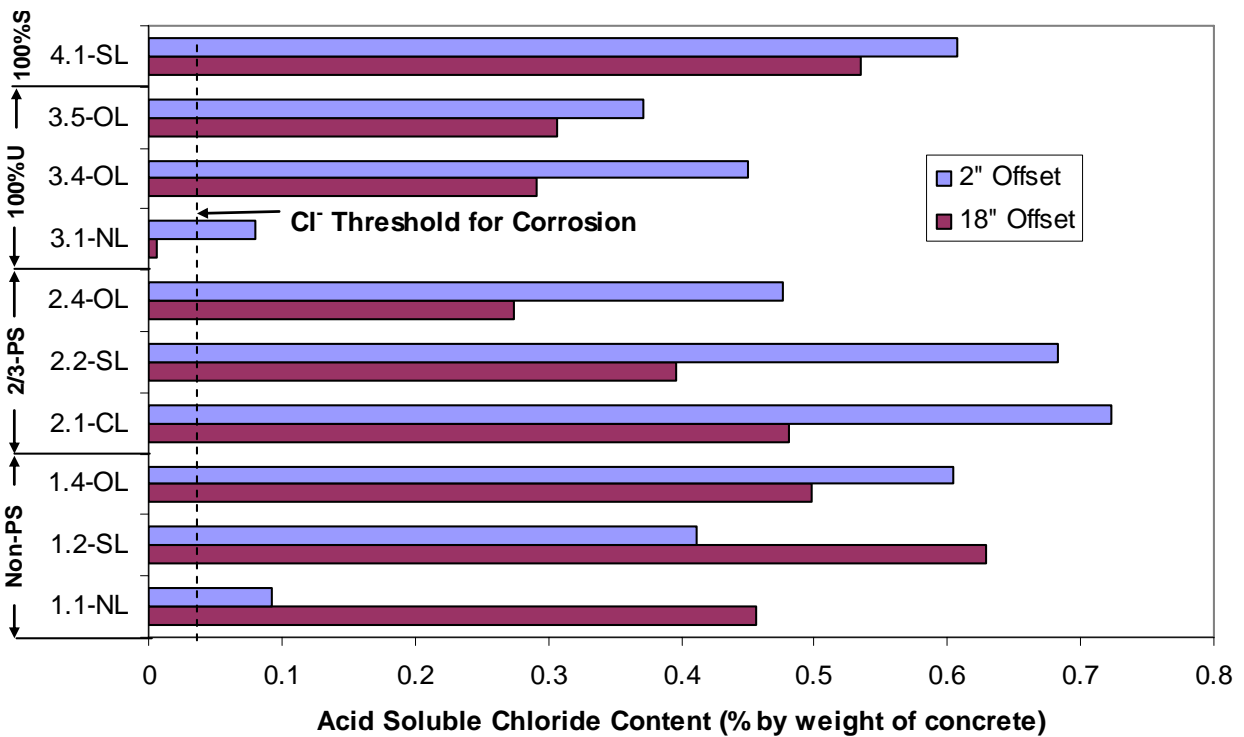


Figure 4.11: Chloride Penetration at Reinforcing Bar Depth-Phase I Beams

Except for the 18" offset in the unloaded fully prestressed specimen 3.1, all chloride levels exceeded the threshold for corrosion - even the reinforced concrete unloaded specimen. While the contents at the 2" offsets were not always the same, in all loaded specimens the contents were far above the threshold, so the difference in values is irrelevant. The only trend observed when comparing specimens with the same level of

prestress is with the fully prestressed beams: Beam 3.1 clearly demonstrated the effect of an uncracked section when compared to beams 3.4 and 3.5.

The chloride penetration at bar depth for the Phase II beams is shown in Figure 4.12 .

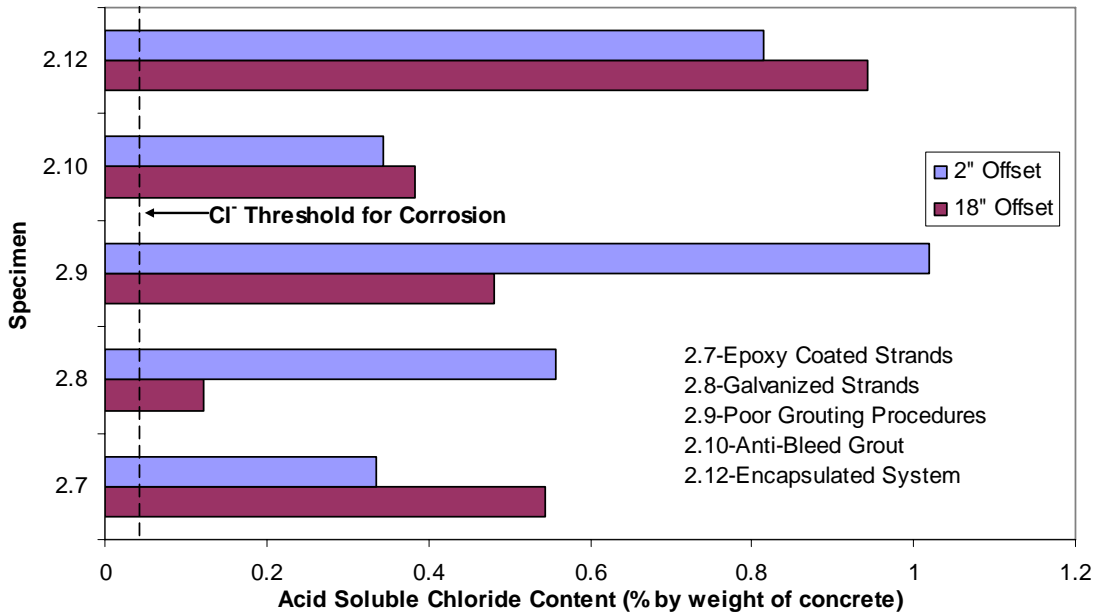


Figure 4.12: Chloride Penetration at Bar Depth-Phase II Beams

All values are well above the threshold for corrosion. The fact that the threshold is exceeded is most likely due to corrosion of the steel reinforcing bars and galvanized ducts. Thus the difference in values among specimens does not reveal any information about the effects of different grouts, strand, or duct type. The values only indicate the potential for corrosion at the levels of the bars and ducts.

The results from the chloride content data are compared to the forensic analysis data in Chapter 6 to determine if they give a correct indication of the relative performance of the specimens.

Chapter 5: Forensic Analysis

At the end of exposure testing, the remaining beam specimens from Phases I and II were autopsied. All reinforcing bars, stirrups and prestressing tendons were removed from the center region of the beams and analyzed. On three beams from Phase II the post-tensioning anchorages were removed for examination. Before autopsy, crack widths and concrete chloride content samples were taken as outlined in Chapter 3. In order to closely examine cracks, the plexiglass ponding enclosure in the center of the beams was removed and the epoxy which had sealed the side face cracks was stripped off.

5.1 AUTOPSY PROCEDURE

5.1.1 Beam Unloading

The beams were kept under a constant loading during exposure testing. To unload the beams a set-up similar to that used for the initial beam loading was used. The unloading setup is shown in Figure 5.1.



Figure 5.1: Beam Unloading (Phase II Beam 2.9 Pictured)

The loaded threaded rods on the beam ends were coupled to additional lengths of threaded rod. Two 30-kip rams were placed so that the rods went through the center holes of the rams. The rams were then pre-extended to match the estimated existing compression in the springs. The compression in the springs was estimated by comparing the loaded springs to identical unloaded springs. The threaded rods were then secured to the top of the rams by a plate and nut. The rams were then loaded to the force in the spring assembly. The force in the rams was monitored with a pressure gauge. Next, the in-place nuts, which were now unloaded, were loosened and moved up. Then the hydraulic pressure was released, unloading the beam. Finally, the loading assemblies were removed from each end of the beams. The Phase II beams after unloading are shown in Figure 5.2. It is interesting to note how much deformation remained in the beams.



Figure 5.2: Phase II Beams After Unloading

The beams were then removed from the reaction beams by a forklift. The reaction beams were placed into storage for future use in the laboratory. The reaction beams are shown in Figure 5.3.



Figure 5.3: Reaction Beams Placed In Storage at FSEL

5.1.2 Cutting of Beams

A 72 in. long, 8-in. deep block was cut from each beam using a large water-cooled saw. The location of the cuts is shown in Figure 5.4.

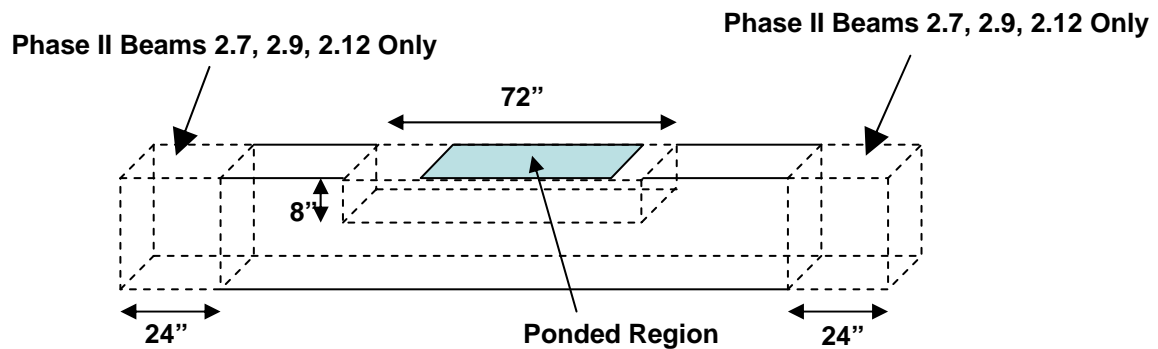


Figure 5.4: Beam Cutting Pattern

This is the same cutting pattern used by Salas³ and Kotys⁴ in the previous autopsies. The centerline of the removed block was 12 in. off the beam centerline. Therefore, an area outside the ponded region could be included for comparison with the area directly beneath the ponded region. Thus a total of 72-in. of each duct and

longitudinal bar were inside the 72-in. long block, and the upper portions of six of the stirrups. For beams 1.1 and 3.1, which had been partially autopsied after four years of testing, 42 in. of material was removed extending from the centerline of the beams. The cutting pattern is shown in Figure 5.5.

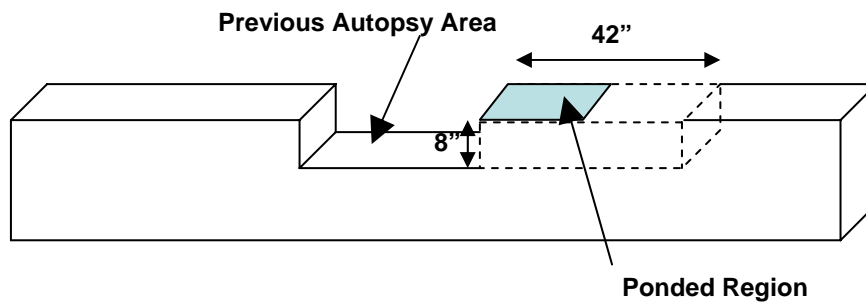


Figure 5.5: Cutting Pattern for Beams 1.1 and 3.1

As shown in Figure 5.4, for the Phase II beams which underwent end anchorage exposure with drippers (Beams 2.7, 2.9, 2.12), 24 in. of the entire beam end were cut from both ends of the beams. Thus a comparison could be made between beam anchorages with saltwater drippers and those without saltwater drippers. The cutting of the beams is shown in Figure 5.6. The cutting was done by FSEL lab technicians. The beams had to be flipped several times with a forklift to complete all the cutting. Once the cuts were made, the blocks were removed from the beam with a forklift. A typical block removed from the center of a beam is shown in Figure 5.7. An example of a removed end anchorage block is shown in Figure 5.8.



Figure 5.6: Cutting of Beams (Phase I Beams Pictured)



Figure 5.7: Typical Center Block Removed from Beams (Phase II Beam 2.7 Shown)



Figure 5.8: Typical End Anchorage Block Removed from Phase II beams 2.7, 2.9, and 2.12 (Beam 2.12 East End Shown)

5.1.3 Removal of Reinforcing Elements

The reinforcing elements were removed from the center blocks using jackhammers and hammer drills. This is shown in Figure 5.9.



Figure 5.9: Breaking up of Block (Phase I Beam 1.1 Pictured)

Since the blocks were upside down, the first elements removed were the grouted post-tensioning ducts, containing the strand. This is shown in Figure 5.10 .



Figure 5.10: Post-Tensioning Ducts Before Removal From Center Block (Phase II Beam 2.12 Pictured)

After further chipping the mild reinforcing steel cage was removed from the block, shown in Figure 5.11 .



Figure 5.11: Mild Steel Reinforcing Cage After Removal From Beam (Phase II Beam 2.10 Pictured)

5.1.4 Removal of Post-Tensioning Anchorages

To remove the anchorages from the end blocks of the three Phase II beams with anchorage exposure, similar methods to those used in removing the autopsy items from the centerline blocks were used. The items removed included the anchorhead, bearing plate, and 18 in. of duct from both tendons. A total of 24 in. of strand was removed from each duct, since the strand went out beyond the anchorhead. The removal of the anchorages is shown in Figure 5.12.



Figure 5.12: Removal of Post-Tensioning Anchorages (East End Anchorage of Beam 2.12 pictured)

5.1.5 Disassembly of Prestressing Tendons

After each duct was removed from the beams, an air powered cutting tool was used to slice the ducts in half longitudinally in order to examine the grout. This was done for both the 6-ft long duct portions removed from the center of the beam, as well as the duct portions from the anchorages. The grout was examined for bleed water voids, evidence of porosity, and cracking. In addition, transverse crack faces on the grout were examined for staining. Once this was complete, the grout was removed and grout chloride content samples were taken every 18 in. along the length of the duct for a total of five samples per duct. For the duct portions in the anchorages, samples were taken every 6 in. from the back of the bearing plate, for a total of four samples per duct. The grout sampled for all ducts was that directly in contact with the strand. Once the strand was removed from the duct, it was unwound in order to examine the interstices between the wires. In

the case of the anchorages, the strand was cut directly behind the anchor head in order to remove it from the anchorhead with a hammer. Then, the wedges were removed from the strand. .

5.1.6 Element Rating System

In order to compare readily the corrosion damage among beams, a numerical rating system was used to rate the corrosion damage in the mild steel bars and stirrups, the galvanized ducts and splices, as well as the prestressing strand within the 72-in. long center block and the anchorages. This is the same rating system used by Salas³ and Kotys.⁴

Mild Reinforcing Steel Rating System

In order to rate the damage in the longitudinal reinforcing bars, the top and bottom of each bar was divided into 36 2-in. intervals. In the case of the stirrups, each 3-in. “leg” was taken as one interval. The remaining portion of the stirrup was divided into seven 2-in. intervals. The interval arrangement for the longitudinal bars and stirrups is shown in Figure 5.13.

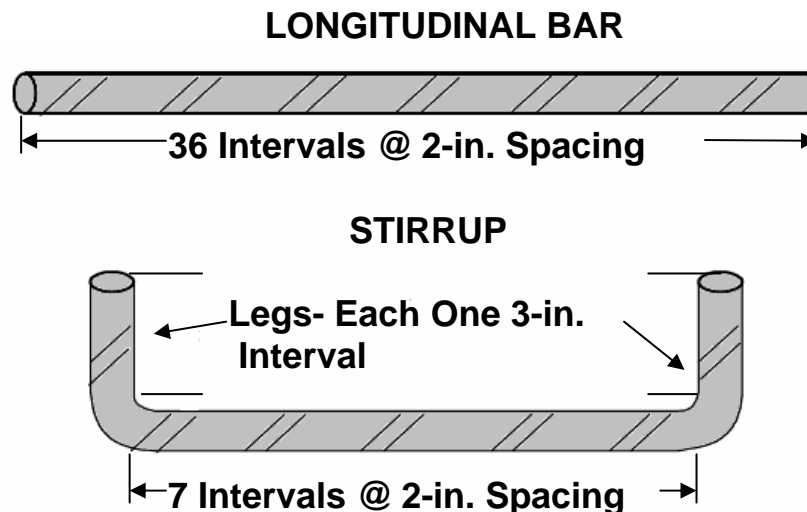


Figure 5.13: Mild Reinforcing Steel Rating Intervals⁴

The numerical rating system used to evaluate each interval of both the stirrups and longitudinal bars is shown in Table 5.1.

Table 5.1: Numerical Rating System For Mild Steel Bars and Stirrups³

Code	Meaning	Description	Rating
NC	No Corrosion	No evidence of corrosion.	0
D	Discoloration	No evidence of corrosion, but some discoloration from original color.	1
L	Light	Surface corrosion on less than one half of the interval, no pitting is present. Surface corrosion can be removed using cleaning pad.	2
M	Moderate	Surface corrosion on more than one half of the interval, no pitting. and/or Any corrosion that can not be completely removed using cleaning pad.	4
P	Pitting	Pit visible to unaided eye.	8
AR	Area Reduction	Measurable reduction in bar cross-sectional area due to corrosion.	a ²

a = Estimated bar cross-sectional area reduction in percent

The cleaning pad used to discern between a rating of 2 or 4 was a 3M Scotchbrite™ pad. The pad was rubbed on the bar with the same pressure used for cleaning pots and pans. In order to determine any area loss in bars, the reduced diameter was measured with a micrometer and the equivalent cross-sectional area loss was calculated. The highest possible rating in a single interval for a longitudinal bar or stirrup would be 10,000. This would indicate the total loss of cross sectional area anywhere in the interval. The rating for an entire longitudinal bar is given by Equation 5-1:

$$R_{Bar} = \sum_{i=1}^{36} (R_{Top\ i} + R_{Bottom\ i}) \quad \text{Eq. 5-1}^3$$

The total rating for all longitudinal bars in a beam is given by Equation 5-2:

$$Total\ Bar\ Corrosion\ Rating = \sum_{n=1}^m R_{Bar\ n} \quad \text{Eq. 5-2}^3$$

Where,

- $R_{Top\ i}$ = corrosion rating on top bar surface, interval i
 $R_{Bottom\ i}$ = corrosion rating on bottom bar surface, interval i.
 $R_{Bar\ n}$ = total bar corrosion rating, bar n
 i = interval, 1 to 36
 n = bar number, 1 to m
 m = total number of longitudinal bars in beam (2 for 100%S and 100%U Beams, 8 for Non-PS and 2/3-PS Beams)

In order to compare beams, as well as to account for the differences in the number of reinforcing bars among the beams, a generalized rating for the longitudinal bars is calculated for beam comparison, given by Equation 5-3:

$$Generalized\ Bar\ Corrosion\ Rating = \frac{Total\ Bar\ Corrosion\ Rating}{m \times 6} \quad \text{Eq. 5-3}^3$$

This gives an average rating per foot of bar.

The total rating for an individual stirrup is given by Equation 5-4:

$$R_{Stirrup} = \sum_{i=1}^9 (R_{Top\ i} + R_{Bottom\ i}) \quad \text{Eq. 5-4}^3$$

The total rating for all stirrups in a beam is given by Equation 5-5:

$$Total\ Stirrup\ Corrosion\ Rating = \sum_{n=1}^6 R_{Stirrup\ n} \quad \text{Eq. 5-5}^3$$

Where,

- $R_{Top\ i}$ = corrosion rating on top stirrup surface, interval i
 $R_{Bottom\ i}$ = corrosion rating on top bar surface, interval i
 $R_{Stirrup\ n}$ = total stirrup corrosion rating, stirrup n
 i = interval, 1 to 9
 n = stirrup number, 1 to 6

Even though there were an equal number of stirrups in each block, an average value for comparison was calculated using a generalized rating given by Equation 5-6:

$$Generalized\ Stirrup\ Corrosion\ Rating = \frac{Total\ Stirrup\ Corrosion\ Rating}{10.5} \quad \text{Eq. 5-6}^3$$

Where 10.5 is the total length of all stirrups in the removed block (in feet).

Galvanized Duct/Galvanized Duct Splice Rating System

Similarly to the longitudinal bars, the galvanized ducts were divided into 36 2-in. intervals. The upper and lower halves of the duct were evaluated separately. In addition, the inner and outer surfaces of the duct halves were also evaluated separately. Thus a total of four surfaces were analyzed. The 12-in. long galvanized duct splices were examined in a similar fashion, with only six 2-in. intervals. The galvanized duct/galvanized splice interval system is shown in Figure 5.14.

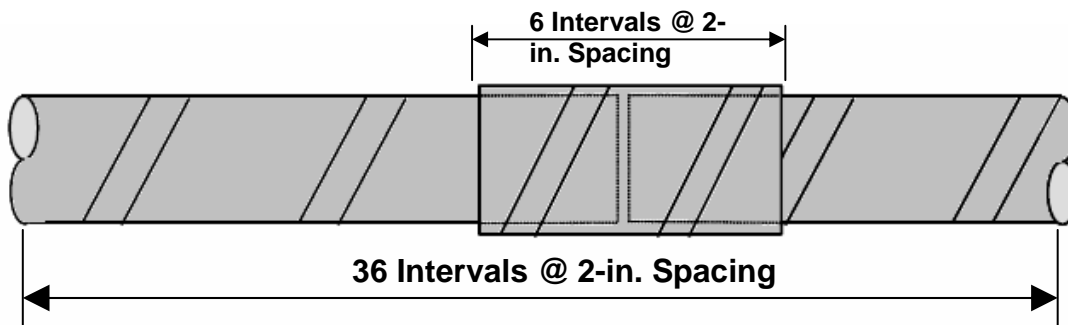


Figure 5.14: Galvanized Duct Rating System⁴

The 18-in. of duct removed from the anchorages was also rated by this system, except with nine intervals. The galvanized duct/galvanized splice rating system is shown in Table 5.2.

Table 5.2: Numerical Rating System for Galvanized Duct/Galvanized Splice³

Code	Meaning	Description	Rating
NC	No Corrosion	No evidence of corrosion.	0
D	Discoloration	No evidence of corrosion, but some discoloration from original color.	1
L	Light	Surface corrosion on less than one half of the interval, no pitting is present.	2
M	Moderate	Surface corrosion on more than one half of the interval, no pitting.	4
S	Severe	Corrosion completely covers the interval. and/or Presence of Pitting	8
H	Hole Through Duct	Hole corroded through duct. Used in conjunction with ratings D, L, M, and S.	32 + A _h

A_h = Area of holes in mm²

The areas of the holes in the ducts were measured with a micrometer. The highest possible rating in one interval for a galvanized duct would be 8171, indicating that the top and bottom of the duct are completely corroded away. The rating for the entire duct is given by Equation 5-7:

$$Total\ Duct\ Corrosion\ Rating = \sum_{i=1}^{36} R_{TopOuter,i} + R_{BotOuter,i} + R_{TopInner,i} + R_{BotInner,i} \quad \text{Eq. 5-7}^3$$

Where,

$R_{TopOuter,i}$ = top outer surface corrosion rating, interval i

$R_{BotOuter,i}$ = bottom outer surface corrosion rating, interval i

$R_{TopInner,i}$ = top inner surface corrosion rating, interval i

$R_{BotInner,i}$ = bottom inner surface corrosion rating, interval i

i = interval, 1 to 36 (1 to 6 for splice, 1 to 9 for anchorage duct).

Since both ducts in a beam are regarded as separate specimens for analysis purposes, each individual duct is assigned a generalized rating. The generalized duct rating is given by Equation 5-8:

$$Generalized\ Duct\ Corrosion\ Rating = \frac{Total\ Duct\ Corrosion\ Rating}{6} \quad \text{Eq. 5-8}^4$$

This gives an average rating per foot of duct.

Prestressing Strand

The strand was also divided into 36, 2-in. intervals. All six outer wires and the inner wire were evaluated separately in each interval. Before evaluation, the strand was unwound so the interstices could be examined. The strand removed from each anchorage was evaluated in a similar fashion, except it was divided into twelve, 2-in. intervals. The strand numerical rating system is shown in Table 5.3.

Table 5.3: Numerical Rating System for Prestressing Strand³

Code	Meaning	Description	Rating
NC	No Corrosion	No evidence of corrosion.	0
D	Discoloration	No evidence of corrosion, but some discoloration from original color.	1
L	Light	Surface corrosion on less than one half of the interval, no pitting is present. Surface corrosion can be removed using cleaning pad.	2
M	Moderate	Surface corrosion on more than one half of the interval, no pitting. and/or Any corrosion that can not be completely removed using cleaning pad.	4
P1	Mild Pitting	Broad shallow pits with a maximum pit depth not greater than 0.02 in.	8
P2	Moderate Pitting	Pitting where the maximum pit depth ranged between 0.02 and 0.04 in.	16
P3	Severe Pitting	Pitting where the maximum pit depth is greater than 0.04 in.	32

The cleaning pad is the same used for the longitudinal bars and stirrups, and is applied in a similar fashion. The depths of the pits were measured with a depth gauge. The classification of pitting is based on tensile tests performed on corroded strand.³ Level P1 indicates pitting which reduces strand strength to 97% GUTS (Guaranteed Ultimate Tensile Strength), Levels P2 and P3 corresponded to 90% and 77% GUTS respectively.³ The total strand corrosion rating is given by Equation 5-9:

$$\text{Strand Corrosion Rating} = \sum_{i=1}^{36} R_{Outer,i} \times n_i + R_{Center,i} \quad \text{Eq. 5-9}^3$$

Where,

$R_{outer,i}$ = corrosion rating on outer wires, interval i

n_i = number of corroded outer wires in interval i

$R_{center,i}$ = corrosion rating on center wire, interval i

i = interval, 1 to 36

Since beams with different reinforcement arrangements had varying numbers of strands in each duct, a generalized value is used to compare the strand ratings in the ducts for each beam:

$$\text{Generalized Strand Corrosion Rating(Per Duct)} = \frac{\sum_{i=1}^m \text{Strand Corrosion Rating}_m}{m \times 6} \quad \text{Eq. 5-10}^3$$

Where,

m = number of strands in each duct: 2 for 2/3-PS Beams, 3 for 100%U Beams, and 4 for 100%S Beams

5.2 RESULTS OF FORENSIC ANALYSIS

The results of the forensic analysis for each individual beam are summarized in the following sections. In the case of photographs showing longitudinal elements such as bars, strand, and ducts, the value on the measuring tape in the photographs coincide with the plots showing the corrosion damage. However, this is not applicable for beams 1.1 and 3.1 since they are partial autopsies. Tables summarizing corrosion ratings are given for each beam. The organization of the data for each individual forensic analysis, including the plots, are done in the same fashion as Salas³ and Kotys⁴ so that comparisons can be easily made between data from both sets of autopsies.

5.2.1 Phase I Beams

5.2.1.1 Beam 1.1 (Non-PS, Unloaded):

1-X-XL-C



Figure 5.15: Beam 1.1-Side View (Left) and Top View (Right)

Table 5.4: Beam 1.1-Corrosion Rating Summary

	Maximum	Total	Generalized
Longitudinal Bars	523	18618	388
Stirrups	740	6668	635

This beam was partially autopsied after 4 years of testing by Salas³ and Kotys.⁴ Approximately half of the ponded region was removed and autopsied. The cut surfaces were sealed with epoxy and exposure testing was resumed. After 8 years of exposure

testing, 42 in. of material to one side of the centerline was removed, including 24 in. with the ponded region.

Beam Appearance

As shown in Figure 5.15 and Figure 5.18, there was severe staining and longitudinal cracking inside the ponded region as well as outside the north corner of the ponded region. The staining was centralized around the location of the bolster strips. Staining was also found around the locations of the chloride sampling points from the previous autopsies. The holes appeared to have never been sealed after the first partial autopsy. On the north side of the ponded region a crack averaging 0.06 in. in width was found along the line of the bolster strips. A transverse crack of 0.002 in. in width was found in the center of the ponded region. On the north side of the beam was an apparent flexural crack with large amounts of staining around it. It is likely that small cracks formed when the beam was handled during the 4-year partial autopsy. The crack width data are given in Figure 5.16. The “Average of Peak Crack Widths” is the average of the peak crack width at each cracked location in the autopsy area. This includes both the longitudinal and flexural cracks. The maximum crack width is the overall maximum crack width found at any point in the autopsy area.

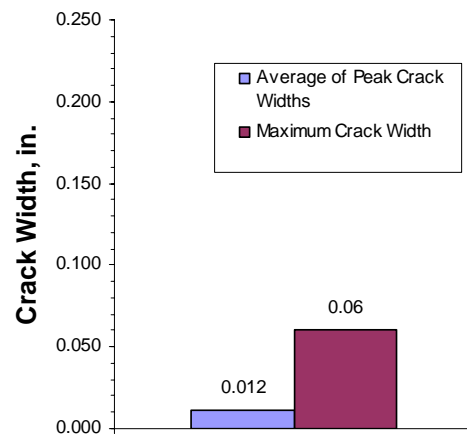


Figure 5.16: Beam 1.1 Crack Widths

Longitudinal Bars and Stirrups

There was pitting and some cross-sectional area loss on all longitudinal bars and most of the stirrups. The stirrup which was outside the ponded region exhibited pitting on its top portion but only moderate corrosion on its legs. The stirrups and bars are shown in Figure 5.17. The ratings for the stirrups and bars along with the beam crack maps are shown in Figure 5.18. In these plots the sum of the ratings for all longitudinal bars in each 2-in. interval is plotted. The total of the ratings for each stirrup along the length of the autopsy area is also shown. The corrosion ratings for the stirrups and bars are summarized in Table 5.4. In order to compare this beam with the other beams, additional stirrup and bar data were extrapolated in order to have a full 72 in. worth of data. This was done by “mirroring” the data from the section currently autopsied.



Figure 5.17: Beam 1.1 Autopsy Elements-Longitudinal Bar (Left) and Stirrup (Right)

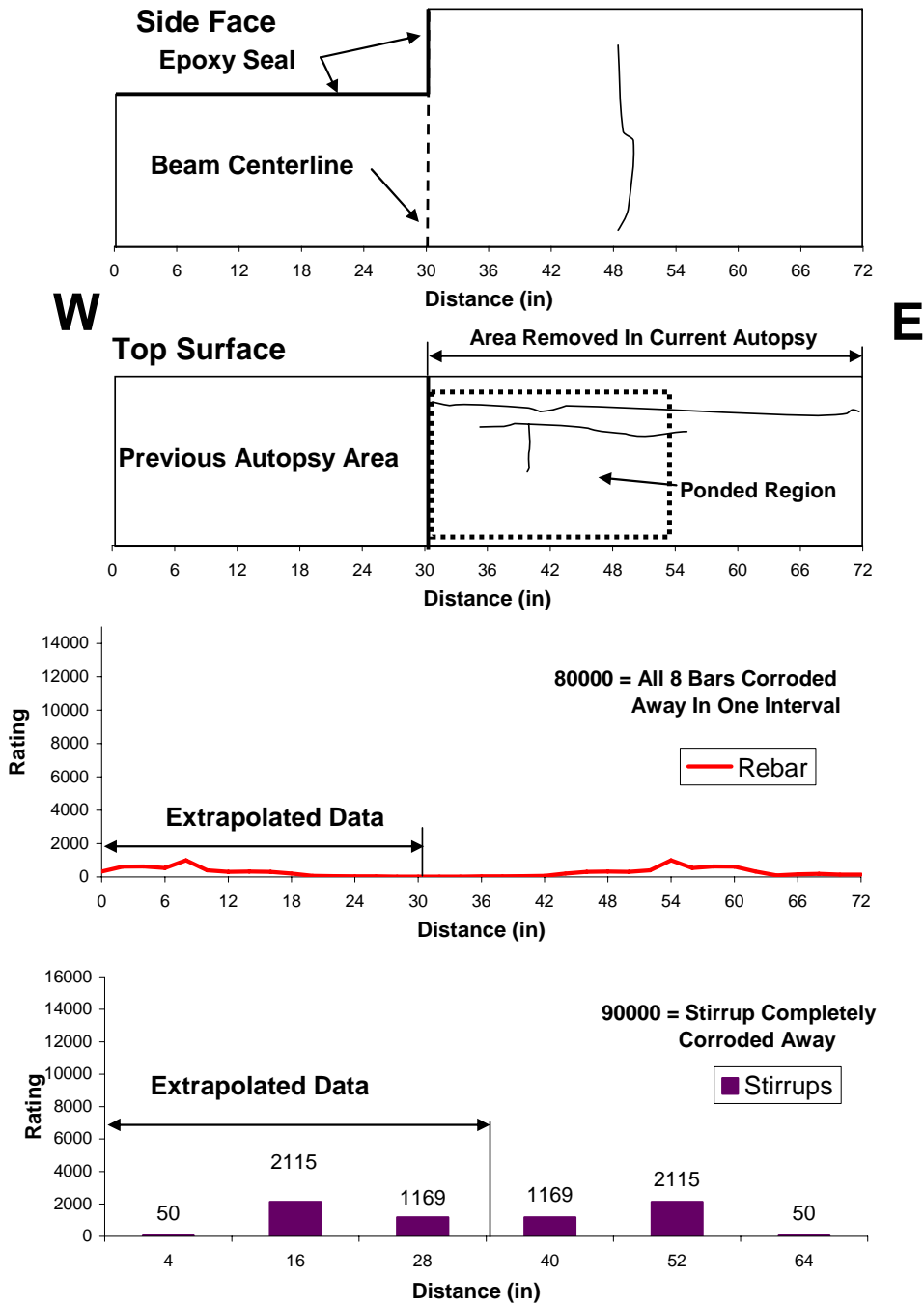


Figure 5.18: Beam 1.1-Crack Patterns and Corrosion Rating Graphs

5.2.1.2 Beam 1.2 (Non-PS, Service Load):

1-X-SL-C



Figure 5.19: Beam 1.2-Side View (Left) and Top View (Right)

Table 5.5: Beam 1.2 Corrosion Rating Summary

	Maximum	Total	Generalized
Longitudinal Bars	3571	119294	2485
Stirrups	4873	41600	3962

Beam Appearance

As shown in Figure 5.19 and Figure 5.23, there was severe staining and cracking both inside and outside the ponded region. There were large 1/8-in. cracks running from the west end of the salt bath through the entire remaining length of the autopsy area. Bolster strip corrosion was found in multiple locations in the ponded region. Some of the flexural cracks coincided with stirrup locations, while flexural cracks were found in other locations as well. Severe staining was found in the area of these flexural cracks. Also, there was longitudinal cracking on the side face of the beam. The combination of longitudinal cracking on the top and side of the beam would suggest severe bar corrosion, since the expansive effect of the corrosion products is essentially pushing the top corners of the beam off. The crack width data are given in Figure 5.21 . After cutting of the beam, it was observed that the longitudinal 1/8-in. cracks actually formed a crack plane right through the level of the severely corroded bars. Thus corrosion of the bars is

responsible for the longitudinal cracking. As the bars corroded, the expansive effects of the corrosion products cracked the concrete. This is shown in Figure 5.20. Note that the block is upside down compared with its position during exposure testing.



Figure 5.20: West End of Autopsy Block-Beam 1.2

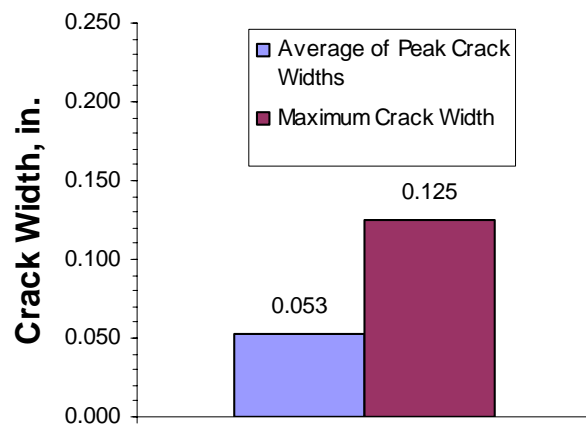


Figure 5.21: Beam 1.2 Crack Widths

Longitudinal Bars and Stirrups

During autopsy, pitting and cross-sectional area loss was found throughout all the longitudinal bars and the stirrups. The most severe section loss in the bars was found in the area of the flexural cracks. The most corroded stirrup was that located 54 in. from the west end of the autopsy area. The corroded bars and stirrups are shown in Figure 5.22. Bar and stirrup corrosion ratings are given in Figure 5.23, and the corrosion ratings are summarized in Table 5.5.



Figure 5.22: Beam 1.2 Autopsy Elements-Longitudinal Bar (Left) and Stirrup (Right)

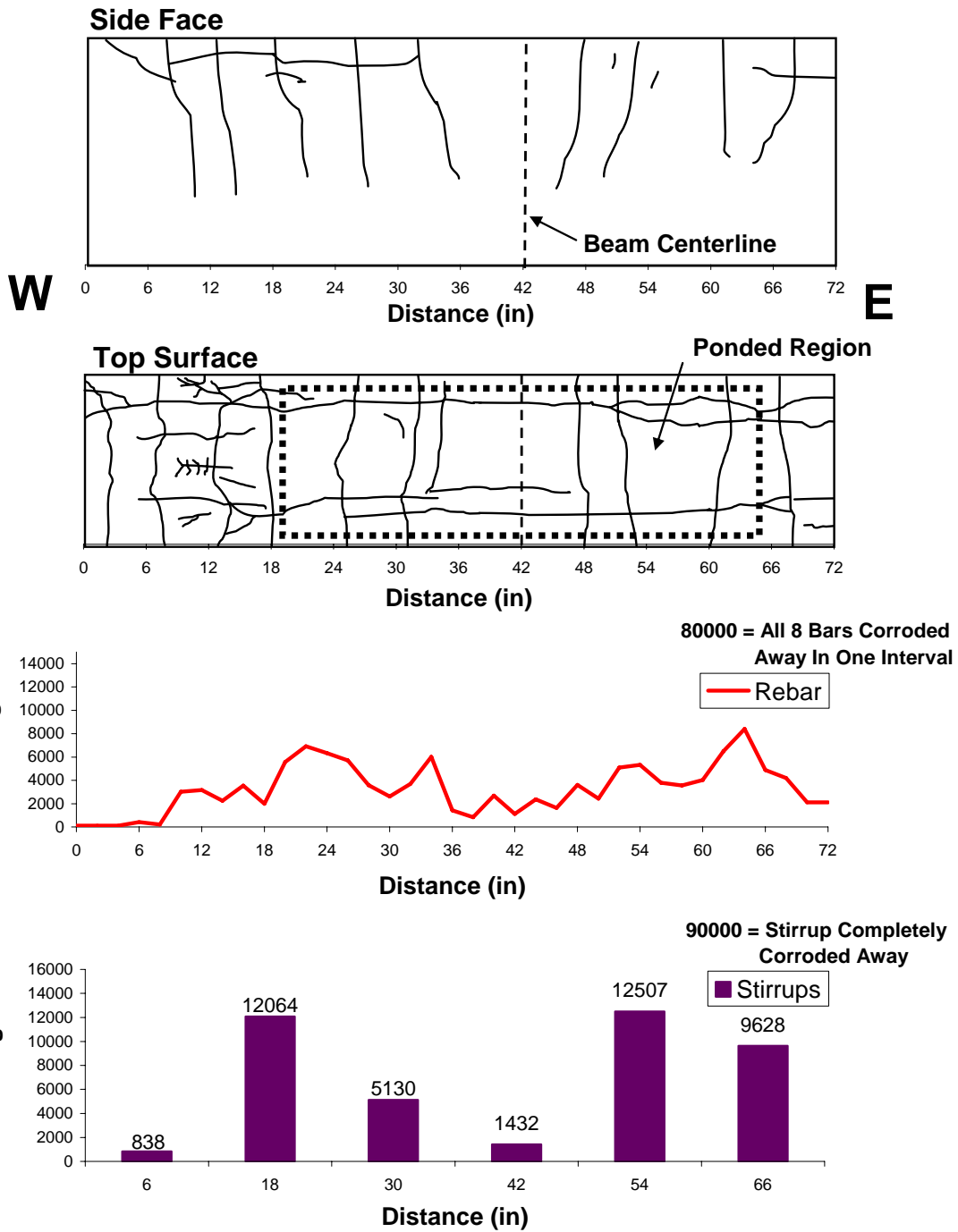


Figure 5.23: Beam 1.2-Crack Patterns and Corrosion Rating Graphs

5.2.1.3 Beam 1.4 (Non-PS, Overload):

1-X-OL-C

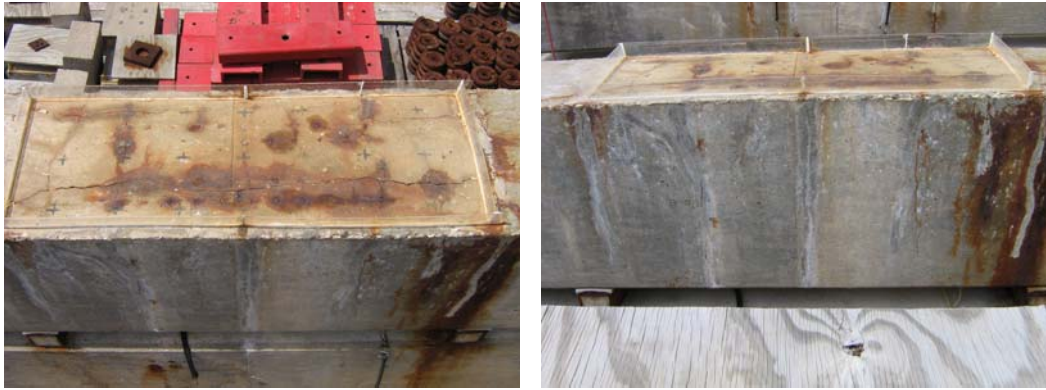


Figure 5.24: Beam 1.4-Top View (Left) and Side View (Right)

Table 5.6: Beam 1.4 Corrosion Rating Summary

	Maximum	Total	Generalized
Longitudinal Bars	3403	108635	2263
Stirrups	3193	38594	3676

Beam Appearance

As shown in Figure 5.24 and Figure 5.27, there was severe staining and cracking throughout the ponded region. The staining was concentrated around longitudinal cracks. These longitudinal cracks typically measured 0.1 in. in width. In general these cracks corresponded to the locations of the steel bolster strips. The maximum width of these longitudinal cracks was 1/8-in.. There was also staining on the side of the beam, especially just outside the west end of the ponded region (This is shown on the far right sides of the pictures in Figure 5.24). Similar to beam 1.2, upon removal of the block from the center of the beam it was found that the longitudinal cracks formed a crack plane right through the bars. The crack width data are given Figure 5.25.

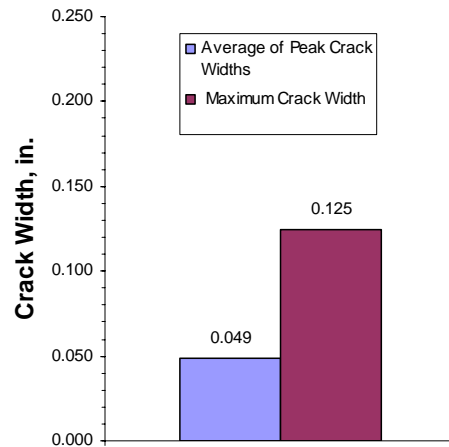


Figure 5.25: Beam 1.4 Crack Widths

Longitudinal Bars and Stirrups

Considerable cross-sectional area loss and pitting was found on all bars and most of the stirrups, with the most severe area loss in the bars corresponding to the locations of flexural cracks. The pitting was less severe outside the ponded region, but present nonetheless. The most severely corroded stirrup corresponded to the flexural crack at 29 in. from the west end of the autopsy area. The worst damage seen on the stirrup was essentially a reduction in diameter from ½-in. to approximately 3/8-in.. As previously stated, considerable staining was seen at the flexural crack at this location. The bars and stirrups are shown in Figure 5.26. Crack patterns and corrosion rating graphs are given in Figure 5.27.



Figure 5.26: Beam 1.4 Autopsy Elements-Longitudinal Bar (Left) and Stirrup (Right)

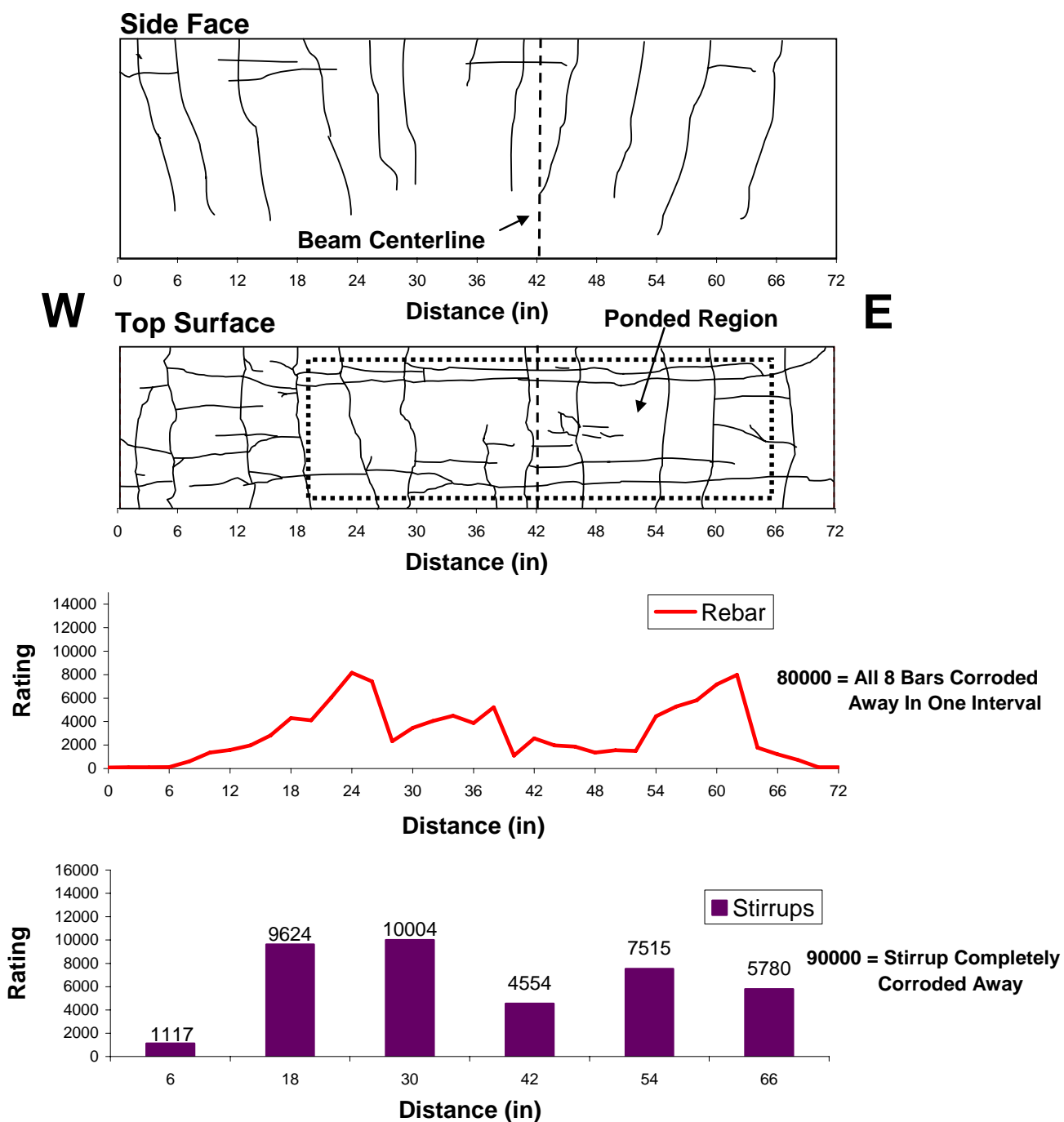


Figure 5.27: Beam 1.4-Crack Patterns and Corrosion Rating Graphs

5.2.1.4 Beam 2.1 (2/3-PS, Small Crack Load):

1-P-CL-C-SD-HS-NG-NS-D1

1-P-CL-C-SD-IS-NG-NS-D2



Figure 5.28: Beam 2.1-Side View (Left) and Top View (Right)

Table 5.7: Beam 2.1 Corrosion Rating Summary

	Maximum	Total	Generalized
Longitudinal Bars	10000	328956	7644
Stirrups	5633	39035	3718
North Duct	4110	84767	14128
South Duct	4714	66997	11166
North Strand	52	1570	131
South Strand	88	3236	270

Beam Appearance

As shown in Figure 5.28 and in the crack maps in Figure 5.32, heavy staining and cracking was observed in the ponded region. Minor staining was seen outside the west end of the ponded region, with small cracks running in both directions. Inside the ponded region, longitudinal cracks following the bolster strips measured about 0.01 in. in width. Severe staining was seen in the area of these cracks. The flexural cracks also showed severe staining on the top of the beam. The largest crack width was from a longitudinal crack about 18-in. to the east of the beam centerline. This crack measured 1/8-in. in width. On the side faces of the beam, the flexural cracks had severe staining emanating from them, which was likely from the corrosion of stirrups because all flexural crack locations corresponded with stirrup locations. Longitudinal cracks with staining were also

found on the side of the beam as well. The large amounts of longitudinal cracks suggest severe corrosion within the beam. Indeed, when the autopsy block was removed from the center of the beam cracking through the bars was seen similar to that in the Non-PS beams. The crack width data for the beam are given in Figure 5.29.

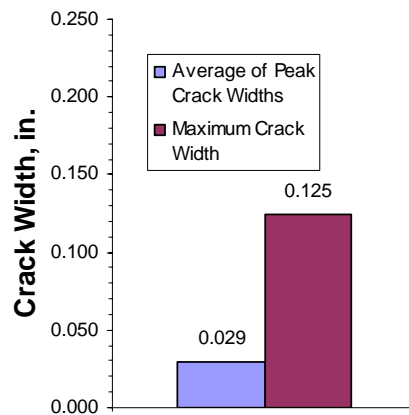


Figure 5.29: Beam 2.1 Crack Widths

Longitudinal Bars and Stirrups

Upon autopsy, it was found that all stirrups and bars suffered severe pitting and cross-sectional area loss (See Figure 5.31). In the area of the flexural cracks, the smaller bars completely corroded away, some losing almost 2-in. in length. The stirrups also had severe pitting and area loss, with the worst stirrup 12-in. to the west of the beam centerline. The ratings along the length of the beam for the bars and stirrups, as well as the other elements of the beam, are given in Figure 5.32. The corrosion ratings are summarized in Table 5.7.

Tendons

The south duct was fitted with an industry standard splice, while the north duct had a heat shrink splice. The industry standard splice suffered tremendous area loss to its top portion and pitting corrosion was found on the remains of the inside surface of the splice. The duct beneath had large holes and pitting. The heat-shrink splice on the south duct showed severe staining and corrosion deposits on the inside. The section of duct beneath the splice was found to be heavily pitted and holed. In this case the holes were

smaller than those in the splice zone of the south duct. The splices are shown in Figure 5.30.



Figure 5.30: Beam 2.1 Duct Splices-South Duct Industry Standard Splice (Left) and North Duct Heat Shrink Splice (Right)

Both ducts were heavily pitted with large holes that caused large surface area loss. The south duct suffered severe surface area loss throughout, with the entire top portion of the duct gone from 14 in. to 18 in. to the west of the beam centerline. The north duct showed similar large surface area loss, however, little corrosion was seen in the portion outside the ponded region. The surface area loss was not as large as that beneath the south duct splice. The ducts are shown in Figure 5.31. The corrosion ratings for the ducts are plotted in Figure 5.32. The ratings are summarized in Table 5.7.

The south duct grout showed no large voids. However, there was some evidence of porosity in the form of bubbles at the top of the grout. The grout was found to be cracked in numerous locations, and staining was found on the crack faces. The maximum chloride content in the south duct grout was 0.237% by weight, far above the corrosion threshold of 0.033%. This maximum value occurred at the far east end of the duct. The north duct grout was similar. However, small surface voids were found on the north duct, and in some cases corrosion products were found inside the voids. The maximum chloride content in the north duct grout was 0.649%, which was found 6 in. to the west of the beam centerline. This is over 20 times larger than the threshold for corrosion. The grout from both ducts is shown in Figure 5.31. The grout chloride contents are plotted in Figure 5.32.

The strands in both ducts were pitted. The two south duct strands showed mild pitting throughout, and moderate to severe pitting on a few wires within the ponded region. Mild pitting was also found on portions of the strands outside the ponded region. The north duct strands had much less pitting than the south duct strand, with only mild pitting found at the 3 flexural crack locations near the beam centerline. The strands are shown in Figure 5.31. Corrosion ratings for the strand are plotted in Figure 5.32 and are summarized in Table 5.7.

It is interesting to note from Figure 5.32 that the reinforcing bar ratings, duct and strand ratings all reach peak ratings at the same locations, which correspond with the location of cracks. Also, the strands from the south duct show more corrosion than the north duct strand. However, according to the chloride content data, the south duct had smaller grout chloride contents than the north duct. It is possible that the industry standard splice allowed more moisture in initially than the heat shrink splice, resulting in more strand corrosion. However, once the ducts corroded away more heavily, the splice type became irrelevant, as chlorides could then enter through the large holes in the ducts.



Longitudinal Bar



Stirrup



South Duct (Top Half)



North Duct (Top Half)



South Duct Grout



North Duct Grout



South Duct Strand



North Duct Strand

Figure 5.31: Beam 2.1 Autopsy Elements

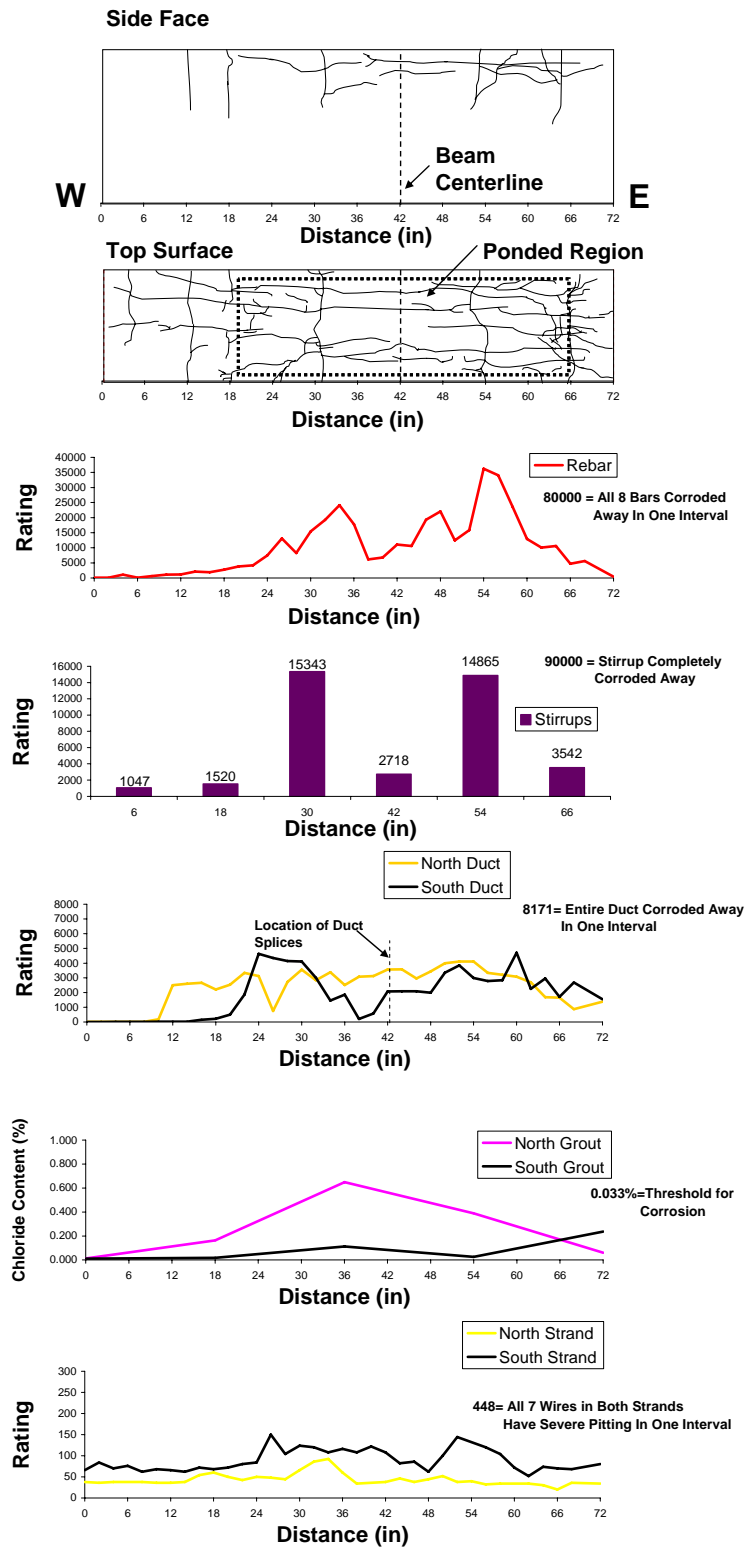


Figure 5.32: Beam 2.1-Crack Patterns and Corrosion Rating Graphs

5.2.1.5 Beam 2.2 (2/3-PS, Service Load):

1-P-SL-C-SD-XS-NG-NS-D1

1-P-SL-C-SD-IS-NG-NS-D2



Figure 5.33: Beam 2.2-Side View (Left) and Top View (Right)

Table 5.8: Beam 2.2 Corrosion Rating Summary

	Maximum	Total	Generalized
Longitudinal Bars	10000	371200	7733
Stirrups	4412	31604	3010
North Duct	6284	79567	13261
South Duct	7166	118394	19732
North Strand	72	2340	195
South Strand	184	4564	380

Beam Appearance

As shown in Figure 5.33 and Figure 5.37, severe staining and cracking was observed inside the ponded region. The staining was concentrated around the flexural cracks at 30, 42, and 53 in. from the west end of the autopsy area. Staining was also observed at bolster strip locations. Longitudinal cracks were observed running along the length of the beam. These cracks typically measured about 0.06 in. in width inside the ponded region. The longitudinal cracks extended outside the west end of the ponded region. The maximum crack width found was located 1 in. inside the west end of the ponded region, where one of the longitudinal cracks measured 1/8-in. in width. Staining was also observed emerging from the flexural cracks on the side of the beam. The large longitudinal cracks and staining suggests severe corrosion within the beam. The crack width data for the beam are given in Figure 5.34.

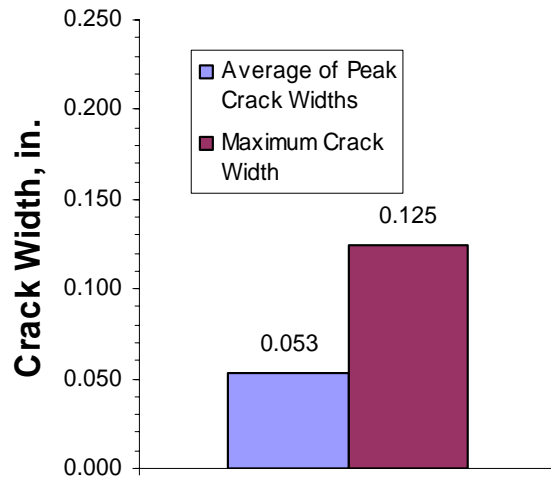


Figure 5.34: Beam 2.2 Crack Widths

Longitudinal Bars and Stirrups

Upon autopsy, it was found that the longitudinal bars and stirrups suffered severe pitting and area loss throughout the autopsy area (See Figure 5.36). Pitting was found even outside the ponded region. Approximately 8-in. of one of the #3 bars was completely corroded away in the vicinity of the flexural crack at 30 in. from the west end of the autopsy area. In the vicinity of the flexural cracks from 42 to 54 in., approximately 6-in. of one of the #3 bars was completely corroded away. The worst stirrup was that 12 in. to the west of the beam centerline. This corresponds to 30 in. in the crack maps and corrosion rating graphs in Figure 5.37. In one location this stirrups diameter was reduced by half. This corresponded to one of the areas of severe staining seen on the exterior surface of the beam. The longitudinal bars and stirrups are shown in Figure 5.36. The ratings for the stirrups and bars are shown in Figure 5.37, and are summarized in Table 5.8.

Tendons

The south duct had an industry standard splice, while the north duct had no splice. The industry standard splice suffered very severe area loss, both to its top and bottom portions. Pitting corrosion was found on the inside of the splice. The length of galvanized

duct beneath the splice suffered severe pitting and the loss of nearly half of the top portion of the duct. The splice is shown in Figure 5.35.



Figure 5.35: Beam 2.2 South Duct Splice

Both ducts were heavily holed and as a result both ducts had tremendous surface area loss. The north duct suffered surface area loss and pitting, even outside the ponded region, with the loss of more than half of the top of the duct in several locations in the vicinity of the centerline of the beam. Pitting was also found on the inside of the duct in the vicinity of the holes. The south duct was more severely corroded than the north duct. The last two feet of the top portion of the south duct were basically missing. Only fragments of the duct ribbing were recovered in this area. At 26 in. from the west end of autopsy area, the duct loss was so severe that the strand could be plainly seen and was severely pitted. The ducts are shown in Figure 5.36. The duct corrosion ratings are plotted in Figure 5.37 and are summarized in Table 5.8.

Corrosion products were found deposited on the grout throughout both ducts. The north duct grout was cracked at multiple locations, with severe staining on the crack faces. The most severe staining was at a crack 30 in. from the west end of the autopsy area. Small voids were found indicating either bleed water accumulation or air pockets. The maximum chloride content in the north grout was 0.290%, which was at a location 12 in. to the east of the beam centerline. This corresponds to a flexural crack location. The south duct grout was also cracked. A large bleed water void was found in the south duct in the vicinity of the beam centerline. The void was about 1.2 in. wide. This void continued through the entire length of the autopsy area. Staining was also found on the

crack faces of the grout, corresponding to locations of severe loss in duct surface area. The maximum chloride content in the south duct was 0.329%, slightly higher than the north duct. The grout from both ducts is shown in Figure 5.36. The grout chloride contents from both ducts are plotted in Figure 5.37.

The strands from both ducts varied in the severity of corrosion. The north duct strands showed moderate corrosion throughout, with mild pitting in the vicinity of the beam centerline. Severe pitting was found on some wires at 30 to 32 in. from the west end of the autopsy area. One of the wires actually broke during unwinding of the strand. This is shown in Figure 5.36. The south duct strand was much more heavily corroded than the north duct strand. Mild pitting was found throughout, with instances of moderate to severe pitting found in multiple locations. At 28 in. from the west end of the autopsy area it was found that three wires on one of the strands had been reduced in diameter by about 33%. One of these wires is shown in Figure 5.36. It interesting to note from Figure 5.37 that the peaks in the south duct strand damage occurred within the vicinity of the centerline crack and the flexural crack at 12 in. to the west end of the centerline. The corrosion ratings for the strand are plotted in Figure 5.37 and are summarized in Table 5.8.

It is significant that the most severe duct damage observed in the south duct was where the large bleed water void occurred. The presence of the void allowed for moisture to reach the inside of the duct more easily. This is also where the maximum chloride content was observed for this duct. The more severe strand damage in the south duct is likely due to the presence of the bleed water void as well since the duct corroded away and less grout “cover” was available to the strand. The presence of the industry standard splice likely allowed an initial entry of moisture, but as is clear from the chloride content data that in the end the presence of the splice became negligible as rest of the duct began to corrode away.



Longitudinal Bar



Stirrup



South Duct



Top of North Duct



South Duct Grout



North Duct Grout



Single Wire from South Duct Strand



North Duct Strand

Figure 5.36: Beam 2.2 Autopsy Elements

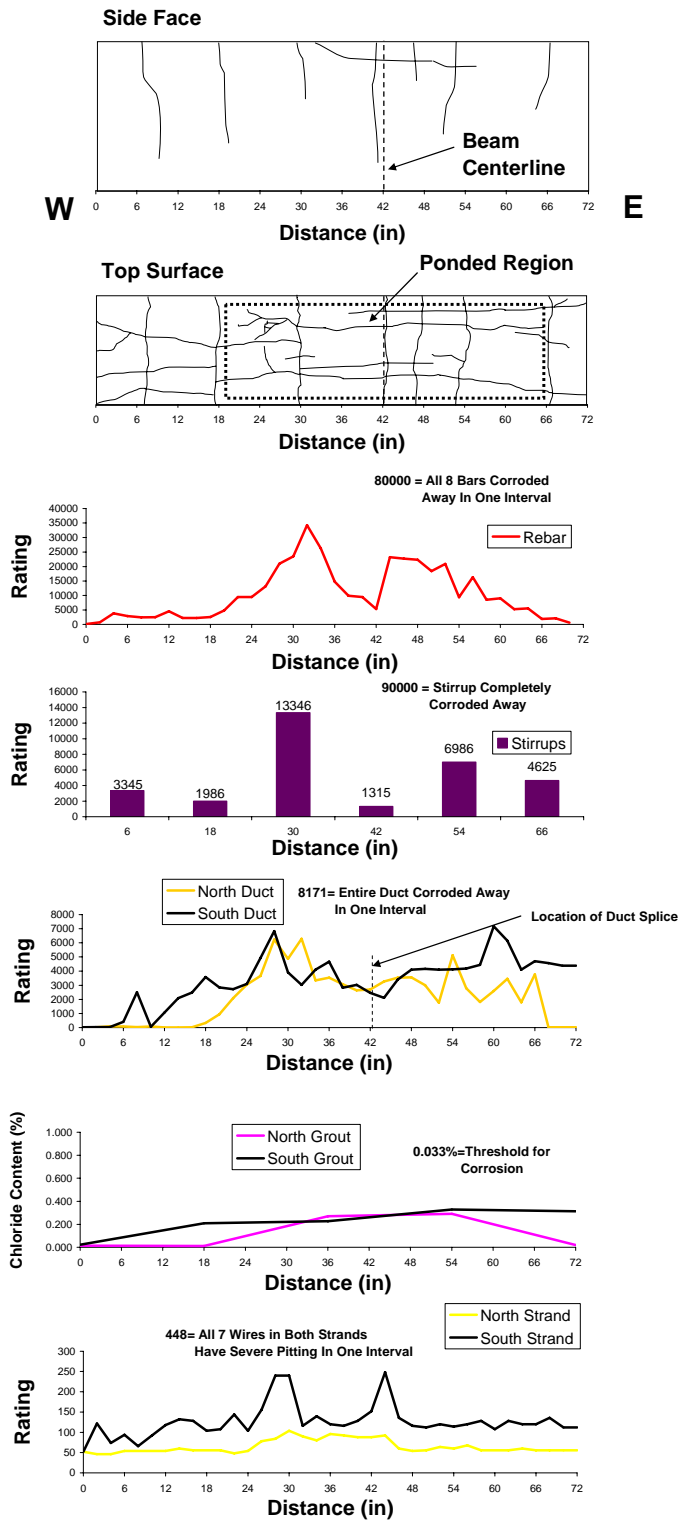


Figure 5.37: Beam 2.2- Crack Patterns and Corrosion Rating Graphs

5.2.1.6 Beam 2.4 (2/3-PS, Overload):

1-P-OL-C-SD-HS-NG-NS-D1

1-P-OL-C-SD-IS-NG-NS-D2



Figure 5.38: Beam 2.4-Side View (Left) and Top View (Right)

Table 5.9: Beam 2.4 Corrosion Rating Summary

	Maximum	Total	Generalized
Longitudinal Bars	10000	168834	3517
Stirrups	1922	15169	1445
North Duct	4257	45914	7652
South Duct	6771	58433	9739
North Strand	40	1972	164
South Strand	48	2436	203

Beam Appearance

As expected, more flexural cracks were observed on this beam than in 2.1 and 2.2 because of the temporary overloading which was done at the beginning of exposure testing. As is apparent in Figure 5.38 and in Figure 5.42, severe staining and longitudinal cracking was observed inside the ponded region. The staining was concentrated around the longitudinal cracks which ran the length of the ponded region. The largest crack width observed for these longitudinal cracks was 1/8-in.. This was at the extreme east end of the ponded region. These cracks continued even outside the ponded region. The cracks seemed to run parallel to the steel bolster strips. Crack width data are given in Figure 5.39. Staining was also seen emerging from the flexural cracks on the side of the beam as well. Overall, the exterior appearance of the beam suggests severe corrosion. When the block was removed from the center of the beam, the longitudinal cracks were found to

form the typical crack plane which went through the corroded bars. The crack widths are given in Figure 5.39, while the crack patterns are plotted in Figure 5.42.

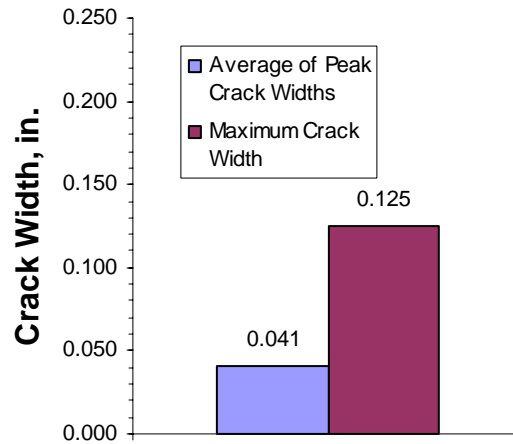


Figure 5.39: Beam 2.4 Crack Widths

Longitudinal Bars and Stirrups

Upon autopsy, all bars and stirrups were found to be heavily pitted and reduced in cross-sectional area (See Figure 5.41). In the case of the longitudinal bars, some pitting was observed even outside the ponded region. The most severe bar damage was approximately 12 in. west of the beam centerline (This corresponds to 30 in. on the crack maps and rating graphs shown in Figure 5.42). This coincides with the location of a flexural crack as well as the severe patches of staining mentioned previously. The bar damage consisted of the total loss of approximately 4-in. of two of the #3 bars, and the loss of around half the cross-sectional area of one of the other nearby #3 bars. The two most heavily corroded stirrups were those located at 12 in. to the west and east of the beam centerline. The stirrup furthest east was reduced in diameter by nearly 25% in one interval. The stirrups and bars are shown in Figure 5.41. The bar and stirrup corrosion ratings along the length of the beam are shown in Figure 5.42, and are summarized in Table 5.9.

Tendons

Both ducts in the beam were spliced at the beam centerline. The south duct had an industry standard splice while the north duct had a heat shrink splice. Most of the top

half of the south duct splice corroded away, while the remainder was pitted. The inside surface had severe pitting adjacent to the holes. The bottom portion of the splice did not have any holes, but was pitted on the exterior in a few locations. The duct portion directly beneath the splice showed large holes and pitting. The north duct heat shrink splice showed discoloration on its inside surface. The portion of duct beneath it had large holes and pitting. Therefore, in this instance both splices performed very poorly in keeping moisture out of the splice zone. The heavy duct corrosion in the splice zone suggests large moisture ingress. The splices are shown in Figure 5.40.



Figure 5.40: Beam 2.4 Duct Splices-South Duct Industry Standard Splice (Left) and North Duct Heat Shrink Splice (Right)

Both ducts were heavily holed and thus had large surface area loss. In the case of the south duct severe surface area loss was seen 12 in. to the west and east of the beam centerline (corresponding to flexural crack locations). The last two feet of the top portion of the duct was nearly corroded away, and only fragments of the duct ribbing were recovered. The north duct showed similar performance, except the last two feet were more intact than the south duct, with large holes instead of complete duct loss. For both ducts, pitting was observed inside the duct in the vicinity of the holes. The ducts are shown in Figure 5.41. The duct corrosion ratings are plotted in Figure 5.42 and summarized in Table 5.9.

The south duct grout had corrosion deposits throughout from the duct corrosion. Bubbles indicating porosity were evident. The grout was cracked and staining was found in some areas. At about 22 in. from the west end of the autopsy area, a large bleed water

void was found. This void became deeper moving east, finally, the grout essentially terminated at about 27 in. from the east of the autopsy area, with only fragments found beyond that point. The highest chloride content measured in the south duct was 0.089%, and was found 6 in. to the west of the beam centerline. The threshold for corrosion is 0.033%. The north duct had a small bleed water void starting at about 7 in. from the east end of the autopsy area. Therefore, the north duct had better grouting than the south duct. The north duct grout had maximum chloride content of 0.455%, which was at location 12 in. to the east of the beam centerline. The grout from both ducts is shown in Figure 5.41, with the chloride contents plotted in Figure 5.42.

The strands in both ducts varied had varied amounts of corrosion. The north duct strands showed light to moderate corrosion in the area outside the ponded region. Inside the ponded region, moderate corrosion was observed on more wires. At 8 to 12 in. east from the centerline (Corresponding to 54 in. on the corrosion rating graphs), mild pitting was observed on both the outer wires and on the center wires on one of the two strands. No pitting was seen on the second strand. This area of pitting corresponds to the location of a flexural crack and where very severe surface area loss was observed in the duct itself. The south duct strand was more severely corroded, with pitting first observed in the center wire at 18 in. to the west of the beam centerline. At 26 in. from the west end of the autopsy area moderate pitting was seen on the center wire. Pitting was seen on the outer wires starting at the beam centerline, and mild strand pitting continued through to the end of the autopsy area. The strands are shown in Figure 5.41, with the corrosion ratings shown in Figure 5.42, and summarized in Table 5.9.

It is very significant to note that the lack of grout at the end of the south duct resulted in more severe damage to the duct and to the strand (In comparison to the north duct) at the end of the duct.



Longitudinal Bar



Stirrup



Top of South Duct



Top of North Duct



South Duct Grout



North Duct Grout



South Duct Strands (Both Strands shown)



North Duct Strand

Figure 5.41: Beam 2.4 Autopsy Elements

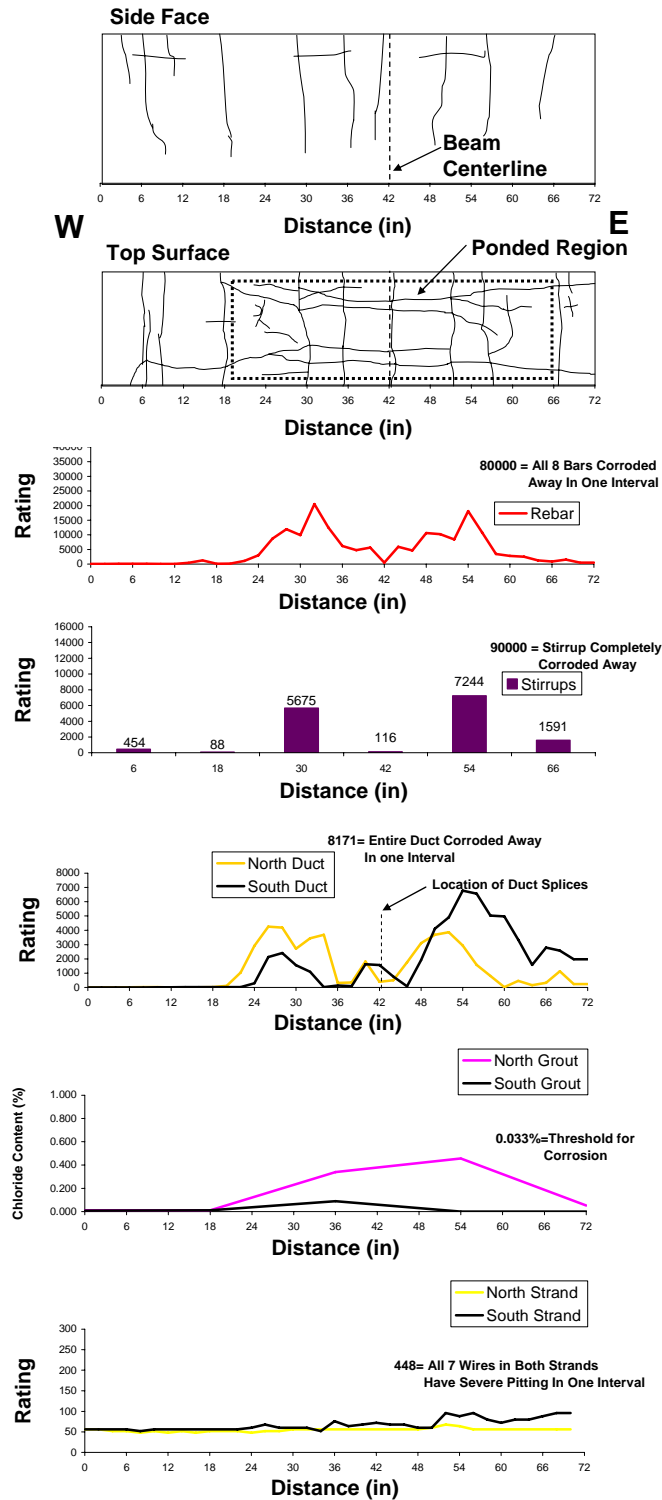


Figure 5.42: Beam 2.4- Crack Patterns and Corrosion Rating Graphs

5.2.1.7 Beam 3.1 (100%U, Unloaded)

1-U-XL-C-SD-HS-NG-NS-D1

1-U-XL-C-SD-IS-NG-NS-D2



Figure 5.43: Beam 3.1-Side View (Left) and Top View (Right)

Table 5.10: Beam 3.1 Corrosion Rating Summary

	Maximum	Total	Generalized
Longitudinal Bars	8	184	23
Stirrups	800	1172	112
North Duct	8	53	9
South Duct	14	26	4
North Strand	32	2662	148
South Strand	28	2475	138

This beam was partially autopsied at 4 years of testing by Salas³ and Kotys⁴. Approximately half of the ponded region was removed and autopsied. The cut surfaces were sealed with epoxy and testing continued. After 8 years of exposure testing, 42 in. of material to one side of the centerline was removed, including 24 in. of the ponded region.

Beam Appearance

As shown in Figure 5.43 and Figure 5.46, the only damage observed on the outside of the beam was spalling and minor staining in the vicinity of the bolster strips. This was at the west end of the autopsy area near the cutting surface from the previous autopsies. No actual cracking was seen on the specimen. Therefore, no crack width data are given.

Longitudinal Bars and Stirrups

In general, the longitudinal bars only showed slight discoloration. However, at the face of the cutting area from the previous autopsies moderate corrosion was found on both bars. The stirrups were slightly discolored with only a few instances of light to moderate corrosion. However, the stirrup which was near the cutting area from the previous autopsies had mild area loss and pitting in its top portion. The stirrups and bars are shown in Figure 5.45, with the corrosion ratings plotted in Figure 5.46 and summarized in Table 5.10. In order to have a fully 72 in. worth of data for comparison to the other beams, additional data was extrapolated by “mirroring” the data about the beam centerline.

Tendons

Since the splices of the ducts were at the beam centerline, only half of the splice remained from each duct to be autopsied. The remaining half of each splice was removed during the previous autopsies. The south duct industry standard splice had small holes and pitting on both the top and bottom near the cut face of the beam. Pitting was observed on the inside of both splice halves as well. The north duct heat shrink splice had discoloration on the inside surface where duct corrosion had taken place. Otherwise, no other discoloration or corrosion deposits were seen on the heat shrink splice. Both splices are shown in Figure 5.44.



Figure 5.44: Beam 3.1 Duct Splices-South Duct Industry Standard Splice (Left) and North Duct Heat Shrink Splice (Right)

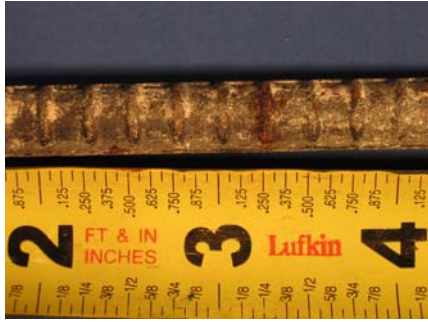
Both ducts were only slightly corroded. The top outside surface of the south duct did have pitting near the previous cutting area, beneath the industry standard splice. Only a few instances of light corrosion were found on the inside and outside of the remainder of the duct. The north duct performed similarly, with pitting found in the same general location as the south duct. In this case the staining was about 1 in. to the east of the end of the heat shrink splice. The ducts are shown in Figure 5.45, with the ratings plotted in Figure 5.46 and summarized in Table 5.10.

The south duct grout showed evidence of a shallow bleed water void on the west end, right at the previous autopsy cutting area. The void was only about 2-in. long and was stained on the inside. Smaller bleed water voids were also seen at the top of the grout, spaced about every 8-in.. These voids terminated about 2 feet from the west end of the autopsy area. The grout also showed bubbles which indicate porosity. The north duct had several small, shallow bleed water voids. The largest was 2 in. long and about ¼ in. deep. This void was located about 10 in. from the west end of the autopsy area. The grout is shown in Figure 5.45. The maximum chloride content for the south duct grout was 0.243%, while for the north duct 0.257%. These two values were found at the far west of the autopsy area, near the cut face from the previous autopsies. The chloride content data is plotted in Figure 5.46.

The strands from both ducts showed light to moderate corrosion throughout. At the cutting area on the west end of the autopsy area, the exteriors of the strand had a large buildup of corrosion products. The light to moderate corrosion for the remainder of the autopsy was concentrated in the interstitial zones. The strand is shown in Figure 5.45, and the corrosion ratings are plotted in Figure 5.46 and summarized in Table 5.10.

The corrosion damage to all of the autopsy elements was concentrated on the west end of the of autopsy area. This corresponds to 42 in. on the corrosion rating graphs in Figure 5.46. The chloride content data clearly shows large chloride ingress at the cut face of the beam. Thus it would appear that the damage to the beam was due to chloride ingress at the cut face of the beam. The moderate strand corrosion in the interstitial areas suggests that moisture which entered at the west end of the autopsy area was transmitted

down the entire length of the strand, causing moderate corrosion on the interstices of the wires. But other than near the previous autopsy area, the lack of serious corrosion on the bars, ducts, and stirrups clearly shows that corrosion is dramatically reduced if cracking is absent.



Longitudinal Bar



Stirrup



Top of South Duct



Top of North Duct



South Duct Grout



North Duct Grout



South Duct Strand



North Duct Strand

Figure 5.45: Beam 3.1 Autopsy Elements

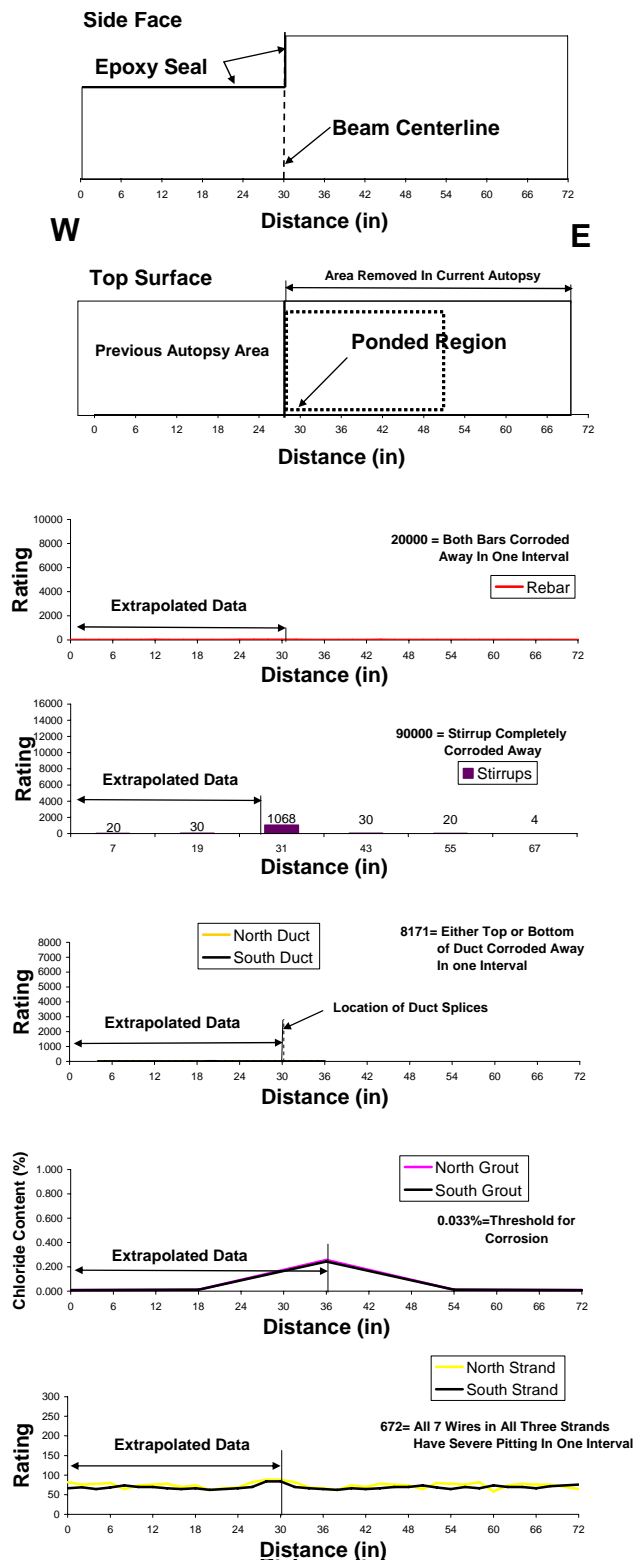


Figure 5.46: Beam 3.1-Crack Maps and Corrosion Rating Graphs

5.2.1.8 Beam 3.4 (100%U, Overload):

1-U-OL-C-SD-HS/HSD-NG-NS-D1

1-U-OL-C-SD-IS/ISD- NG-NS-D2



Figure 5.47: Beam 3.4-Side View (Left) and Top View (Right)

Table 5.11: Beam 3.4 Corrosion Rating Summary

	Maximum	Total	Generalized
Longitudinal Bars	8065	22200	2571
Stirrups	3343	19855	1891
North Duct	4147	49483	8247
South Duct	4089	45187	7531
North Strand	44	3030	168
South Strand	36	2978	165

Beam Appearance

This beam was originally intended to be at constant service load, but in order to crack the beam the previous researchers were forced to overload it. As shown in Figure 5.47 and Figure 5.50, severe staining and cracking was found within the ponded region. No staining was observed outside the west end of ponded region, but staining from bolster strip corrosion was seen outside the east end. Staining was also found on the side of the beam, emanating from the flexural cracks. Longitudinal cracks ran parallel with the bolster strips, and the maximum crack width was 0.06 in., which was measured from one of the longitudinal cracks. The cracks continued outside the ponded region. Longitudinal cracks were also observed on the side of the beam, in the vicinity of the flexural cracks as well. This suggests a large amount of corrosion within the beam. The crack width data are given in Figure 5.48.

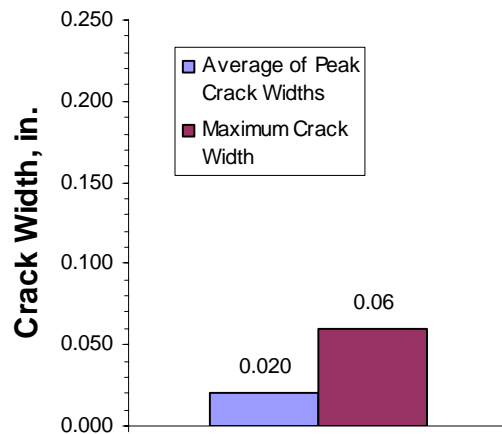


Figure 5.48: Beam 3.4 Crack Widths

Longitudinal Bars and Stirrups

Upon autopsy, it was found that within the ponded region, the bars were mostly pitted with area loss at flexural crack locations (See Figure 5.51). The stirrups were also heavily pitted with cross-sectional area loss. Both #3 longitudinal bars had only mild to moderate corrosion outside the ponded region. Instances of light to moderate corrosion were observed in the areas without flexural cracking that were still in the ponded region. The most severe bar corrosion was at the flexural crack 12 in. to the west of the beam centerline, where one of the bars was reduced in diameter by over 2/3. The bar broke in half at this location upon removal from the beam during autopsy. The other bar had moderate area loss at this location. The stirrups which corresponded to flexural crack locations within the ponded region were severely pitted and suffering from cross-sectional area loss. The area loss was the worst on the stirrup 12 in. to the west of the beam centerline. In one interval the stirrups diameter was reduced to 0.375 in. from an original diameter of 0.5 in.. The stirrup which was outside the west end of the ponded region but still beneath a flexural crack was only moderately corroded. The bars and stirrups are shown in Figure 5.51, with the ratings plotted in Figure 5.50 and summarized in Table 5.11.

Tendons

Unlike the other Phase I beams, beam 3.4 had two splices in each duct. The purpose of two splices was to test the effect of accidental damage to either the industry

standard splice or the heat shrink splice. The south duct was used to test the industry standard splice, with the west-most splice damaged in the form of poor duct taping. The north duct was used to test the heat shrink splice, with the west splice damaged in the form of a 1-in. tear at the seam between the two duct portions. For both ducts each splice was 18 in. either to the west or east of the beam centerline. Upon autopsy, the “damaged” industry standard splice on the south duct was found to be severely corroded. Half of the top portion of the splice was corroded away, with pitting and holes on the remaining portion. The bottom portion of the duct was also severely pitted in some areas, with one end corroded away directly beneath the splice. Pitting was also found on the insides of both the top and bottom halves of the splice. Pitting and holes were also found in the duct directly beneath the splice. The corrosion damage to the “undamaged” splice was similar, but no holes were found on the bottom portion. Holes and pitting were found in the duct portion directly beneath this splice. Both heat shrink splices on the north duct had corrosion deposits on their inside surfaces. The “damaged” splice had smaller deposits on it, while the duct beneath was pitted. The “undamaged” splice had more deposits, and pitting and holes were observed on the duct directly beneath it. The splices are shown in Figure 5.49. Note that the circular hole in the “damaged” heat shrink splice is due to the drilling of chloride samples.

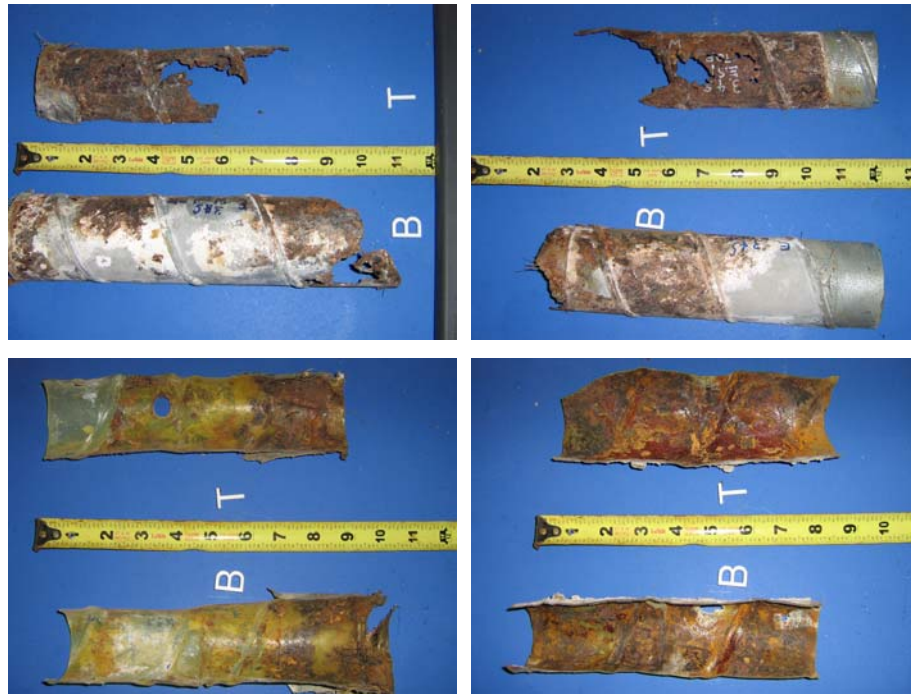


Figure 5.49: Beam 3.4 Duct Splices-South Duct "Damaged" Industry Standard Splice (Top Left) and "Undamaged" Splice (Top Right), North Duct "Damaged" Heat Shrink Splice (Bottom Left) and "Undamaged" Splice (Bottom Right)

Both ducts were severely holed and pitted, thus they had large surface area loss. The south duct was severely pitted and holed within the ponded region. Discolorations to moderate corrosion with some pitting were observed in the duct portion outside the ponded region. Some of the worst damage duct was approximately 12 in. to the west of the beam centerline-corresponding to the location of one of the flexural cracks. In this location the top portion of the duct was nearly corroded away in several intervals. The bottom portion was also heavily corroded with holes and pitting. Another area of major damage was the loss of 6 in. of the top portion of the duct at the end of the autopsy area (east end). The north duct was also holed and pitted, with some of the worst damage again 12 in. to the west of the centerline. At this location the top part of the duct was almost completely corroded away in several intervals. The bottom portion had large holes. However, the worst damage to the south duct overall was the loss of 6-in. of length of the entire top of the duct at the east end of the autopsy area. The ducts are

shown in Figure 5.51, with the corrosion ratings plotted in Figure 5.50 and summarized in Table 5.11.

The south duct grout had large deposits of corrosion products throughout. The grout was also cracked at numerous locations. Small bleed water voids were observed in many locations. Many of the voids had corrosion products inside. Most of the voids were around 1/2-in. in diameter and 1/4-in. deep. There was a large bleed water void at the extreme east end of the autopsy area. This void was wide and 3/8-in. deep maximum. The maximum chloride content in the south duct grout was 0.209%, measured at 18 in. to the west of the beam centerline. The north duct grout was similar, with corrosion products deposited on it throughout. Bleed water voids were seen, with similar sizes to the voids in the north duct. These also had corrosion products in them. The maximum chloride content measured in the north duct grout was 0.091%, found at 12 in. to the east of the beam centerline. The grout for each duct is shown in Figure 5.51. The chloride contents for the grout in each duct are plotted in Figure 5.50.

The three south duct strands were moderately corroded with instances of pitting. Mild pitting was observed on wires just outside the ponded region, with pitting also found on the center wire (this location corresponds to 12 in. on the corrosion rating graphs). The fact that there was pitting on the center wire suggests that the pitting in the ponded region is due to moisture traveling down the strands from the ponded region. Mild pitting with one instance of moderate pitting was found in the vicinity of the flexural crack 12 in. to the west of the beam centerline. Other instances of mild pitting were found near the centerline of the beam. Another concentration of pitting was in the vicinity of the “undamaged” industry standard splice. In this location the center wire of two of the three strands was also pitted. Even though the “undamaged” splice is in this vicinity, it should be noted that the south duct was almost completely corroded away just east of this area. The three north duct strands had moderate to light corrosion, with instances of mild pitting near the east end of the autopsy area. This was also in the vicinity of the “undamaged” heat shrink splice; however, there was also severe holing

and area loss in the duct in this vicinity as well. The strands are shown in Figure 5.51 and the corrosion ratings are plotted in Figure 5.50 and summarized in Table 5.11.

From the plots in Figure 5.50, there is no overall trend between either strand damage or chloride content when comparing the data in the vicinities of the “damaged” or “undamaged” splices in both ducts. It is likely that the severe duct corrosion made the damage to the splices insignificant as the ducts began to corrode away.

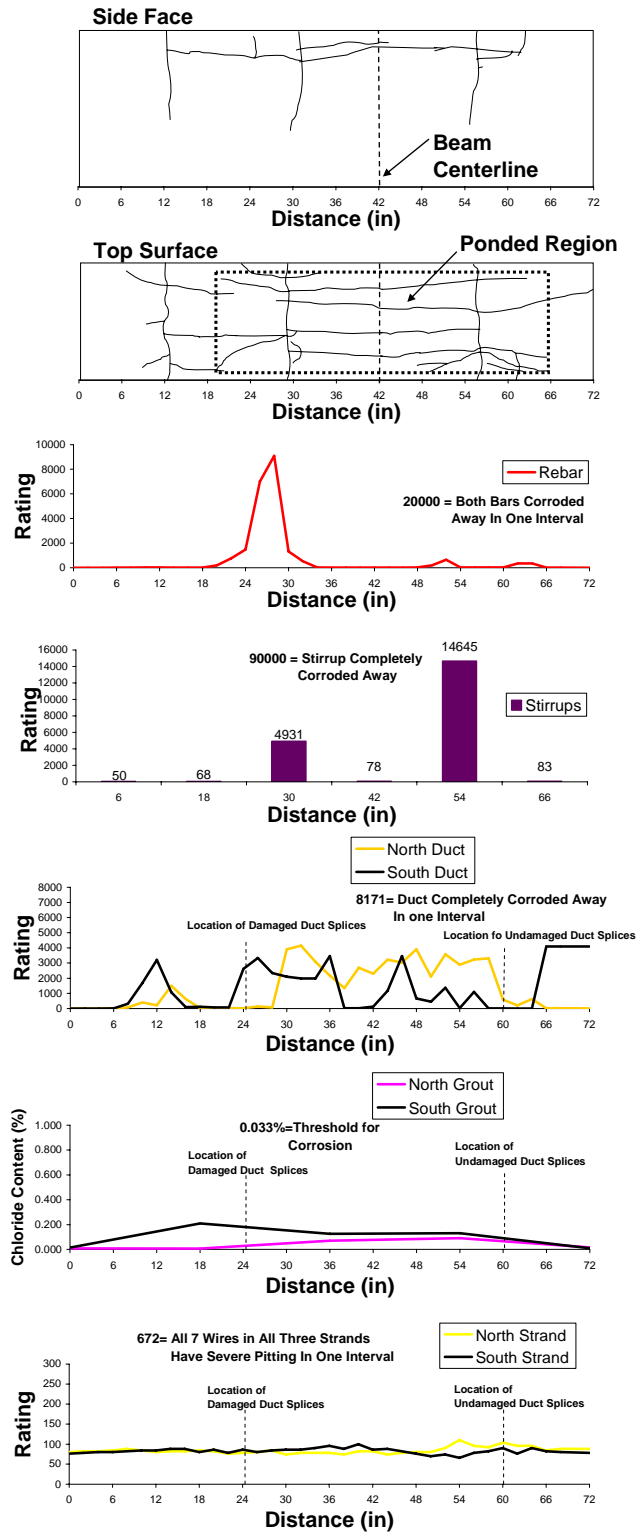


Figure 5.50: Beam 3.4-Crack Patterns and Corrosion Rating Graphs



Longitudinal Bar



Stirrup



Top of South Duct



Top of North Duct



South Duct Grout



North Duct Grout



South Duct Strand



North Duct Strand

Figure 5.51: Beam 3.4 Autopsy Elements

5.2.1.9 Beam 3.5 (100%U, Overload):

1-U-OL-C-SD-HS-NG-NS-D1

1-U-OL-C-SD-IS-NG-NS-D2



Figure 5.52: Beam 3.5-Side View (Left) and Top View (Right)

Table 5.12: Beam 3.5 Corrosion Rating Summary

	Maximum	Total	Generalized
Longitudinal Bars	2514	13822	1434
Stirrups	2720	15495	1476
North Duct	2895	12555	2093
South Duct	3964	23934	3989
North Strand	28	2924	162
South Strand	32	2362	131

Beam Appearance

As shown in Figure 5.52 the beam was heavily stained and cracked. At the beginning of exposure testing the ponded region was partitioned in half in order to improve the watertight integrity of the salt bath. The west portion of the salt bath had larger amounts of staining than the east portion. As shown in Figure 5.52 and Figure 5.56, there were longitudinal cracks with a maximum width of 0.06 in. running parallel to the bolster strips. Staining was observed emanating from these cracks. These cracks continued outside the ponded region to the end of the autopsy area. Outside the ponded region minor staining was seen in the vicinity of the flexural crack just to the west and east of the ponded region. Minor longitudinal cracking was also observed on the sides of the beam, in the vicinity of the flexural cracks. The large amounts of staining and

cracking suggest large amounts of corrosion within the specimen. The crack width data are given in Figure 5.53.

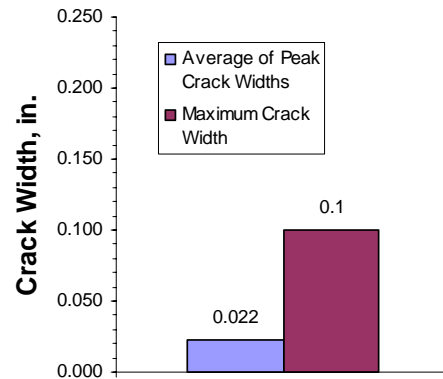


Figure 5.53: Beam 3.5 Crack Widths

Longitudinal Bars and Stirrups

It was discovered during autopsy that both the stirrups and longitudinal bars were heavily corroded inside the ponded region (See Figure 5.55). Instances of pitting and cross-sectional area loss were found on the bars near the flexural cracks in the ponded region. Area loss was observed in the northern most bar for several intervals east from the beam centerline. This was directly beneath one of the longitudinal cracks. The worst bar damage was about 2 in. to the west of the beam centerline, where one of the #3 bars was reduced to ¼-in. in diameter. The other bar was also significantly reduced in area at this location. This location corresponded to the flexural crack in the vicinity of the centerline. Outside the ponded region the bars were only discolored or lightly corroded. The three most heavily corroded stirrups were at the locations of flexural cracks. These bars had significant cross-sectional area loss. The stirrups which were still within the ponded region but not beneath flexural cracks were moderately corroded with only a few instances of some pitting. The stirrups outside the ponded region were only discolored or moderately corroded. The most heavily damaged stirrup was directly beneath the west end of the ponded region. The stirrup had heavy cross-sectional area loss in several intervals, with the bar diameter reduced by around a 1/3. The bars and stirrups are shown in Figure 5.55, and the ratings are plotted in Figure 5.56 and summarized in Table 5.12.

Tendons

Both ducts were spliced at the beam centerline. The south duct had an industry standard splice while the north duct had a heat shrink splice. The top portion of the south duct splice was nearly corroded away, with only large fragments remaining. The bottom portion was heavily pitted with some small holes. Pitting was found on the inside surfaces of both the top and bottom of the splices as well. Pitting and holes were found on the duct surface directly beneath the splice. On the inside surface of the duct directly next to these holes pitting was also found. The north duct heat shrink splice had corrosion deposits on the inside surface. Pitting was observed on the duct surface directly beneath the splice. Pitting was also observed inside the duct directly next to the duct joint. The splices for both tendons are shown in Figure 5.54.



Figure 5.54: Beam 3.5 Duct Splices-South Duct Industry Standard Splice (Left) and North Duct Heat Shrink Splice (Right)

Both ducts were heavily pitted and holed. The large amount of holes produced large section loss in the ducts. The south duct was lightly corroded outside the ponded region. Inside the ponded region the duct was heavily pitted and heavily holed. From 14 to around 24 in. from the west end of the autopsy area (28 to 24 in. to the west of the beam centerline), the top portion of the duct was almost completely corroded away. The inside of the duct was heavily pitted. The bottom portion of the duct was also heavily pitted, on the outside surface and, to a lesser extent, the inside surface. At about 6 in. to the west of the beam centerline the top portion of the duct was also heavily holed. Small holes were found on the bottom of the duct in this area. Pitting was also observed on the inside of the duct. Large holes were also observed on the top portion of the duct at the

east end of the autopsy area as well, with pitting on the inside of the duct also. The north duct was also pitted and holed. The largest amount of damage was just to the west of the beam centerline. At this location the duct had extremely large holes on the top surface. Pitting was observed on the inside of the duct as well. Small holes were also observed on the top of the duct at 18 in. from the west end of the autopsy area. The ducts are shown in Figure 5.55, with the ratings plotted in Figure 5.56 and summarized in Table 5.12.

The south duct grout had small voids at the west end of the autopsy area. These voids were approximately $\frac{3}{4}$ -in. in diameter and a $\frac{1}{4}$ -in. deep. The most significant void was 12 in. from the end of the autopsy area. At approximately 23 in. to the west of the beam centerline, transverse cracks were observed with staining on their faces. When this grout was separated from the strand, corrosion could be seen on the strand directly beneath these cracks. A large bleed water void was found in the vicinity of the beam centerline. It was more than 16-in. long and about $\frac{3}{8}$ -in. deep. Corrosion products from the duct were found inside portions of the void. Several small circular voids were found on the east end of the grout, with duct corrosion products inside. The maximum chloride content measured in the south duct grout was 18 in. from the west end of the autopsy area. The chloride content was 0.184%, far above the threshold for corrosion of 0.033%. The north duct also had small voids on the west end of the autopsy area, with a larger circular void at 18 in.. This void was about 1-in. in diameter and $\frac{3}{8}$ -in. deep. Several more small voids were seen in the vicinity of the centerline, with corrosion products inside. The grout was transversely cracked at multiple locations, with staining on the crack faces in the vicinity of the beam centerline. The maximum chloride content measured in the south grout was 0.076%. This was measured 6 in. to the west of the beam centerline. This is well about the threshold for corrosion of 0.033%. The grout from both ducts is shown in Figure 5.55. The grout chloride content along the length of the autopsy area is plotted in Figure 5.56.

The three strands in the south duct showed light to moderate corrosion overall, with some instances of mild pitting. The mild pitting was found on the center wire of one of the strands at 24 in. to the west of the beam centerline (18 in. on the corrosion rating

graphs). In addition, at approximately 4 in. to the west of the beam centerline mild pitting was also found on a single wire from one of the strands. The three strands in the north duct showed light to moderate corrosion as well, but no pitting. Strands from both ducts are shown in Figure 5.55. The corrosion ratings for the strand along the length of the autopsy area are shown in Figure 5.56, and are summarized in Table 5.12.



Longitudinal Bar



Stirrup



Top of South Duct



Top of North Duct



South Duct Grout



North Duct Grout



South Duct Strand



North Duct Strand

Figure 5.55: Beam 3.5 Autopsy Elements

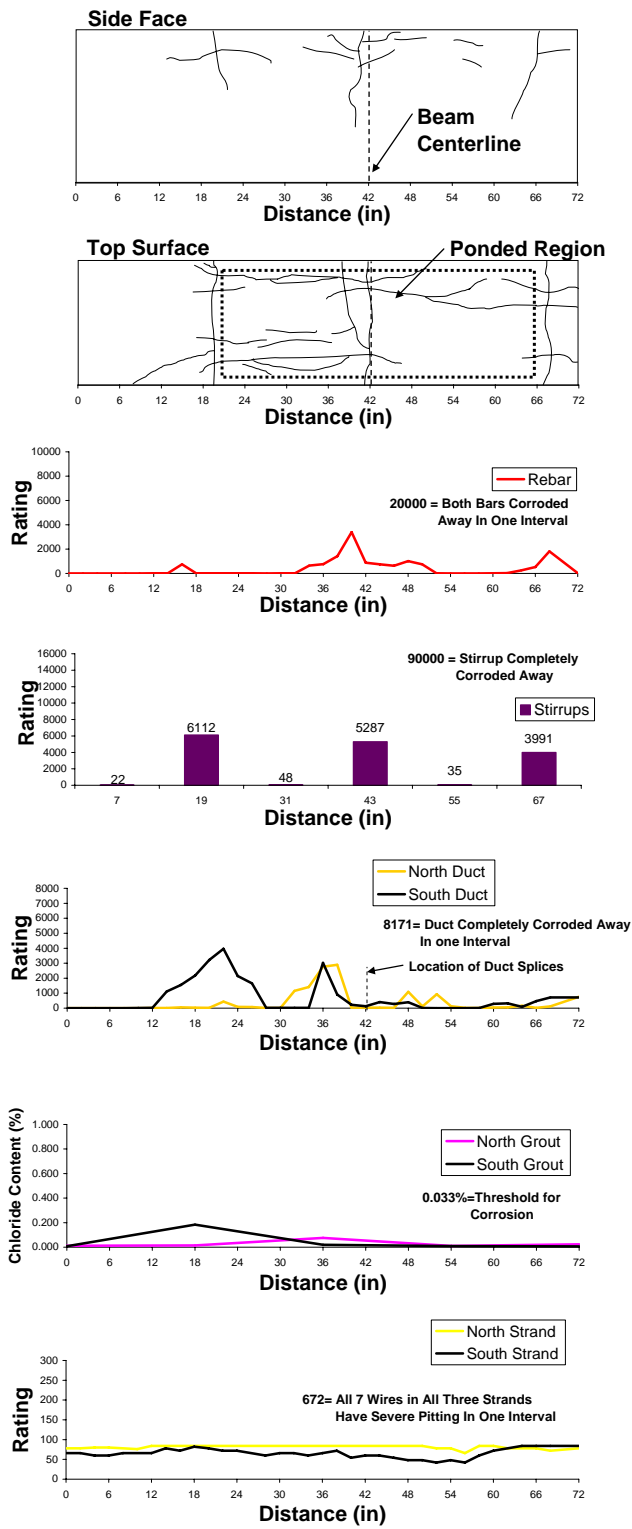


Figure 5.56: Beam 3.5-Crack Patterns and Corrosion Rating Graphs

5.2.1.10 Beam 4.1 (100%S, Service Load):

1-S-SL-C-SD-XS-NG-NS-D1

1-S-SL-C-SD-IS-NG-NS-D2



Figure 5.57: Beam 4.1-Side View (Left) and Top View (Right)

Table 5.13: Beam 4.1 Corrosion Rating Summary

	Maximum	Total	Generalized
Longitudinal Bars	2782	10287	884
Stirrups	2463	16595	1581
North Duct	2029	16399	2733
South Duct	1465	10673	1779
North Strand	28	3190	133
South Strand	32	3410	142

Beam Appearance

As shown in Figure 5.57 and Figure 5.61, the beam was substantially cracked and stained. Patches of staining were found in the ponded region. The staining was concentrated around longitudinal cracks which seemed to follow the bolster strips/longitudinal bars. These cracks were typically between 0.002 and 0.009 in. in width, while the largest longitudinal crack width was 0.016 in.. Longitudinal cracks were also found on the side of the beam, with staining emanating from one of these cracks just outside the west end of the autopsy area. This crack continued almost to the beam centerline. Flexural cracks were also found on the beam. This is significant for this beam because it was designed not to crack under long term loading at service load. Three flexural cracks were found, one at the beam centerline and two additional cracks each 24 in. to the east and west of the centerline. In general these flexural cracks were wider than

the aforementioned longitudinal cracks. Staining was found emanating from the side of the flexural crack at the beam centerline. This crack continued almost to the beam centerline. The largest crack width measured was from the flexural crack just outside the east end of the ponded region. This crack was 0.04 in. in width. This was the only beam where the largest crack width was measured at an actual flexural crack. The crack width data for this beam are given in Figure 5.58.

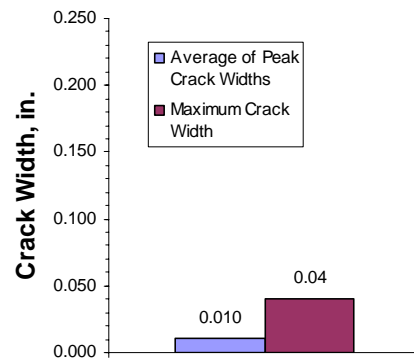


Figure 5.58: Beam 4.1 Crack Widths

Longitudinal Bars and Stirrups

When the beam was autopsied, both the longitudinal bars and stirrups were found to have considerable corrosion (See Figure 5.60). The longitudinal bars were found to be pitted and have cross-sectional area loss near the locations of the flexural cracks in the ponded region. Significant cross-sectional area loss was also found at the location of the flexural crack just outside the west end of the ponded region. Staining was seen at this crack previously. Pitting and slight cross-sectional area loss were found on one of the bars at the location of the flexural crack just outside the east end of the ponded region. The other bar was pitted at this location. The worst longitudinal bar damage was at the centerline flexural crack, where one of the #3 bars was reduced to about a 1/4-in. in diameter. At this location the other bar had moderate uniform corrosion. Pitting was also found in areas where there were no flexural cracks, but where longitudinal cracks were located. The stirrups are bars are shown in Figure 5.60, and the corrosion ratings are plotted in Figure 5.61 and summarized in Table 5.13.

Tendon

The south duct was fitted with an industry standard splice, while the north duct was not spliced. The top portion of the south duct splice was severely holed and pitted. The bottom portion of the splice was also pitted in some locations. Pitting was also found on the inside of both the top and bottom portions of the splice. Pitting and holes were found on the portion of the south duct directly beneath the splice, with pitting also found on the inside of the duct at this location. The south duct splice is shown in Figure 5.59.



Figure 5.59: Beam 4.1 South Duct Industry Standard Splice

Both ducts were pitted and holed thus causing large amounts of surface area loss. In the case of the south duct the surface area loss was concentrated in the area between the western most flexural crack and the centerline flexural crack. Pitting was also found on the inside of the duct in this area. For approximately 12 in. from the centerline of the beam to about 12 in. from the east end of the autopsy area, only slight discoloration was found on the outside of the duct. For the last 12 in. of the autopsy area, however, the duct was pitted and had small holes. This area was outside the ponded region. The north duct was only pitted with some minor holes until about the beam centerline, where the top portion of the duct was almost completely corroded away across several inches. The inside surface of the duct at this location was pitted. Large holes and pitting were also found starting at about 14 in. east of the beam centerline. More large holes were seen further east, terminating about 2 in. short of the end of the autopsy area, where the duct was pitted. The ducts are shown in Figure 5.60, and the corrosion ratings are plotted in Figure 5.61 and summarized in Table 5.13.

Both the south and north grouts were cracked. The south duct grout had a large bleed water void from 30 in. to about 46 in. from the west end of the autopsy area. At its deepest the void was 0.25 in. deep. Numerous corrosion deposits were found both in the void and around it. Small bubbles and small circular bleed water voids were seen east of this point. Very little to no deposition of corrosion was seen on the grout in this area. However, the last 8 in. of grout had corrosion deposit. The largest chloride content at strand level for the south duct grout was 0.04%, close to the corrosion threshold for 0.033%. This value was at 6 in. to the west of the beam centerline. The north duct grout had a large bleed water void from 12 to 28 in. (Again, in reference to the west end of the autopsy area), and corrosion products were found inside the void. At approximately 12 in. from the east end of the autopsy area, staining was found on the face of one of the transverse cracks. Many small bubbles were found on the top of the grout as well. The highest chloride content measured in the north duct grout was 0.06%, also at 6 in. to the west of the beam centerline. This is far above the threshold of 0.033%. The grout from both beams is shown in Figure 5.60. The chloride content along the length of the autopsy area for the grout from both ducts is shown in Figure 5.61.

The four strands in the south duct had light to moderate corrosion. The four strands in the north duct had light to moderate corrosion as well. The strand from both ducts is shown in Figure 5.60. The strand ratings along the length of the beam are shown in Figure 5.61 and are summarized in Table 5.13.



Longitudinal Bar



Stirrup



Top of South Duct



Top of North Duct



South Duct Grout



North Duct Grout



South Duct Strand



North Duct Strand

Figure 5.60: Beam 4.1 Autopsy Elements

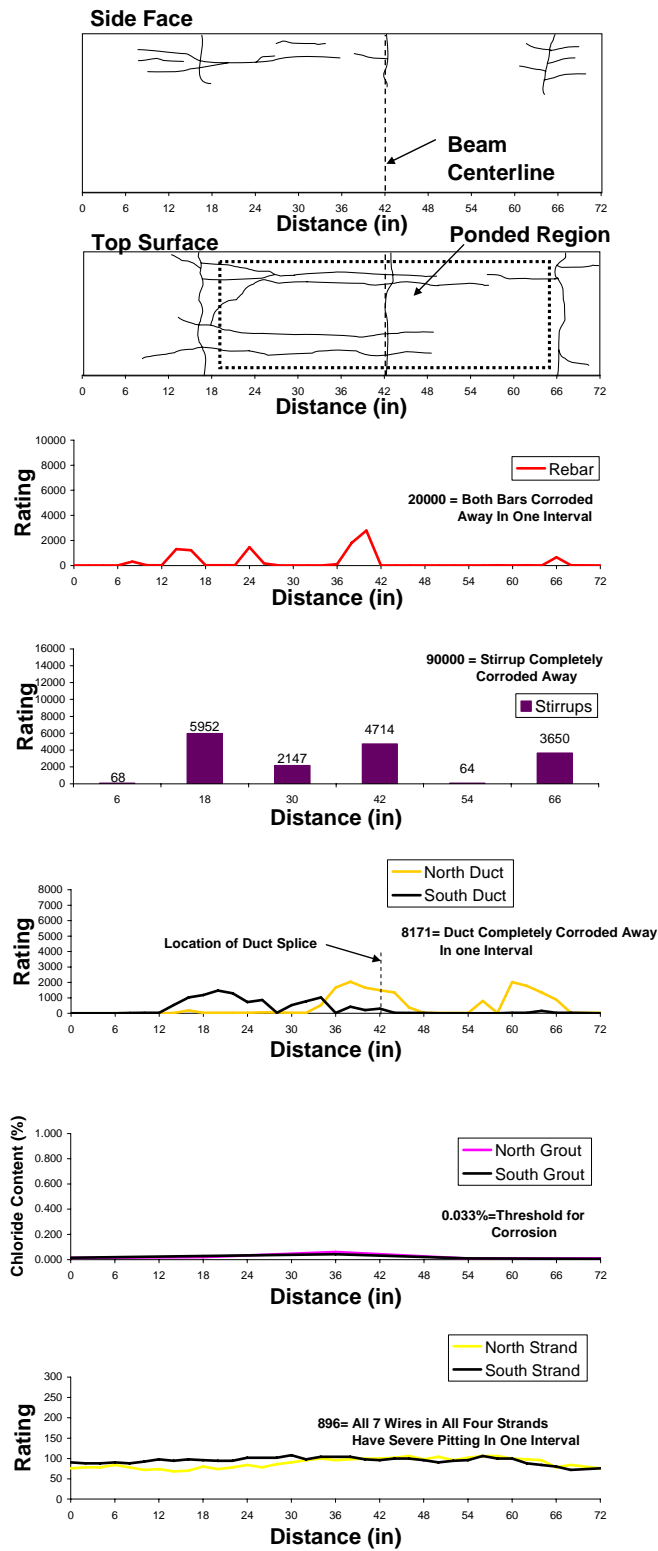


Figure 5.61: Beam 4.1-Crack Patterns and Corrosion Rating Graphs

5.2.2 Phase II Beams

5.2.2.1 Beam 2.7 (2/3-PS, Service Load, Epoxy Coated Strands):

2-P-SL-C-SD-IS-NG-ES-D1

2-P-SL-C-SD-IS-NG-ES-D2



Figure 5.62: Beam 2.7-Side View (Left) and Top View (Right)

Table 5.14: Beam 2.7 Corrosion Rating Summary

	Maximum	Total	Generalized
Longitudinal Bars	5923	125879	2622
Stirrups	1296	13988	1332
North Duct	6152	52523	8754
South Duct	8171	120352	20059
North Strand (Coating Damage)	44	1580	132
South Strand (Undamaged)	56	2586	216

Beam Appearance

As shown in Figure 5.62 and Figure 5.70, staining and longitudinal cracking was found in the ponded region. One major area of staining was at the flexural crack at the beam centerline. The other was at the west end of the autopsy area. At this location the staining was concentrated around a flexural crack and where the hole had been drilled to create a grout vent during beam construction. The hole had been sealed with epoxy after grouting. Staining was also seen on the flexural crack just to the west of the ponded region. Staining was also seen on the side of the beam corresponding with the location of the centerline flexural crack. The maximum crack width was from a longitudinal crack and measured 0.14 in.. This value was measured near the beam centerline. Very little

staining was observed from these longitudinal cracks. Crack width data for this beam are given in Figure 5.63.

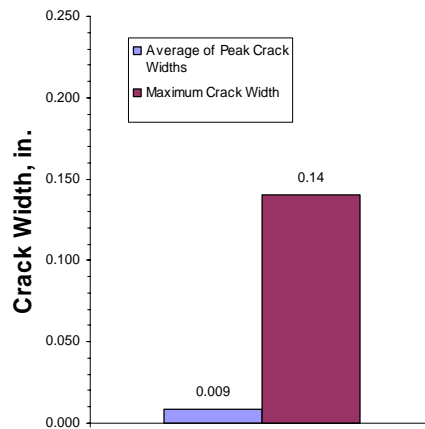


Figure 5.63: Beam 2.7 Crack Widths

Longitudinal Bars and Stirrups

Upon autopsy, pitting and large cross-sectional area loss was found on the longitudinal bars and stirrups throughout the ponded region (See Figure 5.69). The worst damage to an individual bar was at 12 in. to the east of the beam centerline. At this location one of the #3 bars was reduced in diameter to 0.19 in.. The stirrups beneath the ponded region were also heavily pitted with large section loss. The worst stirrup damage was also 12 in. to the east of the beam centerline, where the stirrup bar diameter was reduced from 0.5 in. to 0.4 in. in one interval. The stirrup outside the ponded region was pitted with no section loss. The stirrups and bars are shown in Figure 5.69. The stirrup and bar ratings in the autopsy area are plotted in Figure 5.70, and are summarized in Table 5.14.

Tendons

Both the north duct and south duct had industry standard splices at the beam centerline. The south duct splice was severely corroded with very large area loss. The top portion of the splice had large holes across its length, with pitting. The bottom portion of

the splice was pitted on the outside with a small hole at the centerline. Both the top and bottom portions of the splice were pitted on the inside as well. The top section of the south duct directly beneath the splice was almost completely corroded away. Only fragments were found at the beam centerline. The north duct industry standard splice was also severely corroded. The top portion of the splice was almost completely corroded away, and only fragments were recovered. The bottom of the splice had several holes with pitting throughout. The top portion of the north duct directly beneath the splice was pitted with small holes, while the bottom was only pitted. Both splices are shown in Figure 5.64.

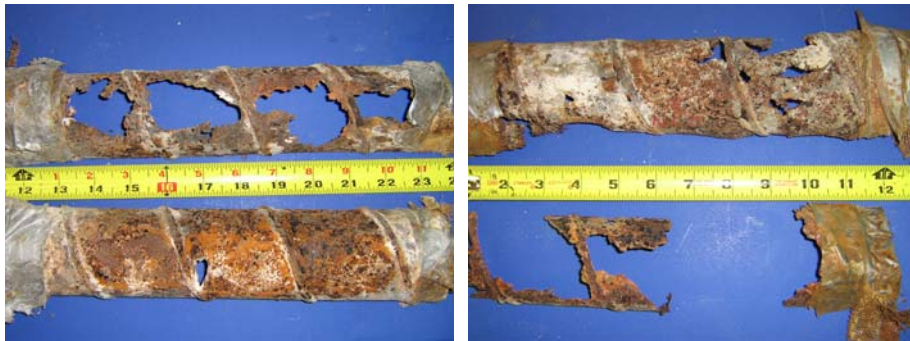


Figure 5.64: Beam 2.7 Industry Standard Duct Splices-South Duct Splice (Left) and North Duct Splice (Right)

Both ducts were severely pitted and holed, resulting in large surface area loss. The top portion of the south duct was pitted even outside the ponded region. Starting at approximately 19 in. from the west end of the autopsy area, several in. of the duct was completely corroded away. At approximately 12 in. from the east end of the autopsy area several in. of duct were also corroded away. Upon inspection of the inside of the bottom of the duct, evidence of abrasion of the epoxy on the strand was found at 14 in. from the west end of the autopsy area. Corrosion deposits which were likely from the strand were found in this area. This is shown in Figure 5.65. This may have occurred at other locations as well, but the severe duct corrosion further east of this location made any other abrasion evidence on the duct impossible to find.



Figure 5.65: Beam 2.7-Evidence of Abrasion of Epoxy Coating from Strand on Bottom of South Duct

The north duct was not as severely damaged as the south duct. At about 18 in. west of the beam centerline several in. of the duct suffered large section loss. Large holes were also found for about 12 in. starting at about 12 in. to the east of the beam centerline. The worst damage was at 26 in. from the west end of the autopsy area, where nearly $\frac{3}{4}$ of the entire duct was corroded away. The ducts are shown in Figure 5.69. The duct damage along the length of the beam is shown in Figure 5.70, and is summarized in Table 5.14.

The south duct grout had a three foot long bleed water void from the far west end of the autopsy area to about 6 in. short of the centerline. In this area large corrosion deposits from the duct were found in the bleed water void. The grout was cracked at multiple locations, and at the grout crack 12 in. from the east end of the autopsy area, a large amount of staining was found on the crack face. The maximum chloride content found in the south duct was at 6 in. west of the beam centerline, where the chloride content was 0.775%. This is very far above the corrosion threshold of 0.033%. The north duct grout had a shallow bleed water void from about 17 to 21 in. west of the end of the autopsy area. From 46 to 48 in., a shallow white colored void was also observed. Transverse cracks were found at multiple locations, and staining was found at the cracks 25 and 27 in. west of the autopsy area. The grout also had many small bubbles indicating a large amount of porosity. The maximum chloride content was 0.415%, measured at 54 in. from the west end of the autopsy area. This is far above the threshold for corrosion. The grout is shown in Figure 5.69, and the chloride content data is plotted in Figure 5.70.

A small amount of epoxy coating on the bottom of the south ducts strands was missing at about 14 in. from the west end of the autopsy area. This confirms the evidence of epoxy abrasion observed on the bottom of the duct. Starting at about 24 in. from the west end of the autopsy area, a large amount of corrosion products as well as damage to the bottom of the strand coating was observed. This is shown in Figure 5.66. The coating on the strand was then chipped off and the strand examined. The coating seemed very brittle and easily cracked when pierced with a screwdriver. After removal of the coating, large amounts of light to moderate corrosion and mild pitting were found on the strands exterior throughout their length. Moderate pitting was found on one of the wires at 18 in. from the west end of the autopsy area. The strand after removal of the coating is shown in Figure 5.66. When the strands were unwound, pitting was also found on the center wire of one of the strands. The unwound strand from the south duct is shown in Figure 5.69 .



Figure 5.66: Beam 2.7-South Duct Strand With Coating (Left) and After Removal of Coating (Right)

In contrast to the south duct strand, the coating of north duct strand was intentionally damaged by the previously researchers, in order to test the effectiveness of epoxy repair kits. As explained in Chapter 2, numerous small holes were made in the epoxy coating on the two strands at five locations: At the beam centerline and 4 holes at approximately 12 in. spacing to the right and left of the centerline. One of the strands had these holes repaired with a standard epoxy repair kit before installation in the beam. An example of one of the holes is shown in Figure 5.67.

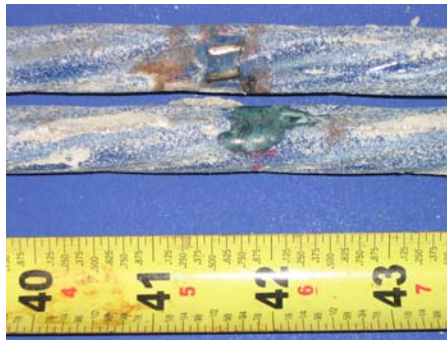


Figure 5.67: Beam 2.7-Example of Strand Coating Damage to North Duct Strand- Patched Strand (Bottom) and Unpatched Strand (Top).

Upon autopsy, corrosion deposits were found on the epoxy next to the unpatched holes. Abrasion damage to the epoxy was found 7 in. from the east end of the autopsy area, where the strand actually made contact with the bottom of the duct. Pitting was found on the exposed strand surface at this location. Upon removal of the coating, light corrosion was found adjacent to the hole locations. Mild pitting was found on the west end of the strands, with instances of pitting found on the center wires. Additional instances of mild pitting were found adjacent to the abrasion damage at the east end of the autopsy area. The strand which was patched also had mild pitting on the west and east ends, as well as light to moderate corrosion. Not as many instances of pitting were observed as in the unpatched strand. Abrasion damage was also found at the same location as the other strand. Light corrosion was found in the vicinity of one of the patched holes, but otherwise the exterior of the strand had little corrosion in the vicinity of the other patched holes. The corrosion ratings for the strand are plotted in Figure 5.70 and are summarized in Table 5.14. The unwound strands are shown in Figure 5.69. In Figure 5.68, the ratings for the patched and unpatched strand from the north duct are plotted separately.

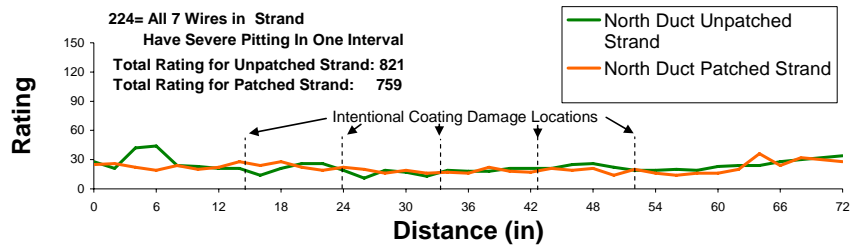


Figure 5.68: Beam 2.7- North Duct Strand Damage Ratings

As shown in Figure 5.68 the total rating for the unpatched strand was slightly larger than the patched strands. However, there is no significance difference between the ratings for the two strands in the vicinity of the holes. The visual inspection of the strand showed no significant corrosion in the vicinity of four of the five patches on the exterior of the strand. So the performance of the patches is fair.

Overall, it would appear that the primary source of moisture ingress for the epoxy coated strand is from abrasion damage caused by contact between the strand and the bottom of the duct during prestressing.



Longitudinal Bar



Stirrup



Top of South Duct



Top of North Duct



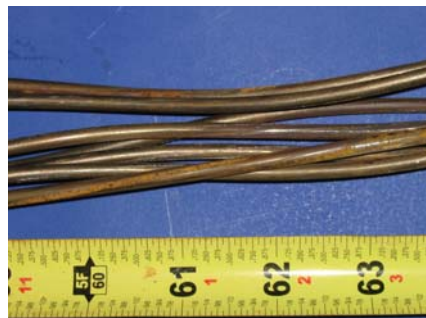
South Duct Grout



North Duct Grout



South Duct Strand (Coating Removed)



North Duct Strand (Coating Removed)

Figure 5.69: Beam 2.7 Autopsy Elements (From Center Portion of Beam)

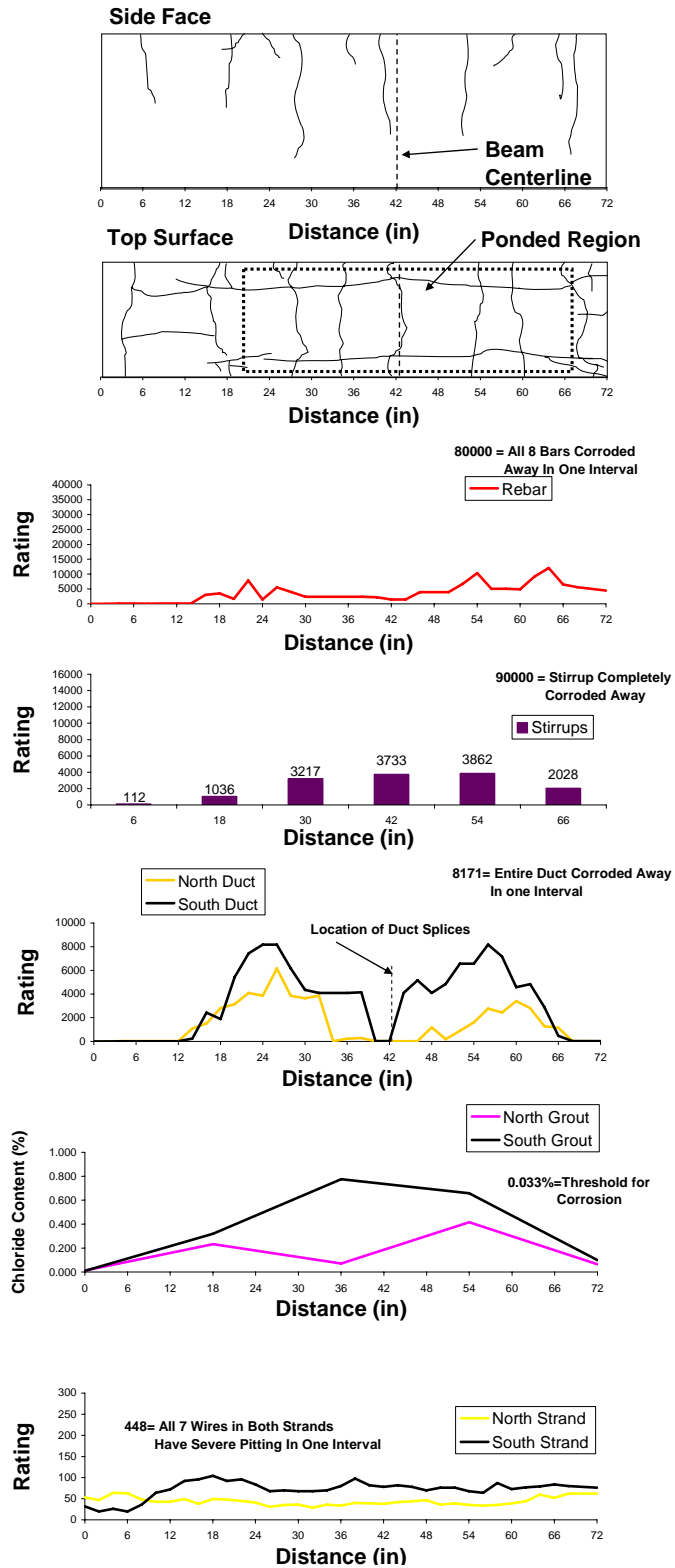


Figure 5.70: Beam 2.7-Crack Maps and Corrosion Rating Graphs

Anchorage



Figure 5.71: Beam 2.7 Anchorage Zones-East End (Left) with Dripper, and West End (Right) Without Dripper

As shown in Figure 5.71, the east end anchorage zone, which had been subjected to exposure testing with a saltwater dripper, had a small patch of staining. This staining was caused by the flow of the saltwater from the dripper. There was a 0.005 in. crack found on the grout which formed the pocket. This was likely a shrinkage crack. The west end anchorage, which had not been subjected to a dripper, also had a 0.005 in. shrinkage crack. As previously stated in Chapter 4, chloride samples revealed no chlorides at the west end, while high chloride content was found at strand tail depth on the east (dripper) end. Approximately two feet of each tendon was removed from each end of the beam ends during autopsy.

West End Anchorage Zone (No Dripper-Control End)

The west end anchorages just after removal from the beam are shown in Figure 5.72.



Figure 5.72: Beam 2.7 West End Anchorages After Removal (Controls): North Duct Anchorage (Top, Left and Right), and South Duct Anchorage (Bottom, Left and Right)

As shown in Figure 5.72, the front of the bearing plate and the anchorhead in both tendons were slightly corroded, while the back of the bearing plates showed no corrosion. The fronts of the wedges also showed some slight corrosion as well. The portion of the north duct in the anchorage zone had light corrosion directly underneath the duct tape seal between the duct and the back of the anchorhead. Light corrosion was also found on the inside of the duct surface in this area. Otherwise the rest of the duct showed no evidence of corrosion. The south duct was similar, with light corrosion also found in the vicinity of the duct tape seal on the outside of the duct. No evidence of corrosion was found inside the south duct itself. The ducts are shown in Figure 5.73. Note that the white substance on the south duct is zinc oxide, which is from the corrosion of the galvanized

coating on the duct. The corrosion ratings for the ducts in the anchorage are given in Figure 5.76 and are summarized in Table 5.15.

The north duct grout showed bubbles indicating porosity, but otherwise nothing else significant was observed in the appearance of the grout. Chloride samples of the grout taken at strand depth revealed negligible chloride content from the back of the anchorhead (Where the first sample was taken), all the way to end of the portion of the duct removed from the anchorage zone. The south duct grout showed evidence of bleed water accumulation for a length of 1 in. behind the anchorhead. Similarly to the north duct grout, negligible chloride content was found at strand depth along the length of the duct at the anchorage. The grout from both ducts is shown in Figure 5.73.

Mostly light to moderate corrosion was found in all the strands from both ducts. However, in the vicinity of where the wedges “bit” into the epoxy coated strand, full penetration of the coating was found in all the strands. In the north duct pitting was found on a single strand on both the center wire as well as some of the outer wires in this vicinity. A single strand in the south duct showed similar mild pitting. The likely source of the corrosion is that moisture from the center of the beam found its way through the interstices into the anchorages. The autopsy elements removed from the anchorage are shown in Figure 5.73. The strand ratings for the anchorage are given in Figure 5.76 and are summarized in Table 5.15.



South Duct



North Duct



South Duct Grout



North Duct Grout



South Strand With Wedges



North Strand With Wedges



South Duct Strand (Coating Removed)



North Duct Strand (Coating Removed)

Figure 5.73: Beam 2.7-West End Anchorage Zone (Control) Autopsy Elements

East End Anchorage Zone (Dripped End)

The east end anchorages just after removal from the beam are shown in Figure 5.74.



Figure 5.74: Beam 2.7 East End Anchorages (Dripped End): North Duct Anchorage (Top, Left and Right), and South Duct Anchorage (Bottom, Left and Right)

As shown in Figure 5.74, both bearing plates and the anchorheads were slightly corroded. The fronts of three of the four wedges were only slightly corroded. But one of the wedges in the south duct had pitting on its front surface. The north duct had pitting on its top inside and outside surfaces in the area right behind the bearing plate, with some light corrosion observed on the inside and outside surfaces of the bottom of the duct in this area. All other portions of the duct showed no evidence of corrosion. The south duct had light corrosion on both the top and bottom portions on the inside and outside surfaces. All other parts of the duct showed no evidence of corrosion. The ducts are shown in Figure 5.75. The duct ratings in the anchorage zones are plotted in Figure 5.76 are summarized in Table 5.15.

The north duct grout was slightly stained from the pitting corrosion on the inside of the duct. There was evidence of bleed water accumulation directly behind the anchorhead. Further towards the interior of the beam there were very small voids

indicating a small amount of bleed water accumulation. The chloride content samples taken at strand level showed negligible chlorides in the grout. The south duct grout showed shallow voids which may have been the result of segregation and/or bleed water accumulation during pumping of the grout. The possibility of segregation is mentioned because the voids did not appear similar to bleed water voids observed previously. A definite bleed water void was seen directly behind the anchorhead. Like the north duct, no chlorides were found at strand depth in the south duct. The grout from both ducts is shown in Figure 5.75.

The north duct strand was lightly to moderately corroded throughout the anchorage, including the portion outside the anchorhead. The south duct strand was similar, except there was mild pitting at the tips of one of the strands outside the anchorhead. At this location five of the six outer wires had moderate pitting, as well as the center wire. Beyond this point only light to moderate corrosion was found on the center wire. In the case of both the north and south strands moderate corrosion was observed directly beneath the locations where the wedges “bit” into the strand and punctured the epoxy coating. The strands are shown in Figure 5.75. The ratings for the strand in the anchorage are shown in Figure 5.76 and are summarized in Table 5.15.



South Duct



North Duct



South Duct Grout



North Duct Grout



South Duct Strand With Wedges



North Duct Strand With Wedges



South Duct Strand (Coating Removed)



North Duct Strand (Coating Removed)

Figure 5.75: Beam 2.7-East End Anchorage Zone (Dripped End) Autopsy Elements

In Figure 5.76, the corrosion ratings for both the ducts and strand for the west end and east end anchorages are shown plotted together for comparison. Note that “Distance From Beam End” is the distance from the respective end of the beam for each respective anchorage. Because the corrosion from the center of the beam spread to both anchorages, in order to detect any corrosion caused by the end dripper the data from the dripped end is compared to the control end to see if there is any increase in corrosion between the two. Thus it is assumed that the corrosion from the center of the beam had an equal effect on both ends of the beam.

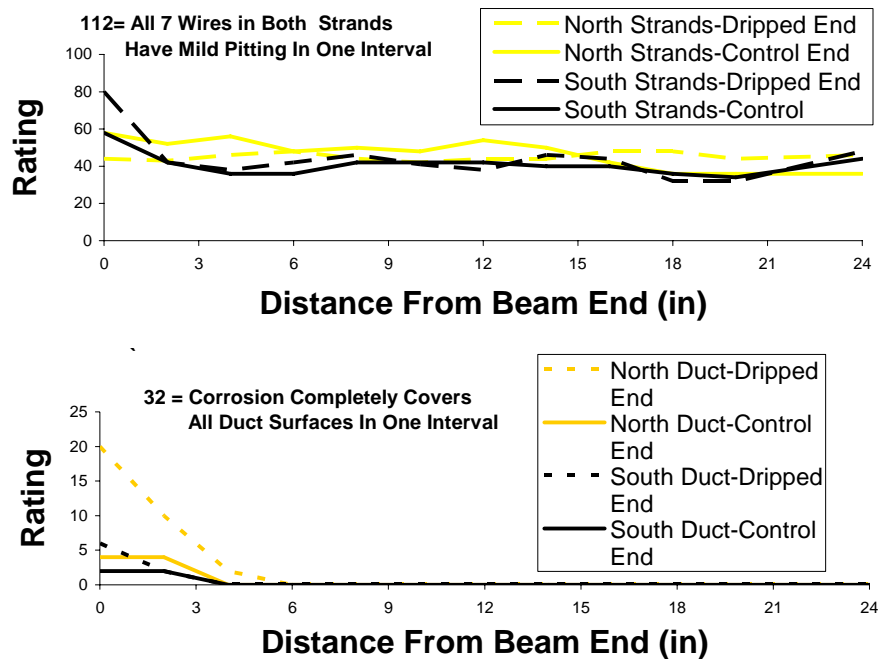


Figure 5.76: Beam 2.7-Corrosion Rating Graphs for Anchorages

In Table 5.15, the corrosion ratings for both anchorages are summarized.

Table 5.15: Beam 2.7-Corrosion Rating Summary for Anchorages

	<u>Dripped End</u>		<u>Control End</u>	
	<u>Maximum</u>	<u>Total</u>	<u>Maximum</u>	<u>Total</u>
North Duct	20	32	4	8
South Duct	6	8	2	4
North Strand	25	541	44	566
South Strand	52	529	44	492

By comparing the data from each tendon in Figure 5.76 and Table 5.15, there is no overall trend between the total strand damage and whether the anchorage has a dripper or not. The corrosion on the strand in the south duct did increase dramatically at the very end of the beam. But since this was observed on both ends of the beam it cannot be attributed to the dripper. It is likely that what has occurred in both ducts is that the large chloride/moisture ingress from the severe corrosion at the center of the beam found its way to the anchorages by way of the strand interstices, since the anchorage is only 7'-6" from the central area of the beam, where, as previously mentioned, very large chloride contents were observed. This is also supported by the fact that no chlorides were found in the grout in the tendons within the anchorage. Subsequently, the effect on the strand from the moisture/chloride ingress from the beam centerline made the chloride ingress caused by the dripper negligible. In contrast, both Figure 5.76 and Table 5.15 clearly demonstrate that the duct damage did increase with the presence of the dripper. All of the major corrosion observed in the ducts was in the vicinity of the duct tape seal or slightly closer to the anchorhead. This is also the location where the steel collar at the back of the anchorhead comes into contact with the galvanized duct. The corrosion was located right inside this area. Therefore, it is possible that a form of galvanic or "two metal corrosion" has taken place, which is when two dissimilar metals are placed together and one of them is corroded due to the difference in electrochemical potential between the two metals.¹⁷ However, in order for this to occur the two metals must already be in a corrosive environment. At the control end bleed water accumulation from behind the anchorhead may have helped initiate this. Meanwhile, at the dripper end, the same occurred but in addition small amounts of chloride ingress from the dripper may have helped accelerate the galvanic corrosion process, resulting in greater corrosion than the control end. These

chlorides may have found their way through the anchorhead and on to the duct surface. However, the chlorides may not have reached the actual level of the strands within the grout. This would explain the lack of chlorides at the level of the strands at the dripped end.

5.2.2.2 Beam 2.8 (2/3-PS, Service Load, Galvanized Strand):

2-P-SL-C-SD-HS-NG-GS-D1

2-P-SL-C-SD-IS-NG-GS-D2



Figure 5.77: Beam 2.8-Side View (Left) and Top View (Right)-Note: These Views are from Opposite Sides of the Beam

Table 5.16: Beam 2.8 Corrosion Rating Summary

	Maximum	Total	Generalized
Longitudinal Bars	10000	117875	2456
Stirrups	2047	16833	1603
North Duct	3654	37304	6217
South Duct	3940	29109	4851
North Strand	56	1274	106
South Strand	42	739	62

Beam Appearance

As shown in Figure 5.77 and Figure 5.82, there was longitudinal cracking and staining centered around the flexural cracks in the ponded region, on both the sides and top surface of the beam. The worst staining was at the centerline flexural crack. As observed in all the other loaded beams, the flexural cracks corresponded with stirrup locations. The maximum crack width was from one of these longitudinal cracks in the ponded region, near the centerline. The crack measured nearly 1/8-in. in width. There was heavy staining at the beam centerline around one of the longitudinal cracks. Patches

of staining were also seen outside the ponded region as well. Crack width data for the beam are given in Figure 5.78.

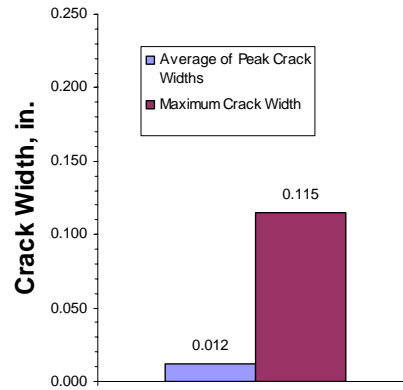


Figure 5.78: Beam 2.8 Crack Widths

Longitudinal Bars and Stirrups

Once the beam was autopsied, pitting and cross-sectional area loss were found on the longitudinal bars and stirrups in the ponded region (See Figure 5.81). The worst reinforcing bar damage was 10 in. to the west of the beam centerline, where one of the #3 bars was completely corroded away in one interval. This corresponded to a flexural crack location. The most corroded stirrup was that at the beam centerline. Here the stirrup was heavily pitted and at one location the stirrup bar diameter was reduced from ½-in. to 3/8-in.. This makes sense since the heaviest amount of staining seen on the exterior of the beam was at the centerline flexural crack. Outside the ponded region the stirrups and bars had mainly moderate corrosion with some pitting. The stirrups and bars are shown in Figure 5.81, with the corrosion ratings shown in Figure 5.82 and summarized in Table 5.16.

Tendons

The splice configuration in this beam was an industry standard splice on the north duct at the beam centerline, with a heat shrink splice on the south duct also located at the beam centerline. The south duct heat shrink splice had a large amount of corrosion deposits on both the inside and outside surfaces, with the duct portion beneath the splice heavily pitted. The top portion of the industry standard splice was essentially corroded

away, with a pitted fragment recovered. The bottom portion of the splice was pitted on both the inside and outside surfaces. The top of the duct portion beneath this splice was very heavily holed resulting in large section loss. Also, the bottom portion of the duct in this area was heavily pitted. Both splices are shown in Figure 5.79.



Figure 5.79: Beam 2.8 Duct Splices-South Duct Heat Shrink Splice (Left) and North Duct Industry Standard Splice (Right)

Both ducts were heavily pitted and holed and thus had large surface area loss. The top portion of the south duct was nearly corroded away at both 12 in. west of the beam centerline and 6 in. to the east of the beam centerline (The beam centerline is at 42 in. in the corrosion rating graphs shown in Figure 5.82). The inside surfaces of the duct were also pitted. The north duct was also heavy holed and pitted, with large amounts of section loss. The worst damage to the north duct was 12 in. to the west of the centerline, where nearly the entire top portion of the duct was corroded away, and the bottom of the duct was holed and pitted as well. Like the south duct, instances of pitting were found on the inside surfaces of the north duct as well. The ducts are shown in Figure 5.81. The duct corrosion ratings along the length of the beam are shown in Figure 5.82 and are summarized in Table 5.16.

The south duct grout had multiple large bleed water voids. The largest was at 26 in. to the west of the beam centerline. The bleed water void at this location was nearly $\frac{3}{4}$ -in. wide. The grout was also transversely cracked, with staining found on several crack faces. The maximum chloride content measured in the north duct grout was 0.662%, far above the threshold for corrosion of 0.033%. This was measured 12 in. to the east of the beam centerline. The north duct grout had two large bleed water voids. The largest was

8-in. long and 1.25 in. wide and was just west of the beam centerline. Here duct corrosion products were found in the void. The north duct grout was transversely cracked in multiple locations with staining found on some crack surfaces. The largest chloride content found in the north duct grout was 0.205%, at 6 in. west of the beam centerline. This value is, again, far above the threshold for corrosion. The grout from both ducts is shown in Figure 5.81, and the chloride contents are plotted in Figure 5.82.

The two south duct galvanized strands had a wide range of corrosion. Both strands were discolored with instances of light to moderate corrosion. There were some instances of mild pitting on only a few wires. Whitish powder, likely zinc oxide, was found in the interstices between several of the wires. The amount of discoloration in the galvanized strand is shown in Figure 5.80. Here, new galvanized strand which was in environmentally controlled storage at FSEL is shown with the galvanized strand removed from the beam. The north duct strand was similar, but with many more instances of mild pitting in multiple locations. The strand from both ducts is shown in Figure 5.81, while the corrosion ratings along the length of the autopsy area are shown in Figure 5.82 and are summarized in Table 5.16.



Figure 5.80: Autopsied Galvanized Strand (Bottom) vs. New Galvanized Strand (Top)

It is significant that pitting and other heavy corrosion was found on the galvanized strand. The overall discoloration of the strand as well as the presence of zinc oxide suggests that the zinc coating had almost corroded away on all the strands, and that the actual steel in the strand was under attack. This is similar to what occurred to the galvanized ducts, where the galvanization only delayed the onset of corrosion in the actual steel.



Longitudinal Bar



Stirrup



Top of South Duct



Top of North Duct



South Duct Grout



North Duct Grout



South Duct Galvanized Strand



North Duct Galvanized Strand

Figure 5.81: Beam 2.8 Autopsy Elements

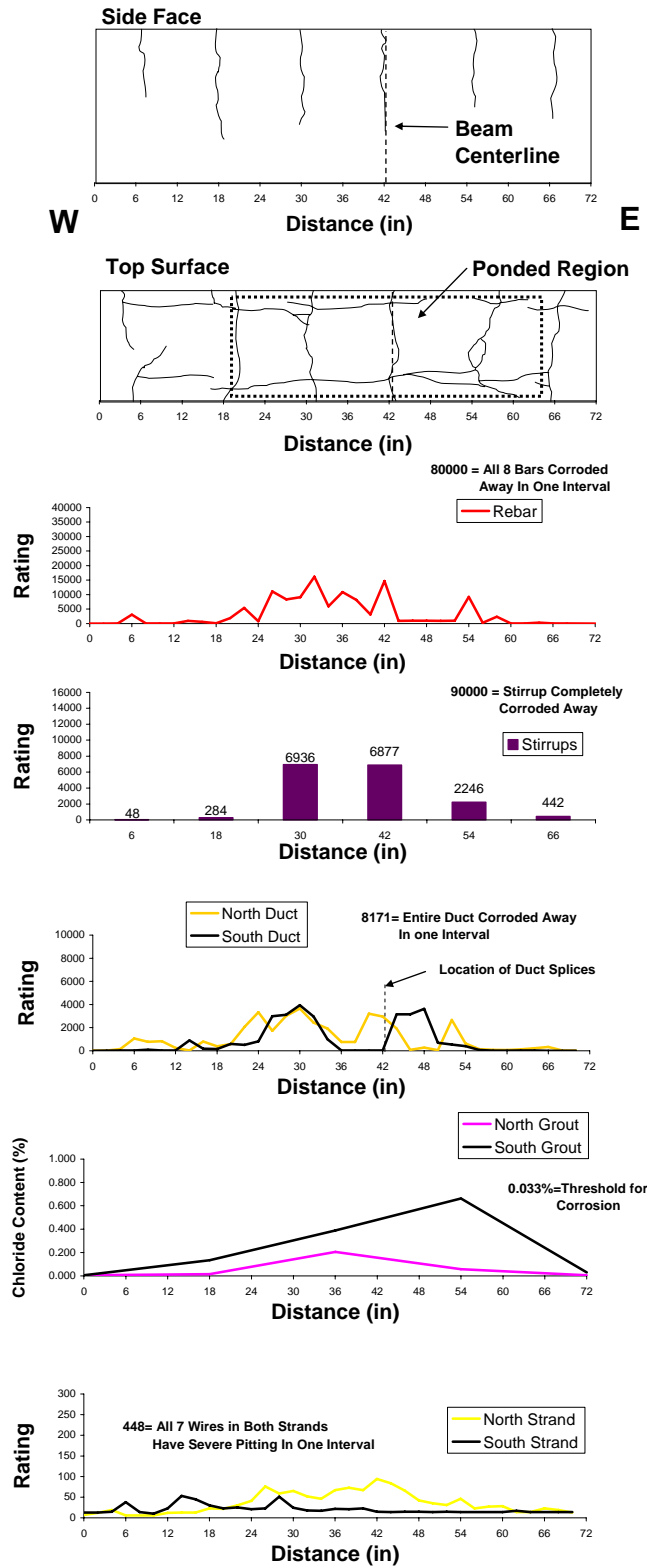


Figure 5.82: Beam 2.8-Crack Patterns and Corrosion Rating Graphs

5.2.2.3 Beam 2.9 (2/3-PS, Service Load, Poor Grouting Procedures):

2-P-SL-C-SD-IS-NG-NS-D1

2-P-SL-C-SD-IS-NG-NS-D2

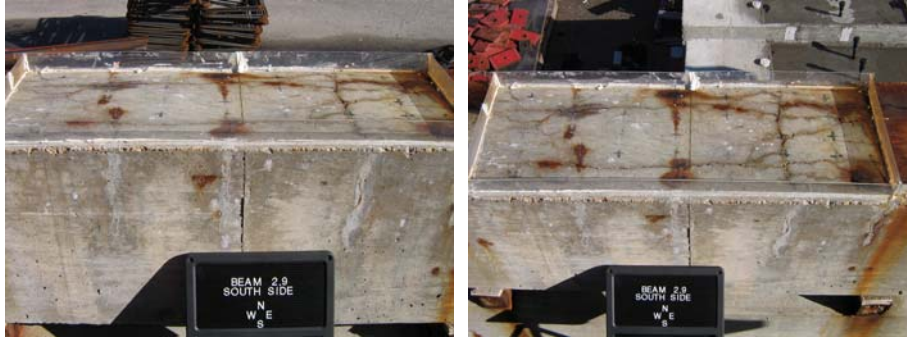


Figure 5.83: Beam 2.9-Side View (Left) and Top View (Right)

Table 5.17: Beam 2.9 Corrosion Rating Summary

	Maximum	Total	Generalized
Longitudinal Bars	10000	492958	10270
Stirrups	1535	21026	2002
North Duct	8171	99193	16532
South Duct	8171	98252	16375
North Strand	44	1648	137
South Strand	48	1680	140

Beam Appearance

As shown in Figure 5.83 and Figure 5.87, there was staining and longitudinal cracking in the ponded region. An additional large patch of staining was observed just outside the east end of the ponded region. The patches of staining inside the ponded region were centered around the flexural cracks. One of the longitudinal cracks in the ponded region continued into the heavily stained area outside the east end of the ponded region. This crack and several other longitudinal cracks continued outside both ends of the ponded region. The largest crack width was recorded near the centerline of the beam, where one of the longitudinal cracks was 0.09 in. in width. Staining was also seen on the side of the beam, emanating from the flexural cracks inside the ponded region. The crack width data are given in Figure 5.84.

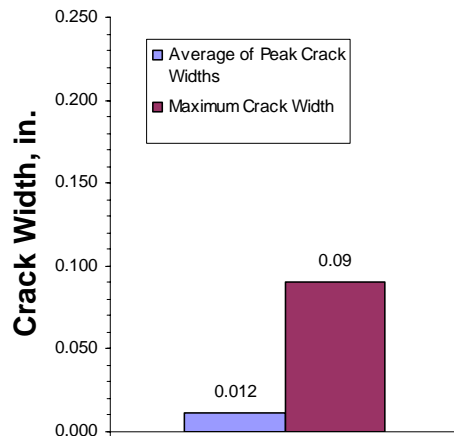


Figure 5.84: Beam 2.9 Crack Width Data

Longitudinal Bars and Stirrups

Upon autopsy of the center portion of the beam, large amounts of pitting and cross-sectional area loss were found on all longitudinal bars and stirrups (See Figure 5.86). In some instances the #3 longitudinal reinforcing bars were completely corroded away for several in. of length. This occurred over a broad area centered about 18 in. west of the beam centerline, where in one 2-in. interval two of the #3 bars were completely corroded away. Loss of bar lengths also occurred intermittently in an area about 18 in. long which was just to the east of the beam centerline. Again, in this area two of the four #3 bars were completely corroded away for several 2-in. intervals. The worst stirrup damage was just outside the east end of the ponded region, corresponding to the location of the heavy staining mentioned previously. The stirrup at this location suffered significant section loss in several 2-in. intervals, and was also heavily pitted. The stirrups and bars are shown in Figure 5.86, while the corrosion ratings for the stirrups and bars within the autopsy area are plotted in Figure 5.87 and are summarized in Table 5.17.

Tendons

Both ducts were spliced with industry standard splices at the beam centerline. Both splices suffered tremendous section loss to their top portions. Only a 3-in. long fragment remained of the top portion of the south duct splice. The bottom portion had very large holes in it. The other areas of the bottom portion were heavily pitted. The duct

portion beneath the splice was heavily pitted and holed. In the case of the north duct splice a 12-in. long fragment of the top portion was recovered, while the bottom portion had a very large hole near its centerline and was severely pitted. The length of the duct beneath the splice was heavily pitted with small holes. The splices are shown in Figure 5.85.

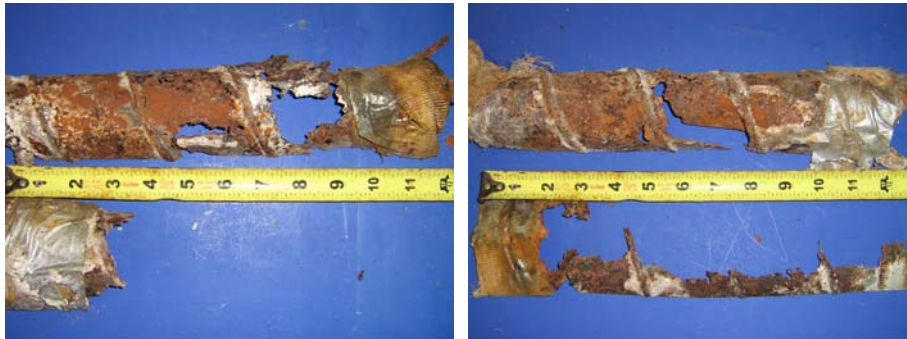


Figure 5.85: Beam 2.9 Industry Standard Splices-South Duct Splice (Left) and North Duct Splice (Right)

Both ducts were heavily holed and pitted, resulting in large surface area loss. The highest amount of damage in the south duct was approximately 12 in. to the west of the beam centerline, where nearly 4-in. of the entire duct was corroded away. The north duct was also heavily holed and pitted, with the entire corroded away for several in. at a location about 18 in. to the east of the beam centerline. The duct corrosion ratings along the length of the beam are shown in Figure 5.87, are summarized in Table 5.17. The ducts are shown in Figure 5.86.

As described in Chapter 2, this beam was used to evaluate the effect of poor grouting procedures. The poor procedures included delays of up to 10 minutes during pumping of the grout, letting air into the pump, and capping the grout vents at the first sign of grout at the vents. Upon autopsy of the tendons, the south duct grout was found to have larger surface bubbles than compared to the beams with the “proper” grouting procedures. Bleed water voids of various sizes were present, and some evidence of segregation of the grout mix was found when examining the faces of the transverse cracks in the grout. This may have been caused by the 10-minute delays in pumping. Many of these transverse crack faces were also heavily stained. An example of the

segregation and staining is shown in Figure 5.86. Note the small bleed water voids at the tops of the grout sections. The maximum chloride content measured in the north duct was 0.267%, this was at the extreme east end of the autopsy area. The north duct was similar, with a large bleed water void near the beam centerline which was 1-in. wide and almost a ½-in. deep. The maximum chloride content measured in the north duct was 0.245%, and was located at 12 in. to the east of the beam centerline. Thus the maximum chloride content for both ducts was far above the threshold for corrosion. The grout from both ducts is shown in Figure 5.86. The chloride content in the grout along the length of the autopsy area is plotted in Figure 5.87.

The two south duct strands had instances of light to moderate corrosion throughout, with some instances of mild and moderate pitting found on one strand in a zone about 20 in. long at the east end of the autopsy area. Here mild pitting was found on some wires, with one case of moderate pitting on one wire at 16 in. to the east of the beam centerline. The other strand had only two instances of mild pitting. One was at the beam centerline and the other was about 18 in. to the west of the beam centerline, in the same general vicinity as where the moderate pitting was found on the other strand in the duct. Both strands in the north duct had mild pitting in the same general areas as the south duct strands, but no instances of moderate pitting were found in either of the strands. The strand is shown in Figure 5.86, and the corrosion ratings for the strand in the autopsy area are given in Figure 5.87 and are summarized in Table 5.17.



Longitudinal Bar



Stirrup



Top of South Duct



Top of North Duct



South Duct Grout



North Duct Grout



South Duct Strand



North Duct Strand

Figure 5.86: Beam 2.9 Autopsy Elements (From Center of Beam)

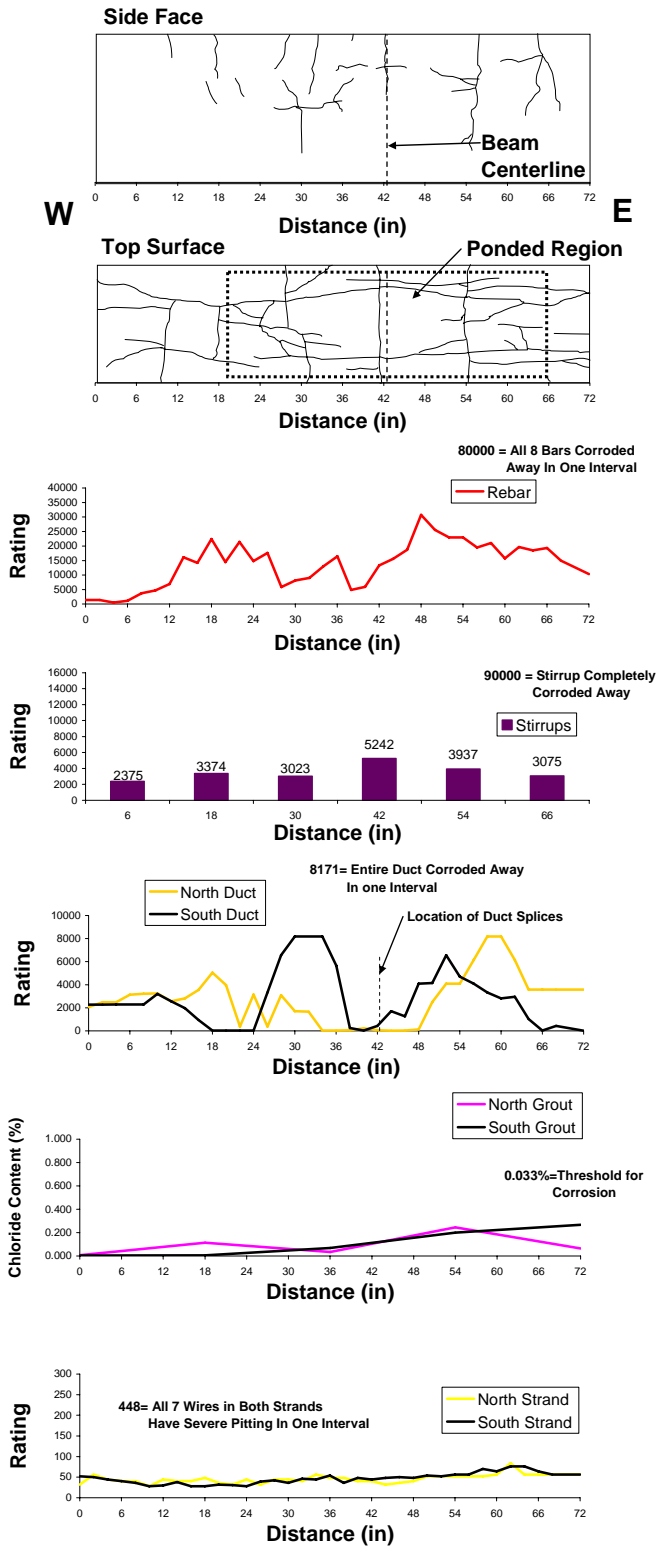


Figure 5.87: Beam 2.9-Crack Patterns and Corrosion Rating Graphs

Anchorage



Figure 5.88: Beam 2.9 Anchorage Zones-East End (Left) with Dripper, and West End (Right) Without Dripper

As shown in Figure 5.71, there were 0.005 in. wide shrinkage cracks on both ends of the beam, where the anchorage pockets had been backfilled. On the east (dripped) end anchorage, there was a large patch of staining right beneath where the saltwater exited from the dripper. Also, on the dripper end a large network of cracks was found directly above the 4x8 concrete cylinder which was used to weigh down the plastic drip pan. The cracks were on the bottom of the beam and then went up the sides approximately 3 in.. These cracks are shown in Figure 5.89.



Figure 5.89: Beam 2.9: Bottom Corner of East End Anchorage Zone

The widest crack width in this crack network was 0.01 in., which was on the side of the beam. A small patch of staining was found right next to this crack. When an attempt was made to remove the 4x8 cylinder, it was discovered that the cylinder was actually pinned beneath the test beam and the reaction beam. This is likely the source of

the cracking on the bottom of the beam. As the beam “crept” downward under sustained load during the nearly 8 years of testing, the cylinder was loaded more and more, and it finally caused local cracking in the beam itself.

West End Anchorage Zone (No Dripper-Control End)

The west end anchorages after removal from the west end of the beam are shown in Figure 5.90



Figure 5.90: Beam 2.9 West End Anchorages (Controls) After Removal-North Duct Anchorage (Top, Left and Right), and South Duct Anchorage (Bottom, Left and Right)

As shown in Figure 5.90, the front of the bearing plate and anchorhead in both tendons were only slightly corroded. The fronts of the wedges also showed slight corrosion as well. The portion of the north duct in the anchorage zone had moderate corrosion on its outside surface inside the duct taped connection between the back of the bearing plate and the duct. Otherwise, no other evidence of corrosion was found on the north duct. The south duct had moderate corrosion in the same location as the north duct, and, some small instances of light corrosion were found on the inside of the duct as well, near where the duct met the bearing plate. The corrosion ratings for the ducts in the anchorage are given in Figure 5.94 and are summarized in Table 5.18. The ducts removed

from this anchorage are shown in Figure 5.91. Note that in the latter figure the duct is shown next to the top half of the back of the bearing plate, which it was in contact with during test. Notice that there are corrosion deposits on that component from the corrosion of the duct.

The north duct grout showed evidence of bleed water accumulation just behind the anchorhead, and deep, but small in diameter, bubbles in the top of the grout. Negligible chlorides were found at the level of the strand in the grout. The south duct had a transverse crack at about 18 in. from the back of the anchorhead. However, the south duct grout did not have the deep bubbles that the north duct grout had. No evidence of bleed water accumulation was found behind the anchorhead in this duct. Similar to the north duct grout the south duct grout had negligible chlorides at the level of the strands. The grout from both ducts is shown in Figure 5.91. Light to moderate corrosion was found on the strands in the north and south ducts in the anchorage zone. Most of the moderate corrosion was concentrated in the interstices, but in the south duct strands moderate corrosion was observed on the outside of the strand at the ends of both tendons outside the anchorhead. The likely source of this corrosion is that corrosion from the center of the beam spread through the interstices down to the anchorages. No corrosion was found where the wedges “bit” into the wires. The strands from both ducts in the west end anchorage are shown in Figure 5.91. The strand ratings in the anchorage are given in Figure 5.94 and are summarized in Table 5.18.



Top of South Duct



Top of North Duct



South Duct Grout



North Duct Grout



South Duct Strand With Wedges



North Duct Strand With Wedges



South Duct Strand



North Duct Strand

Figure 5.91: Beam 2.9-West End Anchorage Zone (Control) Autopsy Elements

East End Anchorage Zone (Dripped End)

As mentioned previously, cracking was found on the bottom of the east end anchorage zone as a result of the 4x8 concrete cylinder placed there to stabilize the saltwater drip pan. When the anchorage block was autopsied pitting corrosion was found on the stirrup directly behind the crack. The chlorides which caused this corrosion likely came from saltwater splash from the drip pan. This explains the staining observed on the side of the anchorage. The east end anchorages after removal from the beam are shown in Figure 5.92.



Figure 5.92: Beam 2.9 East End Anchorages (Dripped End)-North Duct Anchorage (Top, Left and Right), and South Duct Anchorage (Bottom, Left and Right)

As is evident in Figure 5.92, in the case of both tendons more corrosion was found on the face of the bearing plate and anchorhead at the dripped end of the beam than at the control end. However, there was no evidence of corrosion in the area behind the bearing plate. The outside of the top portion of the south duct had severe corrosion in the vicinity of the duct tape connection, and instances of light corrosion on both the outside and inside of the bottom portion of the duct right at the end of the duct at the anchorhead. Light corrosion was also found underneath the duct tape at the duct/bearing plate

interface. It is known from the aforementioned industry standard splices that duct tape does not act as an effective barrier for moisture ingress. But the absence of corrosion on the exposed portion of the duct behind this area suggests that failure of the duct tape was not the likely culprit for the corrosion on the duct behind the anchorhead. The outside of the north duct had light corrosion at the end of the duct behind the anchorhead, on the top surface. At the same end of the duct light corrosion was found on the outside of the bottom surface of the north duct. The ducts from the anchorage are shown in Figure 5.93. The corrosion ratings for the ducts in the anchorages are given in Figure 5.94 and are summarized in Table 5.18.

The south duct grout was cracked in a similar fashion to the grout at the center of the beam. No evidence of staining was found on the crack faces. The north duct grout was also cracked, but again, no evidence of staining was observed on the crack faces. In both ducts the grout chloride content at strand depth was negligible. The grout from both ducts in the anchorage are shown in Figure 5.93.

Moderate corrosion was found on all the strand wires in both ducts. Behind the anchorhead the moderate corrosion was generally found in the interstices. However, in front of the anchorhead, instances of moderate corrosion were found on the outside of the strands in both ducts. No evidence of corrosion was found inside the “bite” marks caused by the wedges in either duct. The strand from both ducts is shown in Figure 5.93. The strand ratings for the anchorages are given in Figure 5.94 and are summarized in Table 5.18.



South Duct



North Duct



South Duct Grout



North Duct Grout



South Duct Strand



North Duct Strand With Wedges



South Duct Strand



North Duct Strand

Figure 5.93: Beam 2.9-East End Anchorage Zone (Dripped End) Autopsy Elements

In Figure 5.94, the corrosion ratings for the ducts and strands in both the end anchorage zones are plotted. This data is also summarized in Table 5.18. The data from both ends are plotted together so that a direct comparison can be made between the control end and the dripped end. The x axis value “Distance From Beam End” is the distance from the respective ends of the beam for each anchorage element. For this analysis it is assumed that the corrosion at the center of the beam had an equal effect on both end anchorages.

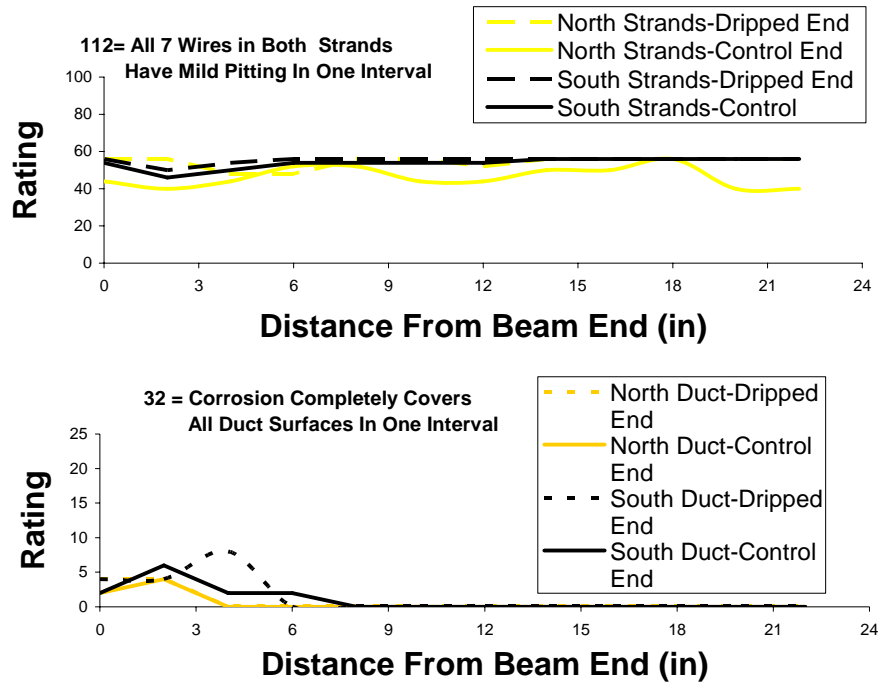


Figure 5.94: Beam 2.9-Corrosion Rating Graphs for Anchorages

Table 5.18: Beam 2.9-Corrosion Rating Summary for Anchorages

	<u>Dripped End</u>		<u>Control End</u>	
	<u>Maximum</u>	<u>Total</u>	<u>Maximum</u>	<u>Total</u>
North Duct	4	8	4	6
South Duct	8	16	6	12
North Strand	28	652	28	556
South Strand	28	664	28	646

In Figure 5.94 there is no increase in strand corrosion at very ends of the beam (Which is “0” on the x axis) in either the dripped end of the beam or the control end of the beam. However, from the same plot and from Table 5.18, an increase in the total

strand corrosion for both ducts between the dripped and the control end is apparent. In the case of the ducts the significant corrosion was found at the bearing plate/duct interface. As demonstrated in Beam 2.7 (Epoxy Coated Strand), the corrosion of the duct at its interface with the bearing plate is likely a form of galvanic corrosion. In Figure 5.94 and Table 5.18 it is clear that the corrosion in the ducts is greater in the end with the dripper. It is possible that chlorides entered through the strand holes in the anchorhead. While this did not penetrate the grout deep enough to produce significant chloride content at the level of the strand in tee grout, it still may have found it's way to the interface between the galvanized steel of the duct and the regular steel of the anchorhead. The presence of these chlorides would then accelerate the galvanic corrosion process between the galvanized duct and the steel bearing plate.

5.2.2.4 Beam 2.10 (2/3-PS, Service Load, Anti-Bleed Grout):

2-P-SL-C-SD-IS-AB-NS-DI

2-P-SL-C-SD-IS-AB-NS-DI

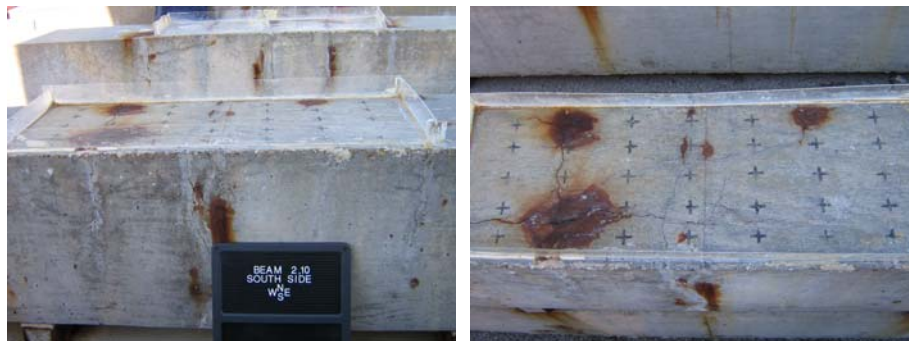


Figure 5.95: Beam 2.10-Side View (Left) and Top View (Right)

Table 5.19: Beam 2.10 Corrosion Rating Summary

	Maximum	Total	Generalized
Longitudinal Bars	4305	57082	1189
Stirrups	1542	19840	1890
North Duct	5592	49464	8244
South Duct	3710	69070	11512
North Strand	26	1040	87
South Strand	36	1136	95

Beam Appearance

As shown in Figure 5.95, and the crack maps in Figure 5.99, there was heavy staining and longitudinal cracking in the ponded region. The heaviest patches of staining were at the intersection of one of the flexural cracks and two of the longitudinal cracks, 12 in. west of the beam centerline. There was also staining on the side of the beam near the flexural crack at the beam centerline. The largest crack width was 0.094 in., and was measured at one of the longitudinal cracks near the beam centerline. There were a few small patches of staining outside the ponded region, but no wide longitudinal cracking. The crack width data are given in Figure 5.96.

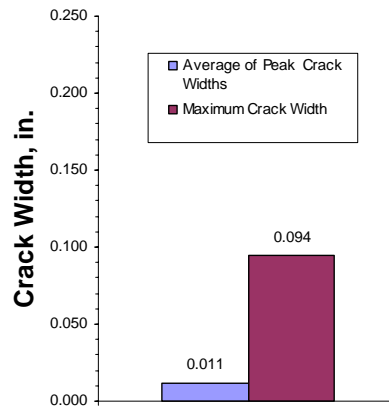


Figure 5.96: Beam 2.10 Crack Widths

Longitudinal Bars and Stirrups

Upon autopsy of the beam, pitting and cross-sectional section loss was found on the stirrups and longitudinal bars (See Figure 5.98). The worst longitudinal bar corrosion was at 16 in. to the west of the beam centerline, where one of the #3 bars was reduced in diameter to 0.25 in.. In the same location the four #4 bars also had considerable area loss. This area roughly corresponds to large patches of staining seen in Figure 5.95. The most highly corroded stirrup was also in this vicinity. In one area this stirrup had a reduction in diameter from 0.5 in. to 0.4 in.. The stirrup and longitudinal bar corrosion ratings are given in Figure 5.99 and are summarized in Table 5.19.

Tendons

Both ducts were spliced at the beam centerline. Both splices were industry standard splices, and were heavily corroded. The top portion of the south duct splice was almost completely corroded away. The top portion of the duct beneath it was nearly corroded away. The bottom of the splice was heavily pitted. The north duct splice had large holes and pitting in the top portion, with the bottom portion heavily pitted on the inside and outside. The top portion of the duct beneath it was pitted and small holes were present as well. Both splices are shown in Figure 5.97

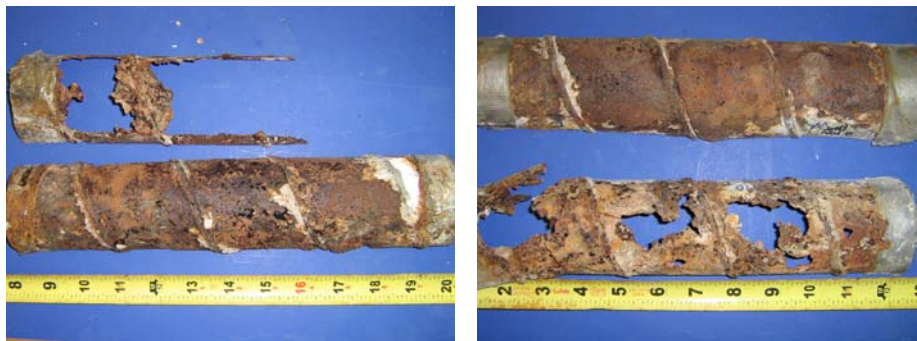


Figure 5.97: Beam 2.10 Industry Standard Duct Splices-South Duct Splice (Left) and North Duct Splice (Right)

Both ducts were heavily pitted with large surface area loss. In the case of the south duct the top portion was almost completely corroded away at about 18 in. to the east of the beam centerline. In the case of the north duct the majority of the top of the half of the duct was corroded away at a location 14 in. to the west of the beam centerline, and at the same location the bottom half of the duct had significant holes as well. The ducts are shown in Figure 5.98, while the corrosion rating graphs for the ducts are given in Figure 5.99 and are summarized in Table 5.19.

Both the south duct grout and north duct grout were an anti-bleed grout mix designed by Schokker². The grout mix was described in Chapter 2. Upon autopsy of both tendons, a large degree of segregation was found in the grout in both ducts. This resulted in shallow voids which ran almost the entire length of the autopsied ducts. Therefore, it appears that the anti-bleed admixture did not fully engage. When viewing the cross section of the grout, directly beneath the shallow void was a distinct layer of more

whitish grout, then grout which was more normal in appearance. The grout at the level of the strands appeared to be better quality than that seen with the grout in the other autopsied beams. The segregation and thus the anti-bleed admixture not engaging may have been caused by the mixing method used, which was mixing the grout for a short period in a bucket with a hand mixer, instead of using a dedicated grout mixer/pump assembly.* In the south duct the maximum chloride content at strand level was 0.162%, which was at 36 in. from the west end of the autopsy area. This is far above the threshold of 0.033%. The maximum chloride content in the north duct was 0.06%, which was at 18 in. from the west end of the autopsy area. The grout is shown in Figure 5.98, and the chloride contents in the grout in the autopsy area are plotted in Figure 5.98.

The south duct strand had light to moderate corrosion, with a few instances of pitting at 14 and 26 in. from the west end of the autopsy area. The north duct strand also had to light to moderate corrosion, but with no pitting. The strands from both ducts are shown in Figure 5.98, with the corrosion ratings plotted in Figure 5.99 and summarized in Table 5.19.

* This determination was based on consultation with Dr. Andrea Schokker of Pennsylvania State University



Longitudinal Bar



Stirrup



Top of South Duct



Top of North Duct



South Duct Grout



North Duct Grout



South Duct Strand



North Duct Strand

Figure 5.98: Beam 2.10 Autopsy Elements

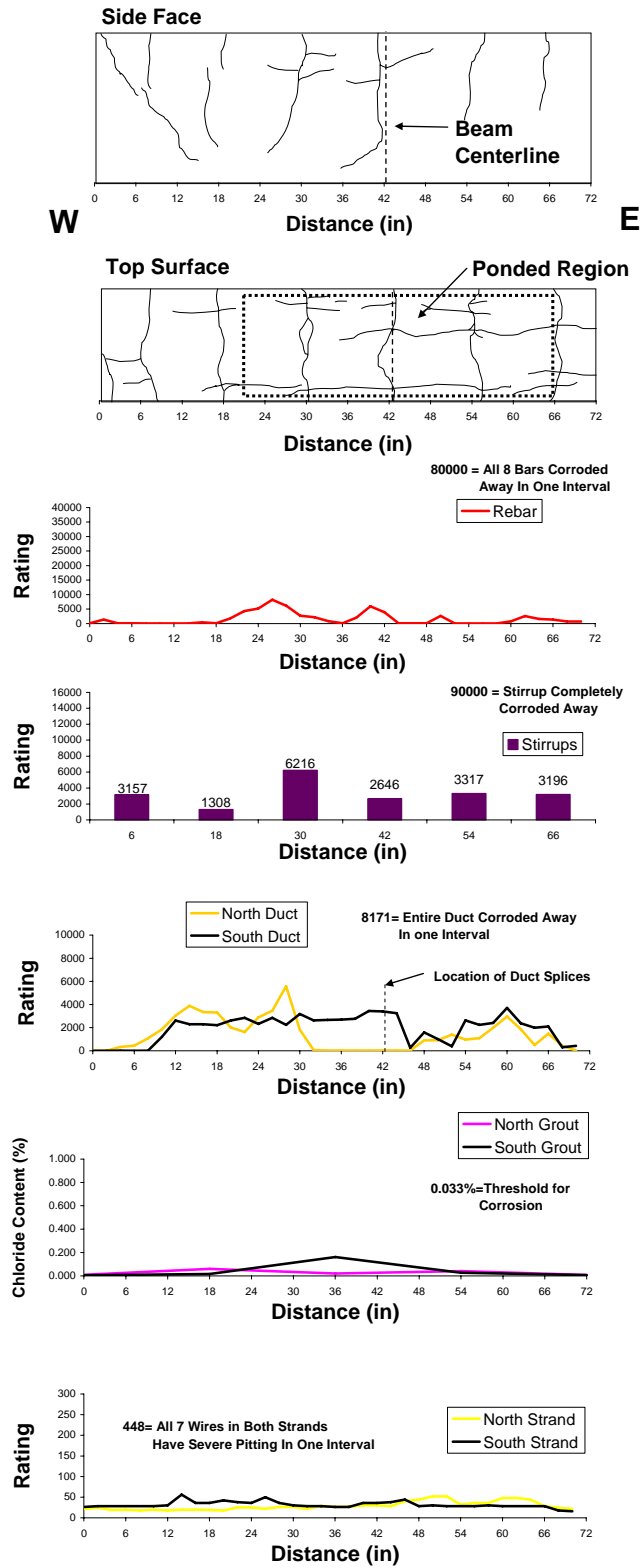


Figure 5.99: Beam 2.10-Crack Patterns and Corrosion Rating Graphs

5.2.2.5 Beam 2.12 (2/3-PS, Service Load, Plastic Duct):

2-P-SL-C-PD-XS-NG-NS-D1

2-P-SL-C-PD-XS-NG-NS-D2



Figure 5.100: Beam 2.12-Side View (Left) and Top View (Right)

Table 5.20: Beam 2.12 Corrosion Rating Summary

	Maximum	Total	Generalized
Longitudinal Bars	10000	281142	5857
Stirrups	3245	35325	3364
North Duct (Plastic Duct)	N/A	N/A	N/A
South Duct (Plastic Duct)	N/A	N/A	N/A
North Strand	52	2064	172
South Strand	56	2060	172

Beam Appearance

As shown in Figure 5.100, and in the crack patterns in Figure 5.105, severe staining and wide longitudinal cracks were seen on the top surface of the beam within the ponded region, with staining also emerging from the flexural cracks on the side of beam. The largest amount of staining on the top of the beam was centered around the intersection of the centerline flexural cracks and the pair of wide longitudinal cracks which ran the length of the ponded region. Staining was also seen emerging from the tops of the flexural cracks both to the west and east of the beam centerline. The largest overall crack width was at 14 in. east of the centerline, where one of the longitudinal cracks was 0.13 in. in width, which is slightly over 1/8-in.. The crack widths are given in Figure 5.101.

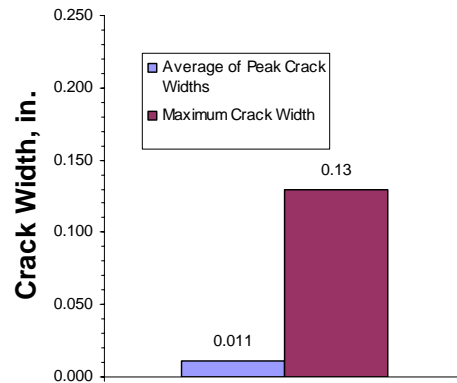


Figure 5.101: Beam 2.12 Crack Widths

Longitudinal Bars and Stirrups

All longitudinal bars and stirrups were pitted with large amounts of cross-section loss (See Figure 5.104). The worse longitudinal bar damage was in an area about 18 in. to the west of the beam centerline, where nearly 6 in. of two of the #3 bars were completely corroded away. The worst stirrup damage was at 12 in. to the east of the beam centerline, where the top portion of the stirrup had its diameter reduced from ½-in. to around 0.375 in.. The stirrup which was at the far west end of the autopsy area, outside the ponded region, had pitting but no cross-sectional area loss. The longitudinal bars and stirrups are shown in Figure 5.104. The corrosion ratings for the bars and stirrups are plotted in Figure 5.105 and are summarized in Table 5.20.

Tendons

The ribbed plastic ducts were continuous in both ducts, so no splices were present to be evaluated. During the breaking up of the block from the beam centerline, it was found that bracing bars had been placed across the bottoms of the stirrups during construction to hold the ducts up. The ducts had then been tied to these bars. This is shown in Figure 5.102. Note that the block is upside down, so the surface on the bottom of the block, facing the ground, was where the saltwater was ponded upon during exposure testing.



Figure 5.102: Beam 2.12 During Autopsy

At multiple locations, including all the stirrup locations, heavy corrosion deposits were seen on the top of the plastic ducts along the length of the autopsy block. Once the ducts were opened, evidence of abrasion was found between the strand and the bottom of the ducts. The abrasion was in the form of deep gouges in the bottom of the duct (See Figure 5.103). The damage was similar to fretting. At a point 12 in. to the west of the beam centerline (54 in. on the corrosion rating graphs), a small hole was found on the bottom of the north duct inside once of these gouges, with corrosion products inside. This was directly over one of the bracing bars which contributed to the damage. Corrosion products were found on the outside of the duct in this area. Severe pitting was found on the strand wire surface which had caused this gouge. Mild pitting was found on two other wires in this vicinity. The other strand in the north duct had mild to moderate pitting on three wires at the same location. Mild pitting was also found on the center wire of this strand, suggesting that the chlorides which had entered the duct had made their way into the interstices of the strand. While at first the remainder of the strand appeared unaffected on the outside, once the strand was unwound moderate corrosion was found on all wires in both strands for rest of the autopsy area. This damage to the north duct is shown in Figure 5.103.



Figure 5.103: Beam 2.12-Abrasion Damage to Interior of North Duct (Left) and Strand From Same Location (Right)

Very small cracking was found in one of the strand gouges on the bottom of the south duct in the exact same location along the length of the beam as the damage to the north duct. This resulted in basically the same situation as that in the north duct. Corrosion products were found in the gouge where the crack was located and mild to moderate pitting was found on three of the outer strand wires, with moderate pitting found on the center wire as well. The other strand had mild pitting on two of its wires in the same area. The strand from both ducts is shown in Figure 5.104, with the corrosion ratings for the strand shown in Figure 5.105 and summarized in Table 5.20. Corrosion ratings for the ducts are not plotted since the ducts are plastic; however, the location of the damage to the ducts is marked on the plot of strand damage. An explanation for this damage is as follows: When the strand was prestressed, it actually pushed down onto the duct, causing damage similar to fretting. Consequently, at a point 12 in. to the west of the beam centerline the plastic ducts had been “squeezed” between the strand and the bracing bar, and as a result the ducts failed mechanically. This damage must have occurred right when the beams were prestressed, even before exposure testing began. As shown in Figure 5.105 once the beam was loaded a flexural crack formed at the point where the ducts were damaged, since a stirrup was located there. Chlorides in the salt bath found their way through the flexural crack and corroded the bracing bar which held the ducts up. The corrosion then spread through the holes in the duct into the strand.

Both ducts were well grouted. The bleed water accumulated on the peaks of the ribs along the length of the duct, preventing large bleed water voids from forming as seen

in the galvanized ducts. The evidence for bleed water accumulation at the peaks of the ducts was large bubbles on the tops of many of the ribs. Negligible chlorides were found in the grout right at the level of the strand. This is surprising considering the aforementioned damage to the duct. What likely happened was the chlorides entered the strands directly and did not absorb into the grout. This is also likely because obviously there was no grout between the damaged areas of the ducts and the strand, so unlike typical strand damage seen in the other autopsies the chlorides did not have to pass through the grout to get to the strand. The chloride contents along the length of the ducts in the autopsy area are shown in Figure 5.105. The grout from both ducts is shown in Figure 5.104.



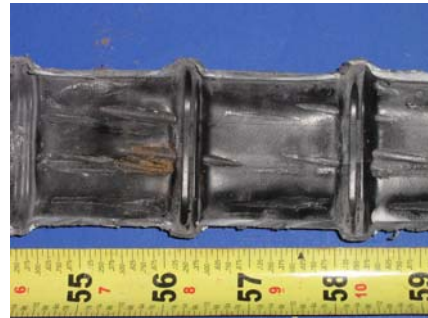
Longitudinal Bar



Stirrup



South Duct



North Duct



South Duct Grout



North Duct Grout



South Duct Strand



North Duct Strand

Figure 5.104: Beam 2.12 Autopsy Elements (Center Portion of Beam)

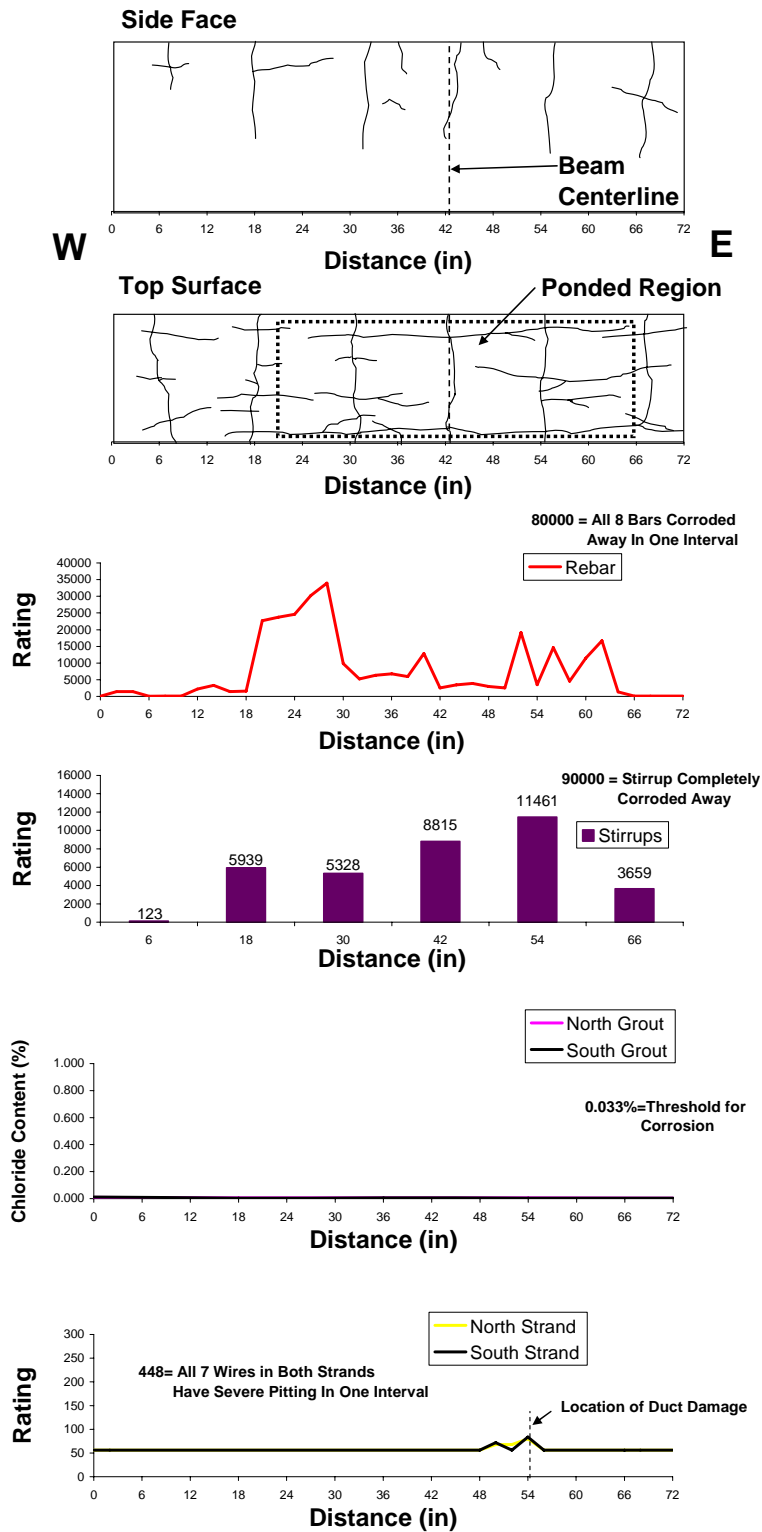


Figure 5.105: Beam 2.12-Crack Patterns and Corrosion Rating Graphs (Center Portion of Beam)

Anchorage



Figure 5.106: Beam 2.12 Anchorage Zones: East End Anchorage With Dripper (Left) and West End Anchorage Without Dripper (Right)

As shown in Figure 5.106, there was staining on the dripped end of the beam where the saltwater had exited from the dripping system. There was no staining on the west end anchorage. No shrinkage cracks were seen on the grout pockets in either anchorage zone. On the underside of the east end anchorage a network of cracks were observed above the 4x8 concrete cylinder used to stabilize the saltwater drip pan. The cracks spread up the sides of the end of the beam around 3 in.. The cracking is shown in Figure 5.107. This photograph was taken once the anchorage block was removed from the beam and flipped upside down. This cracking was likely caused by the same mechanism as the anchorage cracking in beam 2.9.



Figure 5.107: Beam 2.12-Cracking in East End Anchorage Zone

The maximum crack width in this crack network was 0.005 in.. This was measured on the side of the beam. However, there was no staining from any of the cracks.

West End Anchorage Zone (Control End)

The west end anchorages just after removal from the beam are shown in Figure 5.108 .



Figure 5.108: Beam 2.12 West End Anchorages (Control End)-South Duct Anchorage (Top, Left and Right) and North Duct Anchorage (Bottom, Left and Right)

In Figure 5.108, the entire south duct anchorage is shown with the grout cap removed and the grout underneath revealed. The damage to the grout cap occurred during its removal from the anchorhead. The photograph to the right is the face of the anchorhead after the grout was removed. The corrosion seen on both anchorheads is just outside the perimeter of the seal of the rubber ring behind the grouting cap. This corrosion may have caused by bleed water trapped in this area. However, within the perimeter of the seal the anchorhead had no corrosion and the outside of the strands and wedges were nearly pristine in appearance. When the collars behind the anchorheads were opened, the area beneath them was found to be filled with grout and in good condition.

The portion of the south duct and north ducts within the anchorage were in good condition. Some evidence of strand abrasion was found on both ducts, but no punctures

or cracks were found in the ducts. The duct portions from the anchorage are shown in Figure 5.109. Corrosion damage ratings for the ducts are not plotted since they are plastic.

Both ducts were well grouted, and no evidence of bleed water accumulation was found. The grout completely filled the end caps in both ducts, and as previously mentioned, filled the area under the collar. Chloride content testing of the grout in both ducts showed negligible chlorides. Grout from the caps and the collars also showed negligible chlorides. The grout from both ducts are shown in Figure 5.109.

The exterior of the strands from both ducts were in excellent condition, but when the strands were unraveled light to moderate corrosion was found in the interstices throughout the anchorage. What likely occurred was corrosion from the center of the beam spread down the length of the strand through the interstices. The wedges from both ducts had only some instances of slight discoloration inside the anchorhead. The strand from the anchorage is shown in Figure 5.109. The strand corrosion ratings in the anchorage are plotted in Figure 5.113 and are summarized in Table 5.21.



South Duct



North Duct



South Duct Grout Cap



North Duct Grout (From Bottom)



South Duct Strand with Wedges



North Duct Strand with Wedges



South Duct Strand



North Duct Strand

Figure 5.109: Beam 2.12 West End Anchorage (Control End) Autopsy Elements

East End Anchorage (Dripped End)

During autopsy of the end block containing the east end anchorages, moderate corrosion was found on the stirrups above the cracks in the anchorage as mentioned previously. The stirrup is shown in Figure 5.110.



Figure 5.110: Beam 2.12-Corroded Stirrup in East End Anchorage Zone (Dripped End)

The stirrup was likely corroded by saltwater splash from the drip pan when the dripper system was run, since the crack was directly beneath the stirrup and above the drip pan for the saltwater.

The east end anchorages are shown in Figure 5.111.



Figure 5.111: Beam 2.12 East End Anchorages (Dripped End)-South Duct Anchorage (Top, Left and Right), and North Duct Anchorage (Bottom, Left and Right)

As shown in Figure 5.111, the north duct anchorhead and bearing plate had some corrosion, while in case of the south duct there was very little corrosion on the bearing plate or the anchorhead. The north duct anchorhead had corrosion around the o-ring seal, like the anchorages from the other end of the beam. However, the south duct anchorhead had no such corrosion. In the case of both ducts the strand and wedges appeared to be in pristine condition at the anchorhead. When the collars behind the bearing plates were removed, no significant corrosion was found on the bearing plates beneath the collars.

Both the north and south duct portions in the anchorage zone were in good condition. Evidence of abrasion in the plastic duct was found where the strands were in contact with the ducts, but no cracks or holes were found in the ducts. The ducts from the anchorage are shown in Figure 5.112.

Both ducts were well grouted at the anchorage. Very small bleed water voids were seen at some of the peaks of the duct ribs, similar to what occurred in the center of the beam. Grout also completely filled the end cap and the area beneath the collar in the south duct. There was a small void at the top of the cap in the north duct cap. The area

beneath the collar was completely filled with grout in the north duct. Chloride content testing of the grout from the cap and collar as well as the duct showed negligible chlorides in both the north and south tendons. The grout from both tendons is shown in Figure 5.112.

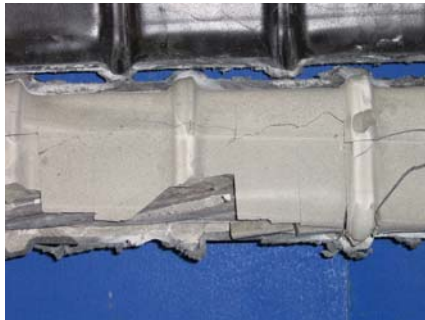
The strands in both ducts had light to moderate corrosion, with the corrosion essentially only in the interstices, similar to the strand from the control end of the beam. The wedges in both ducts only had some very light corrosion. The strands from the anchorage are shown in Figure 5.112. The corrosion ratings for the strand in the anchorages are plotted in Figure 5.113 and are summarized in Table 5.21.



South Duct



North Duct



South Duct Grout



North Duct Cap



South Duct Strand With Wedges



North Duct Strand With Wedges



South Duct Strand



North Duct Strands

Figure 5.112: Beam 2.12 East End Anchorage Zone (Dripped End) Autopsy Elements

In Figure 5.113 the strand corrosion ratings are plotted. Data from both beam ends are plotted together so that a comparison can be made between the dripped end and control end of the beam. It is assumed that the influence of the corrosion of the strands at the center portion of the duct had the same influence on either beam end. The x value “Distance From Beam End” indicates the distance from the respective beam end. The corrosion ratings for the anchorages are summarized in Table 5.21.

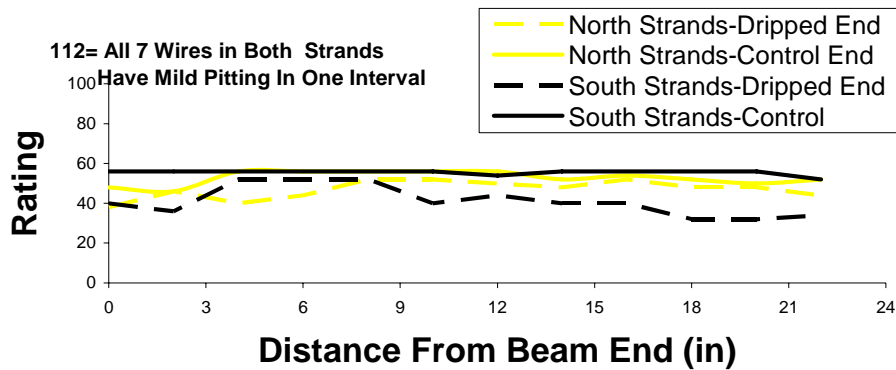


Figure 5.113: Beam 2.12-Strand Corrosion Ratings for Anchorages

Table 5.21: Beam 2.12-Corrosion Rating Summary for Anchorages

	<u>Dripped End</u>		<u>Control End</u>	
	Maximum	Total	Maximum	Total
North Duct	N/A	N/A	N/A	N/A
South Duct	N/A	N/A	N/A	N/A
North Strand	28	562	28	634
South Strand	26	494	28	666

From Table 5.21 and Figure 5.113 it is clear that the strand corrosion did not increase between the control end and the dripped end. In addition, the lack of chlorides in both the caps and collars suggest that the encapsulated system prevented chlorides from entering the duct at all. In addition, the tips of the strands outside the anchorhead in both ends of the beam were in much better condition than the strand tips in the non-encapsulated anchorages (Beam 2.7 and Beam 2.9).

Chapter 6: Analysis of Results

6.1 OVERALL OBSERVATIONS FROM FORENSIC ANALYSIS

6.1.1 Cracking

All of the loaded specimens had longitudinal cracks above the longitudinal reinforcing bars and ducts that in almost every beam were much wider than the flexural cracks from loading. The cracks were the result of the expansive effect of bar and metal duct corrosion products. Thus in most cases there was significant corrosion even in parts of the ponded region where there were no flexural cracks.

6.1.2 Reinforcing Bar Corrosion

The uncoated reinforcing bar damage in the many of the beams was tremendous. In the 2/3-PS beams of both phases I and II many of the #3 bars were completely corroded away across several inches. This would likely result in a substantial decrease in the ultimate strength of the member.

6.1.3 Duct Corrosion and Grouting Voids

In the loaded beams, the galvanized ducts were corroded away in multiple locations. It is also worth noting that the duct corrosion seemed to be worse in areas where grouting voids existed. Indeed, in many cases corrosion products were found in the grouting voids. Thus, poor grouting can have a detrimental effect on the durability of the galvanized duct. This was also found in the 4-year autopsy beams.³

6.1.4 Strand Corrosion

In many cases no corrosion was found on the exterior of the strands but upon unwinding heavy corrosion was found within the interstices. This clearly demonstrates that strand can transport moisture down its entire length. In some of the partially prestressed beams of Phase I the strand corrosion was so heavy that in some cases strand wires were found to be either substantially reduced in area or actually snapped during unwinding of the strand.

6.1.5 Anchorages

The saltwater drippers at the end anchorages caused enough chloride ingress so that the threshold for corrosion was reached at the levels of the anchorhead/strand tails. Indeed, corrosion was found on the anchorheads and strand tips during autopsy. In the case of the anchorages covered with caps, the strand tips were in much better condition. However, any further corrosion from the drippers was difficult to detect because moisture from the ponding at the center of the beam traveled down the strand interstices all the way to the anchorages. This resulted in corrosion in the strands even in the anchorages that were not exposed to drippers. Thus, any differences between ends with drippers and those without drippers were found by comparing the numerical ratings.

6.2 ANALYSIS OF PHASE I VARIABLES

6.2.1 Level of Prestress, Applied Loading, and Crack Width

In order to compare numerically the extent of cracking in each beam specimen, a crack rating was computed using the following equation, adopted from Salas³:

$$\text{Crack Rating for each Specimen} = \sum_{i=1}^m (w^{avg}_i \times l_i) \quad \text{Eq. 6-1}^3$$

Where, w^{avg}_i = average crack width, for crack i

l_i = crack length at end of testing, for crack i

m = number of longitudinal and transverse cracks on the specimen top surface in the 72 inch autopsy area

i = crack under consideration

The rating is essentially the surface area of the cracks in the autopsy area. In Figure 6.1, the crack ratings for each of the beams from Phase I are plotted. Note that “NL” indicates no applied load, “CL” indicates small crack load, “SL” indicates service load, and “OL” indicates overload. In order to obtain a relative sense of the amount of cracking in the beams, a baseline service load rating is shown for each section type. This baseline rating represents the crack rating a fully cracked beam would have under AASHTO maximum allowable service load cracking. It is computed using the typical number of flexural cracks found in the autopsy area in each beam type at service load (9 cracks for Non-PS, 6 cracks for 2/3-PS, and 3 cracks for 100% U and 100% S), and the

Class 1 crack width from AASHTO of 0.017 inches.²⁰ The cracking rating for beam 1.1 was scaled up to account for the fact that only 42 inches were removed during autopsy. This was not necessary for beam 3.1 since it had no visible cracking.

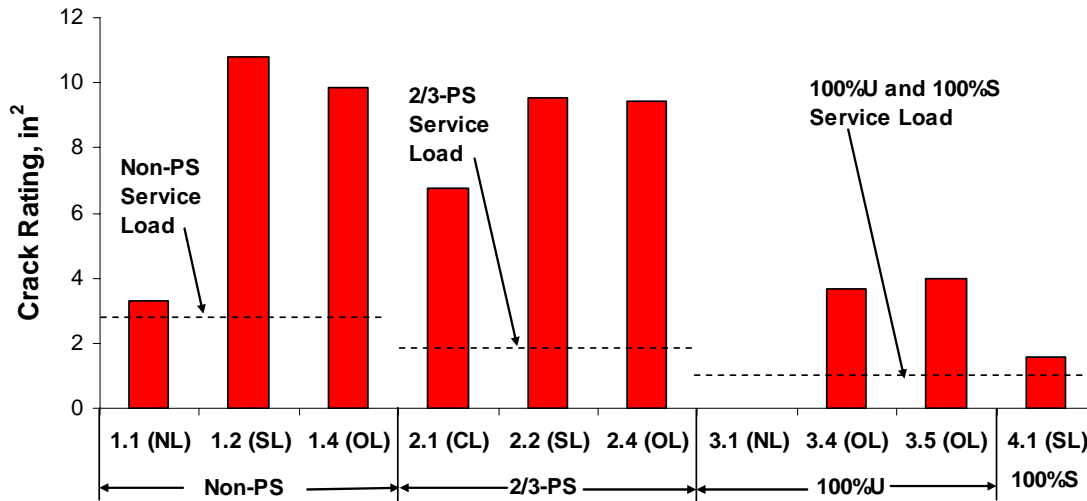


Figure 6.1: Phase I Beams- Crack Ratings

In all loaded beams except 4.1 (100% S) the crack ratings are much higher than the baseline, due to the extensive longitudinal cracking from the duct and bar corrosion. Beam 1.1, which was never loaded, actually exceeded the crack rating for service load just from the effect of the bar corrosion. When comparing specimens with similar loading, it is clear that the long-term cracking was only reduced for the beams that were fully prestressed (100% U and 100% S), since the loaded Non-PS beams and the loaded 2/3-PS beams had essentially the same level of cracking.

When comparing specimens with the same levels of prestress, it is evident from the 2/3-PS beams and the Non-PS beams that once the specimen reaches service load cracking levels there is no real difference in the long-term cracking behavior. However, the 2/3-PS specimen which was initially loaded to only a small crack width did have a considerably lower long-term cracking rating. Even though all the 2/3-PS specimens had wide longitudinal cracks, the somewhat lower rating in this beam was caused by the fact that the flexural cracks were smaller in width than the other 2/3-PS beams.

The longitudinal bar and stirrup generalized ratings for the Phase I beams are plotted in Figure 6.2, along with the crack ratings. In order to obtain a relative sense of the amount of corrosion of the uncoated reinforcement components, a baseline

generalized corrosion rating is shown on the plot. It corresponds to extremely heavy corrosion in which half of the reinforcement would be completely corroded over at least one 2-in. interval in each foot of bar or stirrup.

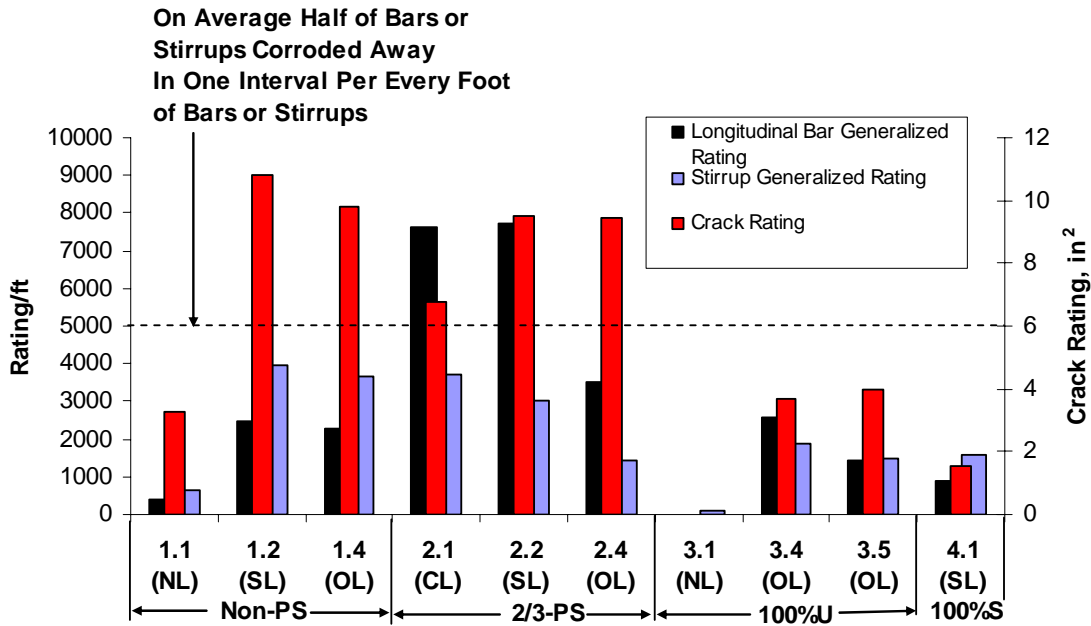


Figure 6.2: Phase I Beams- Stirrup and Longitudinal Bar Generalized Ratings vs. Crack Ratings

Figure 6.2 shows that when comparing specimens with same level of applied load, the stirrup and longitudinal bar damage was substantially less for fully prestressed specimens. The high ratings in the 2/3-PS beams are caused by the fact that the #3 bars were completely corroded away in many locations. The damage was not as severe in the Non-PS beams because the bars were larger (#4's and #5 bars).

Increasing the initial level of loading did not have any appreciable effect on the bar or stirrup damage in the Non-PS or 2/3-PS beams. Of course, the unloaded Non-PS beam (1.1) had little damage due to the lack of an applied load.

Only in the Non-PS beams do the crack ratings follow the trend of the bar corrosion. In the prestressed beams the duct corrosion as well as bar corrosion are contributing to the longitudinal cracking. This explains why the crack ratings do not follow the trend of bar damage in the prestressed beams.

The duct ratings for the Phase I beams are plotted in Figure 6.3, along with the crack ratings. The ducts in each beam are identified by splice type for proper comparison. Again, a baseline generalized rating is provided to indicate the rating corresponding to

very severe corrosion where an entire 2-inch interval of duct is corroded away in each foot of duct.

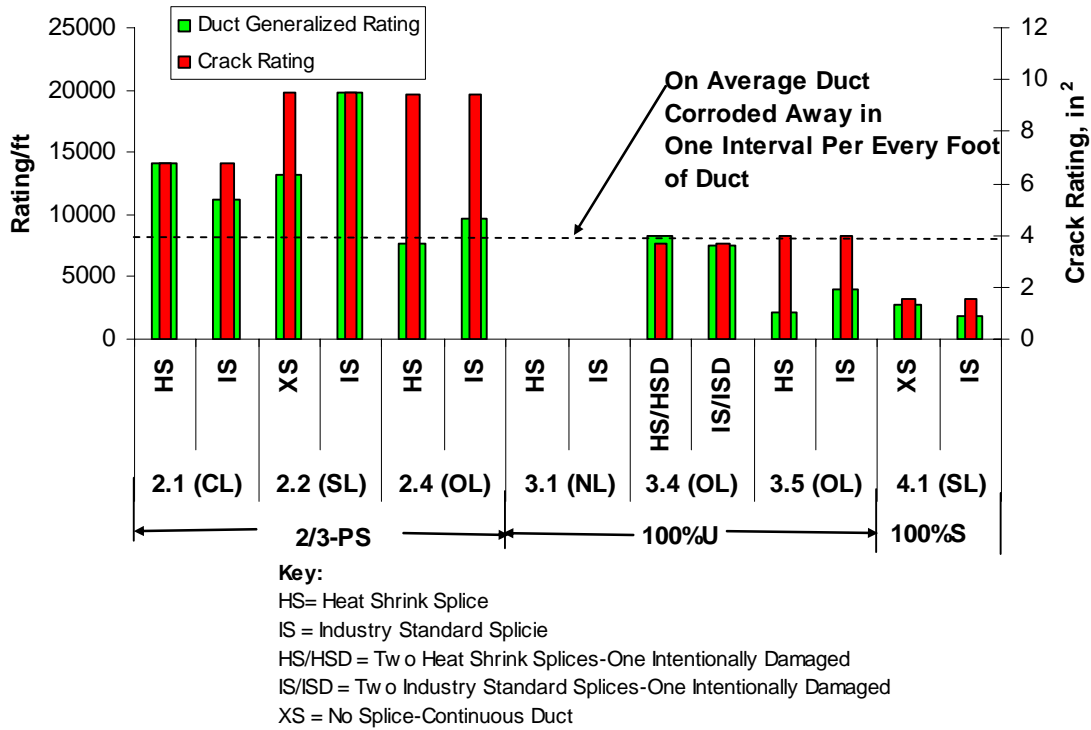


Figure 6.3: Phase I Beams-Generalized Duct Ratings (Organized by Splice Type)

When comparing specimens/ducts with similar loadings and with the same splice types, it is clear that the amount of damage in the ducts clearly decreased once the beam was fully prestressed.

Increasing the level of loading, which can be only be analyzed with the 2/3-PS beams, had no significant effect on the amount of damage in the duct.

There is no trend between the crack ratings and duct corrosion when comparing beams with similar levels of prestress. This is likely from the fact that bar corrosion, not just duct corrosion, is attributing to the cracking.

It is also clear the presence of the splice was not a significant factor in the amount of duct corrosion, since large portions of duct were corroded away even in areas where there were no splices.

The generalized strand ratings for each duct are plotted in Figure 6.4. Again, a baseline generalized rating is provided representing severe pitting occurring in one 2-inch interval for each foot of strand in each duct.

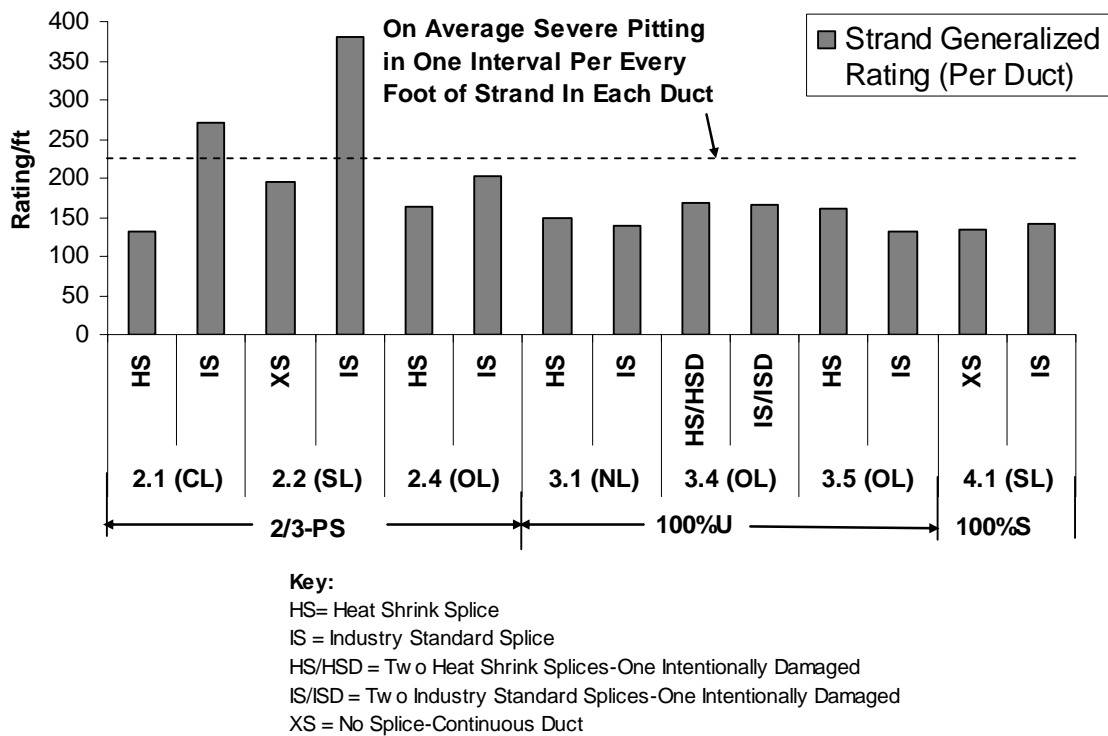


Figure 6.4: Phase I Beams-Strand Generalized Ratings

In Figure 6.4, when ducts with similar loadings and splices are compared, there is in general a decrease in strand corrosion with increased levels of prestress. This is especially true when comparing beams 2.2 and 4.1. However, when comparing the specimens at overload, beams 2.4 and 3.5, there is no difference between the ducts with the heat shrink splices. In general, the differences in strand corrosion are not as dramatic as the differences in bar and stirrup and in duct corrosion. Given the large amount of interstitial corrosion in the strands (mentioned in Chapter 5), it is likely that once a single part of the strand is corroded then the chlorides can be transmitted through the interstices and thus corrode the entire length of strand. .

When comparing the identical ducts in the 2/3-PS beams, there is no clear trend between strand damage and the level of applied load.

The maximum grout chloride contents found in each duct are plotted in Figure 6.5.

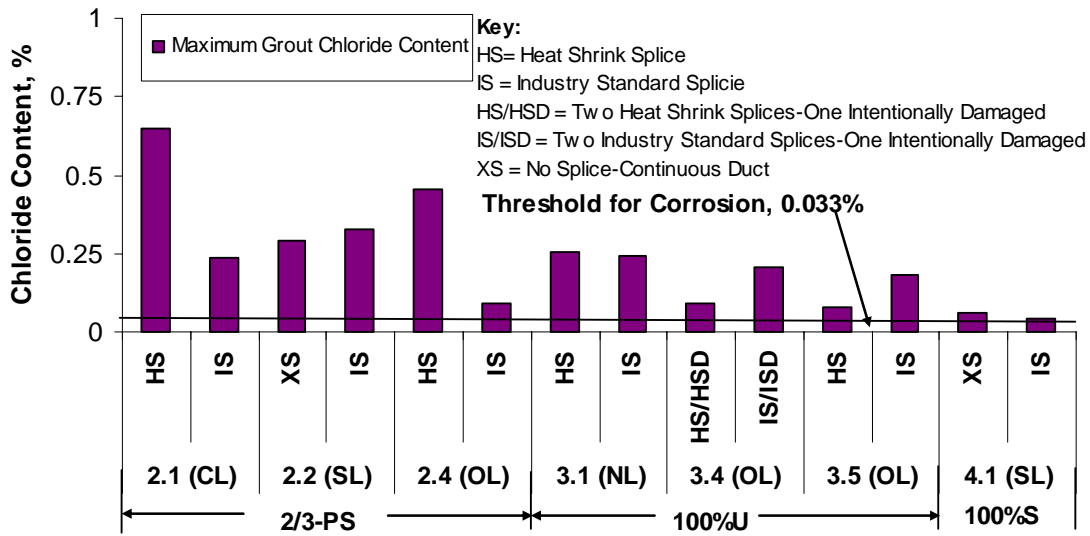


Figure 6.5: Phase I Beams-Maximum Grout Chloride Content in Each Duct

As shown in Figure 6.5, and as mentioned repeatedly in Chapter 5, the maximum chloride contents in all the tendons were higher than the threshold for corrosion of 0.033%. Therefore, any differences between specimens with similar loadings or prestress are inconsequential.

Overall, only when beams were fully prestressed did the overall corrosion decrease in the autopsy elements. In general, increasing the level of initial applied loading had no effect on the amount of damage that was present at the end of exposure testing. This is likely due to the fact that in general the longitudinal corrosion splitting cracks were far wider than the flexural cracks, so they began to dominate the corrosion amount in each beam.

6.2.2 Duct Splice Type and Condition

As is clear from the forensic analysis of Chapter 5, both splice types performed poorly. Heavy duct section loss was found in splice zones with industry standard splices, while pitting and in some cases small holes were found in the splice zones of ducts with the heat shrink splice. In Figure 6.4 the 2/3-PS beams all show that the strand in the ducts with industry standard splices was more corroded than the strand with the heat shrink splices. However, in the case of beam 3.5 (100%U) the strand in the heat shrink spliced duct was more heavily corroded. The chloride content data in Figure 6.5 shows

that there is no correlation between splice type and amount of chloride ingress. In some cases the heat shrink spliced ducts had more chloride ingress, while in some cases the industry standard spliced duct had more chloride ingress. In the case of beam 4.1 the duct with no splice had more chloride ingress than the duct with the industry standard splice. Therefore, it would appear that after 8 years of testing the primary mechanism for chloride ingress in the tendon is the corroded duct. The effect of the splices became less significant as the duct began to corrode away allowing more chlorides into the grout and then into the strand.

As discussed in the forensic analysis of beam 3.4 in Chapter 5, the effect of accidental damage to each splice type was in all likelihood insignificant in comparison to the effect of the tremendous duct loss after 8 years of testing. In addition, as mentioned above, both splices performed poorly anyway so any accidental damage is inconsequential.

6.3 PHASE II VARIABLES

The crack ratings for the Phase II beams are shown in Figure 6.6. The longitudinal bar and stirrup ratings are plotted in Figure 6.7. Note that all Phase II beams are 2/3-PS at service load. Therefore, the same baseline service load crack rating as used in the Phase I 2/3-PS beams is shown.

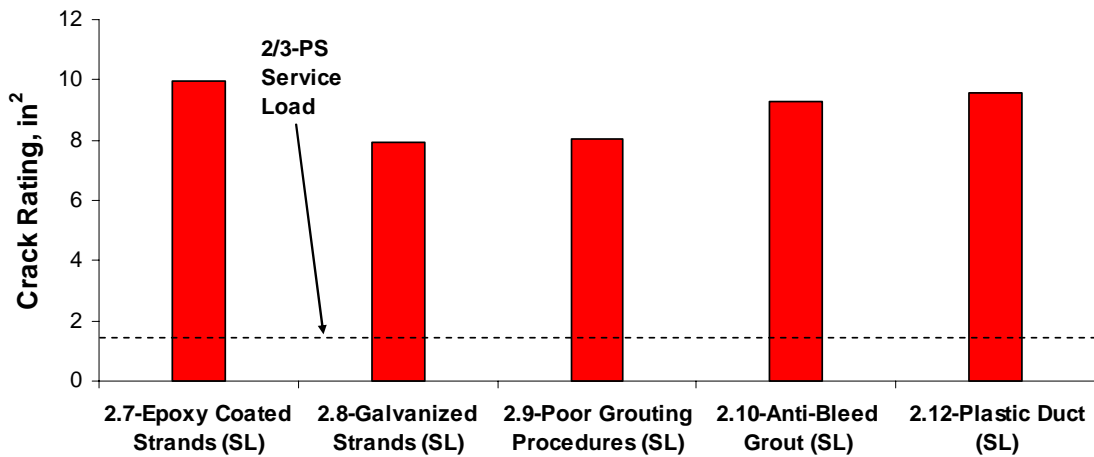


Figure 6.6: Phase II Beams-Crack Ratings

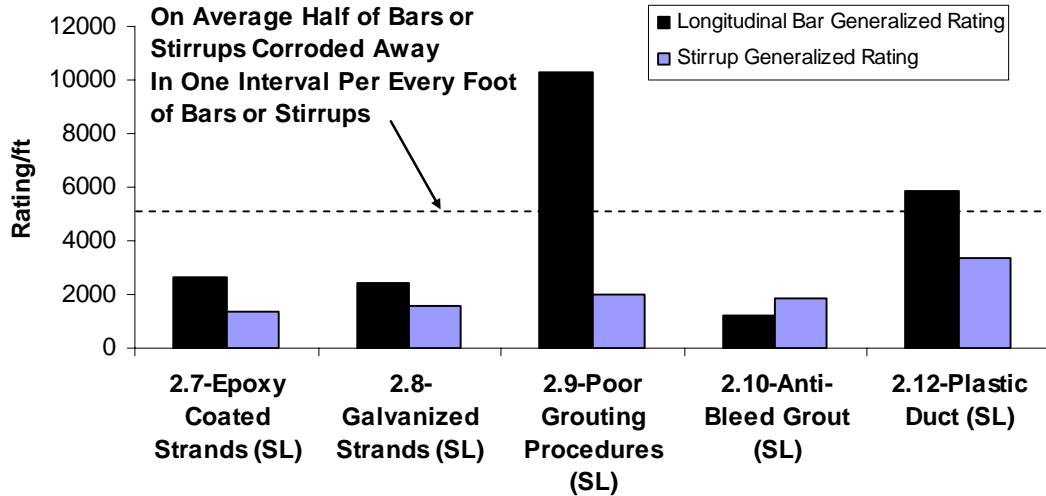
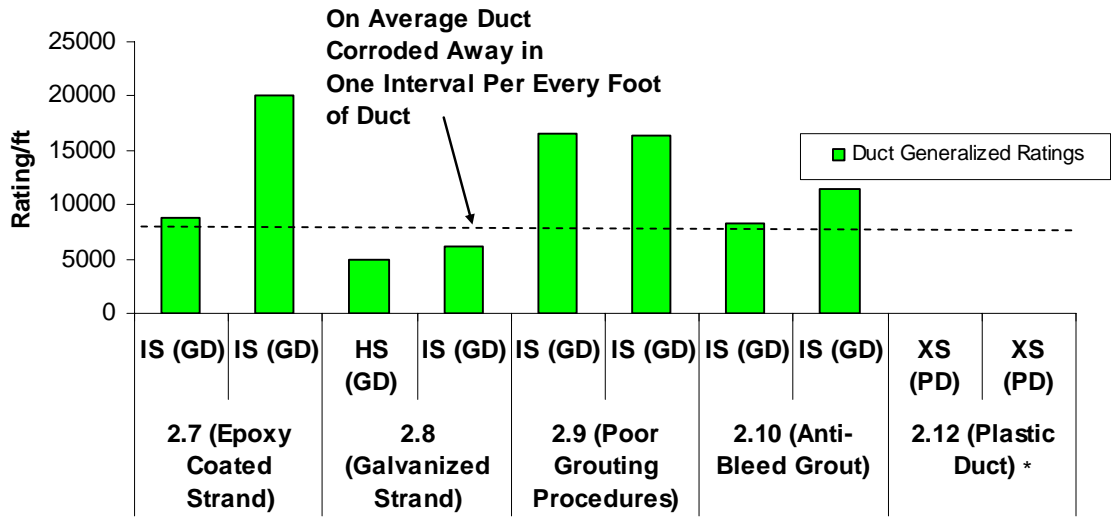


Figure 6.7: Phase II Beams-Bar and Stirrup Ratings

As shown in Figure 6.6, all the Phase II beams exhibited similar very poor long-term cracking behavior. Their cracking behavior is comparable to the 2/3-PS service load beam from Phase I (Beam 2.2).

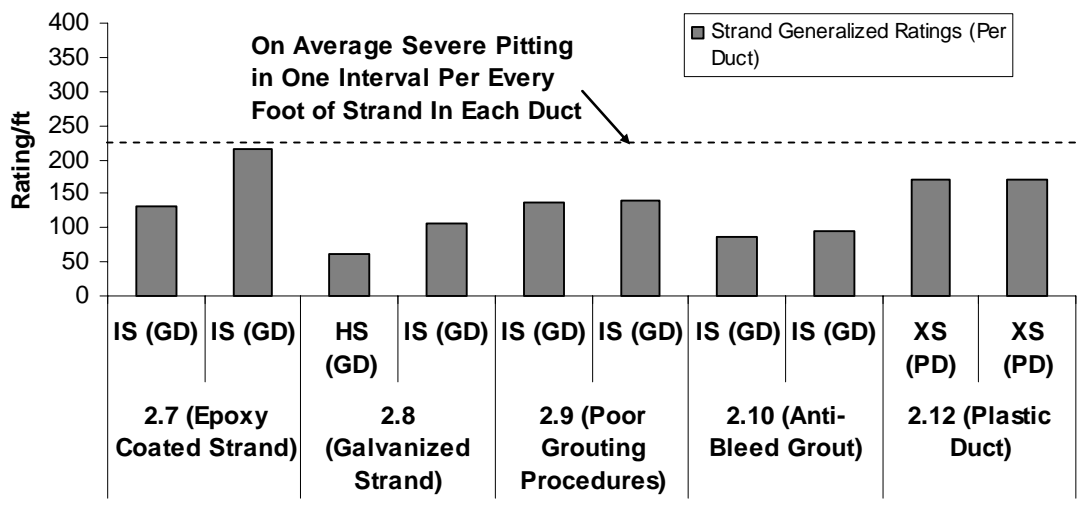
6.3.1 Duct Type

The two duct types tested in the Phase II beams were the plastic duct and the galvanized duct. The duct ratings are plotted in Figure 6.8. The strand ratings and chloride contents for each Phase II duct are plotted in Figure 6.9 and Figure 6.10 respectively.



Key:
 IS (GD) = Galvanized Duct With Industry Standard Splice
 HS(GD) = Galvanized Duct With Heat Shrink Splice
 XS (PD) = Continuous Plastic Duct (No Splice)
 *No Rating for Plastic Duct Since it Did Not Corrode

Figure 6.8: Phase II Beams-Duct Generalized Ratings



Key:
 IS (GD) = Galvanized Duct With Industry Standard Splice
 HS(GD) = Galvanized Duct With Heat Shrink Splice
 XS (PD) = Continuous Plastic Duct (No Splice)

Figure 6.9: Phase II Beams-Strand Generalized Ratings

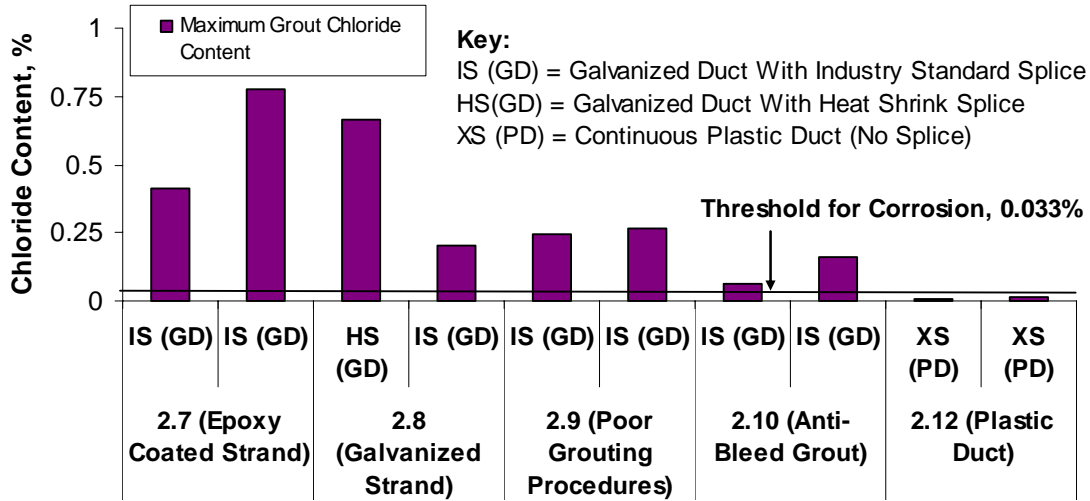


Figure 6.10: Phase II Beams-Maximum Grout Chloride Content in Each Duct

As shown in Figure 6.8 and as was found previously with the Phase I beams, the galvanized ducts performed extremely poorly. As mentioned in Chapter 5, the plastic ducts in beam 2.12 were punctured due to mechanical failure. As shown in Figure 6.9 this resulted in greater strand damage than with the comparable specimen with galvanized duct, beam 2.9 (The proper comparison is with beam 2.9 since it has the same grout type in addition to conventional strand). As shown in Figure 6.10 the chloride content in the plastic duct specimen was still lower than the threshold for corrosion. As explained in Chapter 5, this is likely from the fact that the chlorides entered the strand almost directly through the punctures and as a result only a small amount of chloride may have been deposited into the grout. This puncture problem had been noted previously in the industry. One solution proposed to alleviate this problem is to use metal cradles between any bracing bars and the plastic duct.²¹ However, a metal cradle could corrode in an aggressive environment, so placing sturdy rubber or plastic pads between the duct and any bracing bars may be a better solution. In addition, in previous research done under TxDOT Project 0-4562 in 2004/2005, Luthi, Diephuis, and Icaza⁶ performed pullout and friction tests on industry standard HDPE (High Density Polyethylene) plastic ducts with very small radii of curvature (as little as 10 ft). These plastic ducts were larger in thickness and diameter than those used in this study and would thus be more typically of those widely used in bridge applications. After testing, the ducts were removed and examined. In their study somewhat similar “grooves” were observed in the plastic ducts.

However, the grooves were not as deep and the ducts were not significantly damaged or punctured.¹⁵ In addition, in slab applications (where the VSLAB+™ system used in this study is used) the tendons typically have almost no curvature so the risk of this type of damage occurring would be very small. Thus the VSLAB+™ system would be expected to work for a slab, but not as a draped tendon in a substructure or superstructure. Therefore, with a more “robust” and modern plastic duct system there is little risk of puncture damage occurring in a draped tendon.

It is worth noting that, as mentioned in Chapter 5, the plastic duct did have better grouting performance than the galvanized ducts. This was a result of the ability of the bleed water to accumulate in the peaks of the large ribs in the plastic duct, preventing the formation of large bleed water voids.

With the data from this study it cannot be said for certain that plastic ducts perform better than galvanized ducts. However, if the plastic duct system is “robust” it will likely perform far better than galvanized duct. Indeed, previous research done at the University of Texas with macrocell specimens under project 1405 found that galvanized steel ducts performed substantially better than plastic ducts.³

6.3.2 Strand Type

The three strand types tested were epoxy coated strand, galvanized strand, and conventional strand for comparison.

6.3.2.1 Epoxy Coated Strand

As shown in Chapter 5 and clearly shown in Figure 6.9, the non-flow filled epoxy coated strand used in this study performed poorly in comparison to conventional strand (this comparison is made between beams 2.7 and 2.9 since both have the same type of grout). Abrasion damage to the brittle epoxy coating as a result of prestressing operations allowed chloride ingress onto the strand surface. Because the coating did not also fill the interstices of the strand, the moisture was able to spread throughout the length of the strand. The damage might have been minimized if the epoxy had filled the interstices, so called “flowfilled” epoxy strand. It would also be preferable if the epoxy had better mechanical properties to resist abrasion and wedge tooth penetration.

The effect of coating damage and patch effectiveness was discussed in Chapter 5. It was found that the patches performed fairly well.

6.3.2.2 Galvanized Strand

As presented in Chapter 5 and as shown in Figure 6.9, galvanized strand performed only slightly better than conventional strand. Thus it still performed poorly. The presence of the galvanized coating only delayed the onset of corrosion.

Therefore, in this highly aggressive environment both the galvanized stand and the epoxy coated strand offered no real improvement in long-term corrosion resistance in comparison to conventional strand.

6.3.3 Grouting Procedure

As shown in Chapter 5 the “poor grouting” procedures in beam 2.9 definitely resulted in slightly poorer quality grout than in the other beams. The grout was more segregated and had larger “bubbles” than the control grout used in beams 2.7, 2.8 and 2.12. However, even without the “poor” grouting procedures the grout in these specimens performed poorly as well, also having bleed water voids to the same extent as the grout in beam 2.9. So with the type of grout used, the grouting procedures are already “poor” even without the additional “poor” grouting procedures.

6.3.4 Grout Type

Unfortunately the anti-bleed grout in this study did not perform as well as hoped. It is likely that the mixing procedures used caused segregation and prevented the anti-bleed admixture from fully engaging. This demonstrates the importance of using high quality mixing procedures and equipment when grouting with anti-bleed grout.

6.3.5 Anchorage Protection

As mentioned in Chapter 5, the encapsulated system resulted in better strand protection than in the “uncapped” systems. The strand and wedges at the front of the anchorhead was in much better condition than those in the “uncapped” system. The VSLAB+™ system was shown to be basically watertight due to the lack of chlorides in the grout in the cap and the collar at the dripped end. However, it was difficult to gauge

the extent of the damage from the anchorage exposure cycles due to the fact that moisture ingress from the damage at the center of the beams was able to travel along the strand interstices and reach both anchorages in all the anchorage exposure beams. This clearly demonstrates how strand can act as a vehicle to transport moisture throughout a tendon. However, the tendons in the specimens are shorter than those typically seen in an actual bridge element, so this problem may not be as dramatic in real world applications. In addition, the presence of the galvanic corrosion at the interface of the galvanized duct/bearing plate gives further support to the use of an encapsulated system, where the steel is more of the same type.

6.4 COMPARISON OF DATA TAKEN AT THE END OF EXPOSURE TESTING WITH RESULTS OF FORENSIC ANALYSIS

6.4.1 Half-Cell Potential Data

6.4.1.1 Relative Values of Half-Cell Potential Data vs. Relative Corrosion Damage

In Figure 6.11 the generalized stirrup and bar ratings from the Phase I beams are plotted with the final maximum half-cell reading for each beam. The same is done with the duct ratings in Figure 6.12 .

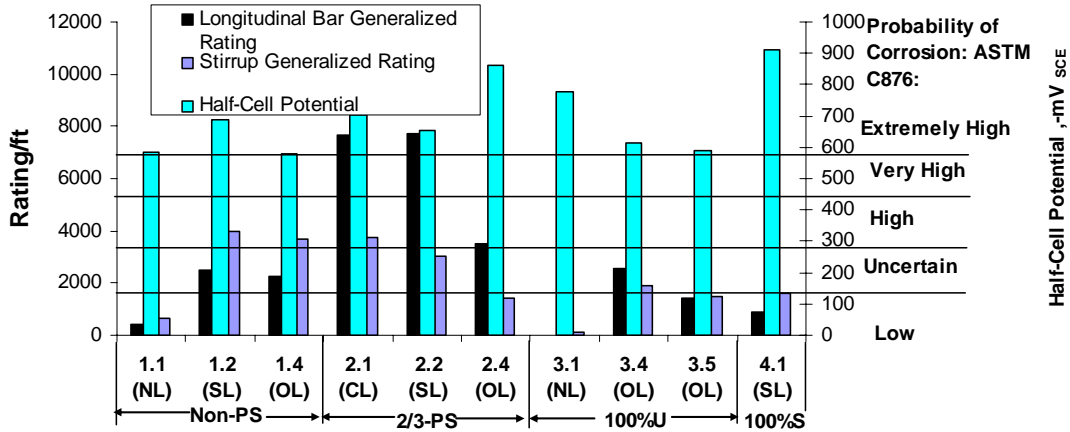


Figure 6.11: Phase I Beams-Stirrup and Bar Generalized Ratings vs. Final Half-Cell Potential Readings

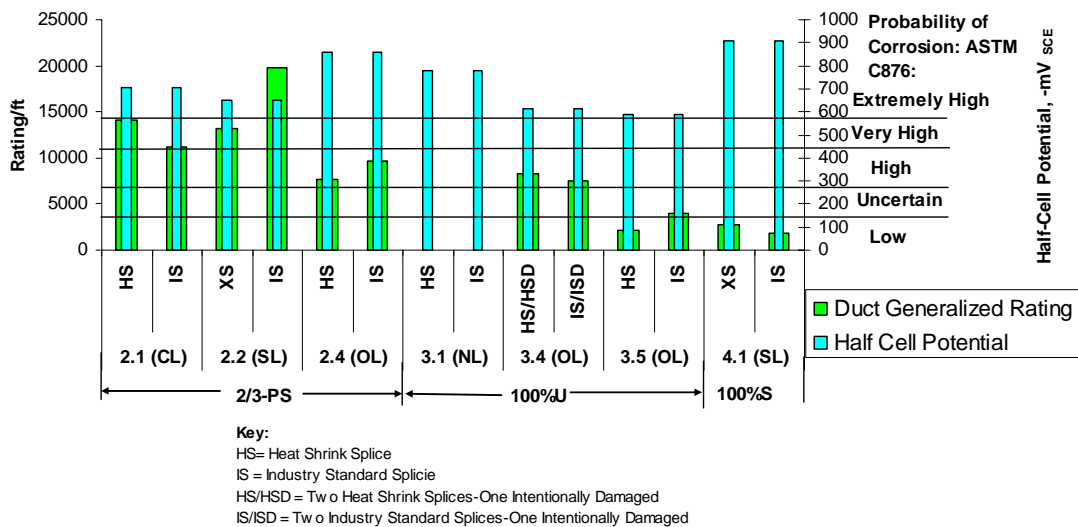


Figure 6.12: Phase I Beams- Galvanized Duct Ratings vs. Final Half-Cell Potential Readings

In Figure 6.11 and Figure 6.12 the half-cell data essentially indicate a greater than 90% probability of corrosion (extremely high probability) for all beams. Indeed, all bars, stirrups, and ducts were at the very least significantly corroded in all specimens. Thus, the half-cell potentials were correct in this matter. However, it is also clear that half-cell readings do not give a good estimate of the relative corrosion damage in the specimens. This is exemplified in Figure 6.11 by beams 3.1 and 4.1, where the relative bar and stirrup damage was low but these two beams had some of the highest half-cell potential readings. This is also true Figure 6.12 for the duct ratings for these beams as well. Only in the Non-PS beams do the half-cell data show the same trend as the stirrup and longitudinal bar data. This is significant because the bars and stirrups are the only elements corroding in the Non-PS beams since the Non-PS beams have no tendons. Since the galvanized ducts are in metal to metal contact with reinforcing bar cage in the prestressed specimens, a circuit is formed between the tendons and the bars and stirrups. Thus there is a large amount of interaction which may be causing the behavior shown in the half-cell potential data. The reinforcing bar, stirrup and duct ratings for the Phase II beams are plotted with the half-cell potential data in Figure 6.13.

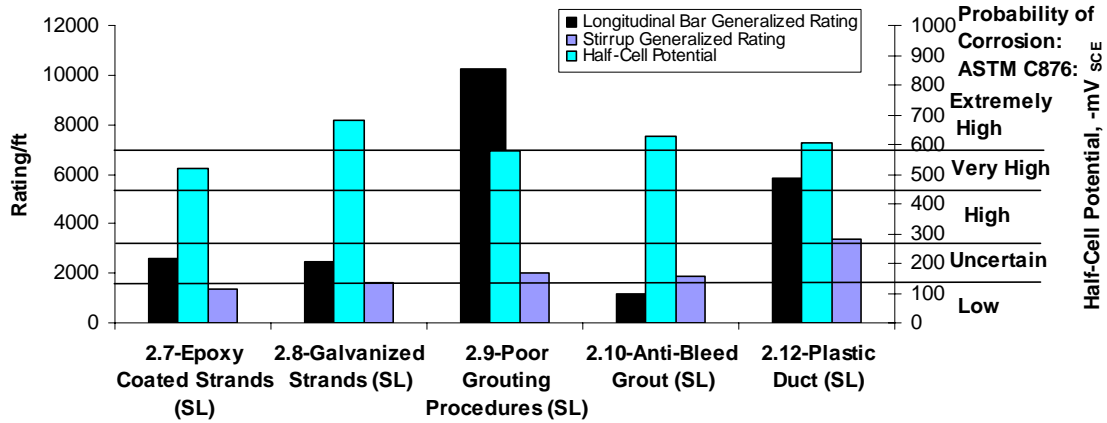
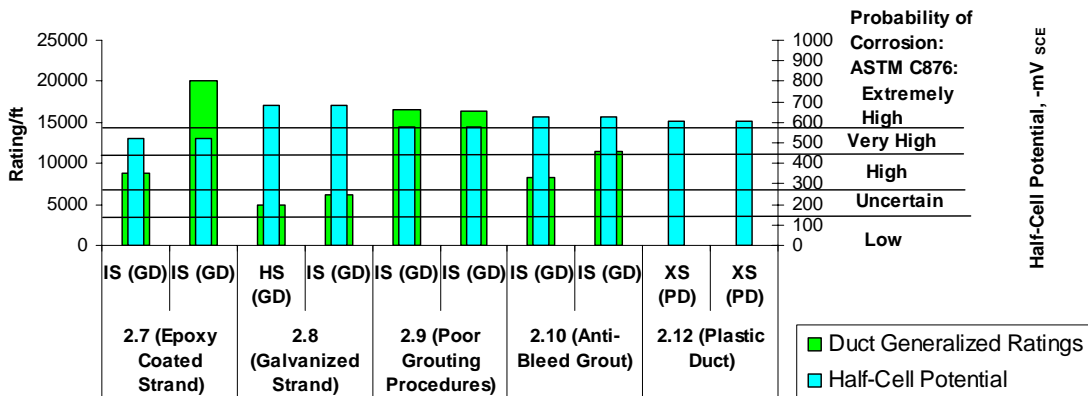


Figure 6.13: Phase II Beam Stirrup and Bar Generalized Ratings vs. Final Half-Cell Potential Readings



Key:
 IS (GD) = Galvanized Duct With Industry Standard Splice
 HS(GD) = Galvanized Duct With Heat Shrink Splice
 XS (PD) = Continuous Plastic Duct (No Splice)

Figure 6.14: Phase II Beams-Duct Ratings vs. Final Half-Cell Potential Readings

In Figure 6.13 all the half-cell potential data from all phase II beams suggested at least a very high probability of corrosion for all beams (All beams except for 2.7 were in the extremely high range). Indeed, the stirrups and the bars in all the beams were heavily corroded. So using the half-cell data to conclude that corrosion was present was accurate. However, there is no clear trend between the amount of the bar and stirrup corrosion damage and the half-cell potential readings. Careful examination of Figure 6.14 reveals that in general the half-cell potential data actually decreased (in absolute value) with increased duct corrosion, but only slightly. All the galvanized ducts in the Phase II beams were heavily corroded at the end of testing. Of course, beam 2.12 (plastic ducts)

which had half-cell potential values in the same range as the rest of the beams, had no duct corrosion. As mentioned for the Phase I beams, the two beams with the least amount of duct corrosion (beams 4.1 and 3.1) had some of the highest half-cell potential readings. Also, the half-cell potentials in the Phase I Non-PS beams were the only readings that agreed with the relative levels of damage in the beams. It is also known from electrochemistry in corrosion that any interaction between zinc and regular steel will result in more negative potentials in the circuit between the ducts and the bars. Therefore, this would all suggest that the zinc in the galvanized ducts is what is causing the incorrect relative behavior of the half-cell data. The interaction of the zinc and the steel reinforcing cage causes very negative values, but once the zinc has sacrificed itself and the duct begins to corrode away the corrosion of the reinforcing bars begins to dominate the half-cell readings. This suggests that the use of half-cell potentials to determine corrosion of ducts and strands is problematic.

6.4.1.2 Time to Initiation of Corrosion vs. Relative Corrosion Damage

In Chapter 4 it was inferred that corrosion initiates at the time when the half-cell data cross the threshold for very high probability of corrosion. In Figure 6.15 and Figure 6.16 the bar, stirrup, and duct corrosion ratings from the Phase I beams are compared to the estimated time of initiation of corrosion based on the half-cell potential data.

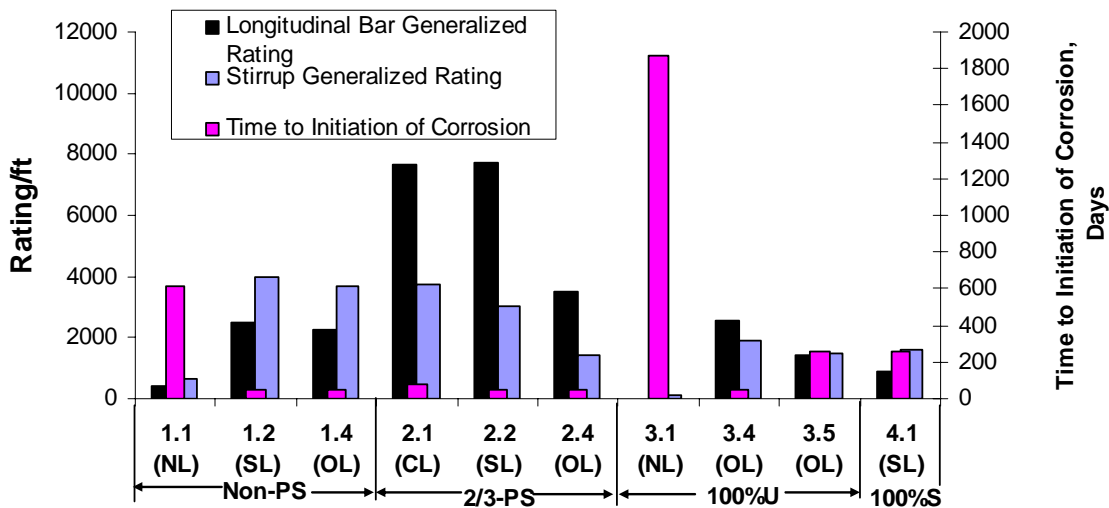


Figure 6.15: Phase I Beams-Stirrup and Bar Generalized Ratings vs. Time to Initiation of Corrosion

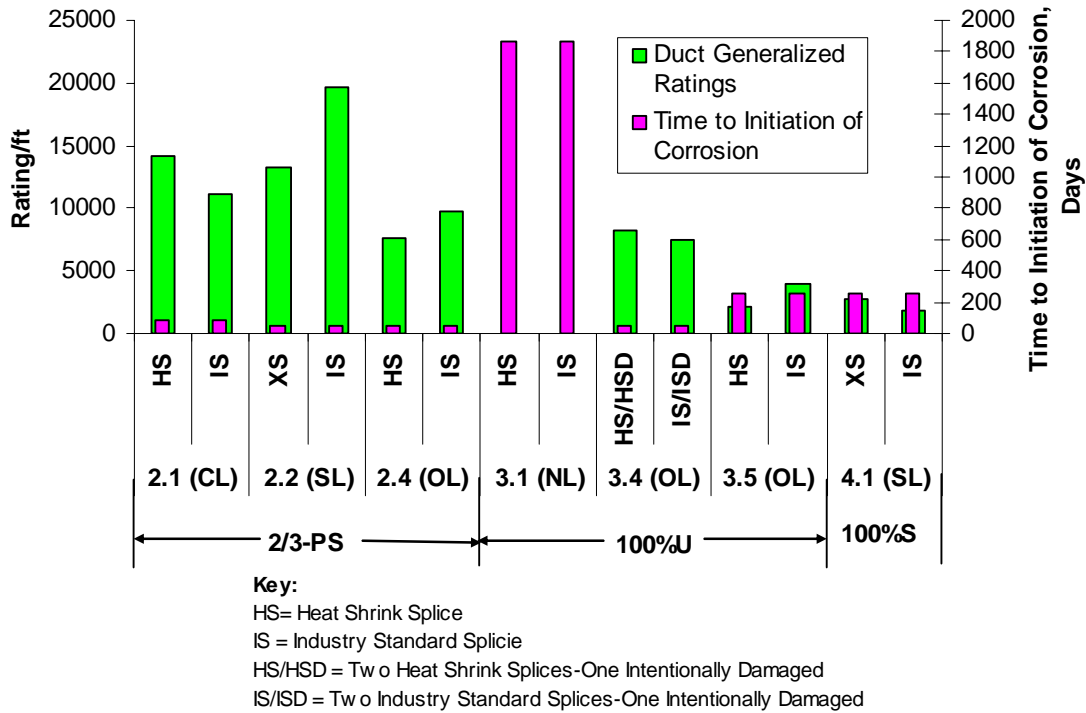


Figure 6.16: Phase I Beams-Duct Generalized Ratings vs. Time to Initiation of Corrosion

As stated in Chapter 4 and as shown in Figure 6.15 and Figure 6.16, the two unloaded beams (1.1 and 3.1) showed much longer times to initiation of corrosion than the other specimens. In the case of the 2/3-PS beams, maintaining the load at small crack levels delayed the onset of corrosion. Also, the time to initiation of corrosion was significantly delayed when the beams were fully prestressed (the service load and overload Non-PS beams and 2/3-PS beams began corroding at the same time). It is clear from Figure 6.15 and Figure 6.16 that the delay in the time to initiation of corrosion had no real effect overall on the final amount of corrosion in the beams. Of course, beams 1.1 and 3.1 had little corrosion due to the lack of cracking due to an applied load, which also delayed the onset of corrosion. This is not surprising considering the fact that all the loaded beams began to corrode within 1 year, which is insignificant considering that the length of exposure testing was a little over 8 years. In Figure 6.17 the Phase II beam stirrup and longitudinal bar ratings are plotted along with the time to initiation of corrosion.

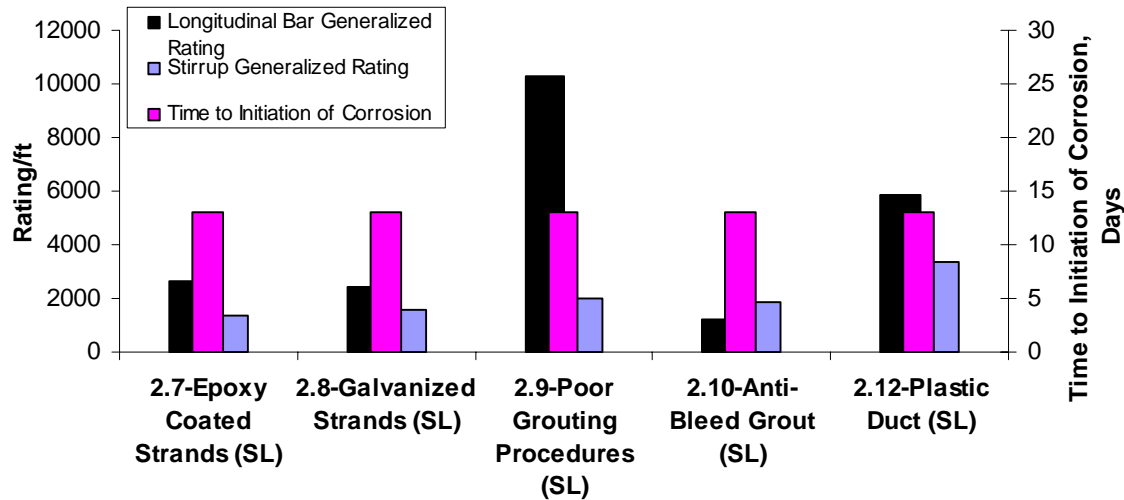


Figure 6.17: Phase II Beams-Stirrup and Bar Generalized Ratings vs. Time to Initiation of Corrosion

As mentioned in Chapter 4 and shown in Figure 6.17, all the Phase II beams indicated corrosion when the first set of readings were taken at 13 days. The bar and stirrup ratings varied among the specimens (as well as the duct ratings, shown in Figure 6.8), but all were very severe. This also suggests that the time to initiation of corrosion in cracked loaded beams has no effect on the final amount of corrosion, since the time to initiation of corrosion among the Phase II beams was the same but the bar, stirrup and duct ratings, while all severe, still varied. Indeed, the time to initiation of corrosion, 13 days, is extremely insignificant when considering the testing time of nearly 8 years.

Overall, the half-cell potential data were correct in indicating that corrosion was present, but it did not give a good estimate of the relative damage in the prestressed beams. Only in the non-prestressed beams was the half-cell data correct in this manner. These errors are attributed to presence of the galvanized ducts. However, in the field, what is more critical is that the half-cells indicate whether corrosion is present or not. The readings accomplished this. There is no way to confirm whether or not the half-cell potential data were correct in indicating that corrosion had initiated on certain days, but in the end the time to initiation of corrosion did not matter due to the length of testing.

6.4.2 Chloride Penetration

The maximum chloride content at the 2 inch depth are plotted with the Phase I stirrup and bar ratings in Figure 6.18 and with the duct ratings in Figure 6.19.

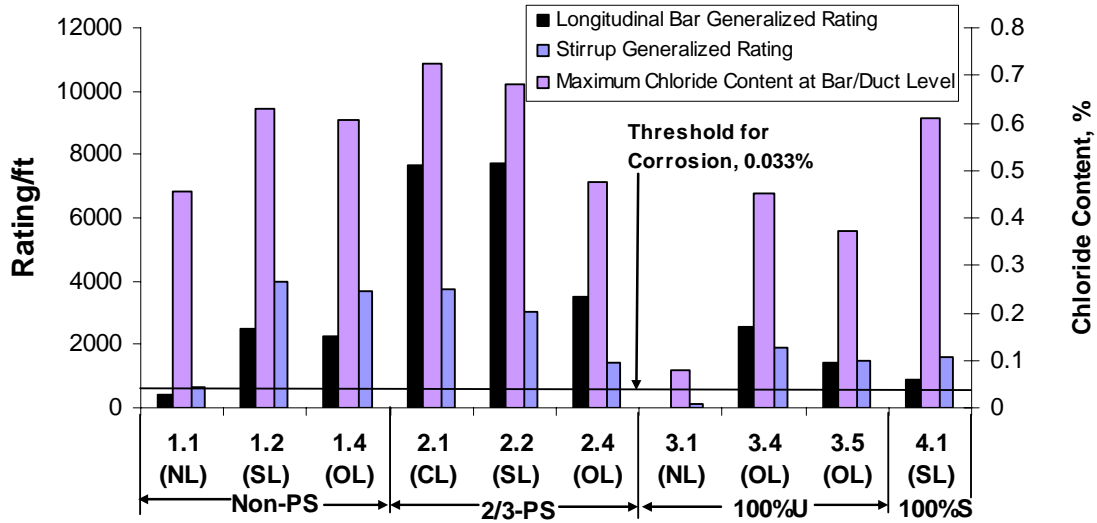


Figure 6.18: Phase I Beams-Maximum Chloride Content at Bar/Duct Level vs. Bar and Stirrup Generalized Ratings

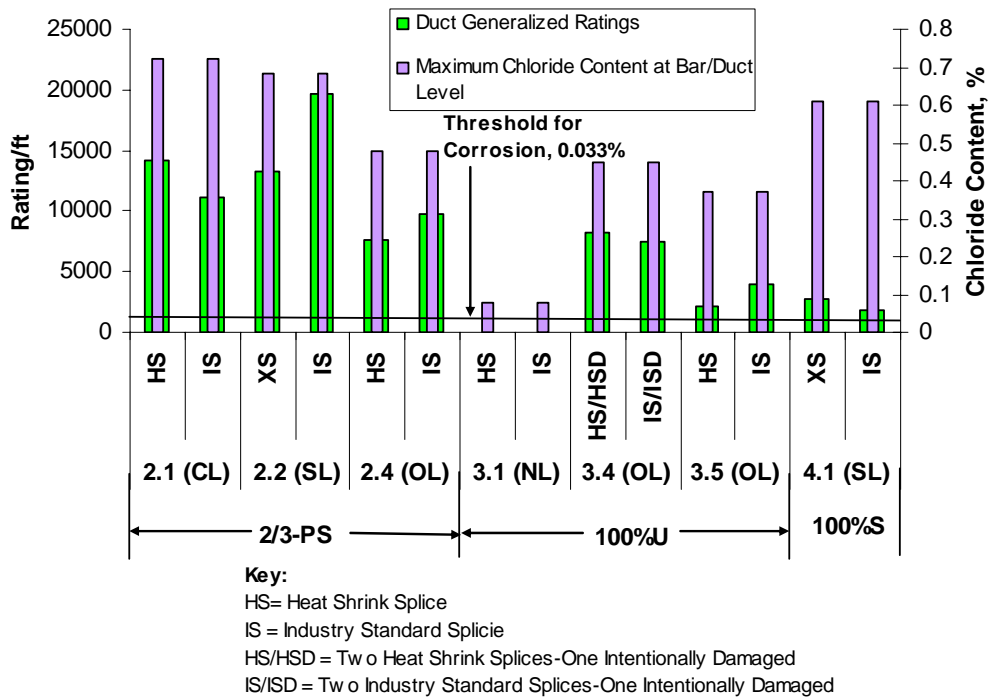


Figure 6.19: Phase I Beams-Maximum Chloride Content at Bar/Duct Level vs. Generalized Duct Ratings

As shown in Figure 6.18 and Figure 6.19 , and as mentioned in Chapter 4, the threshold for corrosion was reached at bar/duct level in the ponded region in all beams. During autopsy the bars and stirrups in all beams were found to be severely corroded.

While the corrosion was typically the highest in the areas of the flexural cracks, it was also significant in areas where there was no flexural cracking. In Chapter 5 it was also noted that many of the beams had wide longitudinal splitting cracking which was from severe bar corrosion. As mentioned in Chapter 4, in several instances the concrete ponding blocks were found to have reached the threshold for corrosion. Therefore, it would appear that chloride ingress due to high concrete permeability was beginning to become significant. The corrosion this caused on the bars and ducts, and in the Phase I beams steel bolster strips, likely initiated the longitudinal cracking. This is also supported by the fact that the unloaded beam 3.1, which had a very low chloride content (but still above the threshold), had no longitudinal cracking. The Phase II bar, stirrup, and duct ratings are plotted with the maximum chloride contents in Figure 6.20 and Figure 6.21.

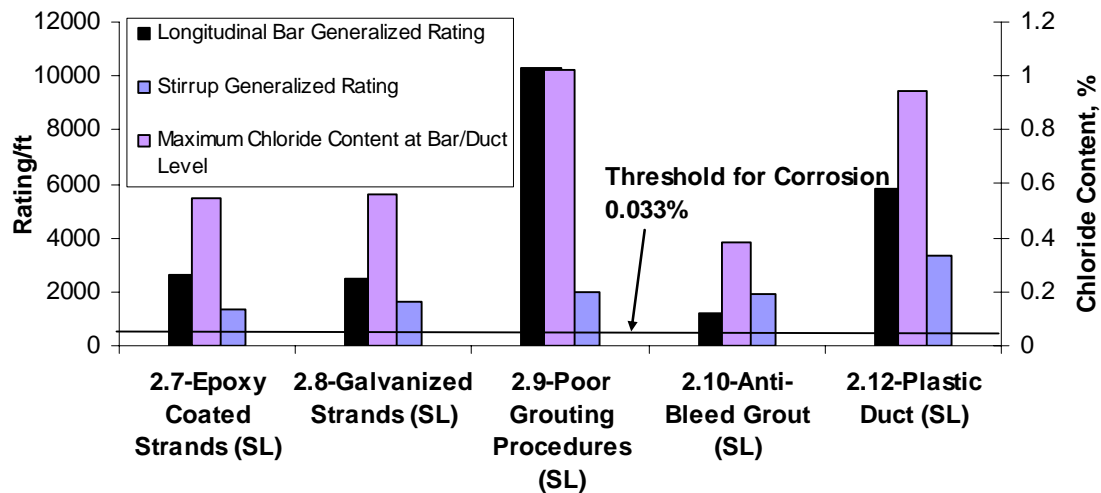


Figure 6.20: Phase II Beams-Maximum Chloride Content at Bar/Duct Level vs. Bar and Stirrup Ratings

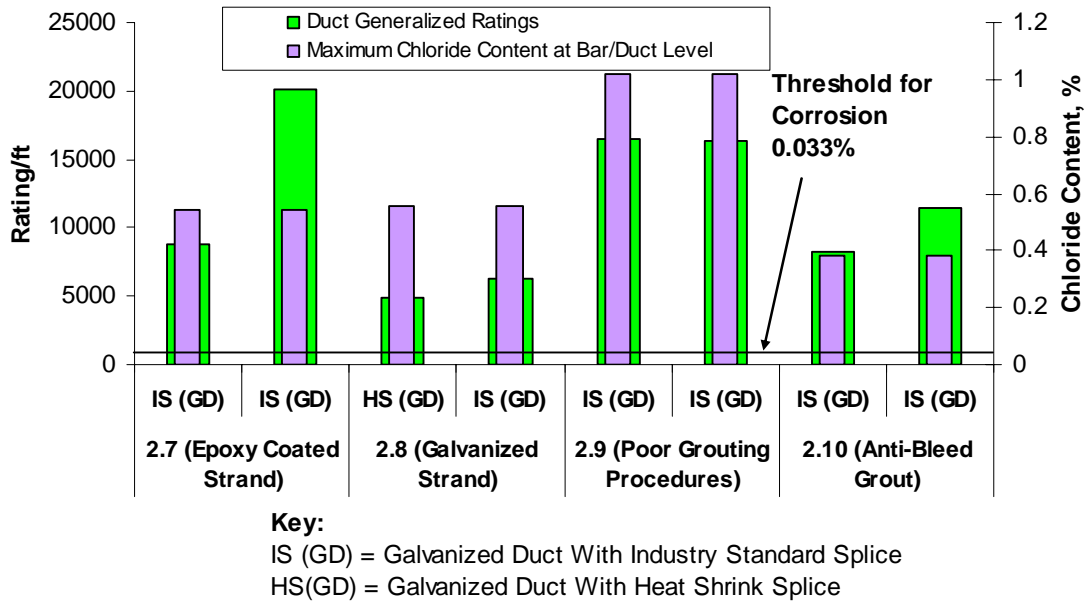


Figure 6.21: Phase II Beams-Maximum Chloride Content at Bar/Duct Level vs. Duct Generalized Ratings

Again, the threshold for corrosion was reached in all beams and severe bar, stirrup and duct corrosion were found. It is interesting to note in Figure 6.20 that the relative bar ratings coincide with relative chloride content. However, the stirrups do not. In Chapter 5 it was noted that in the Phase II beams flexural cracks would formed at stirrup locations. So the stirrups are corroded by chlorides entering at the flexural cracks for the most part. The fact that the relative values of the chloride contents and the longitudinal bar ratings coincide further suggests that concrete permeability, not just flexural cracks, was playing a major role in the corrosion damage of each beam after the long period of exposure.

Overall, when chloride contents above the threshold for corrosion were detected, corrosion was always found. Therefore, sampling chloride contents are an accurate method for determining whether corrosion has taken place.

6.5 EXTENT OF CORROSION DAMAGE AND LENGTH OF TESTING

During the 4 year autopsies performed by Salas³ and Kotys⁴, identical beams to those autopsied in the current study were examined. It is worthwhile to compare the difference in cracking and corrosion ratings between these specimens. The crack ratings of the equivalent beams from the 4 year and 8 year autopsies are plotted in Figure 6.22.

All beams were at service load. No comparison is available for the 100%U beams since beam 3.4, which was originally designated for service load, was overloaded.

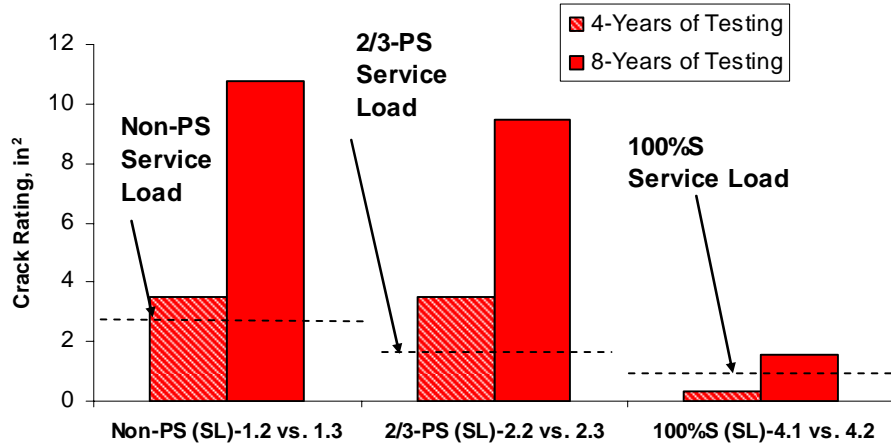


Figure 6.22: Phase I Beams-8 Year Crack Ratings vs. 4 Year Crack Ratings³

The crack ratings increased tremendously after an additional 4 years of testing. Details of the autopsies of the 4-years beams are found in Salas.³ The trends among the beams are similar, but more pronounced with the longer exposure time. In Figure 6.23 the duct ratings for the equivalent 4 year and 8 year prestressed beams are plotted. The strand ratings are plotted in Figure 6.24

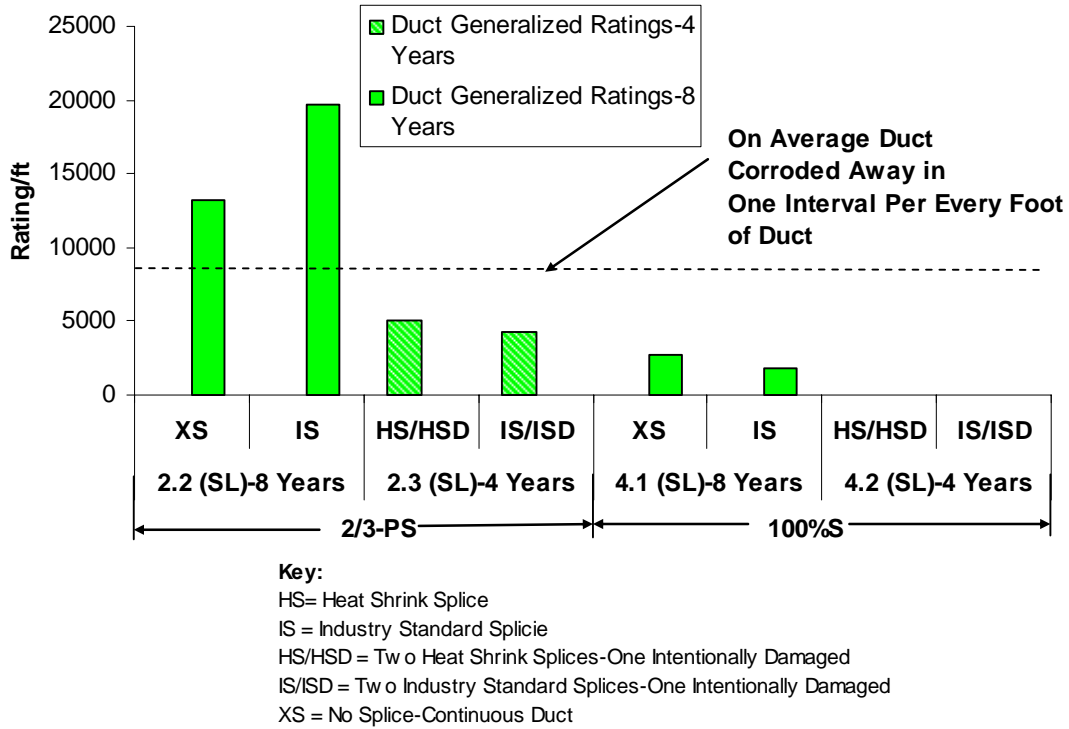


Figure 6.23: Phase I Beams-4 Year Duct Ratings vs. 8 Year Duct Ratings³

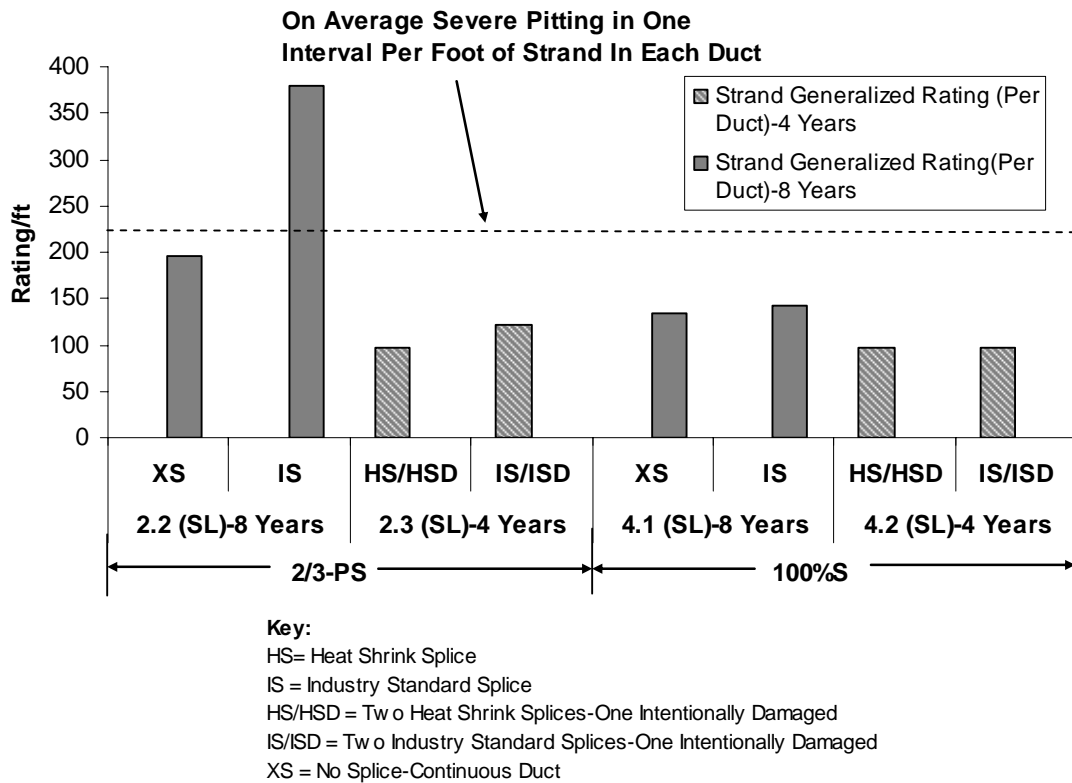


Figure 6.24: Phase I Beams-4 Year Strand Ratings vs. 8 Year Strand Ratings³

From Figure 6.23, it is clear that the duct corrosion increased dramatically after an additional 4 years of testing. This is especially evident in the 100%S beams (4.1 vs. 4.2). In the 4 year autopsies there was little corrosion evident in the ducts, but at 8 years the ducts were heavily holed. The strand ratings in Figure 6.24 show that strand corrosion increased significantly in both the beam types with the additional testing time. It is even more prevalent with the 2/3-PS beams. However, in making make this comparison it must be ignored that different duct splices are used.

6.6 PHASE I BEAMS VS. PHASE II BEAMS

In Figure 6.25 the bar and stirrup ratings for the Phase I and Phase II beams are plotted together for comparison. The Phase II beams are placed alongside the equivalent 2/3-PS beam from Phase I (Beam 2.2). The duct and strand ratings are plotted in Figure 6.26 and Figure 6.27 respectively.

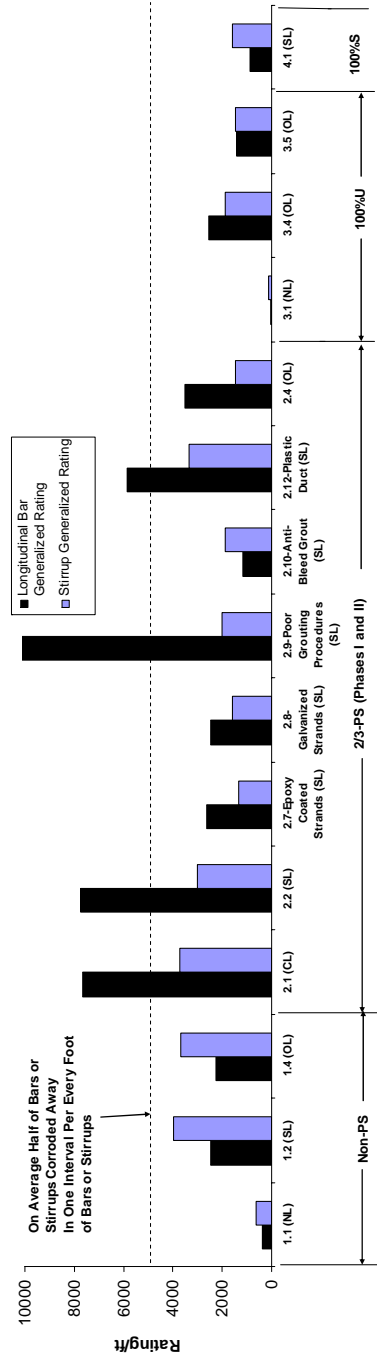
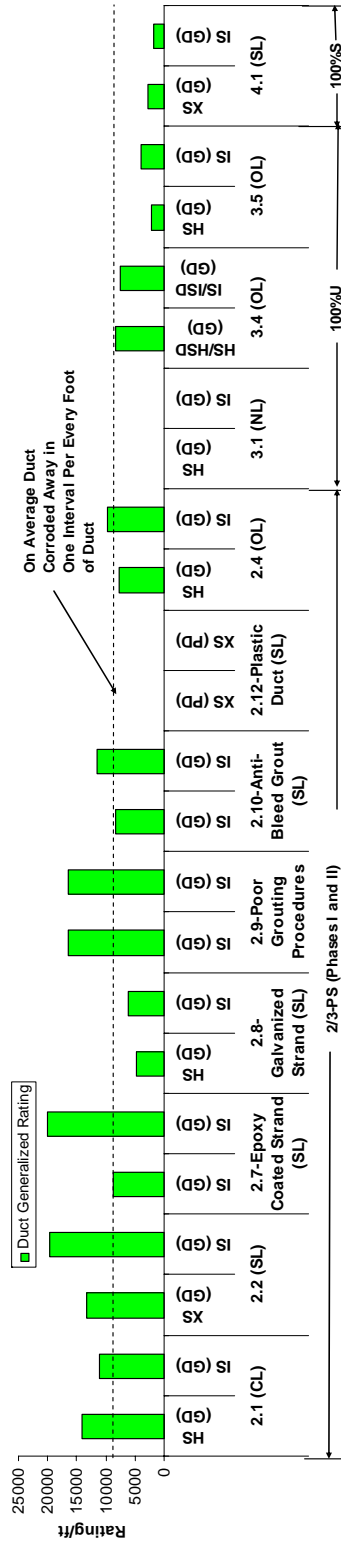


Figure 6.25: Phase I and Phase II Beams-Generalized Bar and Stirrup Ratings



Key:
 HS (GD)= Galvanized Duct with Heat Shrink Splice
 IS (GD)= Galvanized Duct with Industry Standard Splice
 HS/HSD (GD) = Galvanized Duct with Two Heat Shrink Splices-One Intentionally Damaged
 IS/SD (GD) = Galvanized Duct with Two Industry Standard Splices-One Intentionally Damaged
 XS (GD)= No Splice-Continuous Galvanized Duct
 XS (PD) = No Splice-Continuous Plastic Duct
 * = No Rating for Plastic Duct Since it Did not Corrode

Figure 6.26: Phase I and Phase II Beams-Generalized Duct Ratings

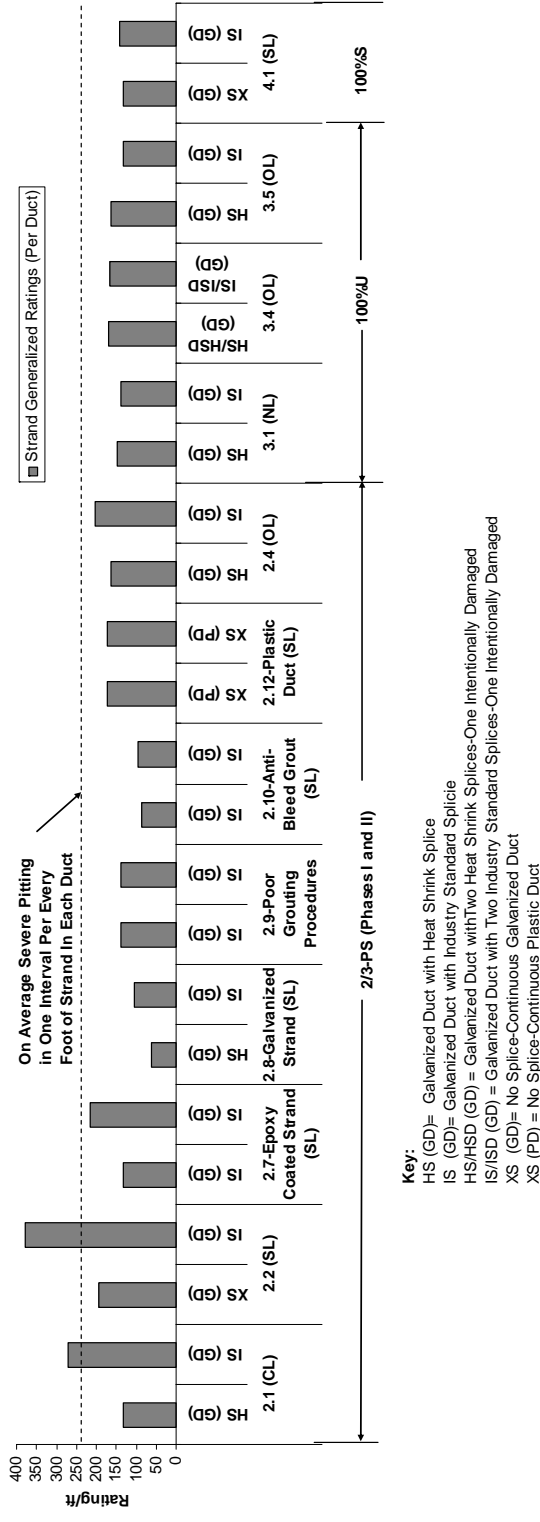


Figure 6.27: Phase I and Phase II Beams-Generalized Strand Ratings

It is clear that Phase II beams (All 2/3-PS at Service Load) performed similarly to the 2/3-PS beams of Phase I. Thus, the difference in testing time between the two phases was negligible and the beams are comparable.

Chapter 7: Design Recommendations & Implementation

7.1 DESIGN RECOMMENDATIONS

Some of the recommendations made below were initially made by Salas³ and Kotys⁴ as a result of the 4 year autopsies. They are included for completeness and were confirmed by the results of the 8 year autopsies.

7.1.1 Mixed Reinforcement

The higher degree of flexural cracking present with partially prestressed beams (also known as mixed reinforcement) resulted in very poor long-term durability. Therefore, it is recommended that mixed reinforcement (partial prestressing) not be used in aggressive environments. Only fully prestressed members should be used in such environments.

7.1.2 Duct Type

Corrugated galvanized metal ducts should not be used in aggressive environments. While future use of corrugated galvanized metal ducts in aggressive environments has already been banned by the Texas Department of Transportation¹¹, it is recommended that any existing post-tensioned bridge structures in aggressive environments that were constructed with such ducts undergo further close inspection if any initial signs of distress such as longitudinal splitting cracks along duct paths are found.

Plastic ducts will likely offer far better protection than galvanized ducts. However, the plastic duct system should be “robust” with high grade couplers. In addition, rubber or plastic bearing pads should be used between the plastic duct and any supporting or bracing bars to minimize the possibility of abrasion of the duct.

7.1.3 Duct Splice Type

Since galvanized metal ducts are no longer in use in aggressive environments in Texas, the industry standard splices are already obsolete. However, heat shrink splices also performed poorly with metal ducts. Heat shrink splices are also used with plastic

ducts. It is possible that this splice type will also perform poorly with a plastic duct. Therefore, more advanced splices/couplers should be used with plastic ducts. One possible type are positive lock couplers with o-ring seals. A series of specimens with advanced plastic ducts couplers are currently under active aggressive exposure to provide quantitative information in this area.

7.1.4 Grout Type and Grouting Procedure

The control grout used in this study would not be allowed by current TxDOT standards. The two main reasons are that it contains expansive admixtures and no anti-bleed admixture¹². Anti-bleed grout with strict grouting procedures will likely result in better grouting. As part of these strict grouting procedures, measures must be taken to ensure proper venting of air from each tendon.

7.1.5 Strand Type

Non-flowfilled epoxy-coated strand should not be used in aggressive environments. Flow-filled epoxy coated strand may offer better performance. Also, a more resilient epoxy coating should be used. Galvanized strand can delay the onset of corrosion, but should be treated as a last line of defense against corrosion.

7.1.6 Anchorage Protection

During the 8-year period of specimen exposure testing, the Texas Department of Transportation, based on experiences in other states, made the requirement that all anchorages be fitted with permanent caps.¹¹The results of this study confirm that this was indeed a proper course of action for TxDOT to take. In addition, any uncapped post-tensioned anchorages with galvanized ducts in existing bridge structures should be subjected to close inspection if in an aggressive environment. In addition, a designer should take into account that it is possible for any moisture ingress from a single point in the tendon to travel throughout the tendon and possibly into the anchorage by the pathways in the strand interstices. Also, similar metals should be used in anchorages to prevent galvanic corrosion.

7.1.7 Reinforcing Bars & Bar Chairs

It is absolutely critical, even in prestressed bridge members, to use epoxy coated bars for non-prestressed reinforcement in aggressive environments. In addition, plastic chairs should be used in aggressive environments instead of steel bolster strips. However, using plastic chairs may result in thermal stresses since plastic has a higher coefficient of thermal expansion. This could have contributed to the splitting cracking seen in the Phase II beams.

7.1.8 Chloride Content

Testing for chloride content at the level of the reinforcing elements is a reliable way to determine the presence of corrosion in a structure.

7.1.9 Half-Cell Potentials

Half-cell potentials are a reliable method to determine the presence of corrosion in post-tensioned bridge substructures. However, they will not indicate whether the corrosion is taking place in the bars, strands, or ducts. This limits the usefulness of the readings. In addition, they can indicate the likelihood of corrosion initiation but not the severity of the corrosion.

Chapter 8: Summary, Conclusions, and Recommendations for Future Testing

8.1 SUMMARY

Fifteen large scale beam specimens with varying levels of prestress were placed under varying levels of loading and subjected to approximately 8 years of aggressive exposure cycles. In some cases the anchorage zones were also subjected to exposure cycles. Non-destructive testing, including half-cell potentials and chloride samples, were taken during testing. In the end, the beams were heavily corroded. Large amounts of staining, spalling, and splitting was observed. The beams were then autopsied and the bars, stirrups, ducts and post-tensioning tendons were examined. Both end anchorages were removed from the beams with anchorage exposure and were also examined.

8.2 CONCLUSIONS

8.2.1 Level of Loading, Level of Prestress, and Initial Crack Width

8.2.1.1 Level of Loading

It was found that once a beam was loaded and flexural cracking introduced any additional loading and widening of the cracks had no effect on the final amount of corrosion.

8.2.1.2 Level of Prestress

Partial prestressing, also known as “mixed reinforcement” offered no real durability advantage over not prestressing at all. Therefore, mixed reinforcement should not be used in aggressive environments. Full prestressing so as to preclude service load cracking delayed onset of corrosion until concrete cover over the bars and ducts was penetrated.

8.2.1.3 Initial Crack Width

Controlling the initial crack width only delayed the onset of corrosion, resulting in no substantial decrease in the final amount of corrosion.

8.2.2 Duct Type

8.2.2.1 Galvanized Steel Duct

The galvanized steel ducts performed poorly. Typically they corroded severely with gaping holes. In many cases the ducts completely corroded away across several inches. Therefore, galvanized steel ducts should not be used in aggressive environments.

8.2.2.2 Plastic Duct

Unfortunately, in the single beam specimen with a plastic duct system, the plastic duct failed mechanically during prestressing when a combination of internal abrasion due to wear from stressing of the strand coincided with a point where the duct passed over a steel bracing bar and then external pressure caused a small hole to form in the duct. This demonstrates that a plastic duct system must be robust and protected from external abrasion. However, the plastic duct also demonstrated better grouting characteristics than the galvanized duct due to its large corrugations. In a previous study with macrocell specimens, more rugged plastic ducts performed substantially better than metal ducts.³ Overall, it is likely that more modern robust plastic ducts will offer much better durability performance than galvanized ducts.

8.2.3 Strand Type

8.2.3.1 Conventional Strand

In the heavily damaged beams the conventional strand was found to be heavily pitted or reduced in area, or, in some cases, actually snapped during unwinding. It was also found that the interstices of the strand can easily transport moisture throughout a tendon, in some cases all the way to the anchorages.

8.2.3.2 *Non-Flowfilled Epoxy Coated Strand*

The epoxy coated strand used in this study had abrasion damage to its coating as a result of the prestressing operations. Chlorides were able to travel down the uncoated interstices and heavily corrode the strand. It was found that the typical patches used to repair coating damage in the strand performed fairly well. In addition, the coating was found to be very brittle with age. At the anchorages full penetration of the coating was found from the wedge teeth with localized corrosion in these areas (this was found at the end of the beam with anchorage exposure). Overall, this type of epoxy coated strand offered no advantage over conventional strand from a durability standpoint. Therefore, non-flowfilled epoxy coated strand should not be used in aggressive environments.

8.2.3.3 *Hot-Dipped Galvanized Strand*

The galvanized strand was substantially corroded with some pitting. While the corrosion was less than in the conventional strand, the galvanized strand still performed poorly. This demonstrates that the galvanization merely delayed the onset of corrosion on the strand itself. Therefore, galvanized strand should not be depended on as a primary line of defense against corrosion.

8.2.4 Grout Type

8.2.4.1 *Control Grout*

The control grout was basically Type I cement with an expanding admixture. This was allowed by TxDOT standards at the time of beam fabrication, but would not be allowed by current standards. The grout was found to be porous and had a large tendency to form bleed water voids. Its discontinuance by TxDOT was fully warranted.

8.2.4.2 *Anti-Bleed Grout*

The anti-bleed grout used in this study was a mix design made by the researchers, not the pre-bagged anti-bleed grout widely used today. Unfortunately, due to the mixing method used, the anti-bleed grout was heavily segregated and as a result the anti-bleed admixture did not fully engage. However, in the area closer to the strands the grout was

of better quality than the control grout. This clearly demonstrates the importance of good grouting procedures. The results of this study do not confirm conclusively that the anti-bleed grout offers better overall performance than the control grout used in the study.

8.2.5 Grouting Method

“Poor” grouting procedures were deliberately used in one beam. This involved poor air venting, poor pumping procedures, and allowing grouting to stop for long periods. The autopsy results showed that the grout had evidence of more porosity and slightly more bleed water voids than in the other beams. However, the poor quality of the control grout resulted in “poor” grouting in the other beams as well. Therefore, the intentional “poor” grouting procedures made little difference in the end.

8.2.6 Anchorage Protection

An encapsulated, plastic duct system typically used for bridge slabs was used in one beam. The primary part of this system was a permanent protective cap with an o-ring seal placed over the anchorhead. This was compared to the then standard detail of coating the anchorage with epoxy and then filling the anchorage pockets with non-shrink grout. The dripping of saltwater at the anchorage caused the chloride content level necessary for corrosion to be reached at the level of the strand tails in the anchorage. Upon autopsy, it was found that the bearing plates and strand tips in the specimens with the standard detail were significantly corroded, while the tips of the strands in the beam with the caps were in pristine condition. Therefore, the use of the caps offers a clear durability advantage.

8.2.7 Galvanized Metal Duct Splice Type & Condition

The industry standard splice type and the heat shrink splice were tested. Both splices were found to perform poorly, allowing moisture ingress into the duct. The effect of accidental damage to the splices was found to be insignificant due to the fact the splices already performed poorly. Duct couplers with o-ring seals may offer an advantage over these splices.

8.2.8 Accuracy of Non-Destructive Measurements Taken During Exposure Testing

8.2.8.1 Half-Cell Potential Readings

The half-cell readings were found to correctly indicate if corrosion was present. However, they could not be used to isolate whether the corrosion was in the bars or the tendon. In addition, the readings did not give an accurate measurement of the relative amount of damage in each beam. Therefore, for field indication of the presence of corrosion half-cell potentials can be useful to a limited extent.

8.2.8.2 Concrete Chloride Samples

Taking chloride samples and determining whether the concrete chloride content threshold for corrosion was reached at bar/duct level was found to be an accurate method for determining the high probability of the presence of corrosion.

8.3 RECOMMENDATIONS FOR FUTURE TESTING

Some of the following recommendations were also made by Salas³ and Kotys⁴. They are included again since the results of the current autopsies make the recommendations all the more apparent.

- Use epoxy coated bars for all non-prestressed reinforcement including stirrups and bracing bars so that non-destructive evaluation indications of corrosion of the post-tensioning tendons is made more apparent. It is likely that epoxy coated bars will not corrode as heavily as uncoated bars. This should greatly reduce the splitting and exposure to chlorides.
- Use plastic chairs so that any corrosion can be attributed to the post-tensioning hardware (assuming that the bars are epoxy coated).
- In future studies the number of variables should be reduced or the number of specimens should be increased.
- If testing anchorage protection, only expose the end anchorage. Do not pond at the center of the beam as well. This way any corrosion in the anchorage can

clearly be attributed to the anchorage exposure cycles and not due to moisture migrating along the beam through the strand interstices.

- In all grouting and especially if using modern anti-bleed grouts, use industry standard mixing equipment and practices.

One possible recommendation may be shortening the length of testing. The new specimens developed for project 4562 have less cover to accelerate chloride penetration.⁵ During the 8 years that the current beams were under exposure, many of the materials and methods used were already declared obsolete even before testing was over. However, it is likely with a shorter testing period that long-term performance of the epoxy coated strand and galvanized strand would not have been as clear.

Appendix A: Corrosion Ratings

Table A.1: Corrosion Ratings for Phase I and Phase II Beams (Center of Beams)

Beam	Beam Specimen Notation	Longitudinal Bars:		Stirrups:		Ducts:		Strand (Per Duct):	
		Total	Generalized	Total	Generalized	Total	Generalized	Total	Generalized
1.1	1-X-XL-C	18618	388	6668	635	N/A	N/A	N/A	N/A
1.2	1-X-SL-C	119294	2485	41600	3962	N/A	N/A	N/A	N/A
1.4	1-X-OL-C	108635	2263	38594	3676	N/A	N/A	N/A	N/A
2.1	1-P-CL-C-SD-HS-NG-NS-D1	328956	7644	39035	3718	84767	14128	1570	131
	1-P-CL-C-SD-IS-NG-NS-D2	328956	7644	39035	3718	66997	11166	3236	270
2.2	1-P-SL-C-SD-XS-NG-NS-D1	371200	7733	31604	3010	79567	13261	2340	195
	1-P-SL-C-SD-IS-NG-NS-D2	371200	7733	31604	3010	118934	19732	4564	380
2.4	1-P-OL-C-SD-HS-NG-NS-D1	168834	3517	15169	1445	45914	7652	1972	164
	1-P-OL-C-SD-IS-NG-NS-D2	168384	3517	15169	1445	58433	9739	2436	203
3.1	1-U-XL-C-SD-HS-NG-NS-D1	184	23	1172	112	53	9	2662	148
	1-U-XL-C-SD-IS-NG-NS-D2	184	23	1172	112	26	4	2475	138
3.4	1-U-OL-C-SD-HS/HSD-NG-NS-D1	22200	2571	19855	1891	49483	8247	3030	168
	1-U-OL-C-SD-IS/ISD-NG-NS-D2	22200	2571	19855	1891	45187	7531	2978	165
3.5	1-U-OL-C-SD-HS-NG-NS-D1	13822	1434	15495	1476	12555	2093	2924	162
	1-U-OL-C-SD-IS-NG-NS-D2	13822	1434	15495	1476	23934	3989	2362	131
4.1	1-S-OL-C-SD-XS-NG-NS-D1	10287	884	16595	1581	16399	2733	3190	133
	1-S-OL-C-SD-IS-NG-NS-D2	10287	884	16595	1581	10673	1779	3410	142
2.7	2-P-SL-C-SD-IS-NG-ES-D1	125879	2622	13988	1332	52523	8754	1580	132
	2-P-SL-C-SD-IS-NG-ES-D2	125879	2622	13988	1332	120352	20059	2586	216
2.8	2-P-SL-C-SD-HS-NG-GS-D1	117875	2456	16833	1603	29109	4851	739	62
	2-P-SL-C-SD-IS-NG-GS-D2	117875	2456	16833	1603	37304	6217	1274	106
2.9	2-P-SL-C-SD-IS-NG-NS-D1	492958	10270	21026	2002	99193	16532	1648	137
	2-P-SL-C-SD-IS-NG-NS-D2	492958	10270	21026	2002	98252	16375	1680	140
2.10	2-P-SL-C-SD-IS-AB-NS-D1	57082	1189	19840	1890	49464	8244	1040	87
	2-P-SL-C-SD-IS-AB-NS-D2	57082	1189	19840	1890	69070	11512	1136	95
2.12	2-P-SL-C-PD-XS-NG-NS-D1	281142	5857	35325	3364	N/A	N/A	2064	172
	2-P-SL-C-PD-XS-NG-NS-D2	281142	5857	35325	3364	N/A	N/A	2060	172

Table A.2: Corrosion Ratings for Anchorages of Anchorage Exposure Beams

Beam	Specimen Notation	Dripped End Strand (Total)	Dripped End Duct (Total)	Control End Strand (Total)	Control End Duct (Total)
2.7	2-P-SL-C-SD-IS-NG-ES-D1	541	32	566	8
	2-P-SL-C-SD-IS-NG-ES-D2	529	8	492	4
2.9	2-P-SL-C-SD-IS-NG-NS-D1	652	8	556	6
	2-P-SL-C-SD-IS-NG-NS-D2	664	16	646	12
2.12	2-P-SL-C-PD-XS-NG-NS-D1	562	N/A	634	N/A
	2-P-SL-C-PD-XS-NG-NS-D2	494	N/A	666	N/A

Appendix B: Half-Cell Potential Data

In Figure B.1 and Figure B.2 the maximum half-cell potentials for each beam at each monthly reading are plotted for the Phase I beams and the Phase II Beams respectively. Despite the fact that both phases were tested for the same time period, they are plotted separately since the testing of the Phase II beams began a year later than the Phase I beams. The probability of corrosion according to ASTM C876¹⁵ is indicated. The crossing of the 90% probability threshold is assumed as the point at which corrosion initiated. In some cases there are gaps in the data due to beam maintenance or equipment issues.

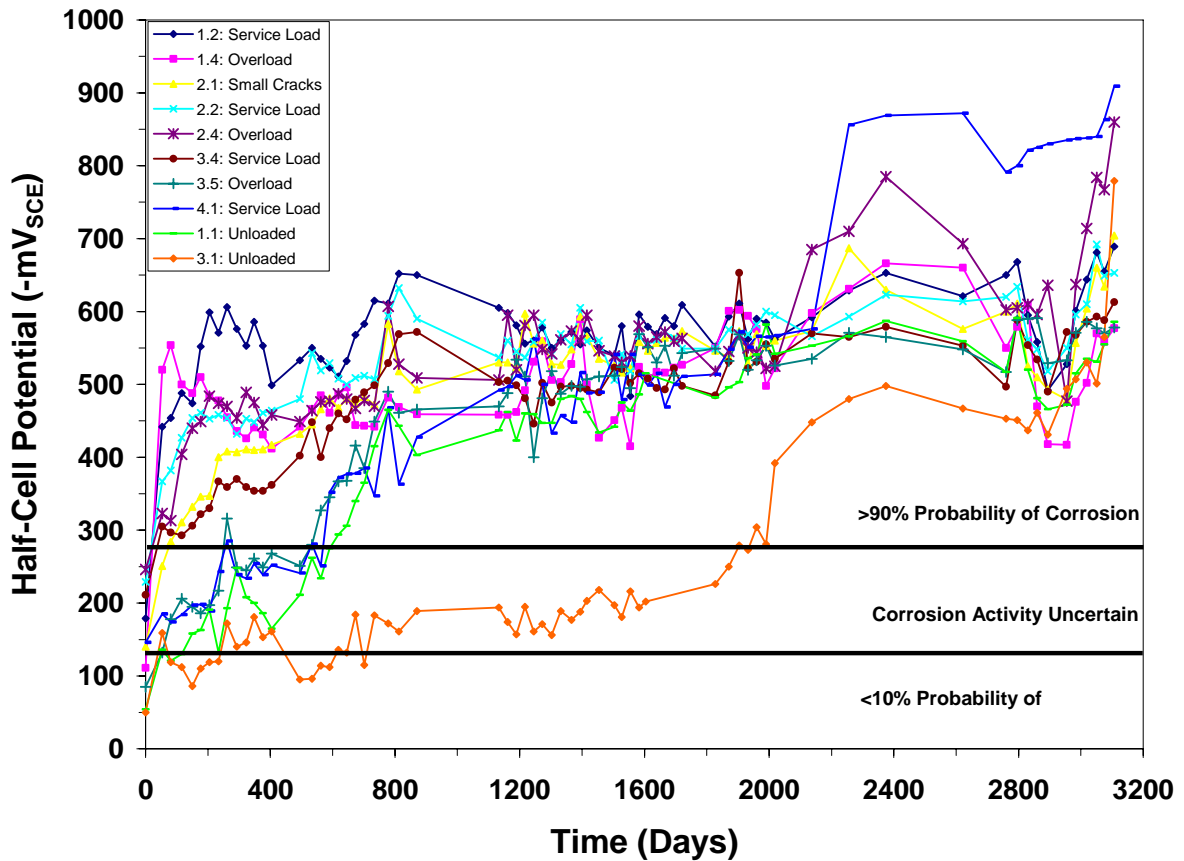


Figure B.1: Phase I Beams-Maximum Half-Cell Potentials for Each Day of Sampling

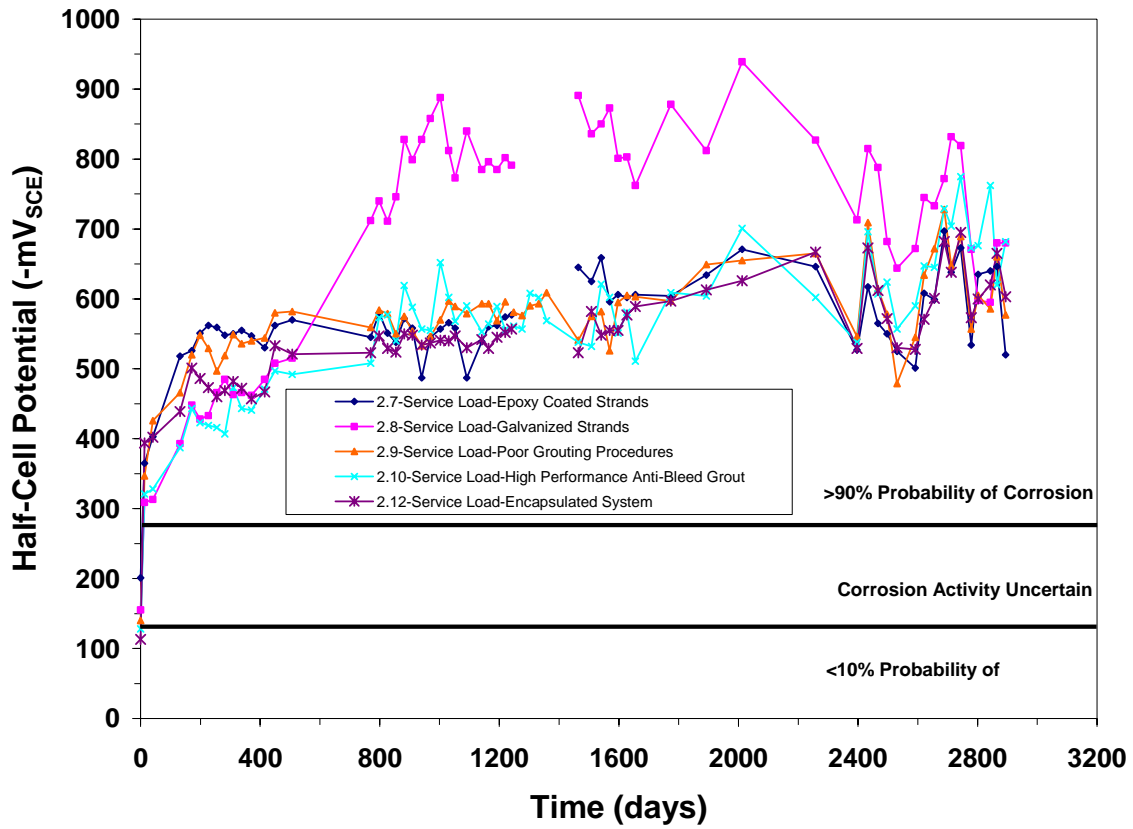


Figure B.2: Phase II Beams-Maximum Half-Cell Potentials for Each Day of Sampling

References

1. West, J.S., "Durability Design of Post-Tensioned Bridge Substructures," Ph.D. Dissertation, The University of Texas at Austin, 1999.
2. Schokker, A.J. "Improving Corrosion Resistance of Post-Tensioned Substructures Emphasizing High Performance Grouts," Ph.D. Dissertation, The University of Texas at Austin, 1999.
3. Salas, R.M. "Accelerated Corrosion Testing, Evaluation and Durability Design of Bonded Post-Tensioned Concrete Tendons," Ph.D. Dissertation, The University of Texas at Austin, 2003.
4. Kotys, A.L. "Durability Examination of Bonded Tendons in Concrete Beams Under an Aggressive Corrosive Environment," M.S. Thesis, The University of Texas at Austin, 2003.
5. Ahern, M.E. "Design and Fabrication of a Compact Specimen for Evaluation of Corrosion Resistance of New Post-Tensioning Systems," M.S. Thesis, The University of Texas at Austin, 2005.
6. Luthi, T. "Factors Affecting Bond and Friction Losses in Multi-Strand Post-Tensioning Tendons Including the Effect of Emulsifiable Oils," M.S. Thesis, The University of Texas at Austin, 2005.
7. French, C., "Durability of Concrete Structures," *Structural Concrete: Journal of the fib*, Vol. 4, No. 3, September 2003.
8. Freyermuth, C.L., "Status of the Durability of Post-Tensioning Tendons in the United States," *Durability of Post-Tensioning Tendons, fib-IABSE Technical Report, Bulletin 15, Workshop 15-16 November 2001, Ghent, Belgium, 2001.*
9. Poston, R.W., and West, J.S., "North American Strategies for Improving Bonded Post-Tensioned Concrete Construction," *Durability of Post-Tensioning Tendons, fib-IABSE Technical Report, Bulletin 15, Workshop 15-16 November 2001, Ghent, Belgium, 2001.*
10. Broomfield, J.P., "Corrosion of Steel in Concrete," 2nd Edition, 2007.
11. Texas Department of Transportation, "Standard Specifications for Construction and Maintenance of Highways, Streets, and Bridges," 2004.

12. Texas Department of Transportation, "DMS 4670, Grouts for Post-Tensioning," 2004.
13. Post-Tensioning Institute, "Specification for Grouting of Post-Tensioned Structures," 2003.
14. American Association of State Highway and Transportation Officials, "Standard Specification for Highway Bridges," 17th Edition, 2004.
15. ASTM, "Standard Test Method for Half-Cell Potentials of Uncoated Reinforcing Steel in Concrete," ASTM C876-91, American Society for Testing and Materials, Philadelphia, Pa., 1991.
16. VSL International, *VSLAB+™*, brochure downloaded from VSL website.
17. Jones, D.A., "Principles and Prevention of Corrosion," 2nd Edition, 1996.

Vita

Gregory Paul Turco was born on October 24, 1982 in Newburgh, New York to Paul and Nancy Turco. After graduating from Westwood High School in Austin, Texas in 2001, he attended the University of Texas at Austin where he received his Bachelor of Science Degree in Civil Engineering in the spring of 2005. In the fall of 2005 he entered the graduate program in the Department of Civil Engineering at the University of Texas at Austin to pursue his Master of Science in Civil (Structural) Engineering.

Permanent Address: 11133 Callanish Park Dr.

Austin, Tx 78750

This thesis was typed by the author.